

**FLAVOUR-SALIVA INTERACTIONS:
IMPLICATIONS OF
SUBMAXILLARY MUCIN AND α -AMYLASE**

VLAD TEODOR DINU, MSc.

**Thesis submitted to the University of Nottingham
for the degree of Doctor of Philosophy**

SEPTEMBER 2019

Abstract

During food ingestion, a large proportion of the aroma and taste compounds remain trapped in the food bolus and are therefore not available for perception. These compounds serve no functional benefit as flavourings and may also have negative health impacts (e.g.hypertension through high levels of salt, diabetes from excess of sugar) to the consumer. Understanding the interactions underpinning the partitioning of aroma and taste compounds from the bolus during oral processing is required to mitigate these adverse effects. Therefore, the focus of this study is on the interactions between functional food ingredients (dietary acidity, salt, polyphenols, polysaccharide mucoadhesives) and two of saliva's most abundant macromolecules, salivary mucin and α -amylase.

Firstly, the macromolecular hydrodynamic integrity of glycoproteins was assessed as a function of pH and ionic strength, as a way of understanding the effects of dietary acid and salt, and evaluate any resulting changes in the aroma release profile. An increase in acidity and saltiness impacted the native state of mucin and α -amylase, through charge shielding effects and aggregation phenomena. Protein interactions with pH and ionic strength are suggested to be, at least in part, responsible for the enhanced flavour perceived in acidic and salty foods. Then, green tea was investigated for its ability to interact with whole human saliva as a means of developing a platform for analysing interactions with food in their native dilute states. The green tea polyphenol epigallocatechin gallate (EGCG) interacted with low molecular weight components in saliva and was found to be an essential step in the formation of green tea aroma.

The development of new mucoadhesive biopolymers for oral processing formulations has received great attention in recent years for enhancing the release of flavour in food. The addition of pullulan to saliva was identified to result in the formation of lower molecular weight and lower viscosity fragments via salivary α -amylase hydrolysis. This property was correlated to an enhanced release of aroma and salt. To address issues associated with the rapid ingestion, a cationic pullulan analogue was developed to aid in its adhesion to submaxillary mucins. Dimethylaminoethyl pullulan (DMAE-Pullulan) was synthesised for the first time, and shown to bind to submaxillary mucin, and also degraded by salivary α -amylase. In addition, an *in-vitro* mucus-like biomimetic was developed for evaluating mucoadhesion and flavour retention by immobilising mucin glycoproteins in calcium alginate gels. This resulted in the formation of bead structures containing mucin and mucin aggregates both on and within the calcium-alginate matrix. Polysaccharides of different ionic properties were tested for their ability to retain flavour compounds onto the surface of the mucus like mimetic. It was found that mucins were the predominant driving force in the interaction with the polymers, with positively charged species showing the highest retention (electrostatic interactions).

Findings from these investigations also added to our current understanding of the interactions between salivary proteins and aroma compounds. Current evidence suggests that high concentrations (>1 %), of aroma compounds i.e. ketones, aldehydes and phenols, can affect the hydrodynamic integrity of proteins. These changes are suggested to directly impact on the structure and function of mucosal proteins.

Acknowledgements

I wish to thank Prof. Ian Fisk, Prof. Stephen Harding, Dr. Gary Adams and Dr. Guy Channell for their supervision, and to Profs. Peter Licence and Christopher Moody for giving me the opportunity to be a part of the EPSRC Centre for Doctoral Training in Sustainable Chemistry. I am also grateful to my internal, Dr. Marcos Alcocer for offering me his advice towards my studies and career, and to the academics (Dr. Rob Linforth, Dr. Gleb Yakubov, Dr. Mary Phillips-Jones), members of staff (Dr. Charfedinne Ayed, Dr. Richard Gillis, Sharon Lim, Jenny Drury), fellow students and friends (Jennifer Wakefield, Thomas MacCalman, Ryan Lithgo, Yudong Lu, Xinxin Li, Kate Hurst, Katy Su, Sophie Lester, Joseph Ali, Brian O’Loinsigh, Azad Kilic and Cordelia Jefferson) who offered me their support. Also, I am grateful to my family for their invaluable support for my personal and professional development.

Publications

Investigations carried out as a part of this project led to the direct publication of five peer reviewed papers:

- Dinu V. et al. (2019). Mucin immobilization in calcium alginate: A possible mucus mimetic tool for evaluating mucoadhesion and retention of flavour. *International Journal of Biological Macromolecules*, *138*, 831-836.
- Dinu V. et al. (2019). An enzymatically controlled mucoadhesive system for enhancing flavour during food oral processing. *npj Science of Food*, *3*, 11.
- Dinu V. et al. (2019). Submaxillary mucin: Its effect on aroma release from acidic drinks and new insight into the effect of aroma compounds on its macromolecular integrity. *Food Biophysics*, *14*, 3.
- Dinu, V. et al. (2018). Analytical ultracentrifugation in saliva research: Impact of green tea astringency and its significance on the in-vivo aroma release. *Scientific Reports*, *8*, 13350.
- Channell G., Dinu V. and Adams G.G. and Harding S.E. (2018). A simple cell-alignment protocol for sedimentation velocity analytical ultracentrifugation to complement mechanical and optical alignment procedures. *European Biophysics Journal*, *47*, 7.

Other papers have been co-authored during my PhD:

- Beji O, Gillis, R.B., Dinu V. et al. (2019). Exploration of temperature and shelf-life dependency of the therapeutically available Insulin Detemir. *European Journal of Pharmaceutics and Biopharmaceutics* (submitted).
- Dinu V., et al. (2020). The antibiotic vancomycin induces complexation and aggregation of gastrointestinal and submaxillary mucins. *Scientific Reports*, (in press).
- Phillips-Jones, M. K, Lithgo, R., Dinu, V. *et al.* (2017). Full hydrodynamic reversibility of the weak dimerization of vancomycin and elucidation of its interaction with VanS monomers at clinical concentration. *Scientific Reports*, 7, 12697.
- Phillips-Jones, M. K. *et al.* (2017). Hydrodynamics of the VanA-type histidine kinase: an extended solution conformation and first evidence for interactions with vancomycin. *Scientific Reports*, 7, 46180.
- Varzakas, T., Alghamdi, A. Alghamdi, H., Linforth, R., Dinu V., et al. (2016). The effect of thermal processing in oil on the macromolecular integrity and acrylamide formation from starch of three potato cultivars organically fertilized. *Cogent Food and Agriculture*, 2, 16.
- Channell G.A., Adams G.G., Lu Y., Gillis R.B., Dinu V. et al. (2018). Use of the Extended Fujita method for representing the molecular weight and molecular weight distributions of native and processed oat beta-glucans. *Scientific Reports* , 8, 11809.

Abbreviations

° C	degrees Celsius
cm	centimetre
g	gram
GC-MS	Gas Chromatography-Mass Spectrometry
L(l)	litre
m/z	mass-to-charge ratio
mg	milligram
ml	millilitre
mm	millimetre
mol	mole
PCA	Principal Component Analysis
ppm	part per million
ppb	part per billion
s/sec	second
µl	microliter
µm	micrometre
AUC	Analytical Ultracentrifugation
APCI	Atmospheric Pressure Chemical ionisation
BSM	Bovine Submaxillary Mucin
c(s)	sedimentation coefficient distribution corrected for diffusion
$D_{\text{trans}} (D_{20,w}^0)$	translational diffusion coefficient (cm^2s^{-1})
Da	Daltons
DLS	Dynamic Light Scattering
dn/dc	refractive index increment (ml/g)
η	dynamic viscosity (mPa s)
η_r, η_{sp}	relative, specific viscosity
$\eta_{\text{red}}, \eta_{\text{inh}}, [\eta]$	reduced, inherent, intrinsic viscosity (ml/g)
GC-MS	Gas Chromatography Mass Spectrometry

J / j	fringe concentration corrected for baseline / uncorrected
k_B	Boltzmann constant (1.381×10^{-16} erg/K)
k_H, k_K	Huggins, Kraemer constants
k_s	Gralén coefficient/concentration dependence of sedimentation coefficient (ml/g)
$g(s)$	least square Gaussian fit of sedimentation coefficient distribution
HSA	Human Salivary α -Amylase
M	molar mass (mol/g)
MALS	Multi Angle Light Scattering
MHKS	Mark Houwink Kuhn Sakurada (power law scaling relationship between M_w and $[\eta]$, S and D respectively)
$M_{n,w,z}$	Number average, weight average, Z average molar mass (Daltons)
N_A	Avogadro's constant (6.022×10^{23} mol ⁻¹)
PBS	Phosphate Buffered Saline
r	radius (cm)
ρ	density (g/ml)
R_g	radius of gyration (nm)
$r_{z,app}$	apparent radius of hydration (nm)
rpm	revolutions per minute
$s^0_{20,w}$ (S)	sedimentation coefficient, corrected to standard temperature and buffer conditions (density and viscosity of water at 20.0 °C) (1S = 1 Svedberg = 1×10^{-13} s)
SEC	Size Exclusion Chromatography
SPME	Solid Phase Micro Extraction
\bar{v}	partial specific volume (ml/g)
ω	angular velocity (rad/s)

List of Figures

Figure 1.1. Schematic representation of the random coil model (adapted from Sheehan, et al., 1986).....	15
Figure 1.2. Domain organisation of human salivary α -amylase monomer. Domain A is shown in orange, domain B in blue and Domain C in red. Obtained from RCSB PDB (file 1SMD).....	20
Figure 1.3. Schematic representation of the main forces involved in the sedimentation process in the solution channel (adapted from van Holde, 1971).....	35
Figure 1.4. Schematic representation showing the principle areas investigated in the current work.....	56
Figure 3.1. Sedimentation velocity, $g(s)$ analysis of BSM showing the sedimentation coefficient distributions (a), and the $c(s)$ analysis at low concentration showing the estimated deconvoluted distribution, $f/f_0 = 3.8$ (b). Run at 20.0 °C at 30, 000 rpm in PBS buffer with ionic strength of 0.1 M (pH 7.0).....	71
Figure 3.2. Dynamic Light Scattering results yielding apparent size distribution of BSM at 1 mg/ml (a), and extrapolation to zero concentration of reduced viscosity of to determine the intrinsic viscosity $[\eta]$ of mucin at neutral pH (b). Experiments performed at 20.0 °C in PBS buffer with ionic strength 0.1 M (pH 7.0).....	73
Figure 3.3. SEC-MALS of BSM showing the RI and UV elution profile of BSM (a), differential molecular weight distribution (b), Mark Houwink-Kuhn Sakurada (MHKS) plot of intrinsic viscosity $[\eta]$, versus molecular weight M_w (c), and Multi-HYDFIT contour plot of the target function (●), showing the M_L and L_P estimates (d).....	74
Figure 3.4. Comparative hydrodynamic properties of BSM at pH 7.0 and at pH 3.0 showing the sedimentation coefficient distribution (a), reciprocal plot of s versus concentration, to determine the concentration dependence	

'Gralén' coefficient (b), the Extended Fujita analysis, $f(M)$ versus M for a loading concentration of 0.25 mg/ml; $\kappa'' = 0.007606$ and $b = 0.483$ (c) and apparent hydrodynamic radius $r_{z,app}$ (d). Experiments performed in PBS buffer with ionic strength 0.1 M (pH 7.0) and Na-citrate buffer with ionic strength 0.1 M (pH 3.0) at 20.0 °C.....76

Figure 3.5. SEDFIT-MSTAR analysis showing the $c(M)$ molecular weight distribution plot and the MULTISIG $c(\sigma)$ transformation yielding the weight average molecular weight distribution (M_w) for BSM at pH 7.0 and at pH 3.0. Centrifuged at 20.0 °C at 10, 000 rpm for 78 hours78

Figure 3.6. APCI-MS results showing the impact of pH on the release of volatile aroma compounds from solutions with 1.0 mg/ml mucin (continuous red line) and from the neutral and acidic buffer solutions (dotted line). Data are shown as mean \pm SE, (n = 3).....80

Figure 3.7. Sedimentation velocity, $g(s)$ and $c(s)$ analyses of HSA showing the sedimentation coefficient distributions of 1.0 mg/ml HSA at different pH. Run at 20.0 °C at 40, 000 rpm in 0.1M PBS (pH 7.0) and 0.1 M Na-citrate buffer (pH 3.0 and pH 5.0).....82

Figure 3.8. GC-MS results showing the effect of pH on the release of volatile aroma compounds from HSA solutions (1.0 mg/ml). Values are expressed as mean \pm SD (n = 3).....84

Figure 3.9. Comparative hydrodynamic properties of BSM at low and high NaCl concentration, showing the sedimentation coefficient distributions at 1.0 mg/ml and reciprocal plot of s versus concentration. Experiments performed in PBS buffer 0.05 M (pH 7.0) before and after the addition of 30.0 mg/ml (1.0 M) sodium chloride.....85

Figure 3.10. Oblate ellipsoid models of BSM under physiological salt concentrations and after the addition of and in the presence of 30.0 mg/ml sodium chloride. Models predicted using HYDFIT and using the concentration dependence 'Gralén' coefficient. Modelled in ELLIPS (Harding et al., 1997).....86

Figure 3.11. GC-MS results showing the effect of NaCl concentration on the release of volatile aroma compounds in the absence of mucin (a), and

in the presence of mucin (b). Values are expressed as mean \pm SD (n = 3).....87

Figure 3.12. Comparative viscosity of BSM solutions in the presence of 0.1 M sodium and 0.1 M potassium chloride. Intrinsic viscosity was determined by plotting the Solomon-Ciuta equation, extrapolated to zero concentration. The experiment was performed using the capillary viscometer at 20.0 °C.....89

Figure 3.13. GC-MS results showing the relative effect of 0.1 M NaCl and 0.1 M KCl on the release of volatile aroma compounds from mucin solutions. Values are expressed as mean \pm SD (n = 3).....90

Figure 3.14. Sedimentation velocity, $g(s)$ and $c(s)$ analyses of HSA showing the sedimentation coefficient distributions of 1.0 mg/ml HSA at different NaCl concentrations (b). Run at 20.0 °C at 40, 000 rpm in PBS buffer (pH 7.0).....92

Figure 3.15. GC-MS results showing the effect of NaCl concentration on the release of aroma compounds in the presence of HSA (1.0 mg/ml). Values are expressed as mean \pm SD (n = 3).....93

Figure 4.1. Sedimentation velocity, $g(s)$ and $c(s)$ analysis for pooled saliva. The plots show the sedimentation coefficient distributions for unstimulated (US) and stimulated (SS) samples. Rotor speed: 40, 000 rpm (120, 000 g), 20.0 °C.....103

Figure 4.2. Relative viscosity showing the quantitative effect of α -amylase added to BSM (1.0 mg/ml) in 0.1M phosphate buffer saline. The polynomial fit is based on 11 data points derived from individual mixtures.....105

Figure 4.3. Sedimentation velocity, $c(s)$ analysis showing the sedimentation coefficient distributions for saliva (blue line), green tea (green) and the result of their interaction (red). Rotor speed: 40, 000 rpm (120, 000 g), 20.0 °C.....106

Figure 4.4. Effect of green tea on the release of aroma compounds from the whole saliva. The dashed green columns express the concentration of

green tea aroma compounds, normalised to one unit, while the red columns represent the headspace concentration of the saliva-tea mixture relative to that of the green tea. The comparison is made by Tukey's post hoc test to calculate the *P*-values ($P < 0.01^{**}$, $P < 0.05^*$). Data is shown as mean \pm SD, (n=3).....108

Figure 4.5. Sedimentation velocity, *g*(s) and *c*(s) analyses showing the sedimentation coefficient distributions for whole US saliva (blue) and what happens upon the addition of epigallocatechin gallate (EGCG) (green). Rotor speed: 40, 000 rpm (120, 000 g), 20.0 °C.....110

Figure 4.6. Sedimentation velocity, *g*(s) distributions for artificial saliva (blue) before and after the addition of 0.5 mg/ml EGCG. Rotor speed: 40, 000 rpm (120, 000 g), 20.0 °C.....111

Figure 4.7. Relative viscosity analysis showing the quantitative effect of EGCG addition to model saliva in 0.1M phosphate buffer saline, pH 7.0..112

Figure 4.8. Principal component analysis bi-plot of aroma release from saliva systems in the presence of model aroma suspension (n=3).....115

Figure 4.9. Principal component analysis bi-plot of aroma release from saliva systems in the presence of orange squash (n=3).....116

Figure 4.10. Relative differences in the release of aroma compounds from α -amylase and mucin solutions in the presence of real (a) and model food (b). The data shown as mean \pm SD, (n=3).....118

Figure 5.1. Results from sedimentation velocity showing the *g*(s) sedimentation coefficient distribution of 0.5 BSM (200 kDa), 0.5 xanthan (200 kDa) and the 1:1 mixture. Run in 0.1 M PBS pH 7.0 at 30, 000 rpm.....130

Figure 5.2. Results from sedimentation velocity showing the *g*(s) sedimentation coefficient distribution of 0.5 BSM (200 kDa), 0.5 pullulan (200 kDa) and the 1:1 mixture. Run in 0.1 M PBS pH 7.0 at 30, 000 rpm.....132

Figure 5.3. Results from sedimentation velocity showing the sedimentation coefficient distribution of 0.5 BSM (200 kDa), 0.2 chitosan

(200 kDa) and their mixture. Run in 0.1 M acetate buffer pH 5 at 30, 000 rpm.....133

Figure 5.4. GC-MS results showing the relative aroma intensity in the headspace from BSM solutions (1 mg/ml) before and after the addition of CMC, pullulan and chitosan. Final polymer concentration was 0.5 mg/ml. Values are expressed as mean \pm SD (n = 3).....133

Figure 5.5. Sedimentation velocity, $c(s)$ analysis, showing the sedimentation coefficient distributions of α -amylase (a), 200 kDa pullulan standard (b), and the result of their interaction (c). Rotor speed: 45, 000 rpm (130, 000 g), 20.0 °C.....137

Figure 5.6. Changes in the apparent z-average hydrodynamic radius of pullulan before and after the addition of HSA (a) and Solomon-Ciuta extrapolations showing the intrinsic viscosity of pullulan upon the addition of HSA (b). DLS size distributions are given as an average of three measurements. Experiments performed at 20.0 °C.....136

Figure 5.7. Results from APCI-MS, conductivity analysis and E-tongue showing the impact of pullulan hydrolysis on the release of flavour, showing the real time data for α -ionone (a), sodium ions (b) and potassium ions (c), respectively. Values are expressed as mean \pm SD (n = 3).....137

Figure 5.8. GC-MS results showing the effect of pullulan hydrolysis on the relative headspace concentration of volatile aroma compounds from in Robinson's orange squash, where 'R' represents the standard squash dilution, 'A1' and 'A2' are increasing α -amylase concentrations of 0.1 and 1.0 mg/ml, and 'P' represents pullulan at a constant concentration of 2.0 mg/ml. Values are expressed as mean \pm SD (n = 3).....139

Figure 5.9. Schematic representation of the chemical modification of pullulan showing the addition of the quaternary amine, glycidyltrimethylammonium (GTMAC) chloride.....140

Figure 5.10. Sedimentation velocity $g(s)$ and $c(s)$ analysis, showing the sedimentation coefficient distributions of GTMAC-pullulan and the result of the interaction with BSM. Rotor speed: 45, 000 rpm (130, 000 g), 20.0 °C.....141

Figure 5.11. Sedimentation velocity $g(s)$ and $c(s)$ analysis, showing the sedimentation coefficient distributions of GTMAC-pullulan and the result of the interaction with HSA. Rotor speed: 45, 000 rpm (130, 000 g), 20.0 °C.....	142
Figure 5.12. Schematic representation of the chemical modification of pullulan showing the addition of the tertiary amine, dimethylaminoethyl (DMAE) chloride (a) and FT-IR spectra of pullulan before after synthesis highlighting the qualitative changes in the spectral intensity correlating to the functional groups (b).....	144
Figure 5.13. Results showing changes in the apparent z-average hydrodynamic radii of DMAE-pullulan, mucin, α -amylase, and the result of their interactions (a), and viscosity results showing the Solomon-Ciuta extrapolation to estimate their intrinsic viscosity $[\eta]$ (b). DLS size distributions are given as an average of three measurements. Performed at 20.0 °C, concentrations were in a 1:1 ratio.....	145
Figure 5.14. Sedimentation velocity, $g(s)$ analysis showing the sedimentation coefficient distributions for DMAE-Pullulan at 0.5 mg/ml (b) and the result of the addition of mucin at 0.5 mg/ml (a) and α -amylase at 0.1 mg/ml (b); and the GC-MS volatile analysis from modified and unmodified pullulan and solutions upon the addition of HSA (d). Rotor speed: 45, 000 rpm (130, 000 g), 20.0 °C.....	146
Figure 6.1. The upper layer of the bovine tongue cut into rectangles prior to treatment with different biopolymer solutions.....	155
Figure 6.2. Environmental scanning electron micrographs of pig gastric mucin (PGM) suspended in 0.1M PBS, pH 7.0 (a), surface alginate bead (b) and the surface of the alginate-mucin bead (c).....	159
Figure 6.3. Apparent zeta potential of solutions containing calcium alginate control beads and mucin beads, showing six replicates.....	160
Figure 6.4. Changes in the weight of control and mucin beads after immersion in different biopolymer formulations for 30 min. Weight change is directly proportional to changes in the hydrated radius of the spheres. Values are expressed as mean \pm SD (n = 3).....	161

Figure 6.5. Sedimentation velocity, $g(s)$ analysis showing the sedimentation coefficient distributions of alginate (2.0 mg/ml) and the result of its interactions with chitosan (1.0 mg/ml) in the presence and absence of 0.01M CaCl_2 . Rotor speed: 40, 000 rpm (120, 000 g), 20.0 °C.....163

Figure 6.6. GC-MS results showing the relative volatile intensity for the mucin beads after immersion in different biopolymer solutions. Volatile aroma compounds are naturally found in the orange squash formulation while the linear aldehydes were additionally added. The comparison is made by Tukey's post hoc test to calculate the P -values ($P < 0.05^*$). Data is shown as mean \pm SD, ($n=3$).....165

Figure 6.7. Conductivity results showing the relative Na^+ and K^+ concentration on the mucin beads after immersion in different biopolymer solutions. Values are determined by subtracting the values of the control beads. Data is shown as mean \pm SD, ($n=3$).....167

Figure 6.8. GC-MS results showing the relative volatile retention on the mucin beads after immersion in different biopolymer solutions. The comparison is made by Tukey's post hoc test to calculate the P -values ($P < 0.05^*$). The data are shown as mean \pm SD, ($n=3$).....169

Figure 7.1. Sedimentation velocity, $g(s)$ analysis showing the sedimentation coefficient distributions of BSM (1.0 mg/ml) and the effect of linear aldehydes (5.0 mg/ml) on this distribution; and (lower) plot of hydrophobicity, $\log P$ against % change in mucin complexation. Rotor speed: 30, 000 rpm (90, 000 g), 20.0 °C.....177

Figure 7.2. Sedimentation velocity, $g(s)$ analysis showing the sedimentation coefficient distributions of BSM (1.0 mg/ml) and the effect of linear ketones (5.0 mg/ml) on this distribution; and (lower) plot of hydrophobicity, $\log P$ against % change in mucin complexation. Rotor speed: 30, 000 rpm (90, 000 g), 20.0 °C.....178

Figure 7.3. SEC-MALS results showing the light scattering (LS) elution profile of BSM, hexanal and the result of their interaction. Insert shows the summary for the hydrodynamic parameters for the main peaks, including

weight average molar mass (M_w) and apparent hydrodynamic radius ($r_{z,app}$).....179

Figure 7.4. Solomon-Ciuta intrinsic viscosity $[\eta]_{sc}$ analysis showing the quantitative effect of hexanal addition to bovine submaxillary mucin (1.0 mg/ml) in 0.1M phosphate buffer saline. The polynomial fit is based on 6 data points derived from separate hexanal/BSM mixtures.....180

Figure 7.5. Sedimentation velocity, $g(s)$ analysis showing the sedimentation coefficient distributions of BSM (0.5-1.0 mg/ml) and the result of its interactions with different phenolic compounds (1 mg/ml). Rotor speed: 30, 000 rpm (90, 000 g), 20.0 °C.....182

Figure 7.6. Raman spectra of BSM ($c= 10$ mg/ml) with and without *p*-cresol (1.0 mg/ml). The mixture was dialysed against a 14 kDa membrane prior to analysis to remove excess *p*-cresol. Performed in 0.1 M PBS pH 7.0 at 20.0 °C.....183

Figure 7.7. Sedimentation velocity, $c(s)$ analysis showing the sedimentation coefficient distributions of HSA (1.0 mg/ml) in 0.1M PBS and the result of its interactions with volatile compounds (10.0 mg/ml). Rotor speed: 40, 000 rpm (100, 000 g), 20.0 °C.....184

Figure 7.8. Results from the E-tongue showing the % change in the intensity of bitterness as a result of α -amylase addition. Experiments performed at 20.0 °C. Values are expressed as mean \pm SD ($n = 3$).....186

Figure 7.9. Sedimentation velocity, $g(s)$ and $c(s)$ analyses showing the sedimentation coefficient distributions of HSA (1.0 mg/ml) and the result of its interactions with quinine hydrochloride (0.2 mg/ml) in 0.1M PBS. Rotor speed: 30, 000 rpm (90, 000 g), 20.0 °C.....187

List of Tables

Table 1.1. The family of mucins (Berry and Corfield, 2014).....	13
Table 1.2. Sugar molecules present within the glycosylated region of mucus glycoproteins (Harding et al., 1999a).....	16
Table 3.1. Summary of AUC, SEC-MALS, DLS and intrinsic viscosity data showing the hydrodynamic properties of BSM in 0.1 M phosphate chloride buffer (pH 7.0) and citrate buffer (pH 3.0).....	79
Table 4.1. Relative viscosity and protein concentrations for pooled unstimulated (US) and stimulated (SS) human saliva. Data shown as mean \pm SD, (n=3).....	104
Table 4.2. Composition of artificial saliva: concentrations of ions and proteins	113
Table 6.1. Titratable acidity (TA) of final orange drinks containing different polymers (error based on \pm 50 μ l 0.1N NaOH).....	16

Table of Contents

Abstract	i
Acknowledgements	iii
Publications	iv
Abbreviations	vi
List of Figures	viii
1. Chapter 1: Introduction	1
1.1. Introduction to Flavour Science	2
1.1.1. Taste and aroma perception	2
1.1.1.1. Taste	2
1.1.1.2. Aroma.....	3
1.1.2. Chemistry of volatile aroma compounds.....	4
1.1.2.1. Aldehydes	5
1.1.2.2. Ketones	6
1.1.2.3. Esters	6
1.1.2.4. Terpenes & terpenoids	7
1.1.2.5. Furans and phenols	7
1.1.2.6. Nitrogen and sulphur containing compounds	8
1.1.3. Flavour industry.....	9
1.2. Introduction to saliva	11
1.2.1. Formation and composition of saliva.....	11
1.2.2. Mucins.....	13
1.2.3. Salivary mucins	17
1.2.4. Salivary α -amylase	18
1.2.4.1. Role.....	18
1.2.4.2. Structure of HSA	19
1.2.5. Flavour bolus interactions	21
1.3. Mucoadhesion	23
1.3.1. Definition	23
1.3.2. Adhesion mechanisms	24
1.3.3. Methods to test mucoadhesion	24
1.3.3.1. Model biomimetic surfaces.....	24
1.3.3.2. Mucoadhesion assays.....	25

1.3.4.	Mucoadhesives	28
1.3.4.1.	Anionic biopolymers.....	28
1.3.4.2.	Cationic biopolymers.....	29
1.3.4.3.	Thiolated biopolymers	30
1.3.4.4.	Non-ionic biopolymers.....	31
1.4.	Hydrodynamic methodology	32
1.4.1.	Analytical Ultracentrifugation (AUC)	32
1.4.1.1.	History	33
1.4.1.2.	Sedimentation velocity (SV) analysis	34
1.4.1.3.	Gross conformation: Wales- van Holde ratio 'R'	37
1.4.1.4.	Generating a sedimentation coefficient distribution	38
1.4.1.5.	Processing methods: g(s) and c(s)	39
1.4.1.6.	Molecular weight distribution: g(s) to f(M) transformation	40
1.4.1.7.	Sedimentation equilibrium (SE) analysis.....	41
1.4.1.9.	Mechanical systems	43
1.4.1.10.	Optical systems	44
1.4.2.	Intrinsic viscosity	45
1.4.2.1.	Theory	45
1.4.2.2.	U-tube viscometry analysis.....	48
1.4.2.3.	Pressure Imbalance Differential Viscometry	49
1.4.3.	Light scattering techniques	49
1.4.3.1.	Dynamic Light Scattering (DLS)	49
1.4.3.2.	Size Exclusion Chromatography: Multi Angle Light Scattering (SEC-MALS)	51
1.4.4.	Analysis of volatile aroma compounds	52
1.4.4.1.	Solid-Phase Micro Extraction coupled with Gas Chromatography–Mass Spectrometry (SPME-GC-MS)	52
1.4.4.2.	Atmospheric Pressure Chemical Ionisation-Mass Spectrometry (APCI-MS)	53
1.4.5.	Differential Refractometry	54
1.4.6.	Vibrational spectroscopy	55
1.5.	Aims of the investigation	56
2.	Chapter 2: Methods	58
2.1.	Sedimentation Velocity (SV).....	58
2.2.	Sedimentation Equilibrium (SE)	59
2.3.	Size Exclusion Chromatography: Multi Angle Light Scattering (SEC-MALS)	60
2.4.	Dynamic Light Scattering (DLS).....	61

2.5.	U-tube capillary (Ostwald) viscometry	61
2.6.	Differential refractometry	62
2.7.	Solid-Phase Micro Extraction coupled with Gas Chromatography– Mass Spectrometry (SPME-GC-MS)	62
2.8.	Atmospheric Pressure Chemical Ionisation Mass Spectrometer (APCI-MS)	63
2.9.	Fourier-transform infrared spectroscopy (FT-IR)	63
2.10.	Raman spectroscopy	64
2.11.	Environmental Scanning Electron Microscopy (ESEM)	64
2.12.	Statistical analysis	64
3.	Chapter 3: Molecular hydrodynamics of bovine submaxillary mucin and salivary α-amylase: effects of salt and pH	65
3.1.	Introduction	65
3.2.	Materials and methods	68
3.2.1.	Samples	68
3.2.2.	Analytical ultracentrifugation (AUC).....	68
3.2.2.1.	Sedimentation velocity (SV)	68
3.2.2.2.	Sedimentation equilibrium (SE).....	68
3.2.3.	SEC-MALS-Viscostar.....	69
3.2.4.	Capillary viscometry	69
3.2.5.	Dynamic Light Scattering (DLS)	69
3.2.6.	Atmospheric Pressure Chemical Ionization-Mass Spectrometry (APCI-MS).....	70
3.2.7.	Gas Chromatography-Mass Spectrometry (GC-MS)	70
3.3.	Results and Discussion	71
3.3.1.	Hydrodynamic characterisation of BSM at neutral pH.....	71
3.3.2.	Effect of low pH on the solution properties of mucin	76
3.3.3.	pH-mucin effects on the release of aroma compounds	80
3.3.4.	pH effects on the release of aroma compounds in the presence of salivary α -amylase	82
3.3.5.	pH-amylase effects on the release of aroma compounds	84
3.3.7.	Salt-mucin effects on the release of aroma compounds.....	87
3.3.8.	Effect of potassium chloride on mucin viscosity	89
3.3.9.	Effect of NaCl ionic strength on human salivary α -amylase .	92
3.3.10.	General Discussion.....	94
3.4.	Conclusion	96

4. Chapter 4: A hydrodynamic study of human saliva. Saliva-food interactions and development of artificial saliva	97
4.1. Introduction	97
4.2. Materials and Methods.....	99
4.2.1. Samples	99
4.2.2. Pooled saliva	100
4.2.3. Green tea	100
4.2.4. Orange squash	101
4.2.5. Sedimentation Velocity (SV).....	101
4.2.6. Differential Refractometer	101
4.2.7. Capillary viscometry	102
4.2.8. Gas Chromatography-Mass Spectrometry (GC-MS)	102
4.3. Results and Discussion	103
4.3.1. Sedimentation fingerprinting of human saliva	103
4.3.2. Saliva interactions with green tea	106
4.3.3. Validating the use of artificial saliva in flavour analysis	113
4.3.4. General Discussion.....	119
4.4. Conclusion	122
5. Chapter 5: Biopolymer mucoadhesives: development of an enzymatically controlled mucoadhesive polymer.....	123
5.1. Introduction	123
5.2. Materials and Methods.....	126
5.2.1. Samples	126
5.2.2. Orange squash	126
5.2.3. Sedimentation Velocity (SV).....	126
5.2.1. Gas Chromatography-Mass Spectrometry (GC-MS)	127
5.2.2. Atmospheric Pressure Chemical Ionization-Mass Spectrometry (APCI-MS).....	127
5.2.3. Dynamic Light Scattering (DLS).....	128
5.2.4. Capillary viscometry	128
5.2.5. INSENT E-tongue.....	128
5.2.6. Conductivity meter analysis	129
5.2.7. Synthesis of dimethylaminoethyl (DMAE) pullulan	129
5.2.8. Fourier-transform infrared spectroscopy (FT-IR)	130
5.3. Results and Discussion	131
5.3.1. Interactions of BSM with polysaccharides.....	131

5.3.2.	Effect of the polysaccharide-mucin interactions on aroma release	134
5.3.3.	The impact of pullulan hydrolysis on flavour release	137
5.3.4.	Developing a cationic pullulan derivative	142
5.3.4.1.	Glycidyltrimethylammonium (GTMAC) synthesis	142
5.3.5.	Interactions with BSM and HSA	147
5.3.6.	General Discussion	149
5.4.	Conclusion	151
6.1.	Introduction	152
6.2.	Materials and Methods	156
6.2.1.	Samples	156
6.2.2.	Mucin beads preparation	156
6.2.3.	Orange drink preparation	157
6.2.4.	<i>Ex-vivo</i> tissue preparation	157
6.2.5.	Retention analysis and weight experiments	158
6.2.6.	Titrateable acidity (TA)	159
6.2.7.	Conductivity meter	159
6.2.1.	Gas Chromatography-Mass Spectrometry (GC-MS)	159
6.2.2.	Dynamic Light Scattering (DLS)	160
6.2.3.	Environmental Scanning Electron Microscopy (ESEM)	160
6.2.4.	Sedimentation Velocity (SV)	160
6.3.	Results and Discussion	161
6.3.1.	Characterization of mucin-alginate beads	161
6.3.2.	Retention of aroma and taste compounds	166
6.3.3.	Comparison to the <i>ex-vivo</i> tongue surface	170
6.3.4.	General Discussion	172
6.4.	Conclusion	173
7.	Chapter 7: Hydrodynamic interactions of mucin and α-amylase with aroma and taste compounds	174
7.1.	Introduction	174
7.2.	Materials and Methods	176
7.2.1.	Samples	176
7.2.2.	Sedimentation Velocity (SV)	176
7.2.3.	Raman spectroscopy	176
7.2.4.	SEC-MALS-Viscostar	177
7.2.5.	E-tongue analysis	177

7.2.6. Capillary viscometry	178
7.3. Results and Discussion	179
7.3.1. Interactions of BSM with aldehydes and ketones.....	179
7.3.2. Interactions of BSM with phenolic compounds	184
7.3.3. Interactions between HSA and aroma compounds.....	186
7.3.5. General Discussion.....	190
7.4. Conclusion	193
8. Chapter 8: Perspectives, Concluding Remarks and Future Work.....	195
8.1. Effect of acidity (pH) and ionic strength (salt)	195
8.1.1. Bovine submaxillary mucin (BSM) characterisation and pH effects	195
8.1.2. Effect of ionic strength.....	197
8.2. Interactions of food and saliva in their native state ...	198
8.3. Development and validation of artificial saliva	200
8.4. Advances in mucoadhesive applications	201
8.4.1. Mucoadhesive biopolymers.....	201
8.4.2. Development of a biomimetic mucus surface	202
8.5. Interactions between salivary proteins and flavour compounds	203
8.6. Future work.....	204
8.7. Conclusion	208
References.....	209

1. Chapter 1: Introduction

Flavour is a term that can be described either objectively, as a sensation arising from the interaction of aroma and taste compounds and mechanical stimuli, or as a subjective experience mediated through the interplay of almost every single human sense. To sensory scientists for instance, flavour is defined as a complex experience that begins before eating, starting with the visual assessment of food and drink, lightness and temperature conditions, sound, and even mood are said to affect our ability to perceive flavour (Smith, 2012). Others, such as those studying food chemistry or physics are not investigating the psychological experiences, but physical measurements of aroma and taste compounds.

Therefore, flavour science is divided between two disciplines: food chemistry and sensory science. The variability of individuals, together with their individual sensitivity thresholds towards acids, sweets, spices or alcohol affects their ability to define flavour in food (Piggott, 2000). As a result, we need to bridge the gap between those who chart the different perceptions of individual tasters and explain how flavour varies as a result of the consumer, to those which say that flavour is solely attributed to the physical and chemical interaction between molecules.

1.1. Introduction to Flavour Science

1.1.1. Taste and aroma perception

1.1.1.1. Taste

One of the first theories of taste perception was proposed almost a century ago by Henning, (1926). He classified taste in terms of a tetrahedron with a triangular base, each corner representing a primary taste, such as sweet, sour, salty and bitter, and any given point in between representing other sub tastes that result from a blend of the primary tastes.

However, more recent models have proposed five or more combinations of fundamental tastes (Breslin and Spector, 2008). One disregarded aspect of Henning's tetrahedron is the non-gustatory aspects of taste. However, these have been discovered with advances in chemistry. For example, savoury (or umami in Japanese) is predominantly evoked by L-glutamic acid, although other peptides have also been found to play a role in savoury taste perception (van den Oord and van Wassenaar, 1997).

In mammals, the gustatory system has evolved in order to identify valuable or dangerous chemicals. For example, carnivorous felines cannot detect sugar as a result of a loss in the sweet receptor gene function (Li et al., 2006). Similarly, alcohol feels sweet to some rodents, who can utilise high ethanol concentrations in fermented grains without being poisoned (Bachmanov et al., 2011). These factors are important to consider when selecting the appropriate model organism for evaluating properties of food and other products.

Most taste receptors are located in the taste buds, which are small papillae structures found on the upper and lateral surfaces of the tongue, as well as in other areas of the oral cavity. They allow parts of the non-volatile taste compounds to come in contact with the receptors, which send signals to the gustatory area of the brain (Chandrashekar et al., 2006).

1.1.1.2. Aroma

While taste is facilitated by the movement of non-volatile food constituents through the bolus and across to the taste buds, the vast majority of food components are odorants, or volatile aroma compounds. These compounds have a tendency to partition into the gas phase, given their very low molecular mass (<300 Daltons) and higher hydrophobicity ($\log P$). Like taste, aroma perception is also mediated by proteins embedded in the membranes of odour receptor cells, located at the rear of the nasal cavity (Firestein, 2001).

Gene sequencing studies indicate the presence of over a thousand similar aroma receptor proteins present in each cell (Menini et al., 1995). However, it is hypothesised that different aroma compounds can bind to the same protein receptor site through competition governed by their chemical structure (e.g. increase in chain length). Binding to the protein receptors generates electric energy, found to generate a cascade of biochemical reactions (Menini et al., 1995). These reactions have been shown to stimulate the production of cyclic adenosine monophosphate (cAMP) and inositol trisphosphate (IP₃), which regulate the opening of sodium and calcium ion channels in the cell membrane. The outcome

provides a quantitative representation of a particular odorant stimulating the receptor cells (Lynch and Barry, 1989).

1.1.2. Chemistry of volatile aroma compounds

The concentrations of aroma compounds present in foods are naturally extremely low (<1 ppm or mg/Kg) (Belitz, Grosch and Schieberle 2009). However, their variation is much greater than for taste compounds, especially in foods that have undergone thermal treatment (e.g. coffee), or fermentation (e.g. cocoa, tea, beer). A total of 7100 compounds have been classified based on their source and chemical class of compounds (Parker et al., 2014). Their odour detection (threshold) is usually over a 100 times lower than that of ethanol (Belitz, Grosch and Schieberle 2009). However, only a limited number of compounds are actually present in foods at concentrations above their odour thresholds, which is the concentration at which a compound can be detected via orthonasal or retronasal olfaction. Such compounds are called key odorants, for example limonene, benzaldehyde, or hexanal. Compounds below the detection level are perceived only if they are artificially added to foods at concentrations above their odour threshold (Grosch, 2001).

The different classes of aroma compounds studied are briefly summarised in the following sections, based on their physical and chemical structures.

1.1.2.1. Aldehydes

Aldehydes are one of the most common compounds present in food, despite having a relatively low odour threshold. The vast majority are linear chained structures starting from ethanal, or acetaldehyde, which is one of the most important commercial compounds (imparting fruity ether like flavour), up to octanal, nonanal, decanal, and even further. Generally, their odour is weaker but more pleasant with an increase in their chain length (higher $\log P$) and molecular weight. An increase in branching can also lower their relative odour but they impart more floral yet subtle fatty notes (Parker et al., 2014).

One important linear aldehyde is hexanal, which imparts a strong freshly cut grass smell, and contributes to the aroma of unripe fruits and vegetables. Hexanal is also formed during thermal treatment of meat, milk or oil. Recent studies have reported a few instances where hexanal and other linear aldehydes are not detected (Kaneko et al., 2011; Kesen, 2013), and this is suggested to arise from irreversibly binding to different protein amino groups.

Branched C5 aldehydes, such as 3-methylbutanal, or isovalaldehyde, imparts malty aroma, essential in many chocolates, teas and other foods that have undergone a thermal treatment (Parker et al., 2014). The relative concentration of 3-methylbutanal, which is a characteristic green tea aroma compound, has been found to increase when in contact with saliva, thus increasing its perception (Dinu et al., 2018a).

The last most important group of aldehydes are cyclic aldehydes, such as benzaldehyde, cinnamaldehyde and vanillin, which are very important commercial ingredients in food and cosmetics, as well as consumer products, and have a pleasant flavour even at excessive concentrations (Parker et al., 2014).

1.1.2.2. Ketones

Ketones have a similar odour and reactivity to aldehydes, though the presence of the carbonyl group, generally at the 2-position (i.e. 2-heptanone, 2-octanone), gives it more subtle aroma. Diacetyl was perhaps the most used ketone due to its pleasant buttery and creamy aroma. However, recent reports found that diacetyl can cause bronchiolitis obliterans (obstruction of bronchioles due to inflammation), if inhaled. As a result, the use of diacetyl has now been banned in a lot of foods and other consumer products in the UK (Allen et al., 2016).

1.1.2.3. Esters

Esters are fruity compounds, fundamental to the aroma of ripe fruit, such as apple and strawberries. Ethyl acetate, ethyl butyrate and ethyl hexanoate are among the most abundant esters, present in virtually every fruity product, although the latter two compounds are also essential compounds in blue cheese and parmesan cheese (Qian and Reineccius, 2003). In addition, the formation of ethyl esters is favoured under higher alcohol concentrations while an increase in chain length favours the

formation of ring esters. These are called lactones and are generally based on a furan or pyran ring, e.g. γ -decalactone, and have much stronger odour (e.g. peach flavour).

1.1.2.4. Terpenes & terpenoids

Terpenes are biosynthesised from basic isoprene units (C_5H_{10}) and are responsible for the characteristic aroma of citrus. One of the most active terpene is limonene, despite its odour threshold being very low (Parker et al., 2014). It is also used as an industrial solvent or in the production of other aroma compounds, such as citral.

The oxygenation of terpenes leads to the formation of terpenoids, such as geraniol, linalool and menthol. The latter is perhaps one of the most familiar, owing to its classic minty aroma and ability to activate the cold-sensing receptors in the oral cavity (Eccles, 1994). Of particular interest is also carvone, due to its ability to exhibit dual aroma characteristics (methol/caraway) depending on its enantiomeric form.

1.1.2.5. Furans and phenols

Furans are indicators of oxidative stability, many of which are formed during thermal processing of foods. They are usually derived from carotenoids and unsaturated lipids and have strong odour thresholds but lack a characteristic note. Common examples are alkyl furans, derived from the oxidation of ω -3 and ω -6 fatty acids, such as 2-ethylfuran and 2-pentylfuran respectively (Parker et al., 2014).

Furans oxidise during Maillard reaction and are called furanones, which have lower odour thresholds. They provide sweet caramel notes, such as 4-Hydroxy-2,5-dimethyl-3(2H)-furanone (HDMF), an important aroma active ingredients in a range of foods, including soft drinks (Buttery and Ling, 1995).

Phenols are very odour active compounds. While they are generally found at extremely low concentrations, they have very strong odours. For example, *p*-cresol is one such compound that imparts smoky, manure like notes. However at low concentrations (ppb), it is an important aroma active compound derived from an intermediate of citral degradation (Parker et al., 2014). It was found that *p*-cresol can interact with the mucus in the oral cavity, and this may help to explain its persistent odour (Dinu et al., 2019a).

1.1.2.6. Nitrogen and sulphur containing compounds

Nitrogen containing compounds are generally found in cooked foods where which produced as a result of the Maillard reaction. Amines are amongst the simplest form of nitrogen containing compounds and usually impart fishy, ammoniac notes. Notable examples are phenylethylamine, 2-methylimino-3-butanone and 2-aminoacetophenone, which are also important in the formation of tortilla chips aroma. One interesting example is methyl anthranilate which has a fruity grape aroma and is used in very high concentrations in confectionery, cosmetics and E-liquids (Tierney et al., 2016).

Linear sulphur containing compounds are an important group of aroma compounds in cooked meat and vegetables, especially in *Brassica* and *Allium* vegetables. More detail can be found at Iranshahi, (2012).

Although this section only covers a small fraction of the thousands of aroma compounds identified, it provides an idea of their chemical diversity. After the arrival of Gas Chromatography Mass Spectrometry (GC-MS) around the 1950s, flavour and fragrance industries have developed exponentially, which significantly reduced the efforts required for the discovery and quantification of aroma compounds in real food systems. This served as a starting point for the extraction and synthesis of nature identical compounds for the use in the food and consumer industries.

1.1.3. Flavour industry

The aroma and fragrance industry has rapidly developed into profitable markets, now serving a large number of retail companies in the food, pharmaceutical, cosmetic and household industries. The total market for flavour and fragrances in 2018 was estimated at £21 billion (Market Research Report, 2019). Up to 60% of the world market is shared between four major companies, such as Givaudan, Firmenich, Symrise and Danisco. These companies spend approximately 10 % of their profits on research and development (Market Research Report, 2019).

With the increased awareness to adopt healthier diets, one particular area that requires constant development of new flavour technologies is low calorie food. According to the World Health Organisation (WHO), 63% of all deaths are due to non-communicable diseases (NCD's) such as

respiratory diseases, cardiovascular diseases, obesity, diabetes, and cancers (WHO, 2011). As a result, increasing efforts are being made to eliminate factors associated with NCD's such as reducing the levels of salt, sugar and fat as well as increasing the levels of dietary fibre in our diet. This led to an increasing amount of pressure on the food industry to develop foods that are lower in salt, sugar and fat. However, consumer acceptance is a major factor and a large number of products fail to deliver consumer satisfaction. This is because many products that have a lower content of salt, sugar and fat have lower organoleptic properties.

Most of the time, fat and sugar are replaced by food polysaccharides, which although are an attractive option in terms of their diverse rheological structure, assisting in the structuring of the product, they reduce the release of aroma and taste compounds. Given the limited time for the compounds to evenly distribute and partition towards the olfactory receptors before food is ingested, the majority of flavour compounds are lost, which has a negative effect on the perception of flavour. Therefore, in order to develop new strategies and improve consumer satisfaction, there is a need to better understand the physical and chemical interactions between food and saliva, which is the first medium encountered by food during oral processing and plays a pivotal role in modulating the release and perception of flavour.

1.2. Introduction to saliva

This section highlights the formation and composition of saliva with emphasis on two major macromolecular constituents, mucin glycoprotein and a major secreted enzyme, salivary α -amylase.

1.2.1. Formation and composition of saliva

Saliva the most abundant secretion, present in the mouth at all times. It is composed of 99% water, with the remaining 1% being made up of proteins and minerals (including sodium and potassium chloride, bicarbonates, calcium and magnesium). A very small fraction also consists of glucose and ammonia (Humphrey and Williamson, 2001).

Saliva is mainly produced by three major salivary glands: parotid, submandibular (or submaxillary) and sublingual. All secretions from the salivary glands are initiated in response to external stimuli, such as food. These changes occur by neurotransmitter stimulation upon the innervation of the sympathetic and parasympathetic nerves (Khutoryanskiy, 2014).

It is considered that sympathetic nerve stimulation leads to the production of salivary proteins, while stimulation of the latter results in the secretion of salivary fluid by the stimulation of K^+ and Cl^- channels. At rest, saliva is predominantly composed of the thicker submaxillary secretions of mucus, while food stimulates the parotid in order to secrete enzymes and other low molecular weight proteins (Schneyer and Levin, 1955).

A smaller amount of salivary secretions also occurs via minor secretory mechanisms present on soft oral tissues. These secretions are regulated

by the VII cranial nerve and are responsible for the production of secretory immunoglobulins and other soluble mucins (Redman, 2012; Salih et al., 2010). These glycoproteins have a significant contribution to the maintenance of oral health and normal structuring of the saliva.

Over a thousand proteins have now been identified in the salivary proteome (Denny et al., 2008). These are widely categorised into six classes: salivary mucins (derived from MUC7 and MUC5B genes), salivary α -amylases, statherins, histatins, cystatins and proline-rich proteins (PRP's). Other significant proportions includes salivary immunoglobulin A (SIgA), DNA (from blood and bacterial cells), carbonic anhydrase, serum albumin, lactoferrin and lactoperoxidase (Khutoryanskiy, 2014).

Stimulation of the salivary glands leads to the formation of the salivary film (Yakubov et al., 2014). These salivary mixtures of mucins and other macromolecules are in a continuous self-assembly process which helps to lubricate to the oral cavity. To some extent, all classes of salivary glands can produce the same type of protein, although the parotid is the major secretor of salivary enzymes i.e. α -amylase, while submaxillary glands are the major producers of soluble mucins (MUC7 derived) (Yakubov et al., 2014). During food stimulation, the parotid is the quickest to secrete enzymes and other small proteins, which subsequently lowers the viscosity of the saliva and facilitates bolus formation in order to support swallowing (Proctor and Carpenter, 2014; Sas and Dawes, 1997). Due to their high relative abundance in saliva, submaxillary mucin and salivary α -amylase are investigated in the current work.

1.2.2. Mucin glycoproteins

Table 1.1. The family of mucins (Berry and Corfield, 2014).

Human Mucins	
<i>Secreted-gel forming</i>	<i>Membrane associated</i>
MUC2	MUC1*
MUC5AC	MUC3A/B
MUC5B*	MUC4
MUC6	MUC12
MUC19	MUC13
	MUC15
<i>Secreted-non gel forming</i>	MUC16
MUC7*	MUC17
MUC8	MUC20
MUC9	MUC21
	MUC22

* Mucins present in the oral cavity.

Mucins are amongst the first macromolecules to be recognized as glycoproteins, being made up of both carbohydrate and protein fractions (Roussel et al., 1988). They appear on mucosal surfaces on almost every part of the body, including the skin, oral cavity, respiratory, digestive, and

urogenital systems (Lang et al., 2007; Perez-Vilar and Hill, 1999). They vary considerably in size, from a few thousand to several million Daltons. The protein domains are rich in threonine and serine which form a bridge between their hydroxyl groups and the N-acetylgalactosamine residues of the carbohydrate region. The carbohydrate fraction can account for up to 90% of the entire molecular weight of the mucin (Steen et al., 1998), although for submaxillary mucins it is lower, about 60% (Tsuji and Osawa, 1986).

Mucins exist in two forms, secreted and membrane-bound. Roussel, *et al.*, (1998) was the first to identify four secretory mucin genes such as, MUC2, MUC5AC, MUC5B, and MUC7 and two membrane-bound mucins, MUC1 and MUC4. Along with the other types of mucins, they are now classified into three categories (Table 1.1.).

Reaching an agreement on their structure and molecular weight was difficult due to their diversity, formation of aggregates, as well as difficulties encountered during purification and solubilisation. Creeth and Denborough, (1970) have been amongst the first to purify mucins by density gradient centrifugation with caesium salts. Other procedures have also been described for example by: Carlstedt et al., (1985) and Sheffner, (1963).

Initial representations such as the "windmill" model were among the first to be described for pig gastric mucin (Allen, 1983). The "windmill" model used to represent mucins as having four heavily glycosylated subunits linked centrally by disulphide bonds. This model was subsequently replaced by three other models such as the "Swollen coil array", "Lectin"

and the "Linear Random Coil" models, all showing some structural similarities by revealing long regions of heavily glycosylated carbohydrate joined together by cysteine rich protein regions (Harding, 1989; Sheehan et al., 1986). Generally, their solution structure is approximated by a random coil model, consisting of linear but glycosylated polypeptide chains linked together by 'naked' disulphide rich protein regions (Figure 1.1).

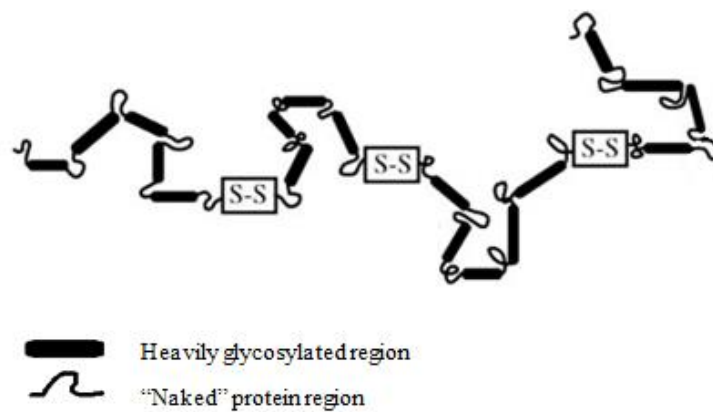
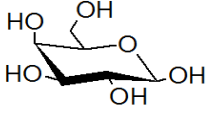
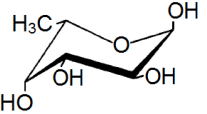
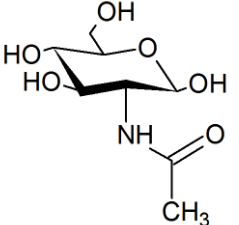
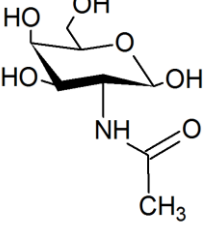
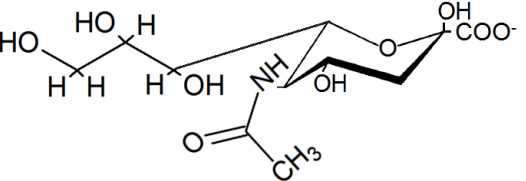


Figure 1.1. Schematic representation of the random coil model (adapted from Sheehan, et al., 1986).

Protein sequencing studies have confirmed that 'naked' regions assist in the coiling of the glycoprotein (Harding et al., 1983a, 1983b). It was found that the O-linked oligosaccharide region can contain up to five different monosaccharids: sialic acid, D-galactose, L-fucose, N-acetylglucosamine and N-acetylgalactosamine (Table 1.2.).

Table 1.2. Structure of sugar molecules present within the glycosylated region of mucus glycoproteins (Harding et al., 1999a).

Monosaccharides present in human mucins	
Galactose	
Fucose	
N-acetylglucosamine	
N-acetylgalactosamine	
Sialic acid	

Mucins have a net negative charge (with an isoelectric point pI , between 2-3) depending on the concentration of sialic acids, found at the end of the carbohydrate chains, but also sulphated proteins along the backbone (Lee et al., 2005; Perez-Vilar and Hill, 1999).

Studies have shown that mucins undergo structural changes favoured by a range of factors including pH and ionic strength. For instance, it was reported that, at higher or neutral pH, their conformation is maintained by the repulsive electrostatic interactions between negatively charged sialic acid groups (Bansil and Turner, 2006a). However, at lower pH the molecules contract and increase in their hydrophobicity, favouring the transition from sol to gel which encourages mucin-mucin interactions and aggregation (Celli et al., 2007; Dinu et al., 2019a). Due to their negatively charged configuration, electrostatic interactions with polycationic biopolymers have been studied for their use as mucoadhesive polymers (Fiebrig et al., 1995a; Harding et al., 1999a).

1.2.3. Salivary mucins

MUC5B and MUC7 were the first salivary mucin gene types to be characterised, also named MG1 and MG2, respectively. Electrophoresis experiments by SDS-PAGE (sodium dodecyl sulfate–polyacrylamide gel electrophoresis) characterised MUC5B types as high molecular weight (>1MDa), while MUC7 types consist of low molecular weight mucins (<300kDa) (Takehara et al., 2013). The structures of the two types of salivary mucins differs considerably. It was found that MUC5B type contains over 5000 amino-acid residues with an overall tri-block structure, similar to early described models. The N termini contains von Willebrand factor type D-domains (vWf), which have a high cysteine content and other charged amino acids responsible for the ability of mucins to gel.

By contrast, MUC7 type mucins are much shorter in length and do not contain vWf domains (Bansil and Turner, 2006a). As a result of lacking these regions, MUC7 type mucins cannot form gels. Differences between macromolecular assemblies of MUC7 and the MUC5B mucin types are important as they could provide valuable information for developing formulations with a certain degree of specificity for one type or the other. However, since human mucin fractions are difficult to obtain in any useful quantities, bovine submaxillary mucin (BSM) is used in the current study. Experiments on bovine submaxillary mucin were amongst the first to be carried to investigate mucin's complex structural assembly (Gottschalk, 1960; Payza et al., 1970). It appears that its glycosylated region makes up to 60 % of the total mass, abundant in sialic acids and N-acetyl galactosamines, similar to the human MUC7 type (Tsuji and Osawa, 1986). In depth analysis of BSM have been reviewed by (Chai et al., 1992; Payza et al., 1970).

1.2.4. Salivary α -amylase

1.2.4.1. Role

Human salivary α -amylase (HSA), is instantly secreted by the parotid upon the stimulation of the acinar cells in the salivary glands. It was found to increase in concentrations up to 7.5 mg/ml, making it one of the most abundant macromolecules in human saliva (Mandel et al., 2010; Zakowski and Bruns, 1985). HSA is a starch digesting enzyme, which initiates the first step in the digestion of food, before being deactivated by the low pH conditions of the stomach (Yakubov et al., 2014). However, it has recently

been shown that HSA may also play a major role in the stomach digestion, as the inside of the food bolus can remain neutral for up to 30 minutes, depending on the food (Bornhorst and Singh, 2013).

It is not so well understood but it is hypothesized that the levels of HSA and its activity may be related to flavour perception, especially in starchy foods. This is because of the specificity of the enzyme for starch and other dextrans. The relationship between decreased bolus viscosity and enhanced flavour perception has received much attention in the past few decades (Cook et al., 2003; Ferry et al., 2004; Vaisey et al., 1969; Walker and Prescott, 2000). This is because stimulation of HSA by starch is linked to a rapid decrease in the physical properties, including a rapid reduction in bolus viscosity. This has been linked to an enhanced flavour perception through a range of cross modal interactions initiating an increased rate of the partitioning of taste and aroma molecules to the olfactory receptors.

1.2.4.2. Structure of HSA

HSA is present as two isoenzymes, both consisting of 496 amino acids. However, one is glycosylated, with an apparent weight average molecular weight of 62 kDa, and the other is a non-glycosylated isoform with a molecular weight of 56 kDa (Bank et al., 1991). Although it was found to form dimers in solutions, HSA functions as a monomer, which catalyses the hydrolysis of α -1,4-glucosidic linkages (Fisher et al., 2006).

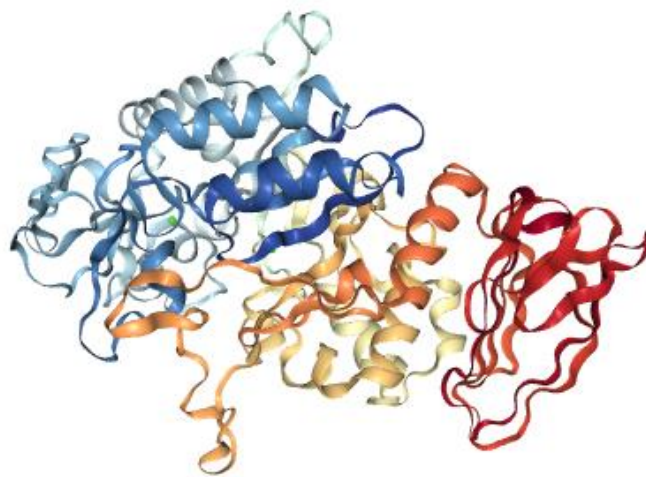


Figure 1.2. Domain organisation of human salivary α -amylase monomer. Domain A is shown in orange, domain B in blue and Domain C in red. Obtained from RCSB PDB (file 1SMD).

The monomer is made up of three domains: *A*, *B* and *C* (Figure 1.2.). Domain *A* is the largest (residues 1-99 and 169-404) and adopts the most common enzyme assemblies, as given by the $(\beta/\alpha)_8$ barrel structure containing the catalytic site, while the *B* and *C* domains are mainly composed of β -strands (MacGregor et al., 2001).

The catalytic site consists of three amino acids, Asp197, Glu233 and Asp300. The Cl^- binding site is in close proximity and is mediated by Arg195, Asn298 and Arg337 while the Ca^{2+} binding site is mediated by His201 of domain *A* and Asn100, Arg158 and Asp167 of domain *B* (MacGregor et al., 2001).

1.2.5. Flavour bolus interactions

It is hypothesised that the surface of the salivary glycoproteins is involved in a range of interactions with food components during oral processing. The transport and release of flavour compounds to the olfactory receptors in the mouth and nose is firstly influenced by the type of food matrix (i.e. solid or liquid), secondly, by interactions with saliva (Taylor, 2002).

Oral processing begins with chewing, followed by the secretion of salivary proteins which facilitate lubrication, digestion and bolus formation. As a result, most of the flavour perceived is a result of bolus and not solely as a function of the food product, which loses its mechanical and chemical properties during mastication.

During oral processing, aroma and taste compounds interact with various components of the bolus, thus limiting their ability to be available for perception. The nature of these interactions are generally classified in to three types (Taylor, 1999): i) direct binding or retention of flavour compounds by food/salivary proteins, ii) partitioning into difference phases such as air, water or lipid, as a function of their hydrophobicity ($\log P$) and iii) viscosity effects (higher viscosity slowing down the rate of release).

Protein binding is the most frequently reported interaction (Guo et al., 2019; Jouenne and Crouzet, 2000; Landy et al., 1995; Zhou et al., 2014). Binding can either be reversible or irreversible depending on the strength of the interaction. For example, aldehydes are known to covalently bind to protein amino groups (Weerawatanakorn et al., 2015), forming Schiff base products or imines while other compounds are suggested to form hydrogen

bonds with food and saliva macromolecules containing nitrogen, sulphur or only oxygen.

For carbohydrates, starch was the most studied for its ability to interact with aroma and taste compounds, and also for its inclusion complexes forming from proposed helical structures in solution (Solms, 1986). The presence of mono and disaccharides has been primarily associated with salting out effects which can actually be very effective carrier mechanisms for the release of flavour (McGorin et al., 1996).

Other than starch, the vast majority of hydrocolloid thickeners (i.e. xanthan, cellulose, alginate, pectin) are generally considered to decrease the release of flavour depending on their concentration (Decourcelle et al., 2004; McGorin et al., 1996). However, research is currently being undertaken in order to improve the functionality of polysaccharides in food and health products.

1.3. Mucoadhesion

Polymer mucoadhesion is proposed to enhance the bioavailability of flavour in food, whereby the use of appropriate polymers, adhesive towards the oral mucosal surface, would aid in reducing some of the negative effects associated with the rapid ingestion.

1.3.1. Definition

Mucoadhesion is described as the ability of biomaterials, such as the matrix of a drug carrier, to adhere to the surface of mucosal membranes by means of interfacial forces of attraction, in order to control the retention time and increase the bioavailability of target molecules. Mucoadhesives are usually tailored for specific tissues in order to increase the bioactive loading concentration at the site of adhesion (Gu et al., 1988; Khutoryanskiy, 2011).

Natural polysaccharides are an attractive option, especially for the food industry, as they are generally non-toxic and offer a good loading ability. Examples include chitosan and also cellulose derivatives such as carboxymethyl cellulose (CMC), although new materials are constantly being developed. Most of them are hydrophilic, and have some hydrogen bond accepting groups i.e. hydroxyl, amine or carboxyl groups (Harding et al., 1999a; Lee et al., 2000; Smart, 2005).

1.3.2. Adhesion mechanisms

In chemical terms, the adhesion between two molecules must involve one of the following bonds: covalent, ionic or hydrogen bonds. Hydrophobic interactions and van de Waals forces may also play a role, though these are often too weak and reversible interactions. Currently, there are six theories describing the potential mechanisms involved in mucoadhesion: wetting theory, fracture theory, electronic theory, adsorption theory, the mechanical theory and the diffusion theory (Mathiowitz and Chickering, 1999; Smart, 2005). Perhaps it is a combination of each of them that defines the process of mucoadhesion.

1.3.3. Methods to test mucoadhesion

1.3.3.1. Model biomimetic surfaces

There are a number of ways of assessing mucoadhesion, although they depend on the state of the mucus surface. The most representative are applications based on real mucosal tissues, such as fresh intestine or fresh tongue, sustainably sourced from local slaughter houses (Fransén et al., 2008; Grabovac et al., 2005a; Lehr et al., 1990a). However, there are severe limitations with this approach such as short life tissue stability, variability within each animal and bacterial cross contamination. In addition, freezing and storing of animal tissues can result in mechanical and functional loss of the mucosa. Therefore, numerous studies aim to develop alternative *in vitro* biomimetic to mucosal surfaces (Khutoryanskiy, 2011, 2014).

A complex example includes the development of mammalian epithelial cell lines, grown on a collagen membrane, such that the surface rheology resembles that of fresh mucus (Kavvada et al., 2005a; Keely et al., 2005a; Sugiyama et al., 1993a; Takahashi et al., 2004a). However, the duration, cost and yield of the final product limits its potential use in industry.

The standard approach is to use commercially available purified mucin powders, isolated from the bovine saliva or porcine gut. They are available at reduced cost and enable the development of a wide range of models, from aqueous solutions, partially hydrated films, or compressed onto polymer membranes (Fiebrig et al., 1995a; Jacques and Buri, 1997; Jones et al., 2009a; Venter et al., 2006a).

Other studies drifted away from the traditional mucus/mucin based systems and developed analogues exclusively from polysaccharides and synthetic polymers. For example, cellulose and locust bean gum gels were used to mimic the rheological and adhesive properties of biological mucus, while some used entirely synthetic polymers (Hasan et al., 2010; Hall et al., 2011).

1.3.3.2. Mucoadhesion assays

Irrespective of the model surface, there are a number of techniques that have been employed in measuring the strength of adhesion. Tensile studies are commonly employed in analysing the detachment force of a candidate mucoadhesive from a solid or semi-solid mucus surface. Variations of this method depend on the sample conditions such as hydration, humidity and temperature (Silva et al., 2012).

Shear assays have been applied to study the changes in the rheology of mucus surface under different treatments. Rotating disc measurements were employed in the analysis of mucoadhesive properties of solids (Bernkop-Schnürch, 2005). This method allows the estimation of the time of disintegration of a dosage form onto a mucosal tissue under dynamic conditions.

Flow assays are used for liquid or semi-solid materials where the ability of a polymer to remain bound to the mucus surface is monitored under continuous flow (Rao and Buri, 1989). In this case, the percentage of target particles that are retained on the mucus surface after washing is quantified as a measure of bioadhesion. A similar wash test is employed in the evaluation of the relative amount of flavour compounds bound a mucus like surface (Dinu et al., 2019b).

For most dilute systems however, viscosity is the method of choice for evaluating the interactions between mucin and polymers (Yakubov et al., 2014). It offers a rapid and convenient means of analysis by studying the flow behaviour of the interactive system. In this case, the mixture is expected to have a higher viscosity than the sum of the viscosities of the mucin and a specific polymer, independently.

Changes in viscosity are governed by physical and chemical interactions, including hydrogen bonding, electrostatic interactions, chain entanglements and covalent bonds (Hassan and Gallo, 1990). Viscosity assays were used to test a wide range of synthetic and natural polymers, including pectin, alginate, carboxymethyl cellulose, thiolated polymers, carrageenan, chitosan and acrylic polymers (Khutoryanskiy, 2014).

Although not very sensitive, turbidity analysis was also used to provide some information, though only for very strong interactions, for instance, with polycations such as chitosan and other cationic polymers. For such systems, an increase in complexation is accompanied by an increase in the turbidity of the solution (Rodriguez et al., 2003; Sogias et al., 2008).

Other studies have employed dynamic light scattering (DLS) and zeta-potential measurements to characterise changes in the size and the surface charge of the system. This is mainly valid for electrostatic interactions, for instance the addition of chitosan was shown to increase the zeta-potential from negative to positive values. By contrast, the addition of anionic polymers resulted in a reduction in zeta potential. The addition of polymers which have similar electrostatic properties to that of mucins, such as hydroxypropylmethylcellulose (HPMC) showed no changes in the zeta-potential (Shen et al., 2009; Takeuchi et al., 2005).

Other molecular hydrodynamic techniques such as analytical ultracentrifugation (AUC) were extensively used in the analysis of mucoadhesion. Changes in the molecular weight and sedimentation coefficient are directly related to the formation of new complexes between the mucin glycoproteins and the polymers. For instance, the sedimentation coefficient distribution ratio of the mucin/polymer complex to that of the mucin ($S_{\text{complex}}/S_{\text{mucin}}$) can be employed as a direct measure of mucoadhesion (Anderson et al., 1989; Deacon et al., 2000; Harding, 2006a; Harding et al., 1999a).

With the arrival of modern spectroscopic techniques and electron microscopy, including Fourier Transformed infrared (FTIR) spectroscopy, Nuclear Magnetic Resonance (NMR) and Atomic force microscopy (AFM) additional ways of evaluating mucus-polymer interactions were enabled (Ducker et al., 1991; Mortazavi, 1995; Patel et al., 2003).

1.3.4. Mucoadhesives

In terms of the chemistry, for a biopolymer to be mucoadhesive it needs to have strong hydrogen donor groups, i.e. amino, hydroxyl, sulphate, or/and carbonyl groups. A good mucoadhesive must have a good loading capacity, therefore higher molecular weight polymers are usually employed. Commonly used polysaccharides are: alginates, chitosan, pectin, dextran, cellulose and derivatives, xanthan, carrageenan and starch. In depth structural analyses can be found in Harding et al., (2016).

1.3.4.1. Anionic biopolymers

Anionic biopolymers such as CMC, sodium alginate and pectin have recently been reported to be mucoadhesive due to their ability to form hydrogen bonds at their carboxylic acid groups. CMC appeared to be a good candidate for oral delivery, largely due to its high range of molecular weights, of up to 4×10^6 g/mol, but also because it is odourless, tasteless and forms transparent solutions (Stelzer and Klug, 1980). The polymer is soluble both in cold and hot water, and can change conformation depending on the pH, ionic strength and concentration. It was also shown

that at low ionic strength and high pH the polymer chains form extended and form stiffer structures, which favour mucoadhesion (Cook et al., 2015a). However, most of the food is acidic and this may limit its adhesive properties. Similarly, a high ionic strength can further reduce a polymers ability to interact with mucin.

As a result of their negatively charged overall configuration, anionic food biopolymers like hydroxypropylmethyl cellulose (HPMC), carboxymethyl cellulose (CMC), pectin, alginate, guar, carrageenan and xanthan, cannot chemically interact with mucins (Fiebrig et al., 1995a; Harding et al., 1999a). While these hydrocolloids can physically interact with mucins to define the composition and rheology of the bolus, they lack the molecular ability to form direct complexes with mucin in solution. Yet, some anionic polysaccharides are still considered mucoadhesive because they have been shown to modify the retention time and release kinetics of target compounds, as a result of the physical and chemical properties of the food thickener i.e. high viscosity, gelation (Khutoryanskiy, 2011). Therefore, while they may have a good loading ability, their ability to effectively release the functional compounds remains debatable.

1.3.4.2. Cationic biopolymers

Polycations such as chitosan (pKa \sim 5.5-7), have extensively been studied for their ability to form strong electrostatic interactions with mucins (Anderson et al., 1989; Chen et al., 2009; Fiebrig et al., 1995a; Harding, 2006a; Pedro et al., 2009). Some authors also highlighted a significant

contribution from hydrogen bonds and hydrophobic interactions (Deacon et al., 2000; Khutoryanskiy, 2011).

While chitosan is found useful in many mucoadhesive applications targeted at the gastro-intestinal region, its application in the oral cavity is restricted. This is because chitosan is so strongly charged that it can precipitate any proteins present in the saliva and cause an unpleasant and astringent mouthfeel, thereby negatively modifying the organoleptic properties of food (Fiebrig et al., 1995a and Cook et al., 2018a). In food and oral applications, the mucoadhesive needs to be tasteless, non-toxic and also milder, but which has a good loading capacity. However, it must also be able to unload the flavour before ingestion (via retronasal olfaction).

Diethylaminoethyl-dextran or DEAE-Dextran, is an example of a cationic mucoadhesive that was shown to interact with mucin (Anderson et al., 1989). However, its mucoadhesive properties were too weak considering the high charge density of the modified polymer. It is suggested that the $\alpha(1-3)$ branches of dextran and the ethyl groups limit the access of the amino group to the sialic acid groups of mucin, due to steric hindrance.

1.3.4.3. Thiolated biopolymers

Thiomers or thiolated polymers are other examples of more recent developments in mucoadhesive formulations. They are synthesised by coupling thiol containing functional groups (SH), capable of forming hydrogen bonds with the sulphate rich regions in mucin (Cook et al., 2015). However, the use of sulphur containing polymers is limited in flavour applications.

1.3.4.4. *Non-ionic biopolymers*

Last but not least, non-ionic neutral polymers, such as dextran, pullulan, guar and schizophyllan, appear to have very poor mucoadhesive characteristics (Nafee et al., 2004). However, it is hypothesised that pullulan may be further tailored to modulate the release of flavour due to its similarity to starch, which are broken down by salivary α -amylase. As a result, potential cationic derivatisation of pullulan is currently suggested to combat some of the issues associated with the rapid ingestion.

1.4. Hydrodynamic methodology

The hydrodynamic techniques used in this investigation include Analytical Ultracentrifugation, Viscometry, Dynamic Light Scattering (DLS), Densitometry, and Size Exclusion Chromatography coupled to Multi Angle Laser Light Scattering (SEC-MALS). The concentrations of volatile aroma compounds released into the headspace were assessed by Solid Phase Microextraction- Gas Chromatography Mass-Spectrometry (SPME-GS-MS), and the real time analysis was monitored by the Atmospheric Pressure Chemical Ionisation Mass Spectrometer (APCI-MS).

1.4.1. Analytical Ultracentrifugation (AUC)

Analytical Ultracentrifugation is a versatile tool in the characterization of proteins, glycans, DNA and molecular interactions along with other state of the art protein characterization capabilities, such as size exclusion chromatography (SEC), Nuclear Magnetic Resonance (NMR), electron microscopy (EM) and light scattering. AUC is especially employed in the analysis of macromolecules and the result of their interactions in biological solute systems, in dilute or in concentrated states (Eisenberg, 2003; Harding, 1994; Schachman, 1989). This is because the technique does not require standards for the molecular weight identification, molecular fixation, separation media or any other matrix interaction material.

The technique relies on the separation of molecules due to a high centrifugal force, in which the separating molecules are monitored by optical detection systems. Generally, molecules separate on the basis of their molecular mass, with heavier molecules sedimenting faster than

smaller and lighter molecules of the same species. However, this is not true for particles of different species (Schuck, 2013). This is because particle shape, flexibility and hydration are also major contributors to molecular separation. For example, small globular proteins sediment faster than elongated or branched polysaccharides of the same molar mass.

1.4.1.1. History

AUC was first established by Theodore Svedberg, who won the Nobel Prize in 1926 for his work on colloidal disperse protein systems. From his AUC studies, he discovered that protein solutions have well-defined molecular weight but with multi-unit associations. This led to the concepts of tertiary and quaternary protein structures, using initially sedimentation equilibrium (SE). But since then, advancements in centrifugation speeds led to the development of Sedimentation Velocity (SV), which worked as a validation technique for confirming the presence of single or multiple components (Correia and Stafford, 2015).

SV experiments became a primary method for investigating the behaviour of readily available proteins (e.g. eggs or blood), and played a major role in characterizing the purity of large scale protein fractionation products from the biopharma industries (Svedberg and Nichols, 1926). With the arrival of the Spinco Model E analytical ultracentrifuge in the 1950's, the Rayleigh interference and the photoelectric scanning absorbance systems used today have arrived (Richards and Schachman, 1959). This led to extensive development in data analysis that could generate a continuous sedimentation coefficient distribution (Baldwin, 1954), which led to the

discovery of 80S yeast ribosomes and the relationship between the 30S and 50S subunits of the 70S ribosomes (Tissières and Watson, 1958). In addition, SV was used to characterize supercoiling in DNA, and conformational assemblies of numerous enzymes and proteins (Correia and Stafford, 2015).

1.4.1.2. *Sedimentation velocity (SV) analysis*

Modern SV is used for analysing purity, state of association, conformation and interactions (Dam and Schuck, 2003a, 2004a). Experiments require high centrifugation speeds, enough to sediment the concentration boundary formed during sedimentation. Multiple scans are taken along the cell pathlength, and correlated to concentration, viscosity and density of the sample. The Svedberg equation is used to derive sedimentation coefficients:

$$s = \frac{v}{\omega^2 r} = \frac{M(1-\bar{v}\rho_0)}{N_A f} \quad (1.4.1)$$

where (s) is the sedimentation coefficient (10^{-13} sec), (v) is the boundary terminal velocity, $\omega^2 r$ is the angular acceleration, (M) is the molar mass, (\bar{v}) is the partial specific volume, (ρ_0) is the solvent density, (N_A) is Avogadro's constant and (f) is the friction coefficient. The Svedberg equation, together with the Stokes-Einstein equation, combine to define all the forces involved during an SV experiment such as:

$$s = \frac{M(1-\bar{v}\rho_0)}{N_A f} \quad (1.4.2)$$

$$f = \frac{k_B T}{D} \quad (1.4.3)$$

$$s = \frac{M(1-\bar{v}\rho_0)D}{N_A k_B T} = \frac{M(1-\bar{v}\rho_0)D}{RT} \quad (1.4.4)$$

where (k_B) is Boltzmann constant, (T) is temperature in degree Kelvin and (R) is the gas constant, the combination of N_A and k_B .

In more simple terms, an SV experiment involves three main forces. The powerful sedimentation force, F_s (away from the centre of rotation) created by the high centrifugal field is counteracted by the two back-diffusion forces of a particle such as, the friction force, F_f (towards the centre) and the buoyancy force, F_b (Figure 1.3.). The buoyancy force depends on the properties of the macromolecule (solubility, hydrophobicity), for instance, proteins/polysaccharides tend to move away from the centre of rotation, while hydrophobic compounds, such as some volatile aroma compounds, have a buoyant force towards the centre of rotation (Figure 1.3.).

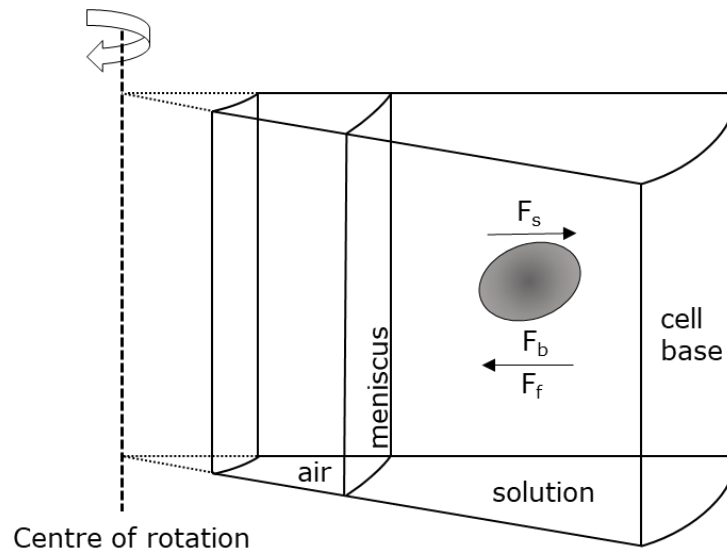


Figure 1.3. Schematic representation of the main forces involved in the sedimentation process in the solution channel (adapted from van Holde, 1971).

As long as the sedimenting force is larger than the diffusion forces, the particles will sediment. Apart from high centrifugation speeds, the rate at which molecules sediment highly depends on the frictional force, F_f , which depends on the overall shape and size of the particle.

For particles larger than water molecules, asymmetry, hydration and charge particles give rise to a phenomenon known as hydrodynamic non-ideality, which is a major contributor in determining the true sedimentation coefficient and molecular weight of a sample, especially for polydisperse particles. Size, asymmetry and hydration contribute to their exclusion volume which along charge and viscosity contribute to hydrodynamic non-ideality effects, which increase with concentration. Therefore, an extrapolation of sedimentation coefficients to zero concentration is required to determine the true weight average sedimentation coefficient

$s_{20,w}^{\circ}$, in Svedberg units S (10^{-13} seconds), where $(s_{20,w})$ denotes the conversion to standard solvent conditions, namely the density and viscosity of water at 20.0 °C, while the (s°) represents the extrapolation to infinite dilution. In this study, uncorrected values are termed 'apparent'. For mixtures and polydisperse systems, non-ideality and viscosity effects have a greater effect on faster, larger components. In this case, the sedimentation can give rise to an apparent monodispersity, since faster molecules are slowed down- for example in mucins, which contain a large distribution of macromolecular components, the larger fractions sediment faster and encounter a region of higher concentration of smaller and slower sedimenting species. As larger species sediment, there is less self-exclusion, therefore smaller species now sediment faster. This phenomenon is giving rise to peak sharpening and underestimates of polydispersity (as in Dhimi et al., 1995).

1.4.1.3. *Gross conformation: Wales- van Holde ratio 'R'*

The extrapolation of the reciprocal of the sedimentation coefficient is a very useful way to obtain information on particle conformation, using the Gralén coefficient (k_s), which is derived from the slope of the extrapolated linear fit multiplied by the weighted average sedimentation coefficient $s_{20,w}^{\circ}$ (Gralén, 1944). Dividing the Gralén coefficient (k_s), by the intrinsic viscosity $[\eta]$, gives the Wales- van Holde ratio 'R', which is used to distinguish between overall shapes of particles (Wales and Holde, 1954). However, theoretical values are limited to a maximum value of $k_s/[\eta]$, of

1.6 for perfect spheres and random coils, with lower values close to 0.1, representing more extended conformations.

1.4.1.4. *Generating a sedimentation coefficient distribution*

Monodisperse systems, under ideal conditions can be directly calculated from knowing the radial distance of the concentration boundary. However, modern analysis of polydisperse systems is based on the Lamm equation (Lamm, 1920), which also takes into consideration the shape of the boundary formed at a given time during sedimentation. Computer algorithms use the Lamm equation to analyse data by iteratively fitting three-dimensional such as:

$$\frac{dc}{dt} = D \left[\left(\frac{d^2c}{dr^2} + \frac{1}{r} \left(\frac{dc}{dr} \right) \right) \right] - s\omega^2 \left[r \left(\frac{dc}{dr} \right) + 2c \right] \quad (1.4.5)$$

where (r) is the radial position of the meniscus, time is (t), and concentration is (c). There are two major packages that can automatically fit the Lamm equation: SEDFIT (Schuck, 2000), which uses the host computer, and UltraScan (Scott et al., 2005), which uses cloud computing (internet). Although UltraScan requires an internet connection, some groups found it to be more useful in analysing heterogeneous particles of different partial specific volumes, \bar{v} . In this work, SEDFIT v14 or later, was used for analysis. The only downsides of SEDFIT is the difficulty to correct for the diffusion of large polydisperse systems.

1.4.1.5. Processing methods: $g(s)$ and $c(s)$

There are two main procedures used to analyse sedimentation velocity data, the $g(s)$ or the $ls-g^*(s)$ (least square Gaussian fit of sedimentation coefficient distribution) against s , and the $c(s)$ method (Schuck, 2000; Schuck and Rossmanith, 2000). Both methods rely on superimposing a discrete model of the raw data by producing fitted data. The fitted data is manually corrected for noise such as TI (Time Invariant) and RI (Radial Invariant). TI noise is removed by searching for patterns which do not change during the run, while RI represents artefacts of Fourier Transform.

The fitted data derived from the two methods of analysis are plotted against the sedimentation coefficient and are normalised to one standard deviation (0.683) for $g(s)$ or two standard deviations (0.95), for $c(s)$ respectively.

It is important to keep in mind that the $g(s)$ distribution is derived independently of diffusion and may not represent the true breadth of the sedimentation coefficient species. However, it can still provide a reasonable approximation of the entire macromolecular concentration. By contrast, the $c(s)$ method is normalised for diffusion by using a weight average frictional ratio using:

$$\frac{f}{f_0} = \frac{M(1-\bar{v}\rho_0)}{N_A 6\pi\eta_0} \left(\frac{4\pi N_A}{3\bar{v}M} \right)^{1/3} \frac{1}{s} \quad (1.4.6)$$

where (f) is the frictional coefficient of a macromolecule and (f_0) is the corresponding coefficient of an anhydrous sphere of the same mass. This

is accurate for monodisperse protein systems having the same frictional ratio, in which case the $c(s)$ can be directly converted to a continuous weight average molecular weight distribution or $c(M)$ plot.

1.4.1.6. Molecular weight distribution: $g(s)$ to $f(M)$ transformation

To obtain molecular weight distribution information for polydisperse systems, such as mucins, it is better to use the extended Fujita model, which is a more recent derivation of the $g(s)$ model (Harding et al., 2011). This uses an approach based on Fujita's original transformation of a $g(s)$ vs s to a molecular weight distribution for random coils. Harding et al. (2011) extended the treatment to general conformations with the aid of the power law or 'scaling' equation linking the sedimentation coefficient and the molecular weight:

$$s = k''M^b \quad (1.4.7)$$

where b depends on the conformation. To transform $g(s)$ vs. s to $f(M)$:

$$f(M) = g(s) \left(\frac{ds}{dM} \right) \quad (1.4.8)$$

where

$$\frac{ds}{dM} = bk''^{1/b} s^{(b-1)/b} \quad (1.4.9)$$

Therefore, to perform the transformation the conformation type or b needs to be known under the particular solvent conditions and at least one pair of s - M values are needed to define the κ'' from Eq. (1.4.7). The method has also been built into the SEDFIT program along with the $g(s)$ vs s method. One disadvantage of the Fujita method is that all the non-ideality drawbacks of the $g(s)$ method are carried over. Therefore, the $f(M)$ plot is usually based on the lowest concentration possible where non-ideality and

self-sharpening effects are minimised. Secondly, this method is not suitable for macromolecules where b is not known. Still, the Fujita transformation is a rapid method for estimating the molar mass distribution of known macromolecules, such as mucins, and can be achieved straight from the SV analysis.

1.4.1.7. Sedimentation equilibrium (SE) analysis

For a direct estimation of molar mass (g/mol), SE experiments are employed. Unlike SV, where high centrifugation speeds are required to sediment the particles, the speed used for SE is lower, such that to achieve a balance between the opposing sedimentation and diffusion forces. After a period of time, an equilibrium is reached where the concentration of the solute moves exponentially towards the cell base but does not sediment. This leads to the formation of a concentration curve, which is analysed at different points in order to determine the molar mass of the sedimenting particle.

Once an equilibrium is reached, the analysis does not require information on particle shape and conformation. However, one needs to know an approximate molar mass range for the particle analysed in order to select the appropriate centrifugation speed. Too much force and some of the larger molecules sediment to the cell base, while under not enough force, the molecules slowly diffuse back to the meniscus. If the molar mass range is uncertain, then several equilibrium speeds are required.

In SE, the concentration distribution between the different radial positions can be explained using the following equation:

$$\frac{d \ln(c)}{dr^2} = \sigma = \frac{\omega^2 M(1-\bar{v}\rho_0)}{2RT} = 2A \quad (1.4.10)$$

where the sigma function σ , of Van Holde et al., (2006) (not to be confused with the same symbol used to represent the standard deviation of a distribution), is related to the reduced molar mass, A of Creeth and Harding, (1982).

SE has to be carefully applied to highly polydisperse systems such as mucins, since too high rotor speeds lead to sedimentation of larger particles, thus leading to underestimates of molar mass (Richards et al., 1968), where shorter solution columns and using different speeds can negate these effects. However, the increasing use of polysaccharides and other polydisperse particles has led to some improvement in molar mass analysis (Morris et al., 2014). Similarly to sedimentation velocity, molecular weights measured at finite concentration are apparent ones ($M_{w,app}$) due to the effects of thermodynamic non-ideality and polyelectrolyte effects.

1.4.1.8. *Analysis of SE data*

Normally, to obtain an estimate for the weight average molecular weight M_w of a macromolecular distribution in solution from a sedimentation equilibrium experiment, an extrapolation of the concentration in the ultracentrifuge cell, c , or $\ln(c)$ to the cell base is required. For monodisperse systems this is not a problem, but for very polydisperse systems, due to the steep rise of the $c(r)$ vs r plot near the cell base, this

can be very difficult. To deal with this, the MSTAR method of Creeth and Harding (1982) was developed, replacing the concentration extrapolation by extrapolation of an operational point average molecular weight $M^*(r)$ – which is much less steeply rising than $c(r)$ – to the cell base. Because of non-ideality, this will still be an apparent value ($M_{w,app}$). The MSTAR methodology is now implemented into SEDFIT (Schuck et al., 2014a), and called SEDFIT-MSTAR (M^*).

MULTISIG is an additional package that can be used to provide a broader resolution of the MSTAR data. The program is designed to provide a continuous distribution of 17 σ terms, which can also be converted into a molar mass distribution (Gillis et al., 2013). Although not as resolving as a sedimentation velocity experiment, the molecular weight distribution so obtained is absolute and does not require assumptions or knowledge of the conformation as with the SV Extended Fujita approach.

1.4.1.9. Mechanical systems

The experiments are carried out in a Beckman Optima X-I analytical ultracentrifuge in a temperature-controlled environment. To prevent overheating of the rotor and adjacent equipment due to the high friction generated by the high speeds, experiments are performed under vacuum, held under 0.7 Pa, with the help rotary or turbo pumps.

The rotors consist of either the 4 holes (An-60Ti) or the 8 holes (An-50Ti) titanium rotors. SV experiments were performed using the 12mm aluminium epoxy resin centrepieces, with sapphire windows, while longer

pathlength (20 mm) titanium centrepieces are used for the SE. Data was captured into text files by ProteomeLab 5.7 (Beckman, Palo Alto, US).

1.4.1.10. Optical systems

Two main optical systems were used to acquire sedimentation data: UV Absorbance and Rayleigh Interference Optics.

UV Absorbance is typically employed for absorbing species such as proteins or nucleic acids. However, it is ineffective for polysaccharides or heavily glycosylated proteins, such as mucins. In addition, a limitation is the duration of a scan, which typically takes about two minutes, depending on the settings employed to scan the entire cell path length. As a result, species of high molecular weight or aggregates may be lost during the scanning process and can therefore lead to underestimates. Absorbance results are presented in .RA files (ASCII), and contain the position relative to the centre of rotation (cm), absorbance (Optical Density, OD) and standard error. The Lambert-Beer Law is used to automatically convert OD to mass concentration (see Parnis and Oldham, 2013).

By contrast, Rayleigh Interference optics are much faster. This is because the monochromatic light passes through the whole sector at once, producing horizontal fringes that are directly bent by the concentration profile in solution. The fringe distributions are converted to .IP files (ASCII) using a Fourier Transform (FT). Sedimentation creates changes in the refractive index, due to changes in the concentration with the radial position, which creates curvature in the fringe pattern. This is called fringe displacement (ΔJ), which is proportional to mass concentration through:

$$\Delta J = c \frac{dn}{dc} \frac{l}{\lambda} \quad (1.4.11)$$

where (d_n/d_c) is the refractive increment, (l) is the cell pathlength, and (λ) is the wavelength used, which for proteins is set at 280 nm.

The two systems can also be combined to get useful information about the sample. For example, using UV Absorbance to identify and quantify absorbing components, and using the RI system for all other types of molecules. This is useful in analysing interactions between proteins and polysaccharides (Harding, 1997).

1.4.2. Intrinsic viscosity

1.4.2.1. Theory

Viscometry is the study of the viscosity of a fluid, which is a measure of the intermolecular forces of attraction within a sample. Intrinsic viscosity can be defined as the measurement of fluid resistance to flow as a result of the hydrodynamic volumes occupied by the molecular components. This is dependent on the chemistry, molecular weight and shape of the molecules in solution (Harding, 1997). This can be defined by the MHKS relation for intrinsic viscosity $[\eta]$:

$$[\eta] = k' M^a \quad (1.4.12)$$

where (k') depends on solvent conditions and (a) is the MHKS shape factor, which depends on the conformation of the particle.

For instance, $a=0$ for spheres, $a=0.5-0.8$ for random coils and $a=1.8$ for a rigid rod (Smidsrød & Andresen, 1978). Therefore, if a macromolecule has a low intrinsic viscosity, is likely that the particle is more spherical. By contrast, high intrinsic viscosities are consistent with larger more elongated molecules, such as DNA or xanthan. Therefore, it is a relatively quick way of identifying which macromolecular solution contains particles that are more globular or more elongated or expanded through hydration.

Firstly, the relative viscosity η_r , is calculated from the ratio of the flow times of the solution (t) to the solvent (t_0) such as:

$$\eta_r = \frac{\eta}{\eta_0} = \left(\frac{t}{t_0}\right) \cdot \frac{\rho}{\rho_0} \quad (1.4.13)$$

where (ρ/ρ_0) is the correction for solution density, where ρ is the density of the solution and ρ_0 is the solvent density, which under very low macromolecular concentrations is usually negligible, assuming the densities are approximately identical.

The intrinsic viscosity $[\eta]$, can be derived from the extrapolation of the reduced viscosity η_{red} to zero concentration c (g/ml), where η_{red} is defined as:

$$\eta_{red} = \frac{\eta_r - 1}{c} = \frac{\eta_{sp}}{c} \quad (1.4.14)$$

where the specific viscosity η_{sp} , describes the change in the relative viscosity η_r of the solution to that of the solvent, which has a value of 1. Alternatively, the intrinsic viscosity $[\eta]$, can also be derived from the extrapolation of the inherent viscosity η_{inh} such as:

$$\eta_{inh} = \frac{\ln(\eta_r)}{c} \quad (1.4.15)$$

where $\ln(\eta_r)$ is the natural logarithm of the relative viscosity.

In a similar way to AUC, extrapolations are required to eliminate hydrodynamic non-ideality effects, arising from charge and/or exclusion volume effects, where self-interactions of macromolecules in solution are concentration dependent. Therefore, reduced or inherent viscosities are extrapolated to eliminate these effects (Harding, 1997). The plots of the reduced and inherent viscosities are called the Huggins and Kraemer plot, respectively (Huggins, 1942; Kraemer, 1938). Usually, the Huggins plot yields a positive slope, while the Kraemer plot yields a negative slope. This is given by the following equations:

$$\eta_{red} = [\eta](1 + [\eta]k_H c) \quad (1.4.16)$$

$$\eta_{inh} = [\eta](1 - [\eta]k_K c) \quad (1.4.17)$$

where K_H and K_k are the Huggins and Kraemer constants, which can also provide useful information about the molecular shape. For instance, a value for K_H ranging from 0.2 and 0.4 corresponds to linear extended structures, while values closer to 1 correspond to more compact, globular molecules (Pamies et al., 2008).

However, a very useful method is the Solomon-Ciuta equation:

$$[\eta] \cong \frac{1}{c} \left(2(\eta_{sp}) - 2 \ln(\eta_r) \right)^{1/2} \quad (1.4.18)$$

developed by combining the Huggins and Kramer relations, which does not require an extrapolation, although it is still useful to check the data at each concentration (Solomon and Ciuta, 1962).

1.4.2.2. *U-tube viscometry analysis*

The U-tube or Ostwald capillary is commonly used for the determination of the intrinsic viscosity. It is a very precise piece of glassware that is immersed in a temperature-controlled water bath. A 2.0 ml solution is injected into a reservoir, and then it is automatically pumped to the top of the capillary and then allowed to fall under gravity. This was done using Schott-Geräte equipment (Schott AG, Germany) in a water bath accurately equilibrated to 20.0 °C. The time taken by the solution meniscus to travel between two points marked on the capillary is automatically recorded. Most times, the process is repeated until the 'flow times' are constant, for an accurate determination of the intrinsic viscosity. This type of measurement can also be used to monitor changes as a function of temperature.

1.4.2.3. *Pressure Imbalance Differential Viscometry*

The method is coupled with the Size Exclusion Chromatography (SEC) instrumentation (described in section 1.4.3.2.). As opposed to standard Ostwald capillary viscometry, this technique measures differences in pressure between the solvent and solution and converting the potential difference in pressure into a relative viscosity (Haney, 1985a, 1985b). A major advantage is that it allows the measurement of heterogeneous samples before or after the sample has been subjected to separation by SEC columns, although may not be very precise at low concentrations or if the SEC columns are blocked (too high concentration). The formula behind the measurement, sometimes referred to as the Solomon-Götesmann equation is identical to the Solomon-Ciuta relation (eq 1.4.18).

1.4.3. Light scattering techniques

1.4.3.1. *Dynamic Light Scattering (DLS)*

DLS, also termed Quasi-Elastic Light Scattering (QELS) or Photon Correlation Spectroscopy (PCS) is used to predict the translational diffusion coefficient and physical size of macromolecules in solution (Harding, 2012). This is achieved by analysing Brownian diffusion of particles suspended in solution, which for larger particles is more pronounced. This is because larger particles scatter more light affecting the intensity of scattered light. The size measured by DLS is an apparent z-average molecular radius ($r_{z,app}$), and is inversely related to the translational diffusion coefficient (D_{trans}) using the Stoke-Einstein equation:

$$D_{trans} = \frac{RT}{6\pi\eta_0 r_H N_A} = \frac{k_B T}{f} \quad (1.4.19)$$

where (R) is the gas constant, k_B is the Boltzmann constant, η is the solution viscosity and T is the absolute temperature (K).

Just like in intrinsic viscosity and the SV, the translational diffusion coefficient is concentration dependent, since exclusion volume effects also affect the rate of Brownian motion. Therefore, an extrapolation to zero concentration is needed to remove non-ideality.

Additional effects of Brownian motion (or rotational diffusion) must be removed. This is particularly useful for more extended structures and is done by extrapolating for the angle of scatter, but in the current investigation it is not performed due to limitations in equipment (Burchard, 1992).

The α -amylase and submaxillary mucin samples used in this study were analysed at only one scattering angle, at 173° . Therefore, it is important to stress that no angular extrapolation was performed to correct for rotational diffusion effects and therefore all DLS values are 'apparent'.

The translational diffusion coefficient is also sensitive to viscosity and temperature, therefore it needs to be normalised to standard conditions such that:

$$D_{20,w} = \frac{293.1}{T} * \frac{\eta_b}{\eta_{20,w}} * D_{trans} \quad (1.4.20)$$

where η_b is the viscosity of buffer, $\eta_{20,w}$ is viscosity of water at 20 °C and (T) is the temperature in Kelvin.

In addition, light scattering techniques are very sensitive to dust and other impurities in the sample, including larger aggregates. Therefore, most samples need to be filtered at least through 0.45 μ m filters before measurement, de-gassed, as bubbles affect light scattering, and the cuvettes need to be air dusted before starting the experiment.

1.4.3.2. Size Exclusion Chromatography: Multi Angle Light Scattering (SEC-MALS)

Size exclusion chromatography (SEC) is a popular technique for the fractionation of macromolecules based on size. The setup consists of a SEC column made up of porous particle beads of certain sizes and porosity (stationary phase). The mobile phase (solvent) passes through the column carrying the solute molecules which are separated at different times, depending their size. There are a number of factors affecting macromolecular separation including temperature, type of molecules, and pore size (Kostanski et al., 2004). One major assumption is that the particles are spherical, therefore errors are high for asymmetric structures.

Combining SEC with light scattering, such as the MALS detector used in this work, can be used to provide estimates of hydrodynamic properties such as molecular weight and size (Van Holde et al., 2006; Wyatt, 1993). The technique is similar to DLS however it involves multiple detectors which reduce the effects of rotational diffusion (Burchard, 1992). The molecular weight is determined from the Zimm equation:

$$\frac{Kc}{\Delta R(\theta,c)} = \frac{1}{M} \left(1 + \frac{q^2 R_g^2}{3} \right) + 2B_2c \quad (1.4.21)$$

where (c) is concentration, (B_2) is the second virial coefficient, θ is the scatter angle at a particular wavelength, and (q) is the wave vector (see Gillis, 2015). Because of the significant dilution caused by the columns, non-ideality effects are usually negligible ($2B_2c$ term in eq. 1.4.21).

1.4.4. Analysis of volatile aroma compounds

1.4.4.1. Solid-Phase Micro Extraction coupled with Gas Chromatography–Mass Spectrometry (SPME-GC-MS)

In the past 20 years, headspace SPME analysis has been a valuable tool in the identification of volatile compounds and other low molecular weight monomers used in the food and other manufacturing industries. It was first invented by Pawliszyn and colleagues in 1989 (Vas and Vékey, 2004). The technique is relatively straightforward, however sample preparation also plays an important role in the accuracy and reliability of results. This is because different compounds have different chemical and physical properties and therefore partition, adsorb and volatilise at different rates.

Aroma compounds are absorbed onto a polymer tube coating a silica fibre. Once an equilibrium is reached in the gas phase, the volatiles are trapped, and their relative concentration is directly proportional to the concentration present in the sample. The captured solutes are then desorbed into the mobile phase (helium gas) of the gas chromatograph and then they undergo separation by the mass spectrometer (Kusch et al., 2013).

1.4.4.2. Atmospheric Pressure Chemical Ionisation-Mass Spectrometry (APCI-MS)

Analysis of volatile compounds in the gas phase was also monitored in real time using the APCI-MS (Gan et al., 2016a; Linforth et al., 1996; Taylor, 2002). As opposed to classical gas chromatography, a major advantage of this technique is that it can measure the selected compounds, based on their mass to charge ratio (m/z), over a period of time. The ionisation is also 'softer', which means that there are fewer fragments produced, and the resulting volatiles can be measured directly in their protonated form ($+H^+$).

Firstly, nitrogen is passed at high rates through a deactivated fused silica tube. The flow of nitrogen produces a Venturi effect which serves to draw a continuous intake of aroma compounds from the gas phase towards the ionisation source. The tube is heated to ~ 150 °C in order to prevent condensation, which can affect the analysis. Upon reaching the ionisation source, the vapours are subjected to a voltage of 4 Kv, in order to protonate the molecules, which releases hydronium ions (H_3O^+). The hydronium ions serve as proton transfer reactions for the volatile aroma compounds. Then, protonated volatile ions are transferred into a vacuum chamber in which they undergo separation by the mass spectrometer.

Although APCI has allowed extensive advancements in flavour analysis, one major drawback is that the soft ionisation is limited in its ability to distinguish between volatiles which have the same molar mass. Therefore, if there are two compounds of the same molecular mass, this leads to competition and inaccurate estimates of volatile concentrations, however

the development of the triple quadrupole version in 2018 has partially resolved this issue (Dion-Fortier et al., 2019). Additionally, the method is limited to non-alcoholic products as it was found that ethanol has a higher affinity for protonation than water, therefore producing protonated ethanol instead of hydronium ions (Sémon et al., 2018).

1.4.5. Differential Refractometry

The concentration of macromolecules was estimated using a differential refractometer, which is an instrument that measures the refractive index of a sample relative to that of the solvent. Although refractive index determination has low sensitivity, mainly because anything in the solution can cause light refraction, this method can provide a rapid means of estimating the total sample concentration.

The technique measures the rate of which macromolecules refract light, and is given by their refractive index increment (dn/dc), which can be found in Theisen et al., (2000). The setup consists of two channels, reference and solution channels. First, a blank scan is performed by injecting approx. 2 ml of solvent in both channels. Then, the solution is injected into the solution channel in order to calculate the total macromolecular refraction. This is given as Brix% (w/v), which is converted to mg/ml using:

$$c(\text{mg/ml}) = \text{Brix}(\%) * \left(\frac{\left(\frac{dn}{dc} \right)_{\text{molecule}}}{\left(\frac{dn}{dc} \right)_{\text{sucrose}}} \right) * 10 \quad (1.4.22)$$

where the dn/dc of sucrose is 0.148 ml/g.

1.4.6. Vibrational spectroscopy

Vibrational spectroscopy is used in the analysis of purity and reaction products in chemical, pharmaceutical and food samples. It has become an integral part in the characterization of newly synthesized polymers. Vibrational spectroscopy can either determine the Infrared or the Raman spectra of molecules, by getting information about the full spectrum of the structure and chemical bonds within a sample. Dry samples are analysed by Fourier-transform infrared spectroscopy (FT-IR) while samples in the aqueous state can be subjected to Raman spectroscopy. In depth methodology can be found at Ferraro, (2003) and Stuart, (2015).

1.5. Aims of the investigation

It is hypothesised that saliva plays a key role in the delivery of flavour molecules to the oral/nasal receptors through its interactions with the food during oral processing. Therefore, in order to identify and propose new ways of maximising the perception of flavour, we need to understand the behaviour and interactions of the key salivary proteins in different food environments, such as pH changes, salt, polyphenols, polysaccharides and other food additives.

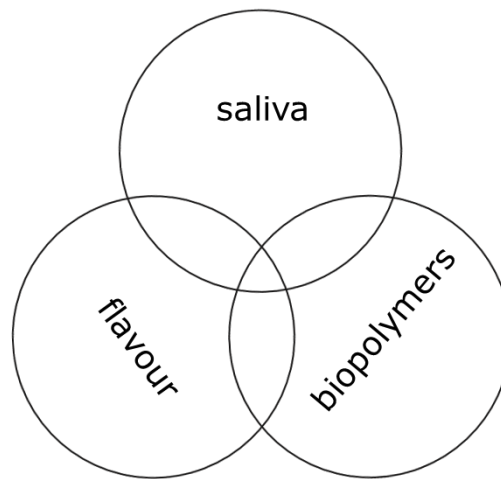


Figure 1.4. Schematic representation showing the interfaces between the fundamental areas of research investigated in the present thesis.

The investigations are positioned at the interface of saliva, food biopolymers and flavour science, as illustrated in Figure 1.3. The scope is to understand some of the effects of the matrix-saliva interactions on the release of aroma and taste compounds, and then suggest novel ways of maximising and evaluating the release and retention of flavour. Hopefully,

knowledge from this work will help in the development of more sustainable food and health products for the consumers.

The structure is as follows:

- Hydrodynamic analysis of two major salivary glycoproteins: submaxillary mucin and salivary α -amylase. The effects of pH and ionic strength on their hydrodynamic properties, and on the intensity of aroma compounds released into the headspace.
- Applications of sedimentation velocity (SV) as a platform for analysing saliva/food interactions (bolus), and develop a substitute for *ex-vivo* saliva; monitoring subsequent changes in the aroma release from the bolus in both model and real food.
- Identifying the role of mucoadhesion in flavour science applications and develop novel mucoadhesives and assays for evaluating the retention of flavour compounds.
- Identify and investigate the effects of aroma and taste compounds on the structure of salivary mucin and α -amylase.

2. Chapter 2: Methods

2.1. Sedimentation Velocity (SV)

For each run, the AUC cells were dismantled, cleaned using water, acetic acid (5.0 %), Neutracon (2.0 %) and ethanol (70 %), assembled and balanced to ± 0.01 g. The cells were optically aligned for the centre of rotation to 0° to reduce peak broadening artefacts (Channell et al., 2018).

The experiments were performed at 20.0°C using the Optima XL-I analytical ultracentrifuge (Beckman, Palo Alto, USA) equipped with Rayleigh interference and Absorption optics. A volume of $395\ \mu\text{l}$ sample and $405\ \mu\text{l}$ solvent respectively were injected into 12 mm double sector epoxy cells with sapphire windows and centrifuged at the required speed. Proteome Lab was used to record changes in concentration versus radial displacement and results were saved in .TXT files.

Raw data was analysed in SEDFIT using the $g(s)$ and $c(s)$ methods of Dam and Schuck (2003) by generating sedimentation coefficient distributions, $g(s)$ vs s , where s is the sedimentation coefficient (in Svedberg units, $S = 10^{-13}$ sec). The $c(s)$ vs s method of Dam & Schuck, although primarily designed for the analysis of mono- and paucidisperse (discrete polydispersity) systems as opposed to continuous polydisperse systems, was employed for the analysis of α -amylase, and pullulan standards. This method was also employed for mucin, although it makes the assumption that all species have the same frictional ratio.

Weight average sedimentation coefficient values from the $g(s)$ vs s distributions were normalised to standard conditions (viscosity and density of water at 20.0 °C) to give $s_{20,w}$. A partial specific volume of 0.64 ml/g was employed for mucin and 0.74 ml/g for α -amylase (Dodd et al., 1998; Fisher et al., 2006). TI and RI noise was removed before fitting the data, which was extracted into Origin 7.5 for presenting the data.

2.2. Sedimentation Equilibrium (SE)

SE mode was employed for the molecular weight experiments. Samples were previously dialysed against a 14,000 Da membrane (Fisher scientific). An equal volume of 140 μ l of samples and solvent was injected into the appropriate channels of the 20.0 mm optical path length double-sector titanium cells with sapphire windows. A rotor speed of 10,000 rpm was employed and scans were monitored every hour. Equilibrium was reached after approximately 70 hours and records of relative concentration distributions were analysed in SEDFIT-MSTAR to yield the weight average molecular mass, M_w (Schuck et al., 2014a).

To reduce non-ideality effects, M_w was plotted at a low concentration of ~ 0.3 mg/ml, with the assumption that it represents the true weight average molecular weight. The relatively new and complementary algorithm MULTISIG was also used to estimate the molecular weight distributions, as instructed by the manufacturer (Gillis et al., 2013).

2.3. Size Exclusion Chromatography: Multi Angle Light Scattering (SEC-MALS)

The SEC set-up consisted of a Postnova Analysis PN7505 degassing unit (Landsberg am Lech Germany), Shimadzu LC-10AD HPLC Pump (Shimadzu UK, Milton Keynes, UK.), fitted with a Spark-Holland Marathon Basic autosampler (Spark Holland, Emmen, The Netherlands) combined with a TSK Gel guard column (7.5 × 75 mm) and TSK Gel G5000, G6000 columns (7.5 × 300 mm) connected in series (Tosoh Biosciences, Tokyo, Japan), fully flushed of column debris. Light scattering intensities were simultaneously detected at 14 angles as a function of elution volume using a DAWN® HELEOS™ II, light scattering photometer connected in series to a ViscoStar® II on-line differential viscometer, an Optilab® rEX refractive index detector (Wyatt Technology Corporation, California, U.S.A.).

A stock solution of 1.0 mg/ml was filtered through a 0.45 µm syringe filter (Whatman, Maidstone, England) to remove any insoluble material or dust prior to injection and then injected into the autosampler. A 100 µl aliquot of each solution was injected onto the columns at ambient temperature. The eluent employed was the PBS dialysate at a flow rate of 0.8 ml/min. ASTRA™ (Version 6) software (Wyatt Technology Corporation, Santa Barbara, U.S.A.) was used to estimate the weight average molecular weight, M_w , weight average intrinsic viscosity $[\eta]$ and radius of gyration R_g , and also molecular weight, $M(V_e)$, intrinsic viscosity $[\eta](V_e)$ and the radius of gyration $R_g(V_e)$ as a function of elution volume (V_e).

The 4mW He-Ne laser was used at a wavelength of 632.8 nm, and the refractive increment for the mucin was taken as 0.181 ml/g. Because of

the low solute concentrations after dilution on the columns non-ideality effects were assumed as negligible.

2.4. Dynamic Light Scattering (DLS)

The experiments were performed using the Zetasizer Nano-ZS detector and low volume (ZEN0112) disposable sizing cuvettes (Malvern Instruments Ltd, Malvern, UK). The samples were measured at (20.00 ± 0.01) °C using the 173° scattering angle and data was collected for 3 runs of 10 second duration per concentration. D_{app} and $r_{z,app}$ values are only apparent values as no angular extrapolation to zero angle was possible to correct for rotational diffusion effects with the current instrumentation (Stetefeld et al., 2016, Burchard, 1992). Size distributions by volume are extracted and plotted in Origin 7.5.

2.5. U-tube capillary (Ostwald) viscometry

Flow times of solvent (t_0) and solutions (t_s) were measured using the semi-automated (Schott Geräte, Hofheim, Germany) U-tube Ostwald capillary viscometer immersed in a temperature controlled water bath at 20.0 °C. A constant volume of 2.0 ml was sampled at a series of dilute concentrations, in order to allow the assumption that no correction was needed for solution density, assuming η_s/η_0 is equal to t_s/t_0 (Harding, 1997). The intrinsic viscosity, $[\eta]$ was calculated according to the Huggins, Kraemer or Solomon-Ciuta relations (see section 1.4.2.).

2.6. Differential refractometry

The Jencons Atago DD-7 differential refractometer was used. First, a blank scan was performed by injecting approximately 2 ml of solvent in both channels. Then, 2 ml of the solution is injected into the solution channel in order to calculate the total macromolecular refraction. This is given as Brix% (w/v), which is converted to mg/ml using eq. 1.4.22 The measurement is repeated at least twice.

2.7. Solid-Phase Micro Extraction coupled with Gas Chromatography–Mass Spectrometry (SPME-GC-MS)

The Trace 1300 series Gas Chromatograph coupled with the single-quadrupole mass spectrometer (Thermo Fisher Scientific, Hemel Hempstead, UK) was used. Samples were incubated at 37.0 °C for 20 minutes with intermittent stirring. Then, the solid phase microextraction (SPME) fibre (50/30µm DVB/CAR/PDMS, Supelco, Sigma Aldrich, UK) was used to extract for 40 min then desorb for 1 min. Separation was carried out by a ZB-WAX capillary gas chromatography column (length 30 m, internal diameter 1.0 mm, 1.00 µm film thickness).

The column temperature was initially at 40.0 °C for 2 min, then increased by 6.0 °C every minute up until 250.0 °C and held for 5 min. Full scan mode was employed to measure volatile compounds (mass range from 20 to 300 Da). A splitless mode was used, and a constant carrier pressure of 18 psi was applied. The areas under the curve were manually corrected for baseline and exported into Origin 7.5 for comparative analysis.

2.8. Atmospheric Pressure Chemical Ionisation Mass Spectrometer (APCI-MS)

The APCI-MS (Platform II, Micromass, Manchester) was used to analyse the concentrations of volatile compounds above the headspace of the solutions under static conditions. Final solution concentration of ~1-10 ppm (parts per million) was sampled with an air flow adjusted to 10 ml/min.

The instrument was set in Selective Ion Recording (SIR) mode to monitor the selected mass to charge ions (m/z) of aroma compounds. The intensity was measured at cone voltage of 50 V, source temperature of 75.0 °C and dwell time of 0.02 seconds. Sampling took place until the signal plateaued. Each peak was integrated in Mass Lynx (Waters, UK) and the area under the curve used to calculate the ion count for the samples using a similar approach used previously (Gan et al., 2016b; Yu et al., 2012).

2.9. Fourier-transform infrared spectroscopy (FT-IR)

Dry samples were subjected to FT-IR analysis. First, they were pressed against the diamond surface to ensure good contact. Measurements were performed in transmission mode on an IRAFFINITY-1S spectrometer equipped with an A219653 attenuated total reflection (ATR) module (Shimadzu, Japan). For each sample, the spectrum was taken as the average of three different measurements at various sites of the dry sample. Spectra were acquired between 500 cm^{-1} and 3500 cm^{-1} at a resolution of 4 cm^{-1} . Measurements were repeated at least twice for reliability.

2.10. Raman spectroscopy

Raman spectroscopy was employed for the analysis of BSM in solution. The experiment was performed using a RamanRXN2 optical system (Kaiser, Boston, USA) and the following conditions: laser wavelength of 785 nm, laser power at sample of $\sim 40 M_w$ with a spectral resolution of 7.5 cm^{-1} , fitted with a NCO-3.0-NIR system. The exposure was 30 seconds for the 10 mg/ml mucin sample. Raman spectra was not corrected for noise and the distribution is a result of an average of 10 scans, without smoothing.

2.11. Environmental Scanning Electron Microscopy (ESEM)

ESEM experiment were supervised by trained staff at the Nanoscale and Microscale Research Centre (nmRC), University of Nottingham. Samples were analysed using a Thermo-Fisher Scientific (Waltham, USA) FEI Quanta 650 ESEM and cooled to $2.0 \text{ }^\circ\text{C}$ by means of a Peltier cooling stage, while the pressure of water vapour in the chamber was adjusted to maintain a relative humidity between 60 to 90 %. An accelerating voltage of 15kV was applied and images were collected.

2.12. Statistical analysis

The AUC analyses were performed in duplicate, while the samples run on the GC-MS were performed in triplicate in a randomised sample order. Tukey's post hoc test was applied to identify significance, and is given as an asterisk '*' directly in the figures ($P < 0.05^*$ and $P < 0.01^{**}$). All figures were made in Origin 7.5.

3. Chapter 3: Molecular hydrodynamics of bovine submaxillary mucin and salivary α -amylase: effects of salt and pH

3.1. Introduction

Past research has generally focused on the study of volatile aroma compounds in the presence of single component systems, such as monosaccharides, salts or some food proteins (Friel and Taylor, 2001; Ruth et al., 1995). However, there is limited research on the effect of saliva and its salivary proteins on aroma release. During consumption of food, saliva is the first medium encountered by the aroma compounds as they travel to the olfactory receptors in the nose (Taylor, 2002).

Saliva consists of a number of macromolecules which protect and lubricate the lining of the oral cavity including mucins, α -amylases, antibodies and other proteins which play a major role in regulating the pH and normal functioning of the saliva (Drobitch and Svensson, 1992). Although its pH is maintained between ~ 5.5 - 7.5 , this decreases during food consumption, thus interfering with the normal functioning of salivary proteins (Cheaib and Lussi, 2013). Changes in pH stimulate salivary glands to produce more saliva in order to compensate for the loss in functionality and to keep the oral cavity lubricated (Hans et al., 2016). But the process is faster at replacing low molecular weight enzymes and smaller peptides, and much slower at replenishing viscous, higher molecular weight mucins, therefore stimulated saliva has a lower proportion of mucin than resting saliva

(Gittings et al., 2015; Dinu et al., 2018a). During this stage, a lower protein content is predicted to contribute to an increase in the partitioning of aroma compounds from the bolus towards the olfactory receptors.

In addition to pH, sodium chloride is another abundant ingredient in the diet, found in bakeries, soup, pasta, confectionery as well as soft drinks. It helps to increase palpability and enhance the release of flavour, including sweetness. For instance, soup contains up to 3 mg/ml of sodium per serving, while cured meats and sausages can contain up to 30 mg/ml salt (Gillespie et al., 2015).

However, a high sodium diet puts the whole population at risk of hypertension and subsequent cardiovascular impairments. For example, in the United States, two thirds of the population have high blood pressure (Institute of Medicine (US) Committee on Strategies to Reduce Sodium Intake, 2010). In 2009, it was estimated that the direct and indirect costs associated with hypertension were over 70 billion dollars. Therefore, authorities throughout the world are now recommending significant reductions of salt in foods in order to reduce some of the consequences associated with its elevated consumption.

In biology, salt and pH have a significant role in regulating the structure and function of proteins (Dominy et al., 2002; Perlmann and Kaufman, 1945). Their use includes stabilisation phenomena and reduction of hydrodynamic non-ideality in charged colloids, i.e. aggregation (Damodaran and Kinsella, 1981). For example, salt ions control the attractive or repulsive interactions between charged groups of proteins,

protein membranes, nucleic acids, carbohydrates and even lipids (Krahn et al., 2019; Singh and Singh, 2015).

It is hypothesised that mucins along with other salivary glycoproteins, play a role in aroma and taste release through the very fine structural or conformational changes induced by the pH and the ionic strength of food. Therefore, in order to maximise flavour release in healthier foods, we need first to understand the behaviour of salivary proteins under the different conditions i.e. pH and salt.

The current study aims to understand the macromolecular hydrodynamics of submaxillary mucin (BSM) and human α -amylase (HSA) under physiological conditions and under acidic and high salt conditions. The solutions of macromolecules are designed to mimic the conditions of the saliva (buffered salts and electrolytes), within the range of the salivary concentration of mucin and α -amylase (Dziemiańczyk et al., 2005; Haward et al., 2011).

AUC was used to explore changes in mucin integrity and conformation, complemented by SEC-MALS, Viscometry and DLS. The hydrodynamic analyses are complemented by GC-MS and APCI-MS analysis to analyse changes in the headspace concentration of aroma compounds under the different treatments.

3.2. Materials and methods

3.2.1. Samples

Bovine submaxillary mucin (Type IS), human salivary α -amylase (type IX-A, A0521) and volatile aroma compounds were obtained from Sigma Aldrich (Dorset, UK). Highly purified RO (reverse osmosis) water was used for the preparation of solutions. The 0.1 M phosphate buffered saline (PBS) was made according to Green, (1933) with salts from Fisher Scientific, UK. The Na-citrate solutions were made by varying the proportion of citric acid and sodium citrate according to Sigma.

3.2.2. Analytical ultracentrifugation (AUC)

3.2.2.1. Sedimentation velocity (SV)

SV experiments were performed as reported in Section 2.1. The speed employed for centrifugation was 30,000 rpm. To eliminate non-ideality, sedimentation coefficients are extrapolated to zero concentration, c using standard $1/s_{20,w}$ vs c plots, also used to derive information on conformation. Comparative molecular weight distributions for BSM in solvents at pH 7.0 and pH 3.0 were also obtained using the $f(M)$ vs M Extended Fujita method of Harding et al. (2011).

3.2.2.2. Sedimentation equilibrium (SE)

For SE, see section 2.2. Prior to the experiment, the samples were dialysed against a 14,000 kDa Mw cut-off membrane (Fisher scientific).

3.2.3. SEC-MALS-Viscostar

SEC-MALS was used in the analysis of mucin at pH 7.0 as according to section 2.3. Due to column limitations, analysis was not possible at pH 3.0.

3.2.4. Capillary viscometry

Flow times of solvent (t_0) and solutions (t_s) were measured using the semi-automated (Schott Geräte, Hofheim, Germany) U-tube Ostwald capillary viscometer as described in section 2.5. The intrinsic viscosity, $[\eta]$ was calculated according to the Huggins, Kraemer and Solomon-Ciuta equations (see section 1.4) by extrapolating to zero concentration.

3.2.5. Dynamic Light Scattering (DLS)

Mucin solutions were also characterised by DLS using the Zetasizer Nano-ZS detector and low volume (ZEN0112) disposable cuvettes (Malvern Instruments Ltd, Malvern, UK) as in section 2.4. The dialysed sample was filtered through a 0.45 μm filter prior to analysis.

3.2.6. Atmospheric Pressure Chemical Ionization-Mass Spectrometry (APCI-MS)

The APCI-MS was used to determine the concentrations of volatile compounds above the headspace as described in section 2.8. The instrument was set in Selective Ion Recording (SIR) mode to record the selected mass to charge (m/z) of the aroma compounds: HDMF (128.13), octanal (128.21), nonanal (142.23), decanal (156.2), linalool (154.25) and *p*-cresol (108.1).

3.2.7. Gas Chromatography-Mass Spectrometry (GC-MS)

The Trace 1300 series Gas Chromatograph coupled with the single-quadrupole mass spectrometer (Thermo Fisher Scientific, Hemel Hempstead, UK) was used, as described in section 2.7. Volatiles were identified by comparison of each mass spectrum with the spectra from the *NIST* Mass Spectral Library.

3.3. Results and Discussion

3.3.1. Hydrodynamic characterisation of BSM at neutral pH

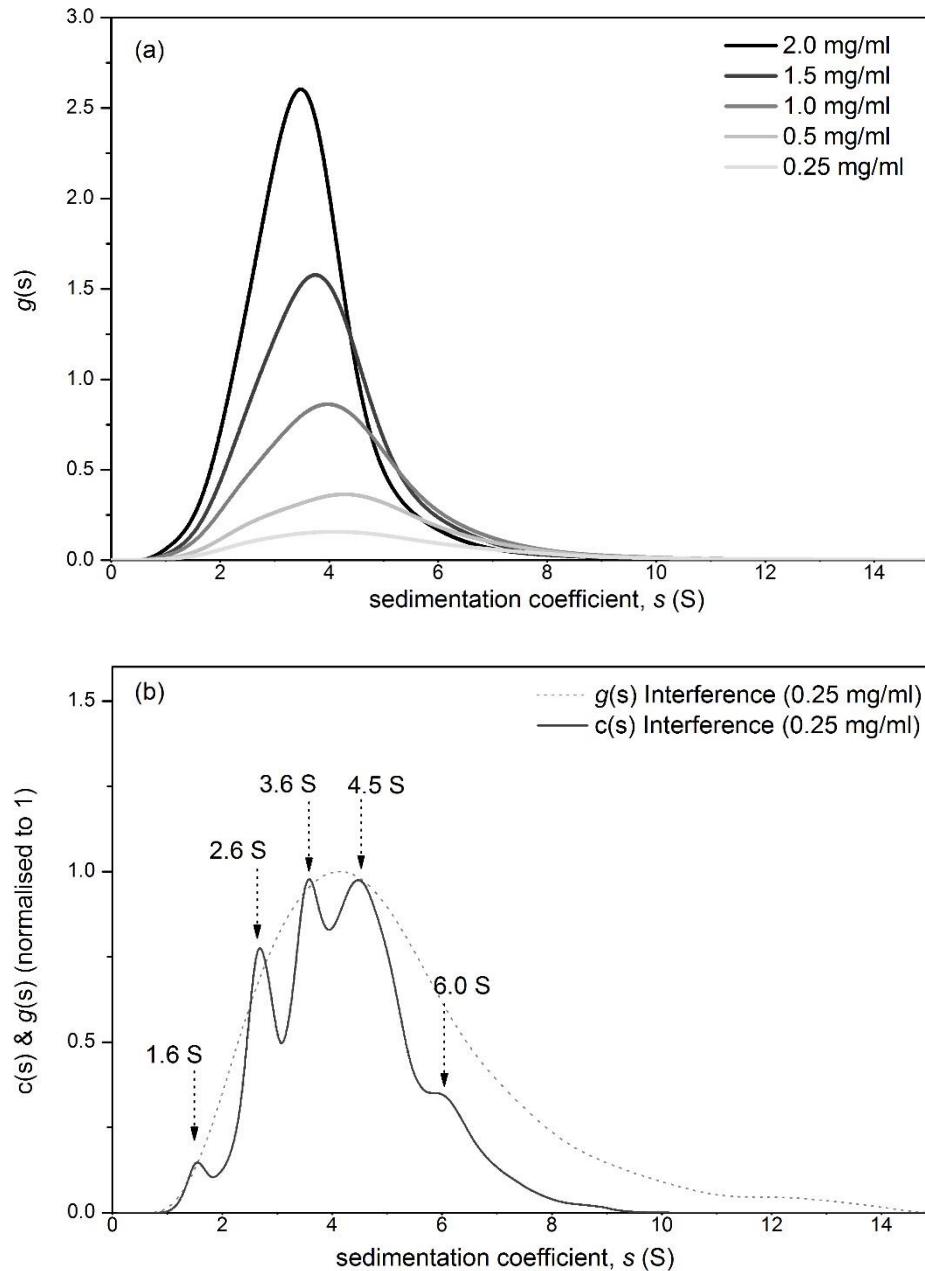


Figure 3.1. Sedimentation velocity, $g(s)$ analysis of BSM showing the sedimentation coefficient distributions (a), and the $c(s)$ analysis at low concentration showing the estimated deconvoluted distribution, $f/f_0 = 3.8$ (b). Run at 20.0 °C at 30,000 rpm in PBS buffer with ionic strength of 0.1 M (pH 7.0).

The sedimentation coefficient distribution of BSM was analysed by $g(s)$ and $c(s)$ methods (Dam and Schuck, 2003b, 2005). The $g(s)$ distribution series at each concentration shown in Figure 3.1.a was used to extrapolate the sedimentation coefficient of the whole sample, $s_{20,w}^0$ (S) corrected to standard conditions (density, temperature). Generally, the analysis confirmed a pauci-disperse sample, with non-ideality effects corresponding to a typical increase in sedimentation coefficient and peak broadening at low concentrations (Figure 3.1.).

The diffusion-deconvoluted model $c(s)$, although less suited for samples of high polydispersity, has resolved five major sedimentation coefficient components at 1.6, 2.6, 3.6, 4.5 and 6 S (Figure 3.1.b). The translational frictional ratio (f/f_0) or simply " f " was 3.8, measured experimentally from the sedimentation coefficient s_{20}^0 , and the weight average molar mass in equation 1.4.2.

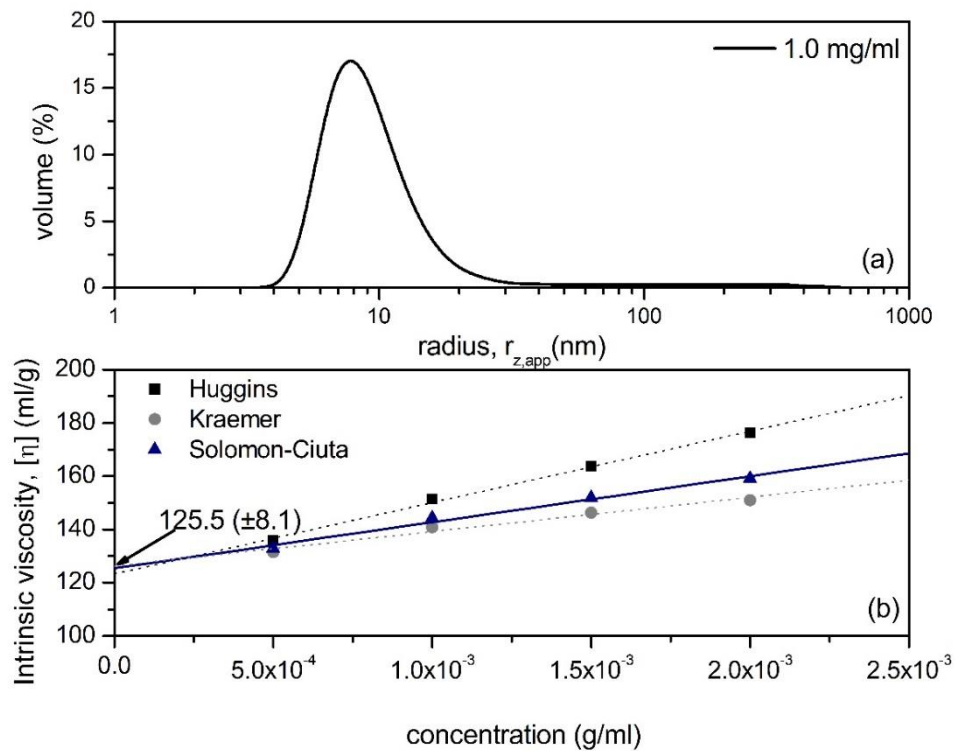


Figure 3.2. Dynamic Light Scattering results yielding apparent hydrodynamic radius $r_{z,app}$ of BSM at 1.0 mg/ml (a), and extrapolation to zero concentration to determine the intrinsic viscosity $[\eta]$ of mucin (b). Experiments performed at 20.0 °C in PBS buffer with ionic strength 0.1 M (pH 7.0).

Figure 3.2. shows the apparent hydrodynamic radius of BSM by volume, as given by DLS, uncorrected for concentration and rotational diffusion effects (Burchard, 1992). The analysis produced an apparent hydrodynamic radius, $r_{z,app}$ of ~ 10 nm corresponding to an apparent diffusion coefficient D_{app} of 2.2×10^{-7} cm²/sec.

The intrinsic viscosity $[\eta]$ in Figure 3.2.b was obtained using the Huggins, Kraemer and Solomon-Ciuta equations (Harding, 1997). Although the extrapolations show a good fitted regression it suggests strong

concentration dependence. Similar intrinsic viscosity values for mucin have been found in other studies, however the slope of the Kraemer extrapolation is usually negative (Goycoolea et al., 1995). Likewise, the Solomon-Ciuta plot represents an average of the Huggins and Kraemer equations and should ideally adopt a horizontal slope. In this case however, positive Solomon-Ciuta indicates concentration dependent aggregation.

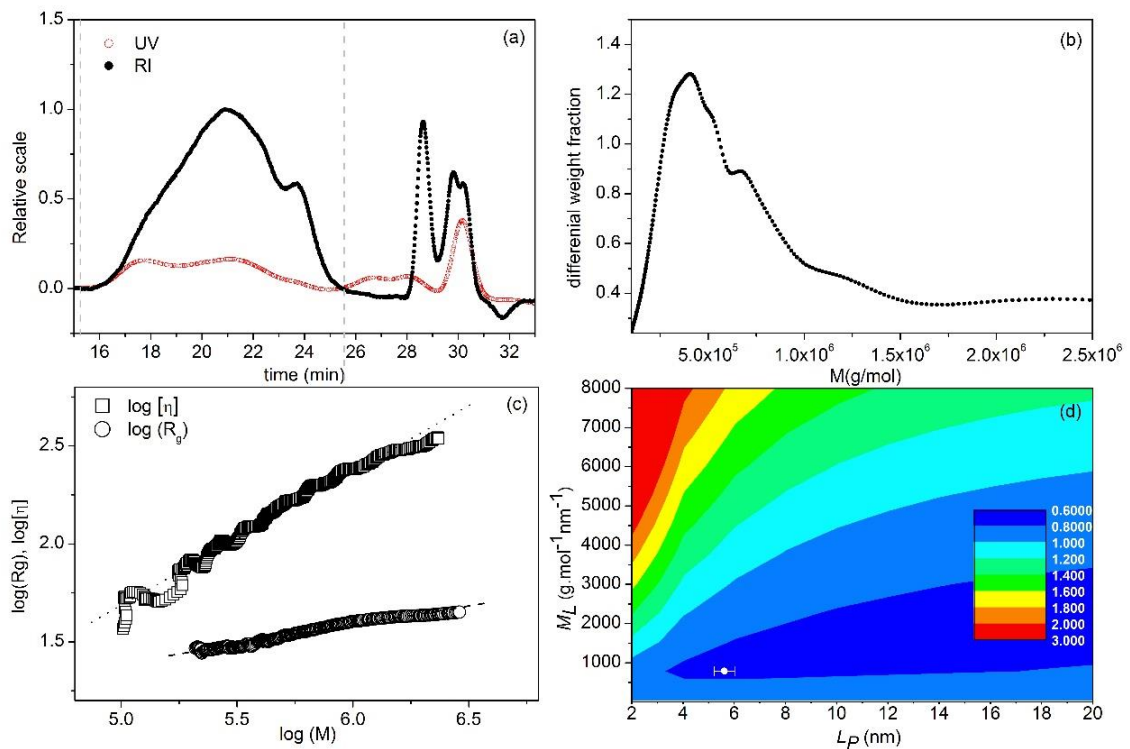


Figure 3.3. SEC-MALS of BSM showing the RI and UV elution profile of BSM (a), differential molecular weight distribution (b), Mark Houwink-Kuhn Sakurada (MHKS) plot of intrinsic viscosity $[\eta]$, versus molecular weight M_w (c), and Multi-HYDFIT contour plot of the target function (\bullet), showing the M_L and L_P estimates (d).

Additional experiments were employed using the SEC-MALS to support the results from the AUC (Figure 3.3.). The Raleigh Interference (RI) and UV elution profiles of BSM in 0.1M PBS (pH 7.0) ranged from 16 min to 25 min. The elution profiles are converted to a molecular weight distribution profile in the ATRA™ software as supplied by the manufacturer (Figure 3.3.b), which was shown to reinforce the multi-component distribution of the $c(s)$ sedimentation analysis.

Data from SEC-MALS was also analysed for the comparison of molar mass and intrinsic viscosity, $[\eta]$ which is used to estimate the conformation of the macromolecule (Figure 3.3.d). The samples show a good correlation between molar mass and intrinsic viscosity, with R_g values of ~ 1.5 nm, consistent with a globular random coil, much lower than those found for other mucins (~ 60 nm in Almutairi et al., 2016).

However, a more quantitative representation of its shape comes from the measurement of the mass per unit length, M_L and persistence length L_p , the later having theoretical limits of 0 for random coils and infinity for a stiff rod (García de la Torre and Harding, 2013). L_p and M_L were estimated in the MultiHYDFIT package, which combines the Yamakawa-Fujii and the Bushin-Bohdanecky relations into a single algorithm that estimates L_p and M_L based on a minimisation of a target function (\bullet), which considers the following hydrodynamic parameters: $s_{20,w}^0(S)$, R_g , D_{trans} , and $[\eta]$ for the entire molecular weight distribution (Bohdanecky, 1983; Ortega and García de la Torre, 2007; Yamakawa and Fujii, 1973). Results yielded a persistence length value, L_p of 5.6 nm (± 0.5) and mass per unit length, M_L of ~ 800 g.mol⁻¹/nm, corresponding indeed to a very tightly packed random coiled structure (Figure 3.3.d).

3.3.2. Effect of low pH on the solution properties of mucin

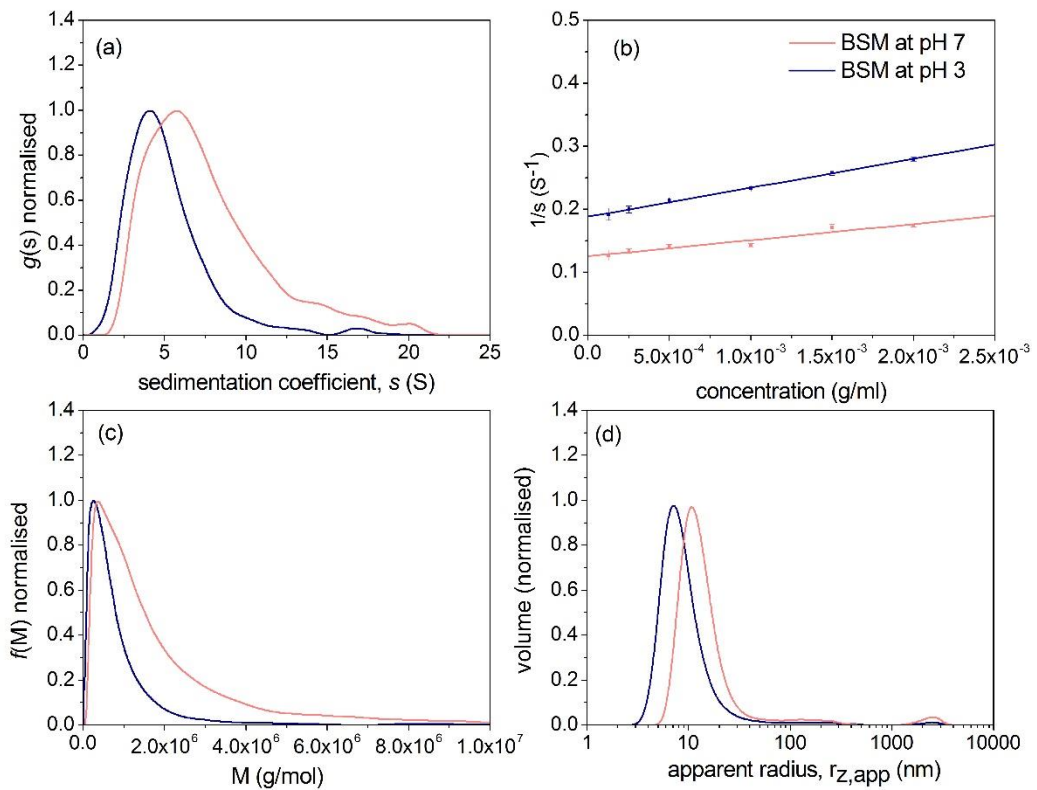


Figure 3.4. Comparative hydrodynamic properties of BSM at pH 7.0 and at pH 3.0 showing the sedimentation coefficient distribution (a), reciprocal plot of s versus concentration, to determine the concentration dependence 'Gralén' coefficient (b), the Extended Fujita analysis, $f(M)$ at a loading concentration of 0.25 mg/ml; $\kappa'' = 0.007606$ and $b = 0.483$ (c) and apparent hydrodynamic radius $\Gamma_{z,app}$ (d). Experiments performed in 0.1 M PBS buffer (pH 7.0) and 0.1 M Na-citrate buffer (pH 3.0) at 20.0 °C.

AUC and DLS were applied to study how lowering the pH of mucin can affect its hydrodynamic properties. The $g(s)$ analysis (Figure 3.4.a) revealed that the sedimentation coefficient distribution has shifted towards higher S ($s_{0,20,w}$) values, from 5.2S at pH 7.0 to 7.9S at pH 3.0. The

reciprocal sedimentation coefficients were extrapolated to zero concentration to determine sedimentation concentration dependence 'Gralen' coefficient k_s , which were (238 ± 9) ml/g at pH 7.0 and (202 ± 18) ml/g at pH 3.0 (Figure 3.4.b & Table 3.1.).

The $f(M)$ transformation was performed according to Harding et al. (2011). The procedure is employed by calculating the kappa (κ'') and (b) parameters (eq. 1.4.7), the latter being determined from the plot of molar mass and intrinsic viscosity (as in eq 1.4.12). Values of b of 0.483 ± 0.010 and κ'' of 0.007606 were calculated, which fits in with previous reports for mucin (Harding et al., 2011). In addition, the molar mass distribution from the $f(M)$ analysis is similar to that from SEC-MALS (Figure 3.3.b).

Figure 3.4.d shows the changes in the apparent hydrodynamic radius of BSM to larger structures, supporting the results from SV and SEC-MALS. Overall, these results suggest a partial pH dependant aggregation and/or possible conformational changes as the pH decreased close to the isoelectric point of mucin (Perez and Proust, 1987).

Generally, the SEC-MALS and the SV analyses (i) confirm a lower molecular weight distribution of BSM at pH 7.0 (100-1500 kDa), as compared to other mucins from other sources (Dodd et al., 1998; Fiebrig et al., 1995b) with the presence of a high molecular weight tail extending to several million Da; (ii) a shift to high molecular weights (and higher apparent hydrodynamic radii) at pH 3.0 which is expected as the lowering of pH to near the pKa of sialic acid means reduced overall negative charge and hence greater tendency to self-aggregate, to some extent similar to gastric mucins.

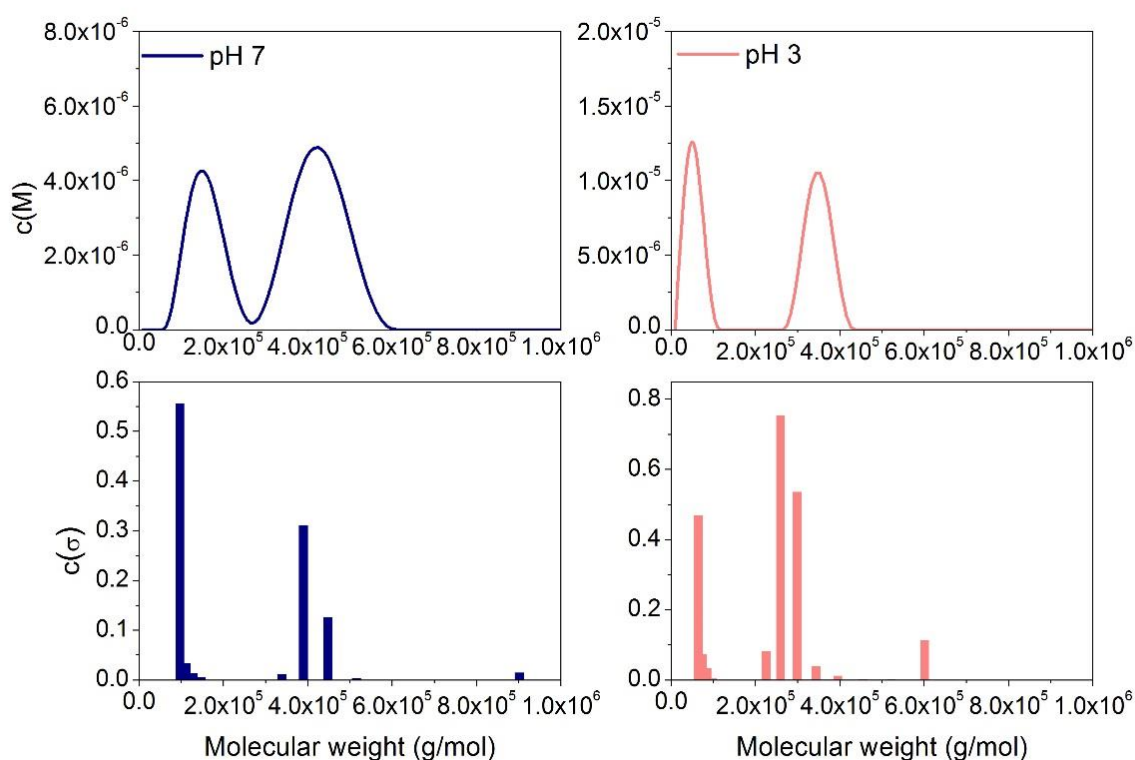


Figure 3.5. SEDFIT-MSTAR analysis showing the $c(M)$ molecular weight distribution plot and the MULTISIG $c(\sigma)$ transformation yielding the weight average molecular weight distribution (M_w) for BSM at pH 7.0 and at pH 3.0 at a loading concentration of 0.25 mg/ml. Centrifuged at 20.0 °C at 10,000 rpm for 78 hours.

In addition, we employed a SE experiment to compare with the results from SV and SEC-MALS. The plots show the weight average molecular weight distributions, $c(M)$ (Schuck et al., 2014b) (Figure 3.5.). MULTISIG was further used to resolve the distributions into more discrete components. While the SE analysis indicates a multi component system, the SE analysis shows a lower weight average molecular weight of BSM at pH 7.0 (~ 300 kDa) as compared to the SEC-MALS and SV analyses.

It is suggested that the centrifugation speed was too fast, leading to the sedimentation of large M_w species to the cell base, causing underestimates. Furthermore, as shown in Figure 3.5., the apparent weight average molecular weight at pH 3 has decreased by ~ 100 kDa, which is thought to be attributed to the loss of the larger mucin aggregates/precipitates to the cell base. Therefore, it is suggested that SE may not be as suitable for the characterization of large protein systems at low pH due to aggregation and denaturation, although the same applies for SEC-MALS where the columns are prone to blockages.

Table 3.1. Summary of AUC, SEC-MALS, DLS and intrinsic viscosity data showing the hydrodynamic properties of BSM in 0.1 M phosphate chloride buffer (pH 7.0) and citrate buffer (pH 3.0).

	pH 7.0	pH 3.0
$s^{\circ}_{20,w}$ (S)	5.2 (± 0.2)	7.9 (± 0.7)
$M_{w,app}$ (kDa)	700 (± 30)	1600 (± 160)
$r_{z,app}$ (nm)	10 (± 3)	15 (± 3)
k_s (ml/g)	238 (± 9)	202 (± 18)
$[\eta]$ (ml/g)	168 (± 5)	127 (± 2)
$k_s/[\eta]$	1.4 (± 0.2)	1.6 (± 0.3)
R_g (nm)	35.1(± 1.2)	-
L_p (nm)	5.6 (± 0.5)	-

Results from the hydrodynamic investigation are given in Table 3.1. The results for pH 7 are lower than one of the first studies on BSM which estimated and $s^{\circ}_{20,w}$ of 6.6 S, a weight average molecular weight of 1100 kDa and an intrinsic viscosity of 165 ml/g (Lyttleton, 1964). In addition, R_g size also estimates appear smaller than gastric mucins determined

previously at ~ 57 nm using the same instrumentation (Almutairi et al., 2016).

It is difficult to conclude how these changes observed in the current work affect mucin conformation. Using the Wales and van Holde (1954) ratio 'R', the values identified in this study were 1.4 ± 0.2 (pH7) and 1.6 ± 0.3 (pH3), both corresponding to random coils. However, within experimental error the results indicate a shift to an even more compact conformation.

3.3.3. pH-mucin effects on the release of aroma compounds

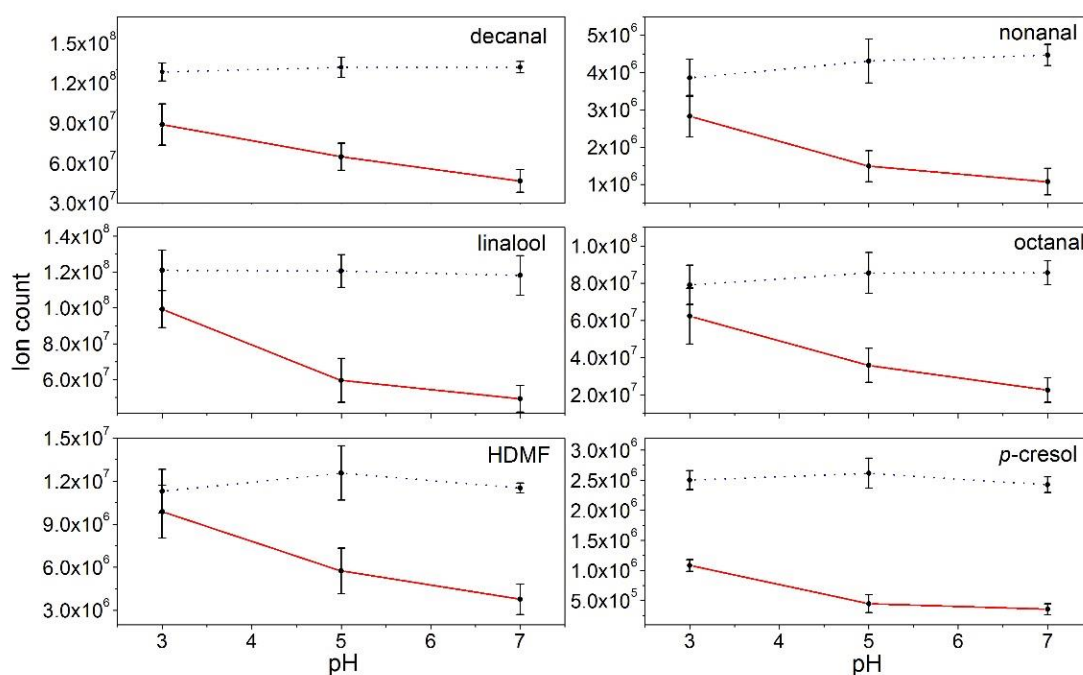


Figure 3.6. APCI-MS results showing the impact of pH on the release of volatile aroma compounds from solutions with 1.0 mg/ml mucin (continuous red line) and from the neutral and acidic buffer solutions (dotted line). Data are shown as mean \pm SE, (n=3).

The compounds are characteristic to lemon flavoured soft drinks, such as *Sprite* and *7UP*, including linalool, HDMF, octanal, nonanal and decanal. The analysis demonstrates how changes in mucin hydrodynamics at low pH affect the partitioning concentration of these compounds. In the absence of mucin (dotted line), results indicated no significant differences in the release of aroma compounds at different pH (Figure 3.6.).

There was a substantial interaction effect which lowered the headspace concentration of the aroma compounds in the presence of mucin, particularly at higher pH. However, lowering the pH was seen to suppress the mucin/aroma interactions. No significant differences ($P < 0.05$) were observed at pH 3.0 between the buffer (control) and mucin solutions, suggesting mucins are somewhat less able to inhibit the release of flavour.

Aggregation may be the leading mechanism by which pH affects mucin solutions, although conformational changes and charge shielding may also play a role in reducing the interactions between the aroma compounds and BSM, hence contributing to an enhanced perception of flavour in acidic drinks.

3.3.4. pH effects on the release of aroma compounds in the presence of salivary α -amylase

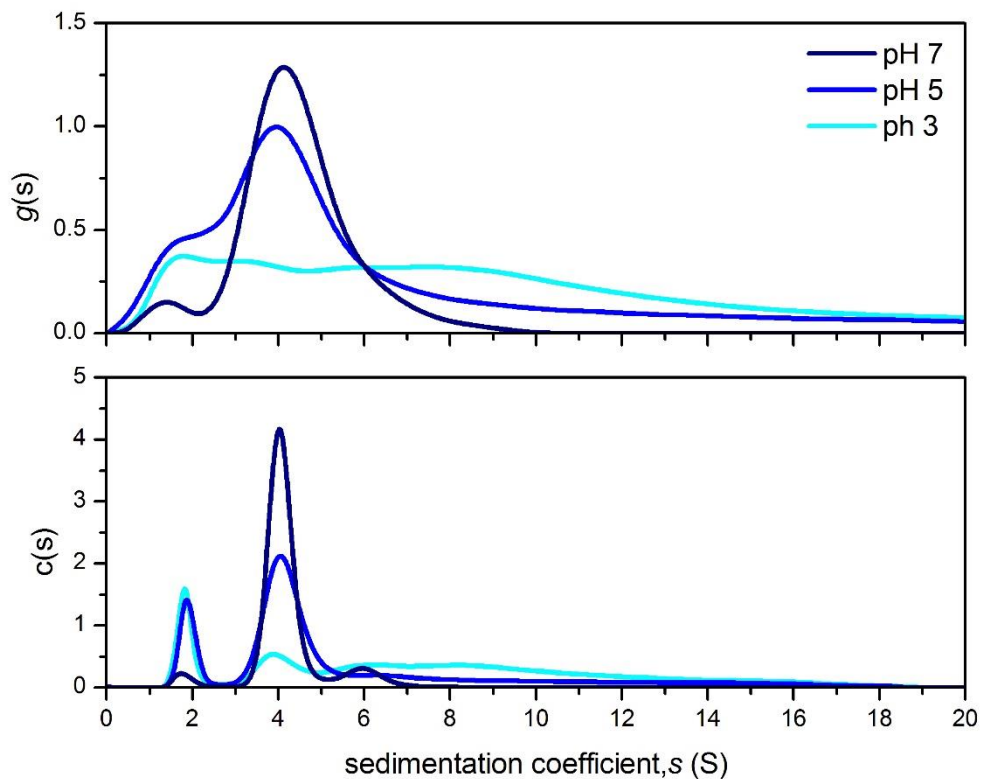


Figure 3.7. Sedimentation velocity, $g(s)$ and $c(s)$ analyses of HSA showing the sedimentation coefficient distributions of 1.0 mg/ml HSA at different pH. Run at 20.0 °C at 40,000 rpm in 0.1M PBS buffer (pH 7.0) and 0.1 M Na-citrate buffer (pH 3.0 and pH 5.0).

Human salivary α -amylase was assessed by SV. The $s_{20,w}$ are not corrected for non-ideality based on the assumption that α -amylase has a near spherical conformation with a low frictional ratio (Gilbert et al., 2003). The analysis suggests the presence of heterogenous components. According to previous reports, it is suggested that the peak at $\sim 4S$ is the amylase monomer and the peak at $\sim 6S$ is the dimer (Isemura and Kakiuchi, 1962), while the $\sim 2S$ component is suggested to be a part of the

enzyme core, which appears to increase in concentration as the pH decreases (Figure 3.7.).

Lowering the pH led to a significant reduction in the concentration of the main component $\sim 4S$, increase in the concentration of $\sim 2S$ component as well as an increase in the concentration of higher order molecular weight aggregates ($>6S$). Unlike mucin, the concentration of the main peak is significantly reduced, suggesting denaturation of protein structure and function. This is related to lack of, or lower levels of surface glycans on salivary α -amylases (compared to mucins), which act to protect the polypeptide backbone (Koyama et al., 2000).

3.3.5. pH-amylase effects on the release of aroma compounds

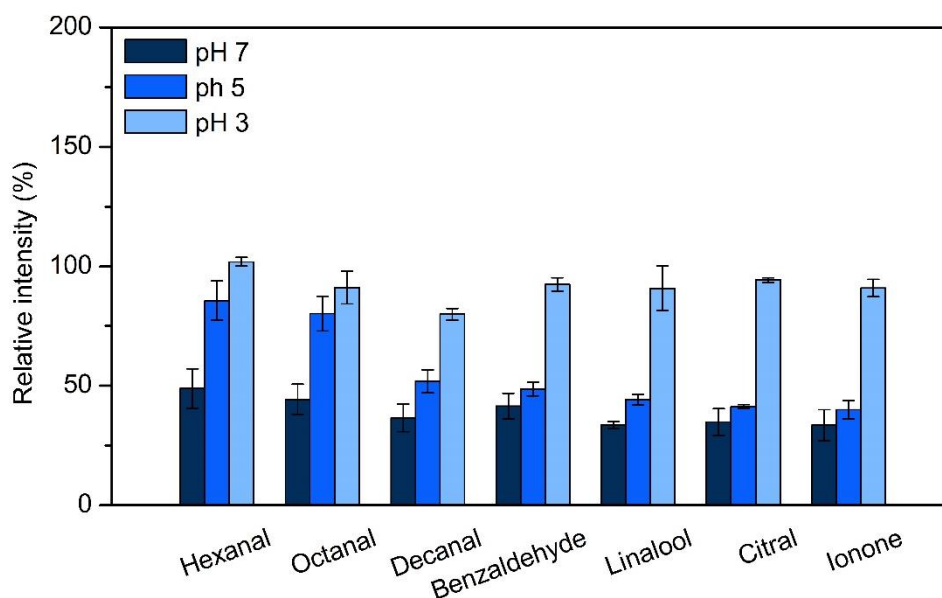


Figure 3.8. GC-MS results showing the effect of pH on the release of volatile aroma compounds from HSA solutions (1.0 mg/ml). Values are expressed as mean \pm SD (n = 3).

To understand how a decrease in pH affects the interactions between α -amylase and aroma compounds, a GC-MS experiment was employed to evaluate the headspace concentrations of aroma compounds (Figure 3.8.). Like mucin-pH interactions, but even more pronounced, a decrease in pH led to a significant increase in the concentration of aroma compounds. As the enzyme completely denatures at pH 3.0, the intensity of all aroma compounds is virtually close to that in pure solvent (100 %). This was to be expected for a typical protein with a low degree of glycosylation, as opposed to submaxillary mucins. Furthermore, it was indicated that, at pH 5.0 and pH 7.0, the intensity of more hydrophobic compounds such as benzaldehyde, linalool, citral and ionone are more affected by the enzyme, showing over 50% reduction in their concentration released into the headspace.

3.3.6. Effect of ionic strength on mucin conformation

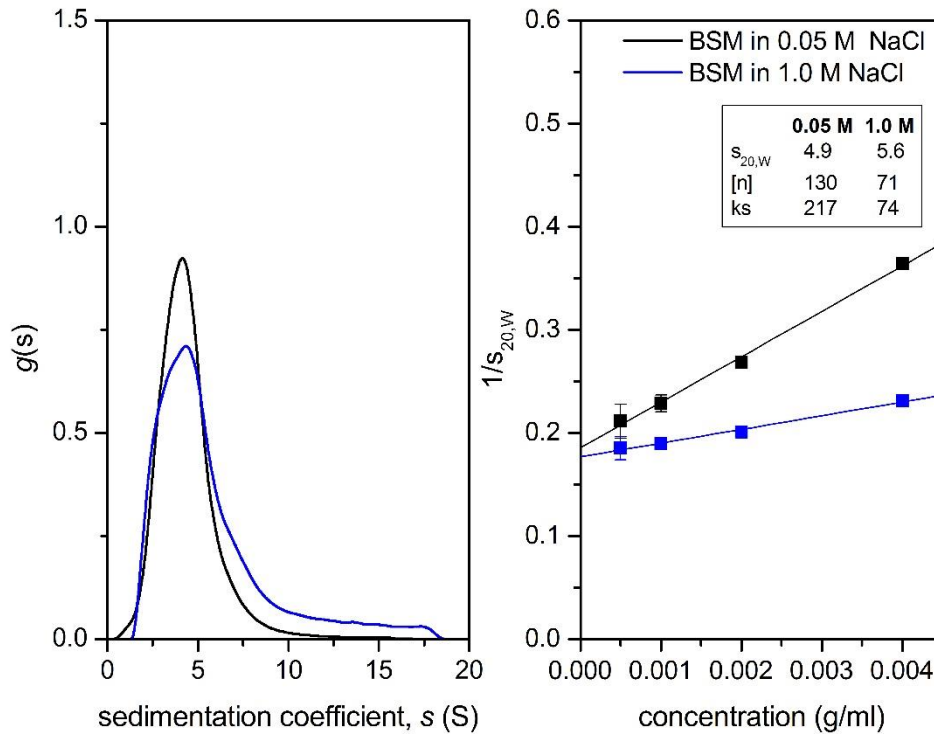


Figure 3.9. Comparative hydrodynamic properties of BSM at low and high NaCl concentration, showing the sedimentation coefficient distributions at 1.0 mg/ml and reciprocal plot of s versus concentration. Experiments performed in PBS buffer 0.05 M (pH 7.0) before and after the addition of 30.0 mg/ml (1.0 M) sodium chloride.

The addition of salt to mucin solutions resulted in the formation of higher molecular weight species, as indicated by the sedimentation coefficient distribution. This led to a reduction in non-ideality, as indicated by the slope of the $1/s$ vs c plot (Figure 3.9.). The effect is attributed to charge shielding effects on sialic acids, sulphate and non-glycosylated protein

regions, which increase aggregation by the reducing hydrodynamic repulsion between the mucin components.

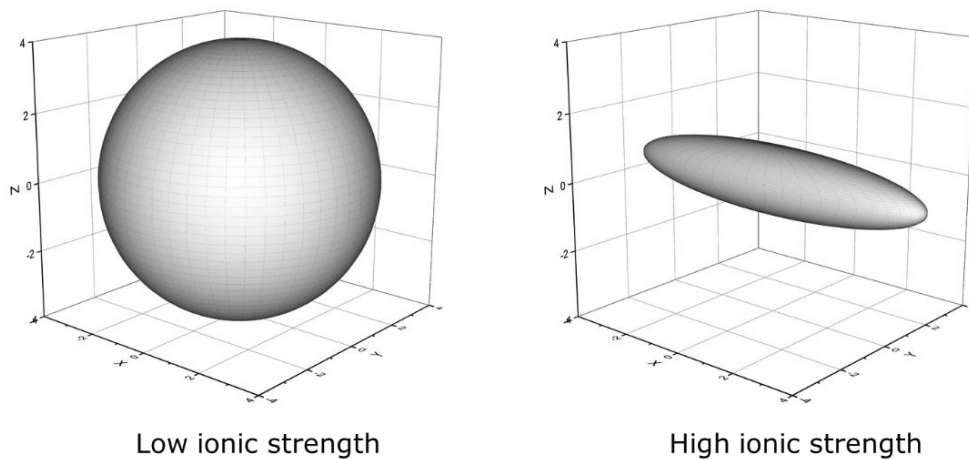


Figure 3.10. Oblate ellipsoid models of BSM under physiological salt concentrations and after the addition of and in the presence of 30.0 mg/ml sodium chloride. Models predicted using HYDFIT and using the concentration dependence 'Gralén' coefficient. Modelled in ELLIPS (Harding et al., 1997).

Using the values previously determined for intrinsic viscosity and molecular weight, changes in the mucin conformation in the presence of high ionic strength were addressed. Using the Wales van Holde ratio 'R' from $k_s/[n]$, we have predicted changes in the conformation of mucin, corresponding to a significantly lower 'R' ratio of 1.04, indicating changes to stiffer structures (Figure 3.10.). It is suggested that the naked protein regions decrease in flexibility as the charge density builds up giving rise to more extended, less hydrated structures. Similar results have been found previously looking at the effect of different salt concentration (calcium and potassium) on hog gastric mucins, suggesting that these changes are partially reversible (Snary and Allen, 1971; Snary et al., 1974).

3.3.7. Salt-mucin effects on the release of aroma compounds

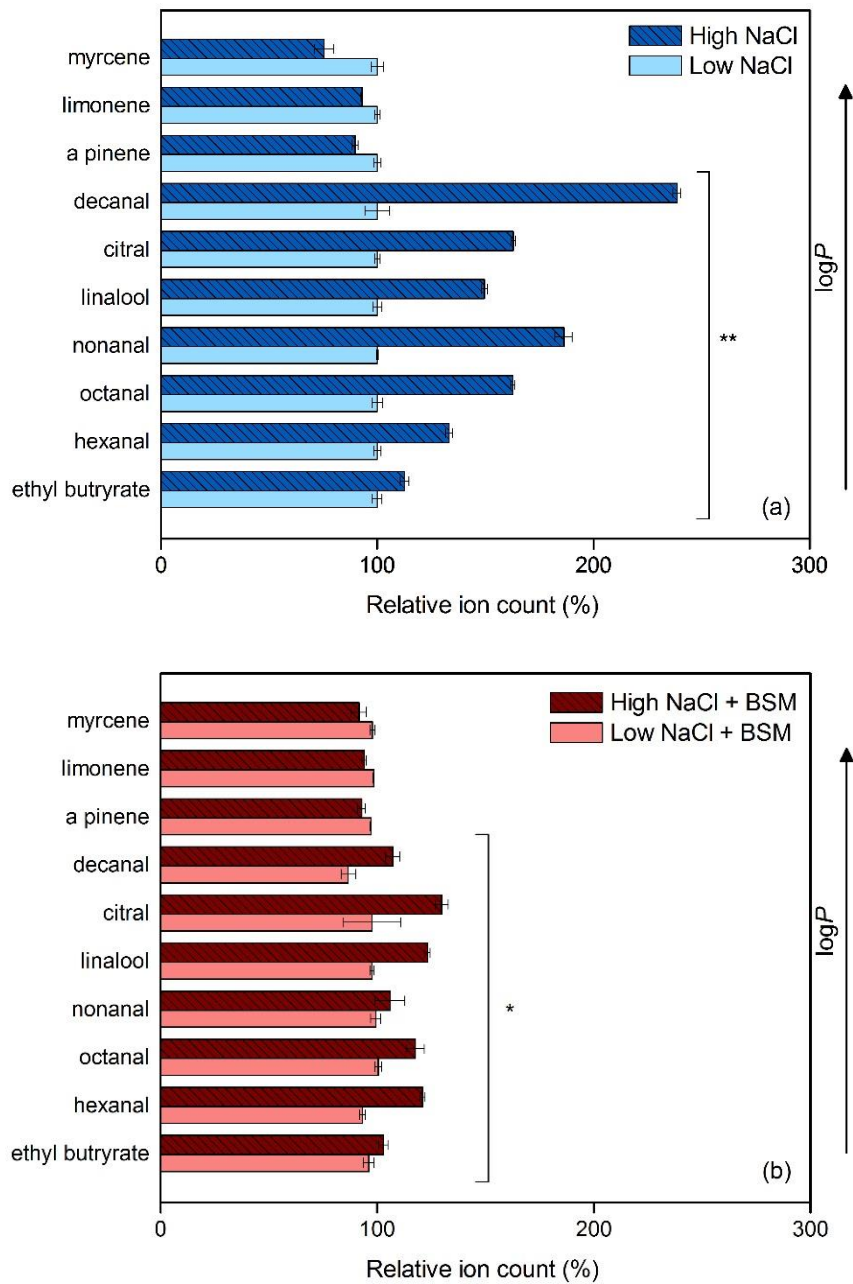


Figure 3.11. GC-MS results showing the effect of NaCl concentration on the release of aroma compounds in the absence of mucin (a), and in the presence of mucin (b). Values are expressed as mean \pm SD (n = 3).

Aroma release was evaluated from a commercial orange juice mixed with BSM solutions at low and high concentrations of sodium chloride (Figure 3.11.a&b). Salting out effects are predominant, whereby the release of aroma compounds was increased significantly by salt addition ($P < 0.01$) (Figure 3.11.a). However, the overall intensity is still markedly reduced by mucin irrespective of the salt concentration, although the relative intensity is still higher at elevated concentrations (Figure 3.11.b). Some compounds such as myrcene, limonene and α -pinene were not significantly affected by the addition of salt.

Current results suggest that the mucin-aroma interactions are not significantly affected by the addition of salt, suggesting that aroma-mucin interactions are more predominantly hydrophobic in nature.

3.3.8. Effect of potassium chloride on mucin viscosity

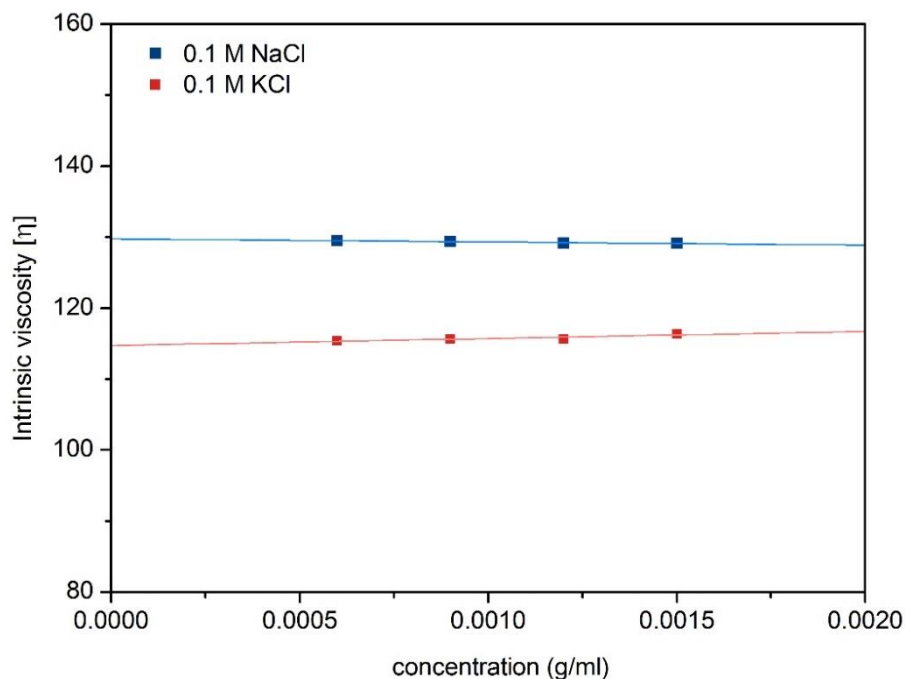


Figure 3.12. Comparative intrinsic viscosity of BSM in the presence of 0.1 M sodium and 0.1 M potassium chloride. Determined using the Solomon-Ciuta relation, extrapolated to zero concentration. The experiment was performed using the capillary viscometer at 20.0 °C.

Potassium chloride (KCl) is one of the lead alternatives to reducing dietary intake of sodium chloride (NaCl). However, it has been associated with an increase in a bitter or metallic taste. Here, we identified differences in the intrinsic viscosity of mucin between sodium and potassium chloride preparations, suggested to play a role in aroma perception.

Differences between the effects of sodium and potassium chloride on the solution structure of BSM were investigated by SV and Viscometry. No significant differences were observed by SV (data not shown), however a decrease was observed in the intrinsic viscosity of mucin in the presence

of KCl (Figure 3.12.). This may be attributed to an increased tendency of mucin to precipitate in the presence of K^+ ions, which are more reactive than in Na^+ ions, according to the Hofmeister series (Baldwin, 1996).

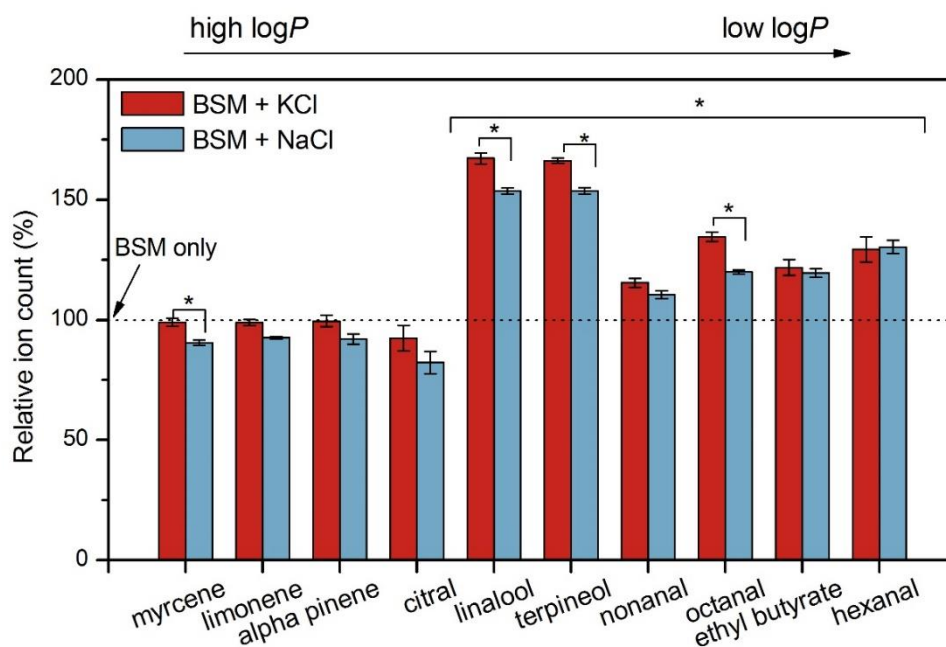


Figure 3.13. GC-MS results showing the relative effect of 0.1 M NaCl and 0.1 M KCl on the release of aroma compounds from mucin solutions. Values are expressed as mean \pm SD (n = 3).

Viscosity results were accompanied by headspace concentration analysis of aroma compounds present in the orange drink (Figure 3.13.). Results suggest that more hydrophobic compounds ($\log P$), are less affected by changes in the ionic strength, although sodium appeared to generally reduce their relative intensity more than potassium. Conversely, the relative headspace intensity of more hydrophilic compounds was significantly increased ($P < 0.05$), especially for compounds containing a hydroxyl group i.e. linalool and terpineol.

Overall, it was found that aroma intensity was higher in the presence of potassium chloride, which may be related to the higher reactivity of potassium, altering native mucin structure and reducing the mucin viscosity, although further experiments are needed to justify the current findings.

A previous study has shown that potassium decreased the viscosity of hog gastric mucin in non-linear stages. For instance, at low concentrations (0.05 M KCl), the viscosity of gastric mucus dropped by approximately 35 % and remained the same until the concentrations of KCl exceeded 0.5 M, after which it dropped again and plateaued (Snary and Allen, 1971). Another similar study revealed that the effect of NaCl on bovine gallbladder mucin viscosity has a biphasic effect where the addition of 0.2 M NaCl caused a gradual decrease in the viscosity until 0.5 M, but after it was found that further addition of salt caused an increase in mucin viscosity (Smith et al., 1989).

3.3.9. Effect of NaCl ionic strength on human salivary α -amylase

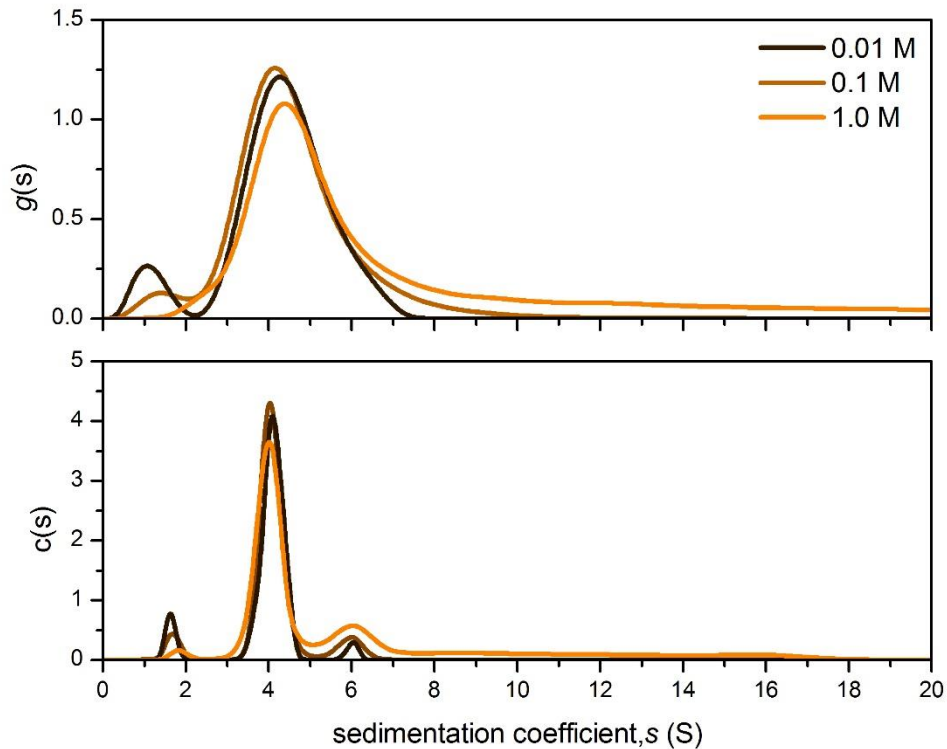


Figure 3.14. Sedimentation velocity, $g(s)$ and $c(s)$ analyses of HSA showing the sedimentation coefficient distributions of 1.0 mg/ml HSA at different NaCl concentrations (b). Run at 20.0 °C at 40, 000 rpm in PBS buffer (pH 7.0).

Changes in the sedimentation coefficient distribution of HSA at different ionic strengths (NaCl) are shown in Figure 3.14. Unlike mucin, which is a random coil, α -amylase is a symmetric globular protein, in which non-ideality affects are lower. But in the same way as mucin, it was found that an increase in the ionic strength leads to an apparent increase in the higher S components and a decrease in the smaller ~ 0 -2 S components.

However, especially for the lower S species, these apparent changes in the sedimentation coefficient may also be related to the higher solvent density which can also affect sedimentation through primary or secondary charge effects. This occurs when the macromolecule sediments under the centrifugal field but the counter-ions lagging behind are generating an electrostatic force which lowers the sedimentation force of the small particles (Fujita 1975; Svedberg and Pedersen, 1940 in Ralston, 2004).

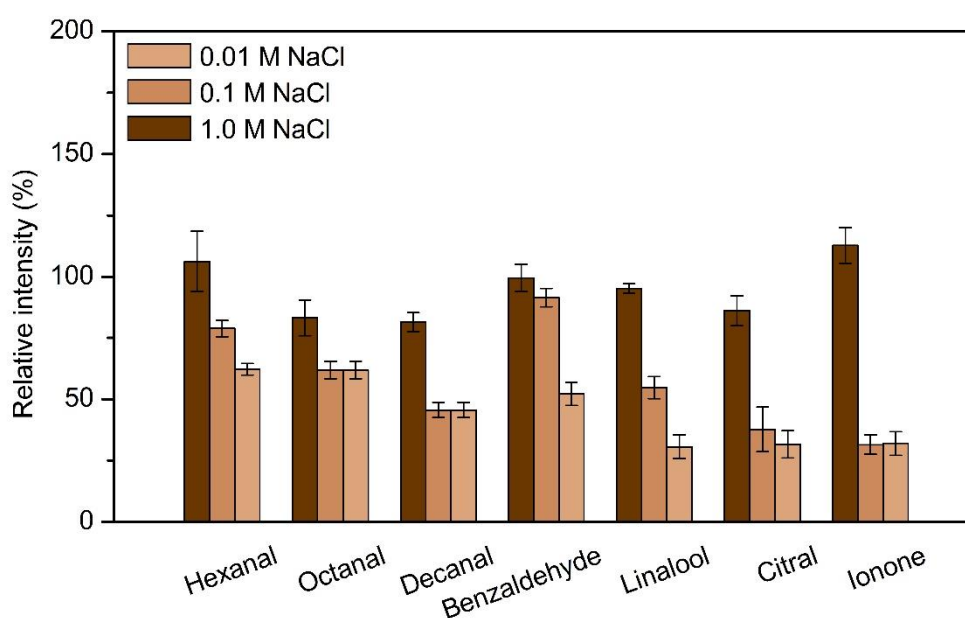


Figure 3.15. GC-MS results showing the effect of NaCl concentration on the release of volatile aroma compounds in the presence of HSA (1.0 mg/ml). Values are expressed as mean \pm SD (n = 3).

The headspace concentrations of the aroma compounds released from orange squash solutions/ α -amylase solutions were evaluated at different salt concentrations (Figure 3.15.). Results suggest significant salting out effects and reduction of amylase-aroma binding. At low salt concentrations

(0.01M and 0.1M), the headspace intensity is significantly reduced by the enzyme (10-60%). However, protein-aroma interactions were significantly lowered by the addition of salt (1.0M) to values close to that of the 1.0M solvent, suggesting that the release from α -amylase solutions is highly affected by changes in the ionic strength compared to submaxillary mucin.

3.3.10. General Discussion

Below pH 7.0, which is the pH of the vast majority of foods, the ionisable amino acids at the protein surface lead to unfolding and disruption of hydrogen bonds. The effects of pH are stronger as it drops below the isoelectric point (pI) of proteins. The two HSA isozymes have a pI of pH 6.0 and 6.9 respectively (Takeuchi et al., 1975). Therefore, at a pH lower than 6, the protein rapidly loses its structure, also indicated by the SV analysis. However, in the case of submaxillary mucin which has a pI of ~ 3 , pH effects are milder and only result in minor structural effects, accompanied by an increase in its tendency to aggregate. This because mucins have a low pH dependant negative charge given by the sialic acidic groups (Dodd et al., 1998).

The concentrations of salt can also affect their structure, thereby affecting their native function (Dominy et al., 2002). Mucin conformational changes are observed at elevated concentrations of sodium chloride. The 'R' ratio of the concentration dependence 'Gralen' parameter k_s , and intrinsic viscosity $[\eta]$, suggested changes to more elongated structures at higher ionic strength. It is suggested that these changes are, at least in part,

responsible for the minor changes observed in the intensity of volatile aroma compounds.

SV was also used to evaluate changes in the sedimentation coefficient distribution of HSA. Although its distribution did not change significantly as a function of salt concentration, being a globular protein, the interactions between the aroma compounds and HSA were significantly reduced by the addition of salt.

3.4. Conclusion

The study showed that bovine submaxillary mucin is partly similar to mucins from other sources (Harding, 1989), having a much more compact structure and lower molecular weight. Having a lower degree of glycosylation (Tsuiki et al., 1961), as opposed to gastric or intestinal mucins (Schömig et al., 2016), the hydrodynamic analysis suggested aggregation and conformational changes at low pH and high ionic strength. These changes correspond to a higher release of flavour but only at pH and ionic strength extremes (pH 3 and 1.0M NaCl). The higher ionic strength was shown to extend the conformation of mucin, the conformation α -amylase remains affected. Charge shielding can be regarded as an effective mechanism in the reduction of protein-aroma interactions, but less effective for bulkier mucin structures, which favour hydrophobic aroma-mucin interactions.

Therefore, the interactions between aroma compounds and the two salivary glycoproteins differ slightly. For mucins, the interactions appear to be more hydrophobic in nature, not being significantly affected by changes in the ionic strength and pH (although the release is higher at pH 3 through mild aggregation/denaturation). However, for α -amylase, the interactions appear more hydrophilic in nature, although pH and salt changes also led to significant reductions in the interaction of hydrophobic compounds (possibly through denaturation and salting out). These differences are important to consider during product reformulation in order to address any of the imbalances caused by the specific interactions with the different proteins.

4. Chapter 4: A hydrodynamic study of human saliva. Saliva-food interactions and development of artificial saliva

4.1. Introduction

Saliva is an inevitable ingredient that influences the processing and uptake of flavour compounds in the oral cavity. However, current methods for the analysis of saliva (e.g. *Salimetrics*, *AlphaLISA*, *Bicinchoninic acid assay* or *GBO Saliva Quantification kit*) are limited in scope and often cannot be used to analyse the interaction products with food (Luther et al., 2010; Topkas et al., 2012). *In-vivo* and *ex-vivo* trials are usually employed but these are not always available during product development. Therefore it becomes difficult to predict how food ingredients interact with saliva during oral processing. Either ethical considerations or limited shelf life, the use of *ex-vivo* saliva is also limited, pushing many researchers to identify alternative ways to analyse the food bolus, for instance by developing analogues for human saliva.

Unstimulated saliva represents a steady and continuous secretion forming the salivary film on the oral epithelium. Under stimulation, there is a marked increase in the concentration of salivary salts, enzymes and other proteins, which change the physiochemical characteristics of saliva. For instance, during food stimulation the contribution made by parotid saliva increases from 30 % to 70 % (Proctor and Carpenter, 2014; Sas and Dawes, 1997). Low molecular weight proline rich proteins (PRP's) and

salivary α -amylase are two major proteins produced by the parotid gland during stimulation (Gibbins and Carpenter, 2012; Mandel et al., 2010). Their increased output is suggested to affect the native structure and function (viscosity, lubrication) of saliva.

Previous studies have shown that salivary proteins interact with polyphenols, which is believed to contribute to the perception of astringency (Baxter et al., 1997; Bennick, 2002; Ramos-Pineda et al., 2019). Due to the high polyphenol content in tea and its antioxidative functions, regular intake of polyphenols and tannins from tea has long been associated with a healthier lifestyle (Cooper, 2012). Green tea polyphenol extract is composed of epicatechin, epicatechin gallate and epigallocatechin gallate (EGCG) (Joiner et al., 2004). Over 50 % of the polyphenols in green tea are EGCG, which were previously reported to have biological effects, including protein inhibition. In addition to its impact on mouthfeel and antioxidative abilities, EGCG has also been considered for the treatment of diabetes and obesity (Lee et al., 2011; Legeay et al., 2015).

In the first section of this chapter, sedimentation velocity (SV) is proposed as an alternative *ex-vivo* tool for probing interactions between the relatively simple food system-green tea and human saliva. Human saliva fingerprinting is based on the sedimentation coefficient distribution, directly derived by fitting the Lamm equation in SEDFIT (Dam and Schuck, 2004b, 2005). GC-MS was used to assess interactions between saliva and green tea in order to investigate their effect on the release of aroma. This contributes to further understanding of how such interactions may affect

aroma delivery from green tea and help to suggest new means of improving the flavour profile in flavoured beverages.

In the second part of the study, an alternative composition of artificial saliva is proposed based on the sedimentation coefficient distribution and the relative concentration of the components in saliva. The effectiveness of the artificial saliva was compared against human sample for their abilities to release the aroma into the headspace. This was tested in the presence of real food (dilute orange squash), as well as a model food system (aroma suspension). GC-MS was used to analyse the relative concentrations of the aroma compounds released from the respective bolus and PCA analysis was used to identify which of the two protein constituents, α -amylase or submaxillary mucin, have a higher influence on the aroma released.

4.2. Materials and Methods

4.2.1. Samples

Bovine submaxillary mucin (type I-S, M3895), porcine pancreatic α -amylase (type VI-B, A3176), human salivary α -amylase (type IX-A, A0521) and the aroma compounds were purchased from Sigma Aldrich (Dorset, UK). Epigallocatechin gallate (PHR1333) was also purchased from Sigma (Poole, UK). The 0.1 M phosphate buffered saline (PBS) was made according to Green (1933), (Fisher Scientific, UK). Milli-Q purified water was used throughout the sample preparation.

4.2.2. Pooled saliva

Pooled stimulated (SS) and unstimulated (US) saliva samples were kindly provided by Dr. Pavel Gershkovich and co-workers from the Centre for Biomolecular Sciences, University of Nottingham. All samples were collected in accordance with the ethical approval R12122013, Faculty of Medicine and Health Sciences Research Ethics Committee, Queens Medical Centre, Nottingham University Hospitals. Participation was voluntary and informed written consent was obtained. All data were held in accordance with the Data Protection Act. Loading and unloading of samples was carried out in a Level 2 microbiological safety cabinet. The samples have been centrifuged at 6,000 RCF (g) to remove the presence of large contaminants such as insoluble mucus, bacteria, dead cells and stored at -80 °C until further use.

4.2.3. Green tea

*Twinings*TM Pure Green Tea (F09542) was purchased from the local supermarket. Samples were brewed according to the manufacturer, in a temperature-controlled environment. The samples were mixed with saliva in a 1:1 ratio when the temperature of the brew cooled down to 60.0 °C. The GC-MS analysis was performed in triplicates.

4.2.4. Orange squash

Robinson's sugar free orange squash was purchased from the local supermarket. Final samples used for the GC analysis were diluted according to the manufacturer, one part concentrate and four parts water. The dilute squash samples were mixed with the saliva solutions in a 1:1 ratio prior to the GC-MS analysis.

4.2.5. Sedimentation Velocity (SV)

Experiments were performed at 20.0 °C using the Optima XL-I analytical ultracentrifuge (Beckman, Palo Alto, USA) equipped with Rayleigh interference as described previously (section 2.1.), along with Absorbance mode, and run at 40,000 rpm (120,000 g). Scans were taken at 2 minutes intervals. The results were analysed in SEDFIT using the $g(s)$ and the diffusion corrected $c(s)$ processing methods using an average partial specific volume of 0.7 ml/g, assuming that the whole sample consists of proteins with the same partial specific volume.

4.2.6. Differential Refractometer

The Atago DD-7 differential refractometer (Jencons Scientific, UK) was used to measure the concentration of saliva. A refractive index increment (dn/dc) value of 0.181 ml/g was employed for estimating total protein concentration, corresponding to that of mucin glycoproteins and α -amylase (Theisen, 1999).

4.2.7. Capillary viscometry

Flow times of solvent (t_0) and solutions (t_s) were measured using the semi-automated (Schott Geräte, Hofheim, Germany) U-tube Ostwald capillary viscometer as discussed previously (section 2.5.). Concentrations of saliva were not corrected for solution density and η_s/η_0 was assumed equal to t_s/t_0 . To a reasonable approximation, relative viscosity also corresponds to the dynamic viscosity (Harding, 1997).

4.2.8. Gas Chromatography-Mass Spectrometry (GC-MS)

The Trace 1300 series Gas Chromatograph coupled with the single-quadrupole mass spectrometer (Thermo Fisher Scientific, Hemel Hempstead, UK) was used as discussed in section 2.7. Saliva control samples were run in parallel and values are subtracted from the mixture.

4.3. Results and Discussion

4.3.1. Sedimentation fingerprinting of human saliva

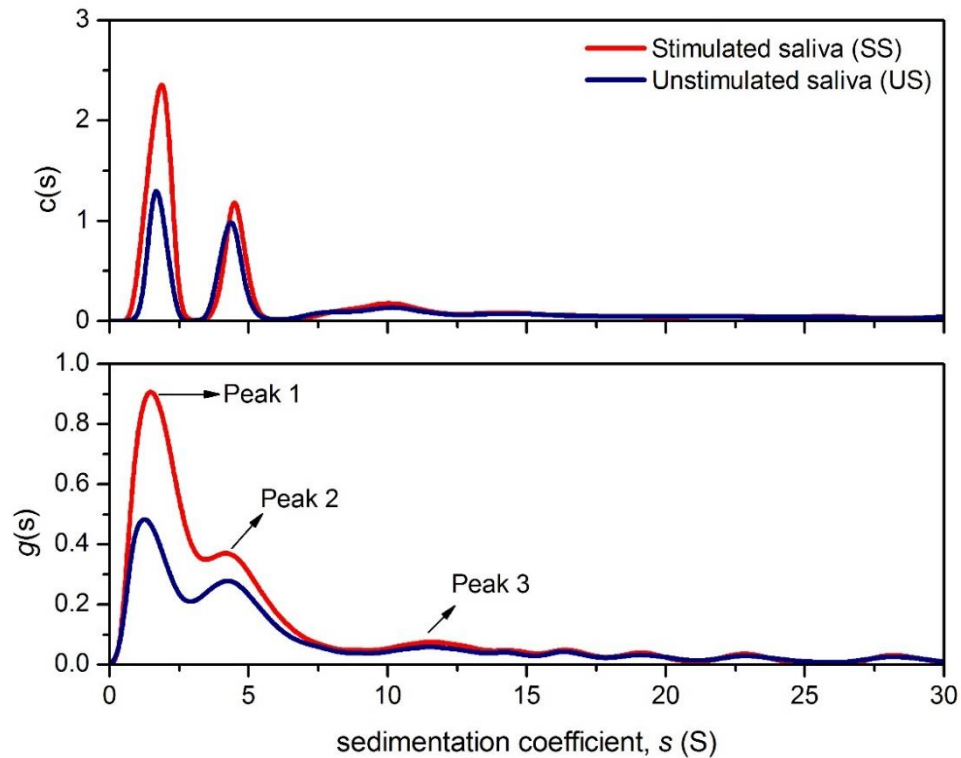


Figure 4.1. Sedimentation velocity, $g(s)$ and $c(s)$ analysis for pooled saliva. The plots show the sedimentation coefficient distributions for unstimulated (US) and stimulated (SS) samples. Rotor speed: 40,000 rpm (120,000 g), 20.0 °C.

Sedimentation coefficient distributions for human US and SS saliva were analysed by $g(s)$ and the diffusion deconvoluted model $c(s)$ (Dam and Schuck, 2004). The experiment confirmed the presence of three major components (Figure 4.1.). As seen in the previous chapter, the values of the apparent sedimentation coefficients for the first and second peaks correspond to a mixture of mucin (4S) and α -amylase respectively ($\sim 1.5S$

and 4S), while the sedimentation coefficient of SIgA (11S) is commensurate with previous established reports (Björk and Lindh, 1974; Mach et al., 1969).

Total protein concentration was approximated using the differential refractometer. Each individual fraction was then calculated in terms of the proportion of each peak using the integration tool in SEDFIT and are presented in Table 4.1. The relative viscosities (t_s/t_0) of SS and US samples were calculated against the 0.1 M PBS buffer.

Table 4.1. Relative viscosity and protein concentrations for pooled unstimulated (US) and stimulated (SS) human saliva. Data points are shown as mean \pm SD, (n=3).

Saliva	Total conc. (mg/ml)	Relative viscosity	Peak 1	Peak 2	Peak 3	Other
US	2.36 (± 0.09)	1.045	0.85 (± 0.03)	0.94 (± 0.05)	0.28 (± 0.02)	0.28 (± 0.03)
SS	3.41 (± 0.15)	1.035	1.91 (± 0.05)	0.95 (± 0.05)	0.28 (± 0.05)	0.19 (± 0.07)

It was shown that the SS sample had a higher relative protein concentration than US (Table 4.1.). From the SV trace, it is indicated that Peak 1 (1.5S), is largely responsible for the higher concentration of SS saliva while the concentration of the second peak remained constant at \sim 1.0 mg/ml.

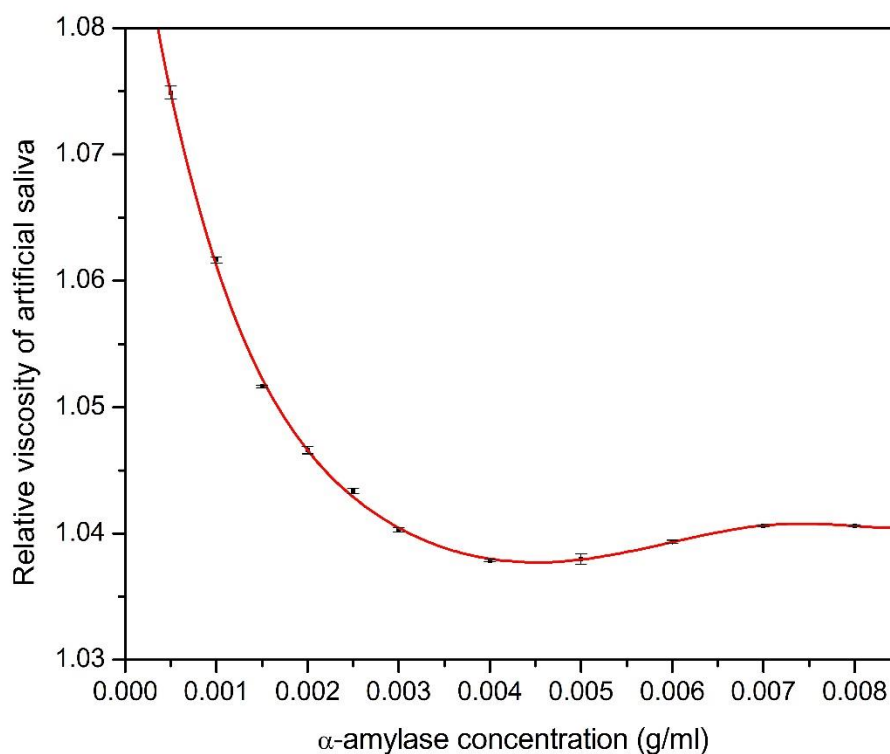


Figure 4.2. Relative viscosity showing the quantitative effect of α -amylase added to BSM (1.0 mg/ml) in 0.1M phosphate buffer saline. The polynomial fit is based on 11 data points derived from individual mixtures.

Results in Figure 4.2. show that there is a decrease in the relative viscosity of BSM upon increasing the α -amylase concentration. The concentration of BSM remained constant at 1.0 mg/ml while the concentration of porcine pancreatic α -amylase increased from 0.5 mg/ml to 8.0 mg/ml, to represent physiological ranges found in the human saliva, with the average concentration being estimated at 2.64 ± 1.8 mg/ml (Mandel et al., 2010).

The mucin content in pooled saliva largely corresponds to MUC7 type, since MUC5B types are known to gel and have likely been removed during preparative centrifugation steps, due to their very large molecular size (2-50 MDa). Consequently, the viscosity results obtained in this study may

differ from the true viscosity of the *in-vivo* saliva. Though, results are in agreement with other studies showing a lower viscosity for SS. This is suggested to be attributed to the higher proportion of the peak 1 components from the SV data, such as low molecular weight fractions, PRPs and α -amylase, which have very low intrinsic viscosity (globular conformation), therefore lowering the dynamic viscosity the system (Figure 4.2.) (Sas and Dawes, 1997; Dodds et al., 2015).

4.3.2. Saliva interactions with green tea

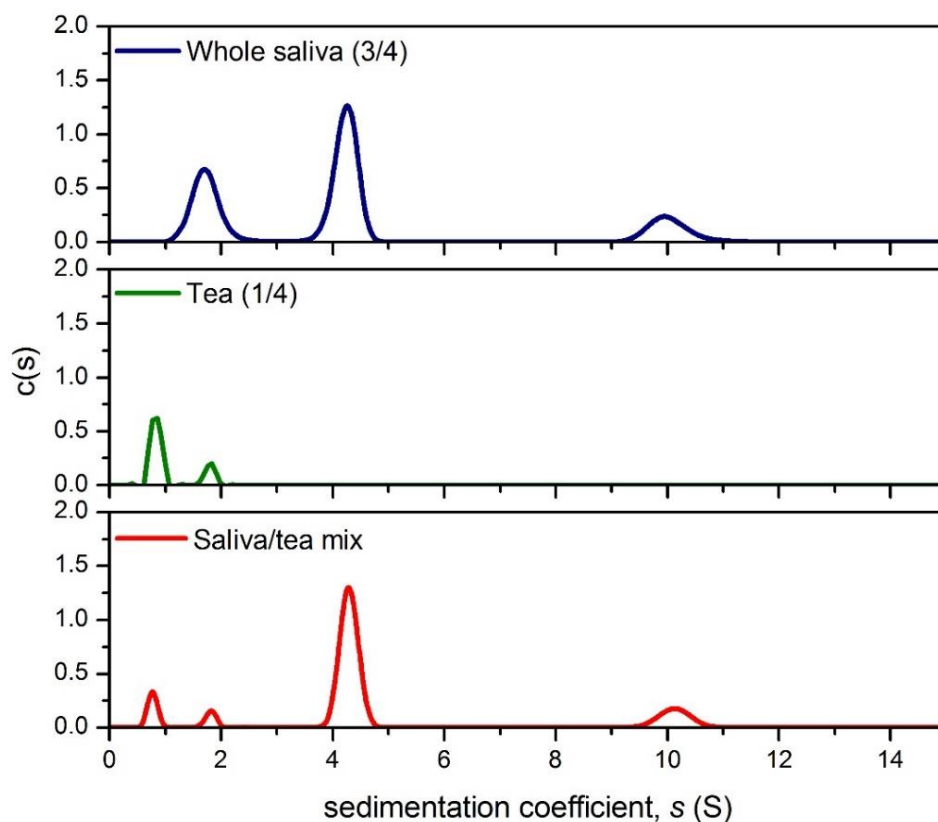


Figure 4.3. Sedimentation velocity, $c(s)$ analysis showing the sedimentation coefficient distributions for saliva (blue line), green tea (green) and the result of their interaction (red). Rotor speed 40, 000 rpm (120, 000 g), 20.0 °C.

The next step was to characterize the interactions between saliva and green tea (Figure 4.3.). To increase resolution, the mixture of green tea and human saliva is analysed by the $c(s)$ method, with distributions recorded using interference optics. While the saliva sample shows the presence of the three characteristic peaks observed previously, the green tea sample (diluted) resolved the presence of minor macromolecular components, at $\sim 1S$ and $\sim 2S$.

In the mixture, the distribution of sedimentation coefficients in saliva resulted in complete loss of peak 1. This indicates a direct interaction between green tea and the components of peak 1. By contrast, there are no significant changes in the distribution of the second and third peaks.

To study the effect of this interaction on aroma development, a GC-MS experiment was performed to analyse changes in aroma partitioning upon mixing with saliva (Figure 4.4.). A 1:1 volume ratio was employed, corresponding to 5.0 ml of saliva and 5.0 ml of tea. The green tea control has also been diluted 1:1 with water, to account for any changes due to dilution.

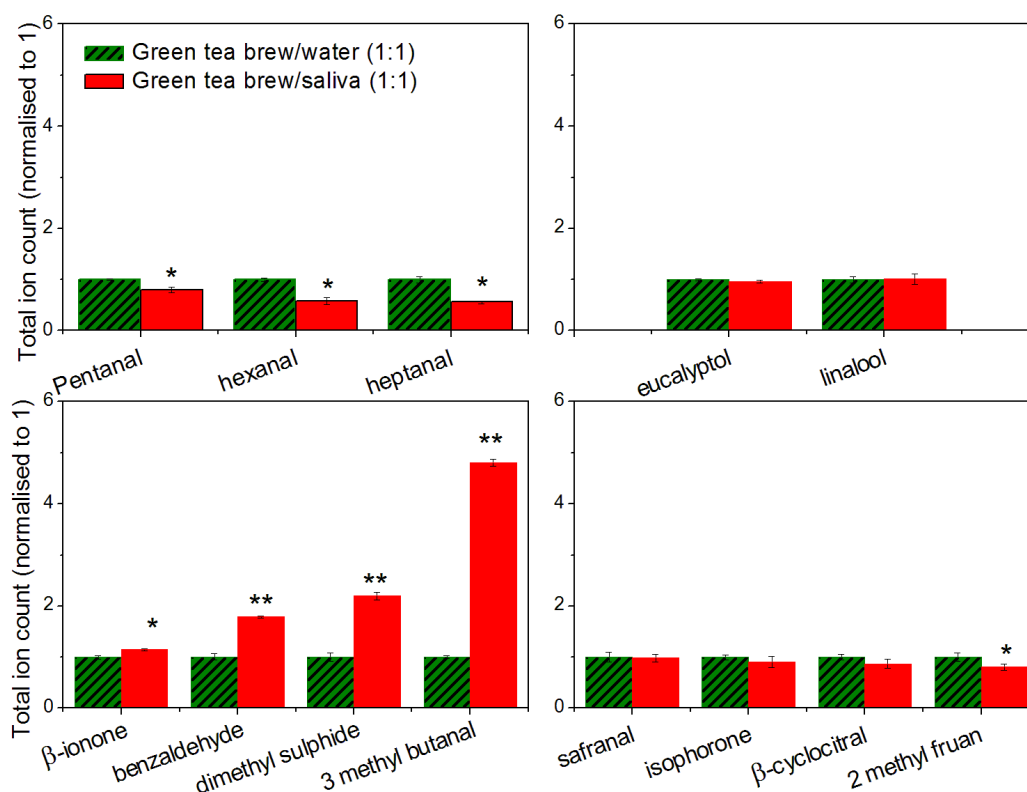


Figure 4.4. Effect of green tea on the release of aroma compounds from the whole saliva. The dashed green columns express the concentration of green tea aroma compounds, normalised to one unit, while the red columns represent the headspace concentration of the saliva-tea mixture relative to that of the green tea. The comparison is made by Tukey's post hoc test to calculate the *P*-values ($P < 0.01^{}$, $P < 0.05^{*}$). The data are shown as mean \pm SD, ($n=3$).**

Of the green tea aroma compounds the 13 most abundant compounds were quantified by GC-MS based on the signal to noise ratio detected. It was found that the addition of saliva had a significant effect on the partitioning of a number of volatile compounds. Although terpene alcohols such as eucalyptol and linalool showed no significant change in their

headspace concentration ($P>0.05$), there was a significant decrease in the relative abundance of linear aldehydes ($P<0.05$), such as pentanal, hexanal and heptanal. These effects are suggested to be attributed to Schiff base adduct formation between the N-terminal amino groups of salivary proteins and the carbonyl groups of the aldehydes (Godoy-Alcántar et al., 2005; San George and Hoberman, 1986).

A sharp increase in the relative intensity was detected for β -ionone, benzaldehyde, isovaleraldehyde and dimethyl sulphide ($P<0.01$). Dimethyl sulphide has been previously reported to be formed during heating of tea (Kiribuchi and Yamanishi, 1963), while the other compounds are known to be formed either by oxidative deamination of amino acids, or by carotenoid oxidation (Ho et al., 2015).

It was also revealed that oxidation of amino acids by tea quinones can produce characteristic odours such as isovaleraldehyde (3, methyl butanal) and isobutanal (Sanderson and Grahmann, 1973). In addition, quinone oxidation of β -carotene is converted to β -ionone, while other compounds including benzaldehyde, have been shown to be formed by the hydrolysis of glycosidic bound volatiles (Gui et al., 2015). In part, this is suggested to arise from the action of α -amylase, which itself is a glycoside hydrolase acting on α -glucoside bonds.

Other studies reported that catechin 3-gallates are potent inhibitors of α -glucosides, such as α -amylase (Yilmazer-Musa et al., 2012). As a result, it is suggested that EGCG promotes the release of these volatile compounds due to their affinity to bind the lower S proteins found in saliva such as enzymes and other low molecular weight proteins.

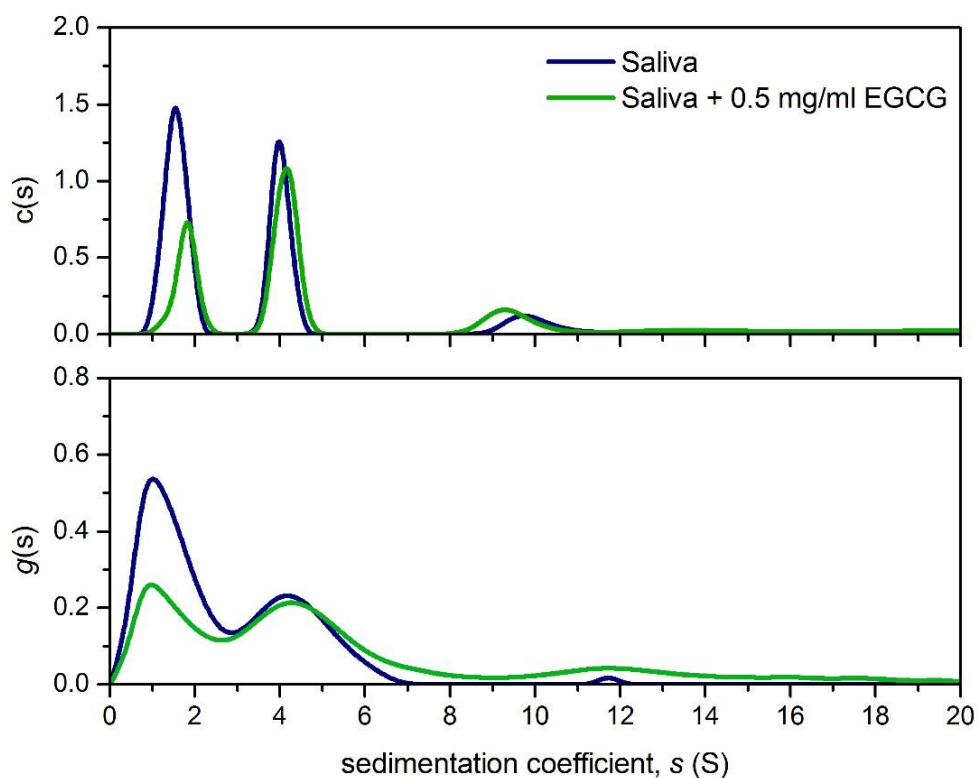


Figure 4.5. Sedimentation velocity, $g(s)$ and $c(s)$ analyses showing the sedimentation coefficient distributions for whole US saliva (blue line) and what happens upon the addition of epigallocatechin gallate (EGCG) (green line). Rotor speed: 40,000 rpm (120,000 g), 20.0 °C.

Next, an SV experiment was carried out to confirm the interaction with EGCG (Figure 4.5.). The experiment was performed using whole US saliva, to which 0.5 mg/ml epigallocatechin gallate (EGCG) was added (Figure 4.5.). The data confirmed a direct interaction between EGCG and Peak 1 components. In an analogous manner, this was validated by using artificial saliva, based on 1.0 mg/ml BSM and 1.0 mg/ml porcine pancreatic α -amylase (Figure 4.6.).

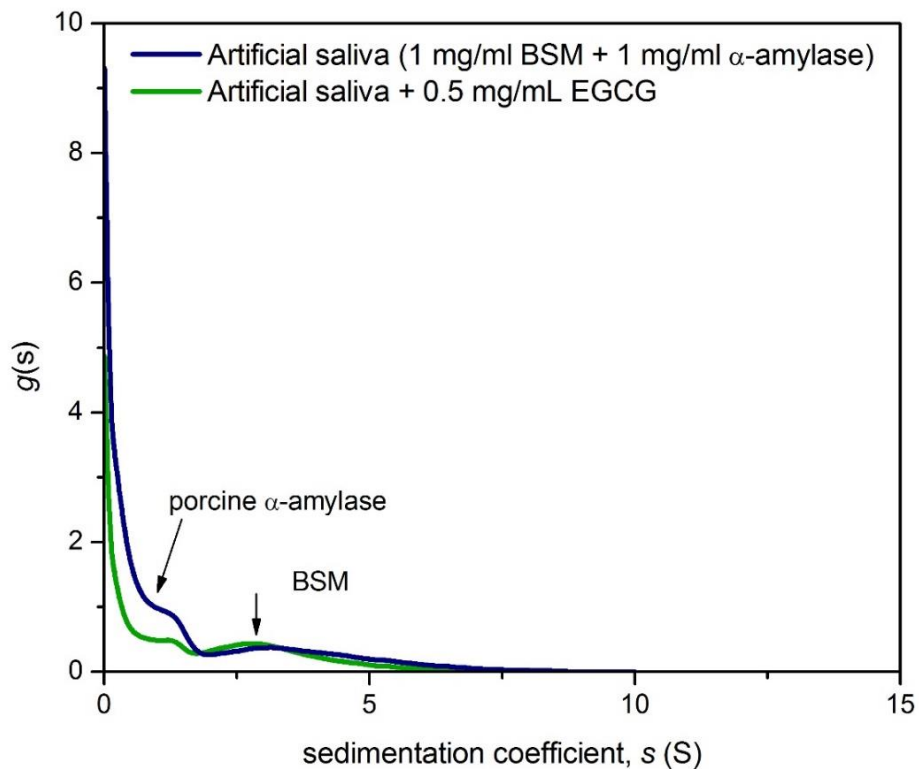


Figure 4.6. Sedimentation velocity, $g(s)$ distributions for artificial saliva (blue) before and after the addition of 0.5 mg/ml EGCG (green). Rotor speed: 40,000 rpm (120,000 g), 20.0 °C.

Based on the area under the curve, it was found that the concentration of porcine α -amylase has decreased by 47% upon EGCG addition, commensurate with our results from the real system. The effects of EGCG on the viscosity of saliva were further investigated (Figure 4.7.). The assay is based on five data points derived from separate solutions. Each solution had a constant concentration α -amylase (1.0 mg/ml) and BSM (1.0 mg/ml) and different EGCG concentrations were added into.

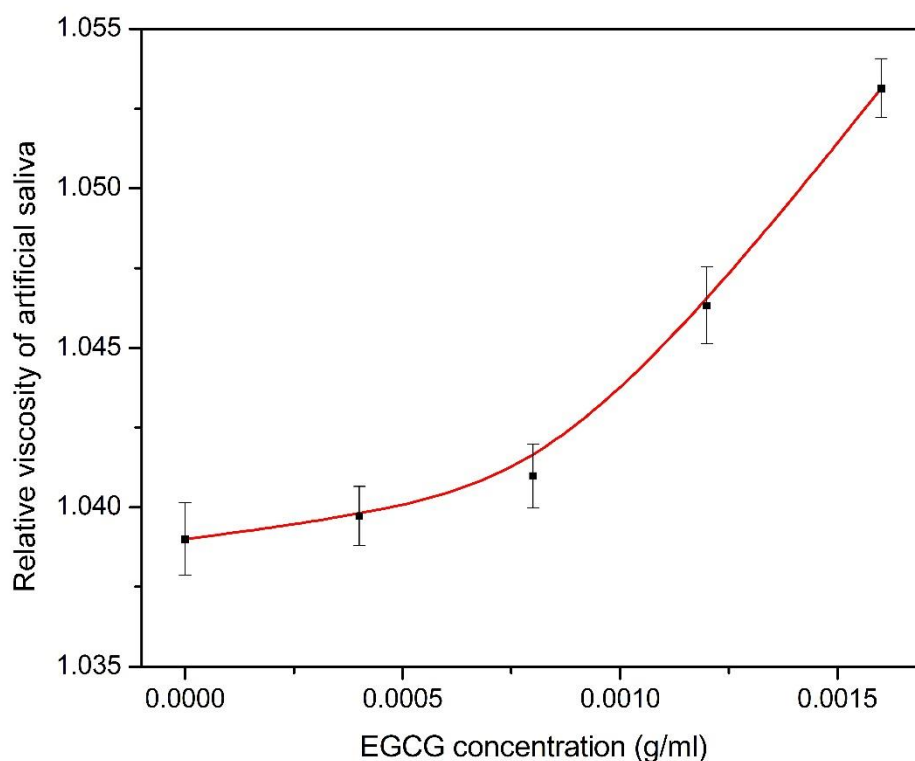


Figure 4.7. U tube relative viscosity analysis showing the quantitative effect of EGCG addition to artificial saliva in 0.1M phosphate buffer saline, pH 7.0.

It was found that increasing the concentration of EGCG resulted in a dose dependent increase in the viscosity of artificial saliva. This is thought to be related to lowering of the α -amylase concentration by EGCG, and from the increased friction resulting from its precipitation, which may also play a role in the astringent sensations perceived during tea consumption.

4.3.3. Validating the use of artificial saliva in flavour analysis

Table 4.2. Composition of artificial saliva: concentrations of ions and proteins.

Composition	Concentration
<i>Phosphate-buffered saline*</i>	0.1 M (pH 6.8)
<i>Calcium chloride</i>	0.1 mg/ml
<i>Mucin (BSM)</i>	1.0 mg/ml
<i>α-amylase</i>	2.0 mg/ml

*see Green (1993)

The next set of experiments are designed to develop and test an artificial saliva preparation based on mucin and α -amylase as the macromolecular constituents. The macromolecular concentration estimated previously was used to develop the composition of the artificial saliva (Table 4.2.).

The increase in the concentration of the 1.5S components in SS was suggested to be attributed to the increased production of low molecular weight proteins via parotid stimulation. Here, the artificial saliva was based on human salivary α -amylase (HSA) and bovine submaxillary mucin (BSM). CaCl_2 was also added as it is essential for enzymatic activity (Table 4.2.).

GC-MS was used to measure the aroma intensity in the presence of different preparations of artificial and real human saliva. Both model and

real foods (orange juice) were used to gain a deeper understanding of the effects of other food co-ingredients present in real food (i.e. citric acid, polyphenols, carbohydrate). Principal component analysis (PCA) was used to reduce the dimensionality of the data and explain the largest source of variance. The aim of the model food system, containing only a suspension of aroma compounds, was to investigate interactions solely attributed to the aroma compounds, excluding the effect of other ingredients found in the orange squash.

The PCA results for the model food (aroma suspension) suggest that the release profile is dependent significantly on the salivary composition, as indicated by principal component F1 explaining 87.19 % of the variance. As expected, it was shown that the release is higher in the absence of proteins (water) and gradually decreases as the system becomes more complex (Figure 4.8.). In addition, PCA results suggest that 12.04 % of the variance is due to more hydrophobic compounds, such as α -pinene and limonene, which increased in the presence of HSA, while the intensity of more hydrophilic compounds (linalool, menthol and menthone) is higher in the presence of BSM (Figure 4.8). Similar results have been reported in Chapter 3 and previously (Pagès-Hélary et al., 2014).

For the model food system, it was shown that the more complex the salivary composition, the more representative it is to human saliva with regards to aroma released. This was to be expected, although in the next experiment, aroma release was investigated from real food (orange squash), to study the influence of other co-ingredients present, such as citric acid, cellulose gum and orange pulp (Figure 4.9.).

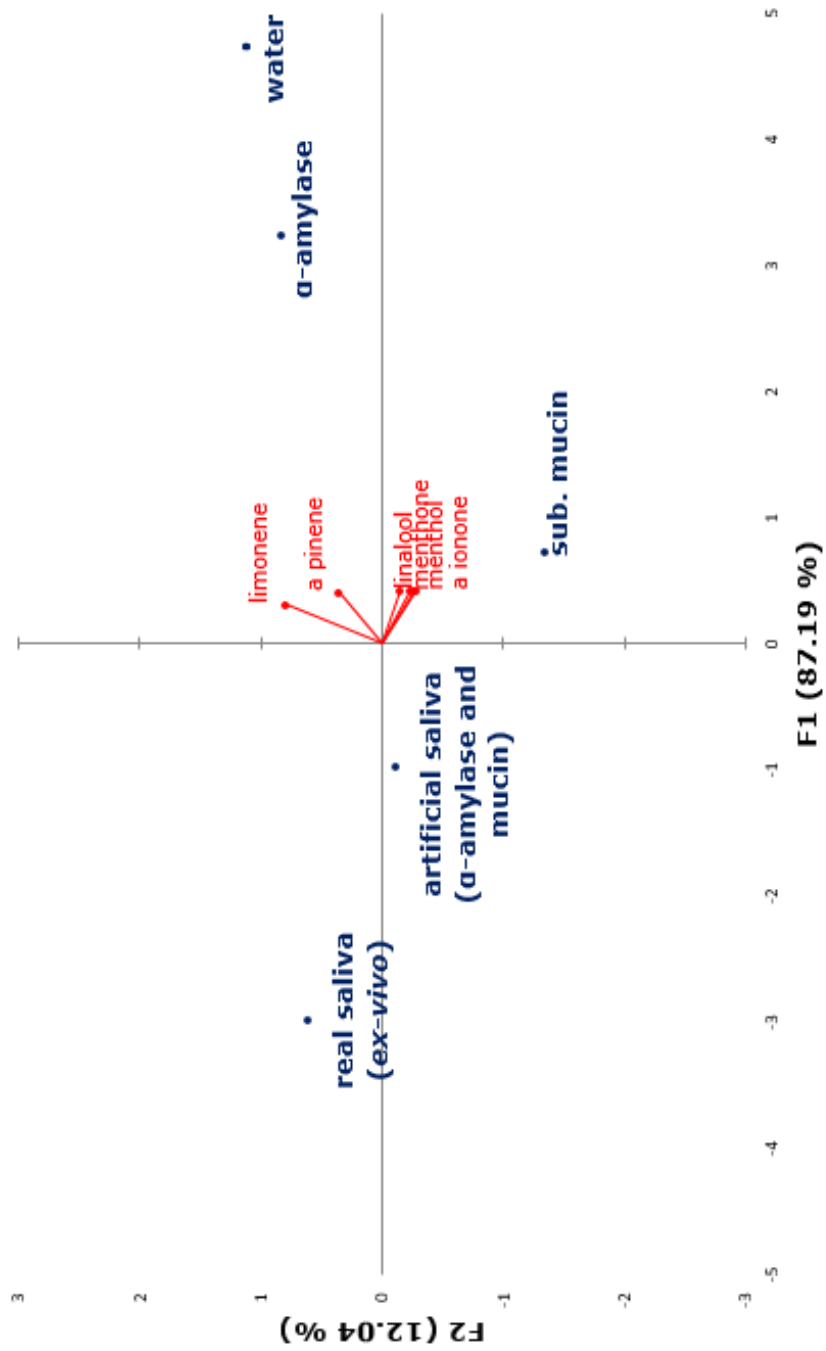


Figure 4.8. Principal component analysis bi-plot of aroma release from saliva systems in the presence of model aroma suspension (n=3).

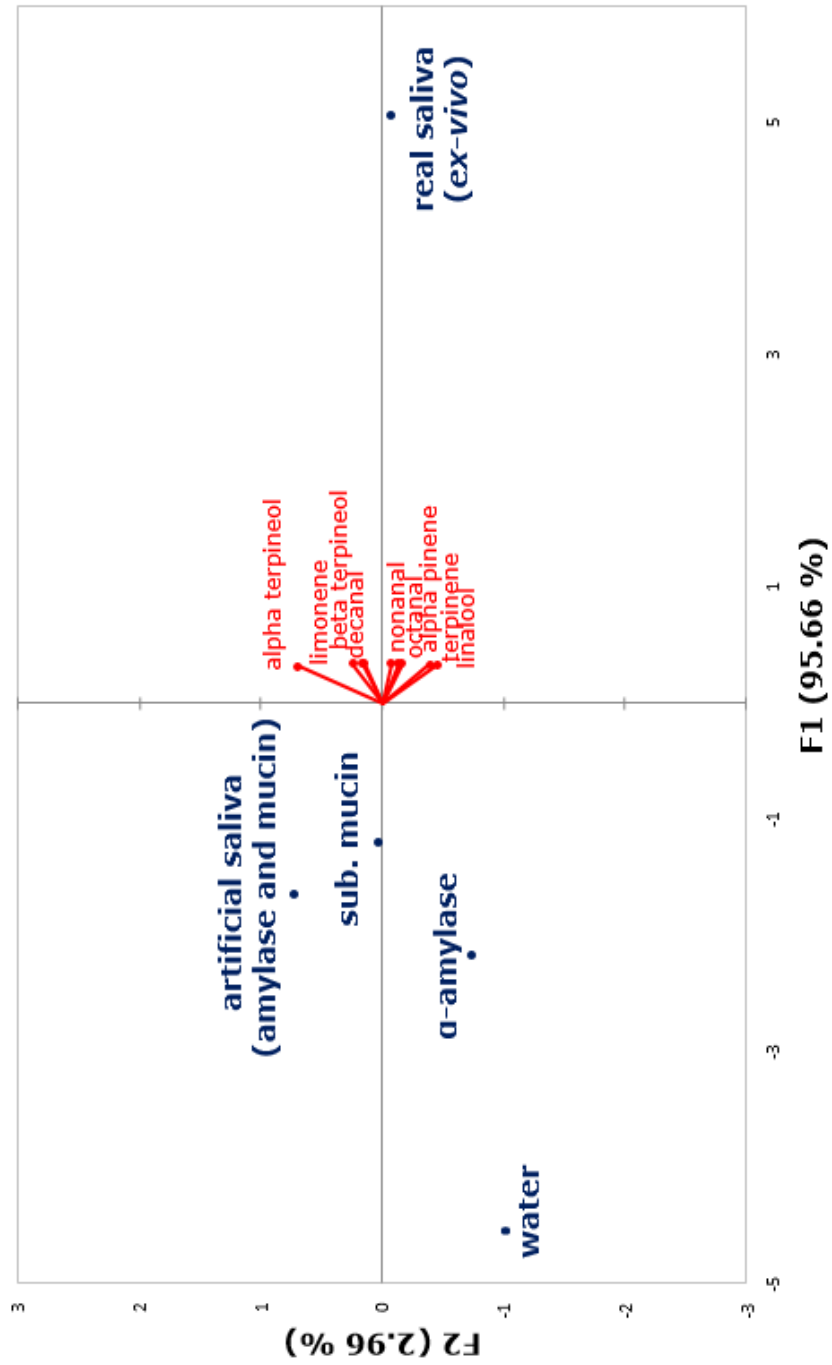


Figure 4.9. Principal component analysis bi-plot of aroma release from saliva systems in the presence of orange squash (n=3).

A significant interaction involving the other squash co-ingredients was observed, different from the model food system. 94.6% of the variance is explained by PC1, indicating the artificial saliva system is significantly different human *ex-vivo* saliva. It is suggested that part of these differences are attributed to a lower pH of the orange drink (pH 4) which causes the precipitation of proteins and other unglycosylated salivary proteins, not present in the artificial saliva composition.

Some of the major differences in the magnitude of the release of aroma compounds between the real and model food are illustrated in Figure 4.10. For real food (orange squash), there were no significant differences between mucin or α -amylase, suggesting their effects are inhibited by the product co-ingredients. However, in the presence of the model aroma suspension, the intensity was significantly lower in the presence mucin.

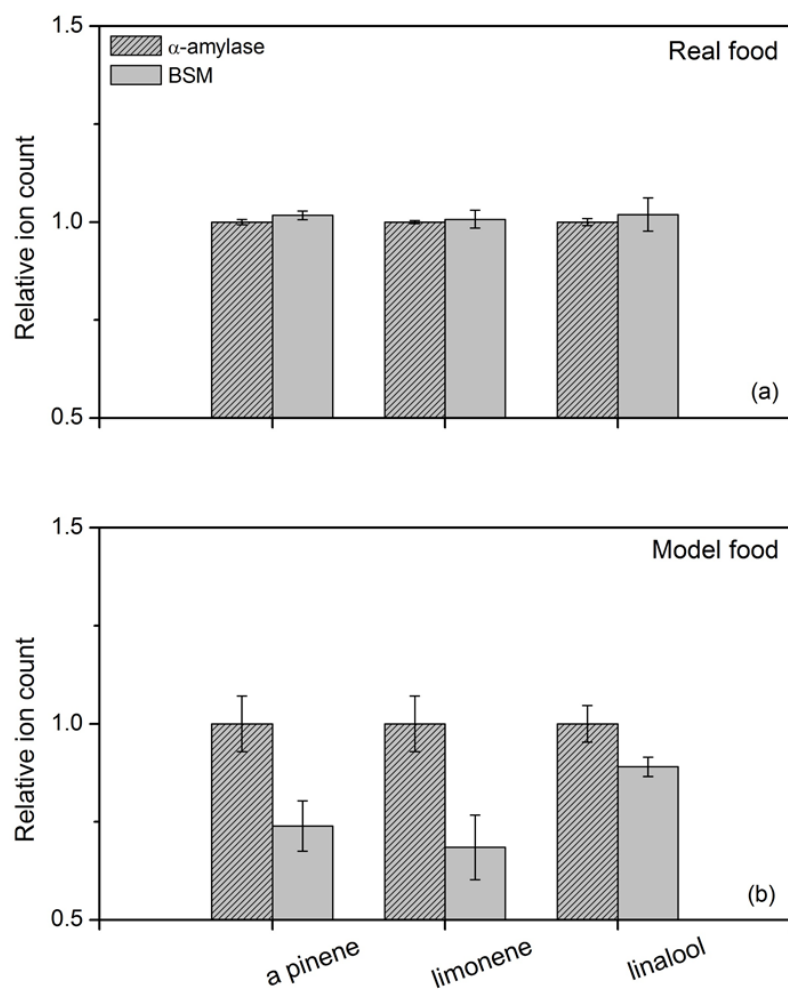


Figure 4.10. Relative differences in the release of aroma compounds from α -amylase and mucin solutions in the presence of real (a) and model food (b). The data are shown as mean \pm SD, (n=3).

4.3.4. General Discussion

There are limited published reports on the hydrodynamic properties and concentrations of mucin, α -amylase and other proteins in saliva, partly due to different collection protocols or different quantification techniques. Although it is difficult to compare reported values, the present results are in agreement with other findings (Björk and Lindh, 1974; Kejriwal et al., 2014; Mach et al., 1969).

The viscosity reported by other groups varies depending on the type of instrumentation and post collection protocols. However, lower protein concentration in the stimulated samples (SS) is consistent with the majority of findings (Gittings et al., 2015; Humphrey and Williamson, 2001), and this has been agreed to result from the increased output of the parotid gland, secreting more enzymes and other low molecular weight proteins. Our results have shown that by increasing the α -amylase concentration, the viscosity of saliva is reduced, attributed to the lower intrinsic viscosity of α -amylase.

The sedimentation coefficient for Peak 2 ($\sim 4S$) is similar to BSM which was shown to have a weight average molecular weight of $\sim 500-700$ kDa, in agreement with previous findings for MUC7 type mucins (Mehrotra et al., 1998). Secretory IgA (SIgA) is commonly found in saliva, and plays a critical role in mucosal immunity (Hurlimann and Zuber, 1968). It exists as a dimer, joined together by a J-protein domain and is known to have an $s_{20,w}$ value of 11S and a molecular weight of 385 kDa (Mach et al., 1969; Björk and Lindh, 1974), which is consistent with the current findings.

Using a combination of SV-AUC and GC-MS, it was first shown that the interactions between green tea and saliva are key in the formation of the characteristic aroma profile. This has been attributed to an interaction between saliva with EGCG, one of the most abundant green tea polyphenols. In other studies, this interaction has been studied by X-Ray crystallography and shown that the three hydroxyl groups of the epigallo and gallate groups form specific hydrogen bonds with the amino residues of α -amylase (Lee et al., 2011). In addition, the degree of binding has been reported to be correlated with the number of galloyl rings on the polyphenol chains (Narukawa et al., 2010).

Currently, the main proteins used in the development of artificial saliva are pig gastric mucin (PGM), bovine submaxillary mucin (BSM) and a wide range of α -amylases (as in Ruth et al., 1995). As great differences exist between these macromolecules, there is a need to develop a more standardised artificial saliva composition for the analysis of food.

The accessibility of readily available lyophilised powders has been shown to bridge some of the gaps between *ex-vivo* (saliva) and *in-vitro* systems. However, their different molecular composition can have an effect on the analysis. For example, as opposed to submaxillary mucins, the chemical and physical properties of PGM differs significantly. For example, they contain a higher proportion of carbohydrate (~90%), along with a number of on Willebrand factor type D-domains, which contain a larger proportion of cysteine and other charged amino acid residues, facilitating mucus gelation during acidic conditions. This is the reason why gastric mucins are designed to protect the stomach during digestion (Bansil and Turner, 2018; Madsen et al., 2016).

By contrast, bovine submaxillary mucins (BSM) have a much lower carbohydrate content (~60 %) and a higher proportion of negatively charged sialic acids localised both centrally and in terminal regions of the polypeptide chain (Frenkel and Ribbeck, 2015; Liao et al., 2016). In addition, commercial PGM preparations contain non mucin protein fractions, such as bound albumin, which can have a different effect on the biophysical functionality of mucin solutions (Sandberg et al., 2009).

While some studies reported no differences with regard to the release of flavour from model solutions containing PGM or BSM (Friel and Taylor, 2001), the properties and co-ingredients of the food can interact differently with the seemingly related proteins. For example, sigma porcine pancreatic amylase (A3176) contains high amounts of lactose, also seen in the small (<0.5S) species of the sedimentation coefficient distribution (Figure 4.6.) and this may also interfere with the analysis.

Some more complex artificial saliva compositions are reported in the literature. They include a mixture of distilled water, potassium phosphate, sodium chloride, potassium chloride, calcium chloride, sodium nitrate, sodium bicarbonate, mucin and α -amylase (van Ruth et al., 2001; Van Ruth and Roozen, 2000). However, the levels of carbonic acid in resting saliva remains constant around 1.3 mM/l, corresponding to 0.039 mg/ml. In stimulated saliva, the bicarbonate ion concentration depends on the flow rate which depends on the type of food stimulus triggering the secretion of carbonic anhydrase VI by the parotid and submaxillary glands (Llena-Puy, 2006).

4.4. Conclusion

SV can be a useful tool for testing the interactions between human saliva and simple systems, such as green tea. The analysis allowed for the identification of interacting species from the sedimentation coefficient distribution. It was revealed that the reaction between green tea and saliva leads to the formation of a characteristic aroma profile, such as a decrease in linear aldehydes and an increase in the concentration of β -ionone, benzaldehyde and isovaleraldehyde.

The SV data for pooled saliva was also used to estimate the relative concentrations of α -amylase and submaxillary mucin, used to develop an artificial saliva system, as a platform for aroma analysis. It is suggested that the artificial system proposed can be useful in analysing flavour-bolus interactions, but only in unrealistic model systems, where there is a cumulative effect of α -amylase and submaxillary mucin, shown to mimic the *ex-vivo* saliva (similar to Van Ruth and Roozen, 2000). However, it was shown that in real food systems, the use of artificial saliva is not valid therefore rendering the need to perform *in-vivo* or *ex-vivo* trials.

5. Chapter 5: Biopolymer mucoadhesives: development of an enzymatically controlled mucoadhesive polymer

5.1. Introduction

Mucoadhesion has extensively been a subject of research for the food industry and academia in the recent years (Cook et al., 2018b; Harding, 2006b; Mackie et al., 2017a; Smart, 2005). However, it still remains a loosely understood concept in flavour applications. While its main purpose is designed to enhance drug loading capacity and residence time at the site of action, a good mucoadhesive must also have a very good unloading capability (Harding, 2006b).

Oral mucoadhesion has attracted the attention of the food industry with regard to improving the bioavailability of flavour during oral processing, particularly useful in lower calorie, reformulated foods. This is because the flavour, alongside texture, are important factors impacting consumer choice, whose decisions are often driven by products that smell and taste better (Ulla et al., 2016).

The issue is that the flavour perceived is determined by the rate of release of aroma and taste compounds from the salivary bolus, towards the aroma and taste receptors, before the food is ingested. Otherwise, the flavour molecules and other bioactive compounds, are rapidly lost through ingestion and are therefore not available for perception.

Biopolymers have always been an attractive option for modifying the flavour and texture of food. Many of them are anionic polysaccharides which have been used as stabilising agents and thickeners, such as xanthan, pectin, and cellulose derivatives (Cook et al., 2003, 2018b). While many research groups have tried to evaluate and compare their mucoadhesive properties, there is limited evidence to suggest that anionic polysaccharides are, in chemical terms, adhesive towards the mucus layer (Fiebrig et al., 1995b; Harding, 2006b).

Polysaccharides with carboxylic acid and hydroxyl groups are recognized as desirable candidates in mucoadhesive applications (Peppas and Buri, 1985). For anionic polymers, interactions have solely been attributed to physical chain entanglements and hydrogen bonding (Fiebrig et al., 1995b). A review by Cook et al., (2017) lists a variety of ionic and non-ionic mucoadhesive candidates and their respective performance.

Mucins can form strong electrostatic interactions via their acid groups or sulphate groups (Bansil and Turner, 2006b; Takehara et al., 2013). As a result, neutral and anionic food biopolymers cannot form electrostatic interactions with mucus. While densitometry and rheology assays were employed to characterise their mucoadhesive interactions (Harding, 2003), it was shown that neutral polysaccharides such as dextran, scireloglucan, hydroxypropyl-cellulose and anionic polymers such as pectin, xanthan and carboxymethyl cellulose (CMC) are not mucoadhesive (Fiebrig et al., 1995b; Lehr et al., 1992).

Starch is a polysaccharide that enhances flavour and taste properties more than other colloids of the same viscosity, which is partially due to the

decrease in the bolus viscosity, which enhances the rate or release of aroma and taste compounds (Escher et al., 2000; Ferry et al., 2004). Therefore, the starch like polymer-pullulan, although much less viscous, may have strong resonances in the encapsulation and release of flavour compounds.

Pullulan is produced by fermentation of starch and other glycans by *Aureobasidium pullulans*. It is a linear polymer consisting of $\alpha(1-4)$ linked maltotriose and infrequent maltotetraose units, linked together by $\alpha(1-6)$ glycosidic bonds. Depending on fermentation conditions, the linear polymer has been found to contain up to 6% tetrasaccharide units, which allow access to the active site of salivary α -amylase to hydrolyse the polymer (West and Strohfus, 1996). As a result, it is hypothesized that its *in-vivo* degradation may result in an enhanced perception of flavour, due to an increased rate of release of aroma compounds reaching the olfactory receptors (Ferry et al., 2004).

Additionally, it is proposed that the synthesis of a cationic pullulan analogue would reduce the loss of flavour through ingestion by adhering to the anionic mucus surface of the oral cavity, along with some of the entrapped flavour compounds, provided the cationic derivative does not affect the functioning of the enzyme.

In this study, we first take advantage of SV-AUC to illustrate changes in the sedimentation coefficient distribution of bovine submaxillary mucin (BSM) in the presence of neutral, anionic and cationic polysaccharides. After, we investigate their interaction effects on the release of aroma compounds from a real food system. Lastly, cationic pullulan derivatives

were synthesised and characterised for their ability to interact with human salivary α -amylase (HSA) and BSM.

5.2. Materials and Methods

5.2.1. Samples

Bovine submaxillary mucin (type I-S, M3895), human salivary α -amylase (type IX-A, A0521), P200 kDa pullulan standard (01615), a 200 kDa chitosan derivative, with a degree of deacetylation DA \sim 70%, and aroma compounds were purchased from Sigma Aldrich (Dorset, UK). The unfractionated 200 kDa pullulan was purchased from Carbosynth. The 0.1 M phosphate buffered saline (PBS) was made according to Green (1933).

5.2.2. Orange squash

Robinson's sugar free orange squash concentrate was purchased from the local supermarket. Samples were diluted according to the manufacturer, one part concentrate and four parts water/buffer. For the GC headspace analysis, the samples were mixed with the polymer solutions such that the concentration of squash is always constant. Highly purified RO (reverse osmosis) water was used throughout the sample preparation.

5.2.3. Sedimentation Velocity (SV)

Experiments were performed at 20.0 °C using the Optima XL-I analytical ultracentrifuge (Beckman, Palo Alto, USA) with the Rayleigh interference

optics at 30,000 rpm as discussed in section 2.1. Results were analysed in SEDFIT using the $g(s)$ and the $c(s)$ processing methods, the latter valid for the high degree of fractionation/low polydispersity of the P200 pullulan standard.

5.2.1. Gas Chromatography-Mass Spectrometry (GC-MS)

The Trace 1300 series Gas Chromatograph coupled with the single-quadrupole mass spectrometer (Thermo Fisher Scientific, Hemel Hempstead, UK) was used, as described in section 2.7. Volatiles were identified by comparison of each mass spectrum with the spectra from the *NIST* Mass Spectral Library.

5.2.2. Atmospheric Pressure Chemical Ionization-Mass Spectrometry (APCI-MS)

The APCI-MS was used to analyse the concentrations of single volatile compounds above the headspace as described in section 2.8. The final concentrations of the compounds were 1 ppm and the air flow was adjusted to 50 ml/min. Sampling time was recorded until the signal intensity started to decrease. The release curves are based on the data points imported directly from the chromatogram.

5.2.3. Dynamic Light Scattering (DLS)

The experiments were performed using the Zetasizer Nano-ZS detector and low volume (ZEN0112) disposable sizing cuvettes (Malvern Instruments Ltd, Malvern, UK). The samples were measured at a final concentration of 1.0 mg/ml at $(20.00 \pm 0.01)^\circ\text{C}$ using the 173° scattering angle collected for 3 runs of 10 seconds. The contribution of rotational diffusion effects to the autocorrelation function is assumed negligible (Burchard, 1992).

5.2.4. Capillary viscometry

Flow times of solvent (t_0) and solutions (t_s) were measured using a semi-automated (Schott Geräte, Hofheim, Germany) U-tube Ostwald capillary viscometer as previously discussed in Section 2.5. The intrinsic viscosity, $[\eta]$ is given by the Solomon-Ciuta equation.

5.2.5. INSENT E-tongue

Digested and undigested pullulan solutions were made in 30 mM potassium chloride buffer and poured into the sample cups in triplicate ready for analysis by the Taste Sensing System TS-5000Z. Manufacturer guidelines were used for analysis and data extraction. The experiment was kindly performed by New Food Innovation specialists as in previous studies (Pein et al., 2014; Tahara and Toko, 2013).

5.2.6. Conductivity meter analysis

Dissolution of sodium was evaluated using a Mettler Toledo conductivity meter (Ohio, USA). A 1 ml sodium chloride solution (0.1 mg/ml) was dissolved in a beaker containing native and digested pullulan solution. The HSA signal was subtracted from the digested solution. Data was recorded every 2 seconds until a plateau was reached (~20 s). For this analysis, a 1 ml solution of sodium chloride was added at a concentration of 1.0 mg/ml into a 50 ml pullulan solution, equivalent to the dissolution of 0.2 mg of sodium, under constant magnetic stirring and maintained at 25.0 °C. Three replicates were performed and normalised by relative conductivity.

5.2.7. Synthesis of cationic pullulan derivatives

Glycidyltrimethylammonium (GTMAC) pullulan was first synthesised by using the method of Heinze et al., (2004). Briefly, 20 g of Sigma 200 kDa pullulan was suspended in 10M sodium hydroxide solution to activate the pullulan hydroxyl groups. Then 53 ml of GTMAC was added dropwise at stirred for 6 h at 60 °C. The final solution was adjusted to pH 7 using 0.1M HCl.

The dimethylaminoethyl (DMAE) addition reaction was performed using an adapted version of San Juan et al. (2007)²⁴. 5 g of Pullulan (Carbosynth, 200 kDa) was dissolved in 25 ml of distilled water and mixed with a 25 ml 10M sodium hydroxide solution. Then, 35 g of 2-chloro-N,N-dimethylethylamine hydrochloride was added to the mixture and left stirring at 60 °C for one hour. After the reaction was completed, the mixture was washed four times with 50 ml diethyl ether and diluted in

water to a concentration of 10 mg/ml, and adjusted to pH 7 using 0.1M HCl.

Final solutions were further cleaned of any organic solvents and concentrated in a rotary evaporator, after which was dialyzed in PBS buffer against a 14.000 Da (g/mol) membrane for two days. The resulting solution was freeze-dried which resulted in the formation of white and odourless lyophilized powder, stored at 4° C.

5.2.8. Fourier-transform infrared spectroscopy (FT-IR)

The resulting DMAE-pullulan (powder) was subjected to FT-IR analysis. Measurements were performed in transmission mode on an IRAFFINITY-1S spectrometer equipped with an A219653 attenuated total reflection (ATR) module (Shimadzu, Japan). For each sample, the spectrum was taken as the average of three different measurements at various sites of the dry sample. Spectra were acquired between 500 and 3500 cm^{-1} at a resolution of 4 cm^{-1} . Dry pullulan samples were pressed against the diamond surface to ensure good contact. Measurements were repeated twice for reliability.

5.3. Results and Discussion

5.3.1. Interactions of BSM with polysaccharides

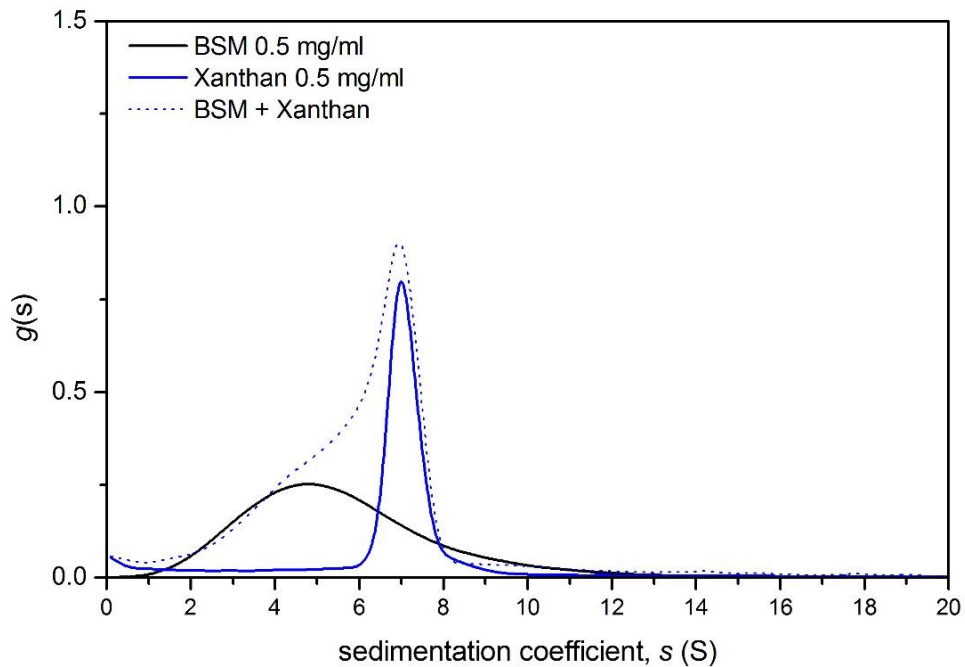


Figure 5.1. Results from sedimentation velocity showing the $g(s)$ sedimentation coefficient distribution of 0.5 BSM (200 kDa), 0.5 xanthan (200 kDa) and the 1:1 mixture. Run in 0.1 M PBS pH 7.0 at 30,000 rpm.

Experiments on a series of anionic polysaccharides were performed, including alginate, gum arabic, xanthan and CMC. No significant change in the ratio of the sedimentation coefficient distribution was seen upon the addition of the anionic polymers, despite possible weak interaction sites at the carbonyl, hydroxyl or carboxyl groups as seen in Figure 5.1, showing the lack of any interaction between BSM and Xanthan.

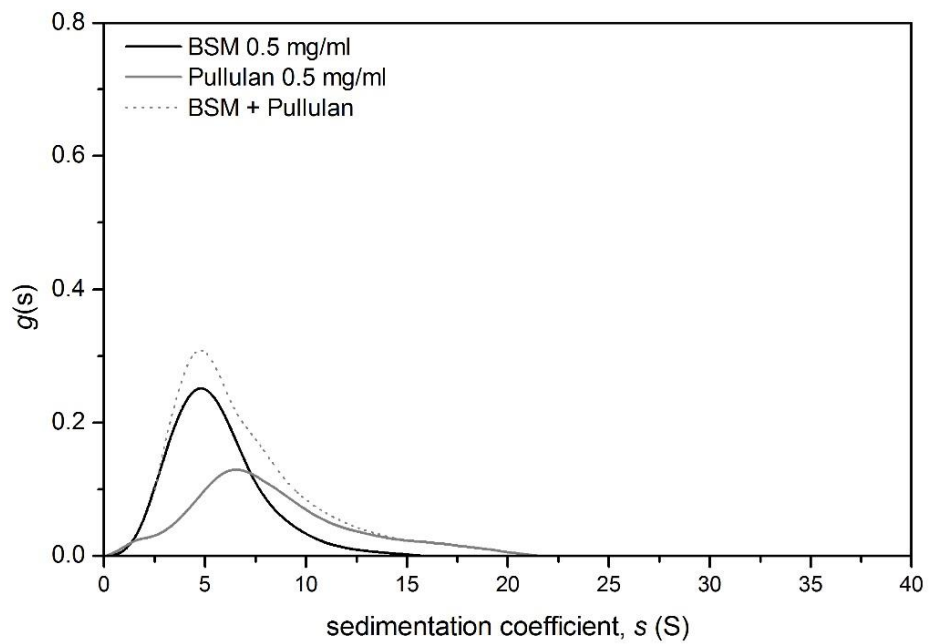


Figure 5.2. Results from sedimentation velocity showing the $g(s)$ sedimentation coefficient distribution of 0.5 BSM (200 kDa), 0.5 pullulan (200 kDa) and the 1:1 mixture. Run in 0.1 M PBS pH 7.0 at 30,000 rpm.

In the same manner, mucin interactions with neutral polysaccharides such as dextran and pullulan revealed no apparent changes in their sedimentation coefficient distribution, as illustrated in Figure 5.2.

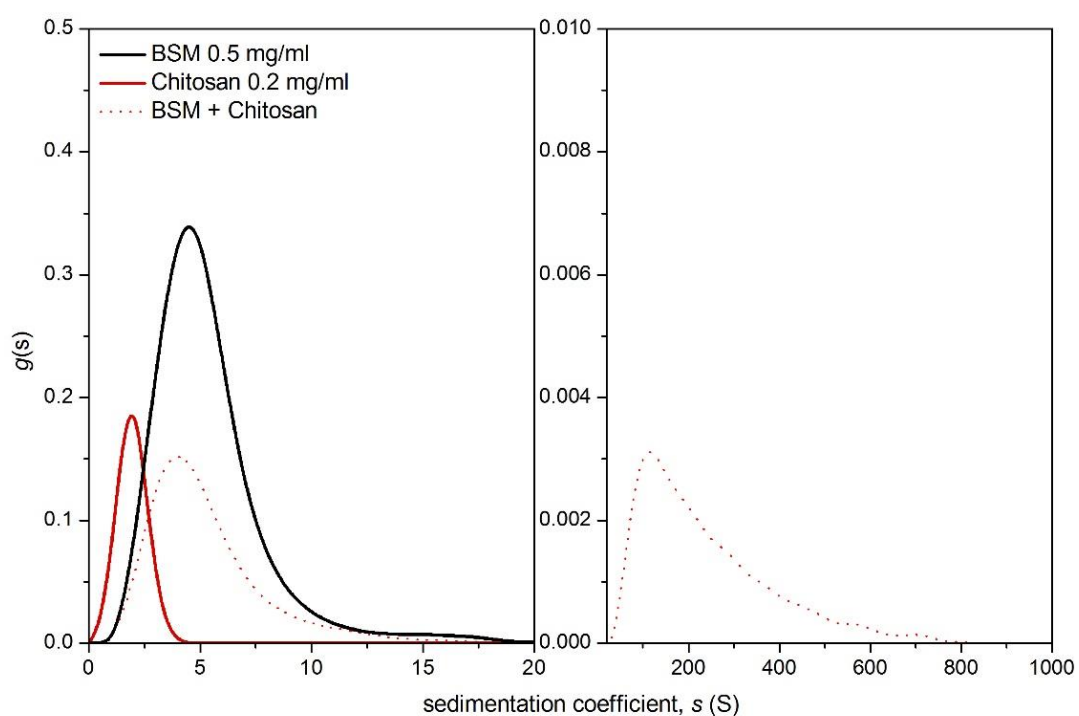


Figure 5.3. Results from sedimentation velocity showing the sedimentation coefficient distribution of 0.5 BSM (200 kDa), 0.2 chitosan (200 kDa) and their mixture. Run in 0.1 M acetate buffer pH 5 at 30,000 rpm.

Next, a 200 kDa chitosan derivative was used to illustrate strong electrostatic interactions between the positively charged amino groups of chitosan and the acidic functions of the mucin carbohydrate chains (Figure 5.3.). This test can only be performed at pH 5 or less, due to the poor solubility of chitosan at neutral pH, but which is representative of most food environments.

Firstly, it was shown that the addition of 0.2 mg/ml chitosan to 0.5 mg/ml BSM lead to a marked reduction in the mucin concentration, indicating a direct interaction between the macromolecules. Secondly, this led to the

formation of a long distribution of high molecular weight species ranging from 20 S to 900 S, corresponding to large mucin-chitosan complexes.

5.3.2. Effect of the polysaccharide-mucin interactions on aroma release

While mucoadhesive interactions are essential in loading the flavour onto the mucosal surface, another important parameter is the ability to rapidly unload the aroma molecules from the mucus-polymer complexes, which depends on the product. In liquid formulations, most of the aroma and taste compounds are lost by ingestion, therefore a rapid release of the aroma from the bolus is the aim of flavour mucoadhesives. Therefore the ability of anionic, neutral and cationic polysaccharides to modify aroma release was next evaluated using the GC-MS in the presence of mucin solutions.

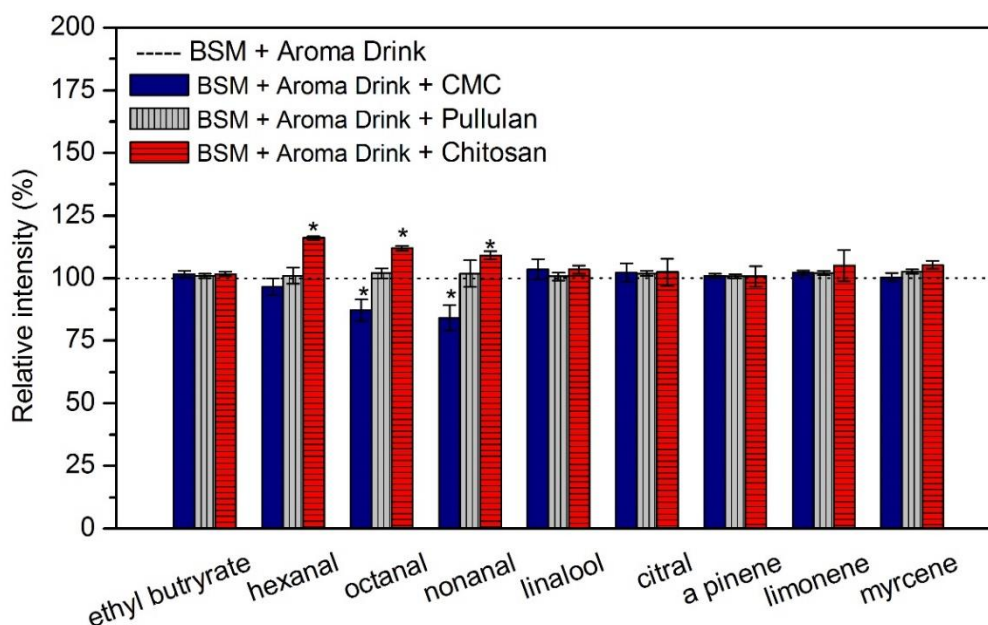


Figure 5.4. GC-MS results showing the relative aroma intensity in the headspace of BSM solutions (1.0 mg/ml) before and after the addition of CMC, pullulan and chitosan at a polymer concentration of 0.5 mg/ml. Values are expressed as mean \pm SD (n = 3).

The addition of the different polysaccharides led to minor changes in the relative headspace intensity of the aroma compounds, with the exception of linear aldehydes (hexanal, octanal, nonanal) which were influenced by the charge of the different polysaccharide excipients (Figure 5.4.). For instance, the concentrations of hexanal, octanal and nonanal were markedly reduced after the addition of anionic CMC, possibly through carbonyl-carbonyl interactions between the carboxyl functions of CMC and the carbonyl groups of the linear aldehydes (Allen et al., 1998).

The aroma intensity generally increased in the presence of the cationic polymer. This is attributed to a partial reduction in mucin concentration and the formation of larger S complexes (Figure 5.3.). However, it was

found that the relative concentration of linear aldehydes was significantly higher in the presence of chitosan, possibly caused by competition for mucin binding by chitosan amino groups, suppressing interactions with the carbonyl containing aldehyde compounds. The use of higher concentrations chitosan may lead to a higher headspace intensity, but its use in food is linked to negative mouthfeel effects (through its strong mucin complexation) and GI issues.

The addition of pullulan led to no apparent changes in the headspace concentration upon its addition to the mucin solution. This is partially attributed to the very low viscosity of pullulan and the lack of any electrostatic interactions with mucin.

It is worth mentioning that despite different charge and molecular properties of the added polymers results show minor changes in the intensity of aroma compounds in the headspace, at the concentrations used. However, there is an imbalance in the release of aldehydes (hexanal, octanal and nonanal) as can be evidenced by the addition of anionic CMC and chitosan, but not with neutral pullulan. Therefore pullulan is further investigated, and also due to its resemblance to starch, known to enhance aroma release through a reduction in bolus viscosity by the action of salivary α -amylase.

5.3.3. The impact of pullulan hydrolysis on flavour release

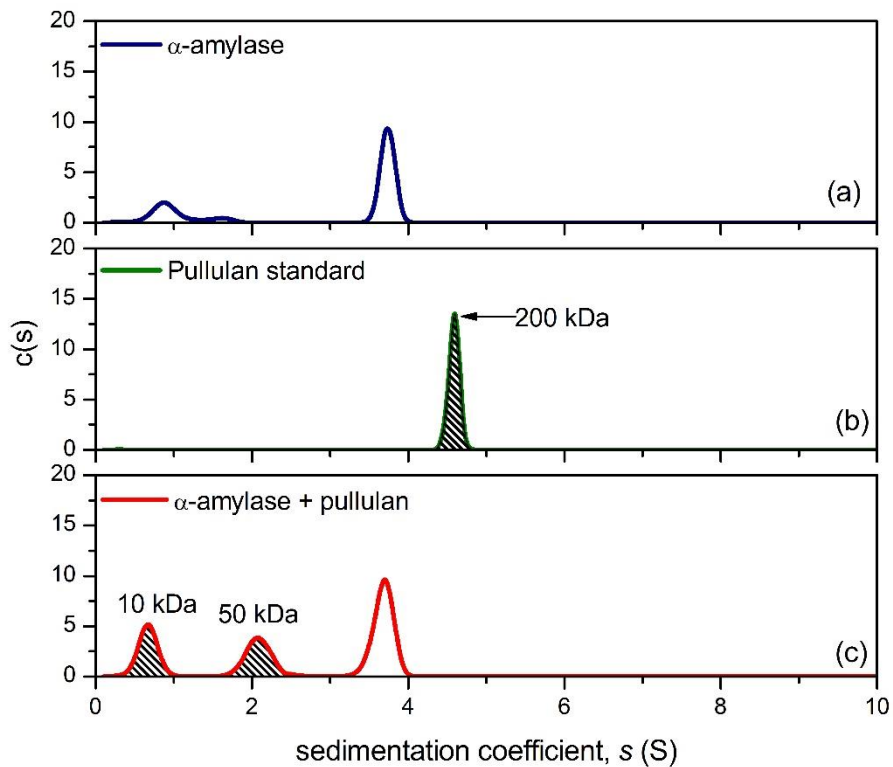


Figure 5.5. Sedimentation velocity, $c(s)$ analysis, showing the sedimentation coefficient distributions of α -amylase (a), 200 kDa pullulan standard (b), and the result of their interaction (c). Rotor speed: 45,000 rpm (130,000 g), 20.0 °C.

The analysis was performed using highly a purified 200 kDa molecular weight pullulan standard, which yielded a single, monodisperse peak at ~ 4.6 S (Figure 5.5b). The addition of salivary α -amylase revealed the formation of degradation fragments corresponding to major peaks at ~ 2 S and ~ 0.8 S respectively (Figure 5.5c). Note that a proportion of the monodisperse peak at ~ 0.8 is partly attributed to the presence of the

smaller component of HSA (Figure 5.5.a). Relative molecular weights for the digested fractions are suggested to be between 10 kDa and 100 kDa, respectively. For the rest of the investigation, an unfractionated food grade 200 kDa pullulan was used.

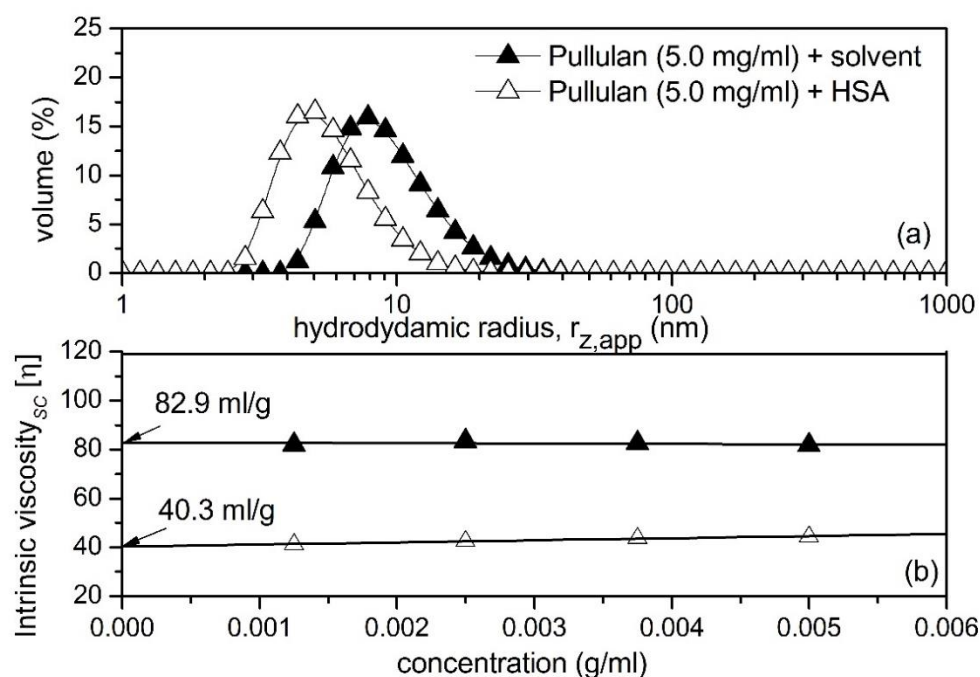


Figure 5.6. Changes in the apparent z-average hydrodynamic radius of pullulan before and after the addition of HSA (a) and Solomon-Ciuta extrapolations showing the intrinsic viscosity of pullulan upon the addition of HSA (b). DLS size distributions are given as an average of three measurements. Experiments performed at 20.0 °C.

DLS and viscosity experiments were employed to determine the ability of HSA to hydrolyse pullulan. Undigested pullulan showed an apparent z-average hydrodynamic radius, $r_{z,app}$, of ~ 8.5 nm, which was not visible upon the addition of α -amylase, resulting in a z-average of ~ 5 nm (Figure 5.6.a). In addition, viscosity data shows that the addition of HSA results in a twofold decrease in the intrinsic viscosity $[\eta]$, as indicated by the

Solomon-Ciuta extrapolation (Figure 5.6.b). Combining DLS and viscometry, we can confirm that HSA is capable of digesting pullulan, producing smaller fragments of lower molecular weights and lower viscosity. The next important question was to test these effects on the release of aroma and taste compounds.

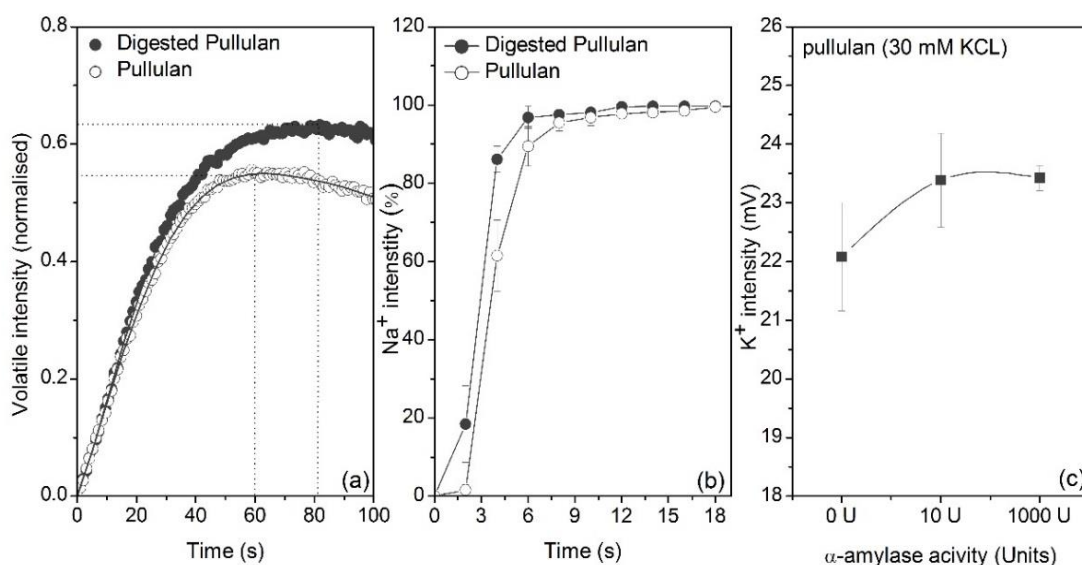


Figure 5.7. Results from APCI-MS, conductivity analysis and E-tongue showing the impact of pullulan hydrolysis on the release of flavour, showing the real time data for α -ionone (a), sodium ions (b) and potassium ions intensity (c). Values are expressed as mean \pm SD (n = 3).

The results in Figure 5.7.a shows the peak intensity and persistence of aroma compound α -ionone, before and after pullulan digestion. In the presence of native pullulan (4 mg/ml), the headspace concentration reached a plateau, while it continued to increase for an additional \sim 20 seconds in the presence of the degraded sample. Although the time scale of the APCI analysis is not representative of the very short amount of time

needed to consume a drink, the system confirms the effect of pullulan digestion on aroma release.

A similar trend is observed in Figure 5.7.b, in which conductivity analysis indicates an increase in the rate of release of sodium ions. This suggests that the availability of sodium may be increased as a function of polymer degradation. The intensity of potassium was further tested as a function of enzyme concentration using the taste evaluation INSENT E-tongue (Figure 5.9.c). Although not significantly different, results suggest that an increase in the α -amylase concentration can enhance the availability of K^+ ions.

In addition, the hypothesis was tested using a commercial orange drink 'R' in the presence and absence of pullulan 'P' (Figure 5.8.). Results suggest that α -amylase 'A', which is naturally present in saliva, reduces the headspace concentrations of the compounds, and the effect is concentration dependent (A1, A2 in Figure 5.8.). However, the presence of pullulan suppressed this effect and enabled a higher concentration of aroma compounds to be released into the headspace.

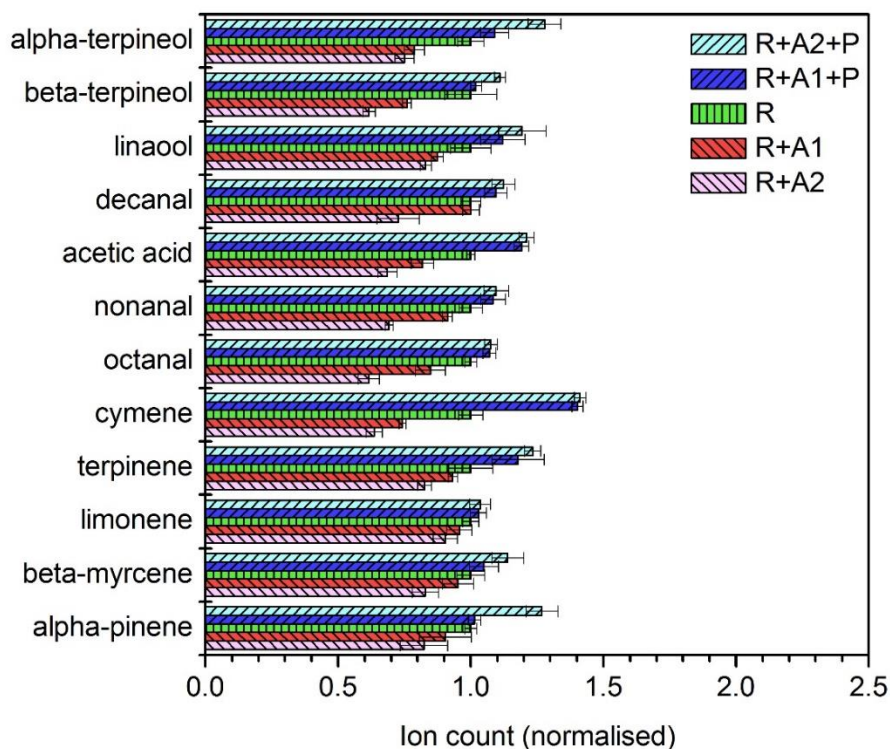


Figure 5.8. GC-MS results showing the effect of pullulan hydrolysis on the relative headspace concentration of aroma compounds found in Robinson’s orange squash, where ‘R’ represents the standard squash dilution, ‘A1’ and ‘A2’ are increasing α -amylase concentrations of 0.1 and 1.0 mg/ml, and ‘P’ represents pullulan at a constant concentration of 2.0 mg/ml. Values are expressed as mean \pm SD (n = 3).

Given that α -amylase can be secreted to very high concentration during food stimulation (up to 8 mg/ml), results suggest that the aroma intensity can be enhanced by the presence of pullulan, despite the presence of citric acid which might interfere with the normal functioning of the enzyme.

The issue regarding rapid food ingestion is now addressed in the next section. For most products, such as squash or other soft drinks, oral transit time corresponds to only a couple of seconds. Therefore, this forms the

basis for the development of a mucoadhesive polymer system which can be initiated by the action of HSA. It is suggested that by modifying the chemical properties of pullulan, such that it becomes adhesive towards the oral mucus, some of the issues associated with the rapid ingestion can be reduced.

5.3.4. Developing a cationic pullulan derivative

The investigation began with the coupling of amino functional groups onto the polysaccharide backbone to make it polycationic, but without interacting with the enzyme.

5.3.4.1. Glycidyltrimethylammonium (GTMAC) synthesis

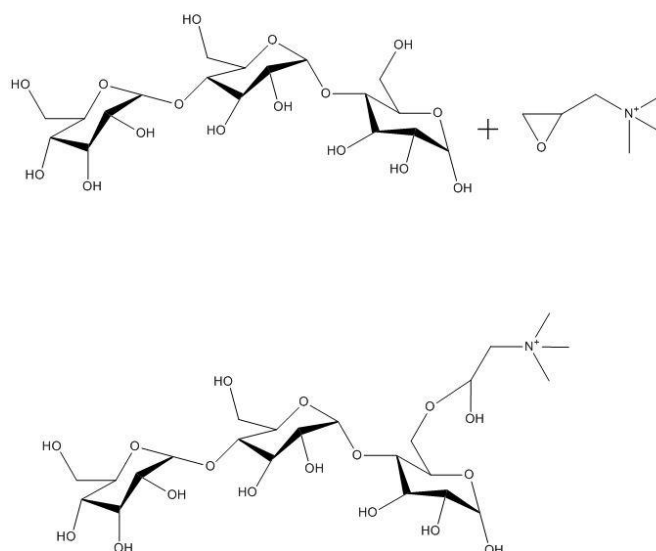


Figure 5.9. Schematic representation of the chemical modification of pullulan showing the addition of the quaternary amine, glycidyltrimethylammonium (GTMAC) chloride.

Cationic starch is commonly used in the food and non-food industries, such as the paper industry. Most commonly, GTMAC is used to develop cationic starches with a low degree of substitution in order to improve the functionality of paper (Bendoraitiene et al., 2006; Rwei et al., 2014). In this study, the method of Heinze et al., (2004) was also applied for developing GTMAC-pullulan using glycidyltrimethylammonium chloride in an aqueous mixture of sodium hydroxide (Figure 5.9.).

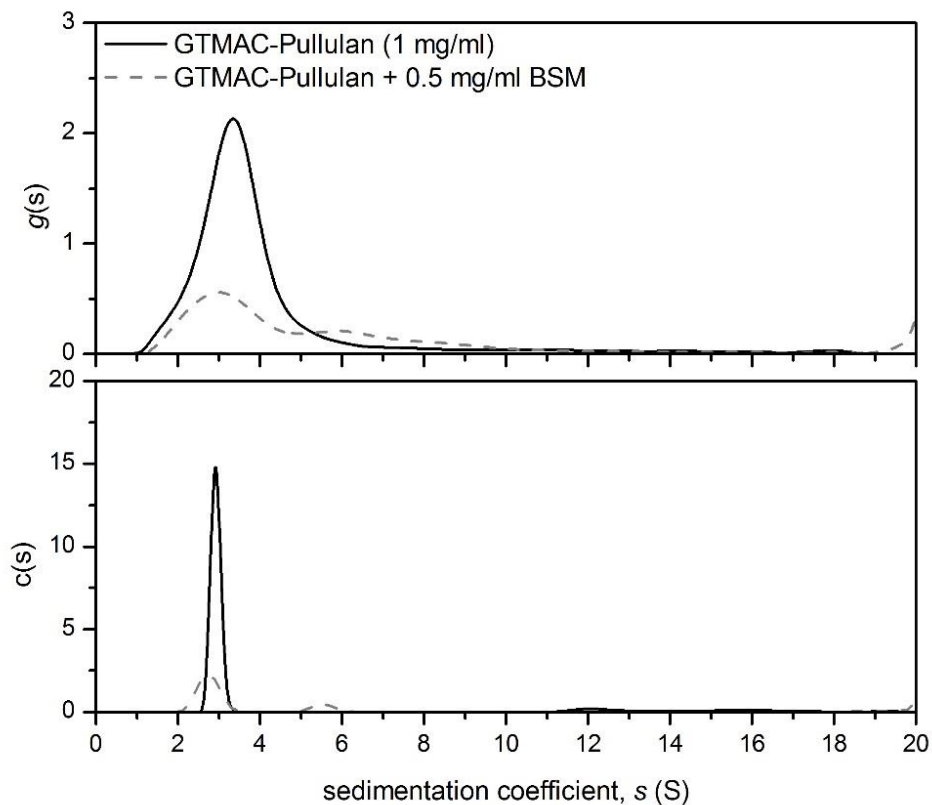


Figure 5.10. Sedimentation velocity $g(s)$ and $c(s)$ analysis, showing the sedimentation coefficient distributions of GTMAC-pullulan and the result of the interaction with BSM. Rotor speed: 45, 000 rpm (130, 000 g), 20.0 °C.

A significant interaction was observed between BSM and GTMAC-pullulan which led to a decrease in the concentration of BSM, yielding species with apparent sedimentation coefficients greater than 100 Svedberg (Figure 5.10.). This is similar to chitosan-mucin complexation indicative of the strong electrostatic interactions between the quaternary amino group and the acid groups of mucin.

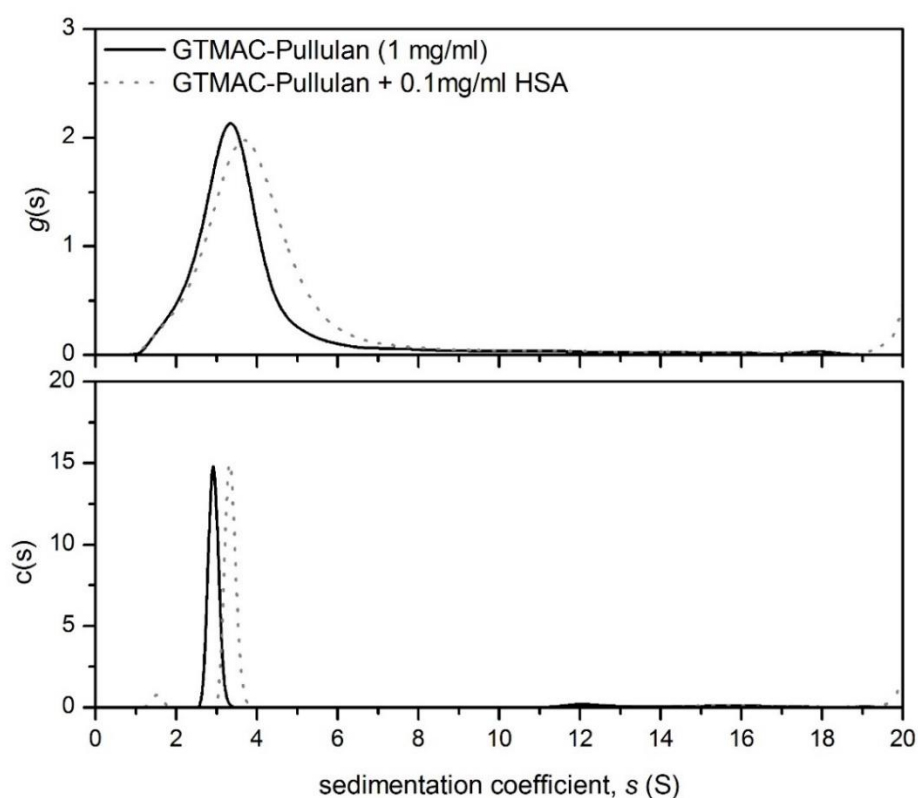


Figure 5.11. Sedimentation velocity $g(s)$ and $c(s)$ analysis, showing the sedimentation coefficient distributions of GTMAC-pullulan and the result of the interaction with HSA. Rotor speed: 45, 000 rpm (130, 000 g), 20.0 °C.

SV analysis was also employed to check the ability of HSA to break down the modified polymer. However, the addition of 0.01 mg/ml α -amylase to the 1 mg/ml solution of GTMAC-pullulan led to minor changes in the sedimentation coefficient distribution. An apparent increase in the sedimentation coefficient distribution is observed, attributed to the HSA control or HSA/polymer interactions (Figure 5.11.). Nonetheless, this suggests that the enzyme is unable to degrade the modified polymer.

5.3.4.2 Dimethylaminoethyl (DMAE) synthesis

The more promising candidate was dimethylaminoethyl as a grafting agent (Figure 5.12.). The reaction was performed using an adapted version from Juan et al., (2007) (see section 5.2.10.). The polymer was dialysed against a 14, 000 Da membrane and the resulting material analysed by FT-IR (Figure 5.12.a).

By comparing the IR spectra of the native sample, the absorption bands for DMAE-pullulan at $\sim 900\text{ cm}^{-1}$ and $\sim 3050\text{ cm}^{-1}$ correspond to stretching and wagging vibrations of the amino group, while the strong absorption at 1390 cm^{-1} and 1460 cm^{-1} correspond to the CH_2 and CH_3 vibrations of the dimethylaminoethyl chain. A characteristic CO group is observed around 1720 cm^{-1} , while broader and weaker vibrations are observed in the region $1800\text{-}2500\text{ cm}^{-1}$, which indicate the presence of the CN bonds of the amino group (Figure 5.12.b).

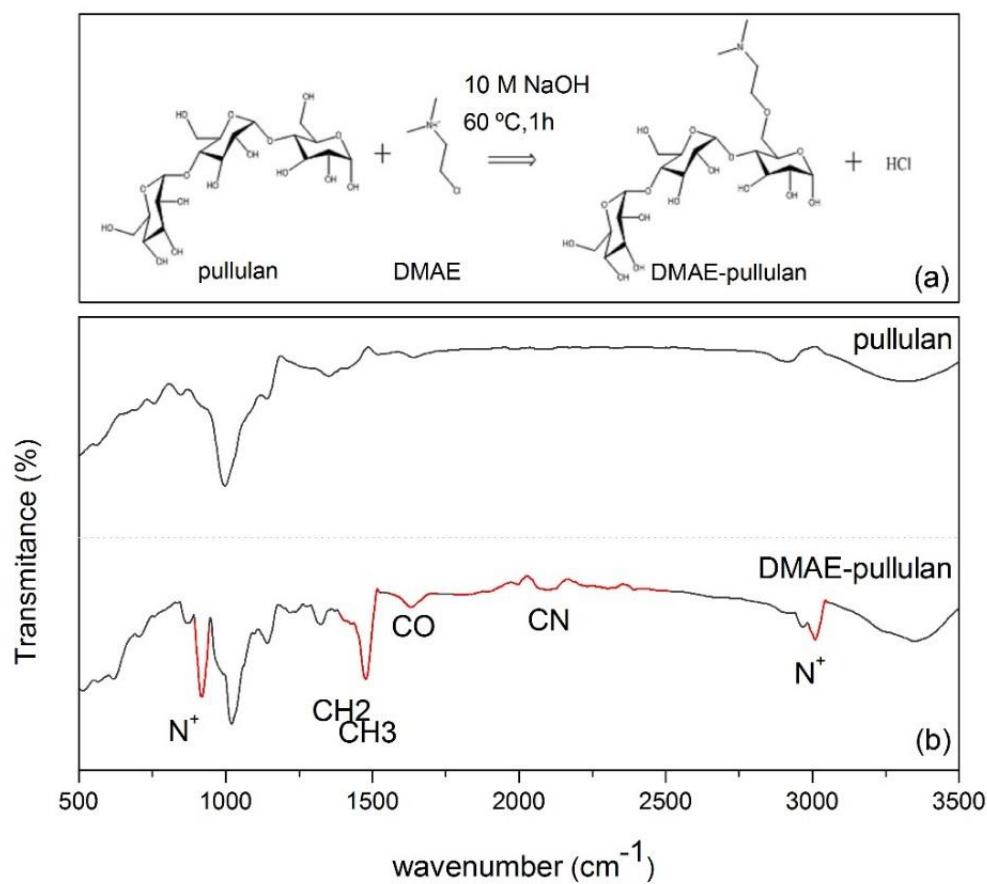


Figure 5.12. Schematic representation of the chemical modification of pullulan showing the addition of the tertiary amine, dimethylaminoethyl (DMAE) chloride (a) and FT-IR spectra of pullulan before after synthesis highlighting the qualitative changes in the spectral intensity correlating to the functional groups (b).

The FT-IR analysis suggests that the DMAE group was successfully grafted onto the pullulan backbone. Next, we addressed the hydrodynamic interactions between DMAE-pullulan and the two salivary macromolecules.

5.3.5. Interactions with BSM and HSA

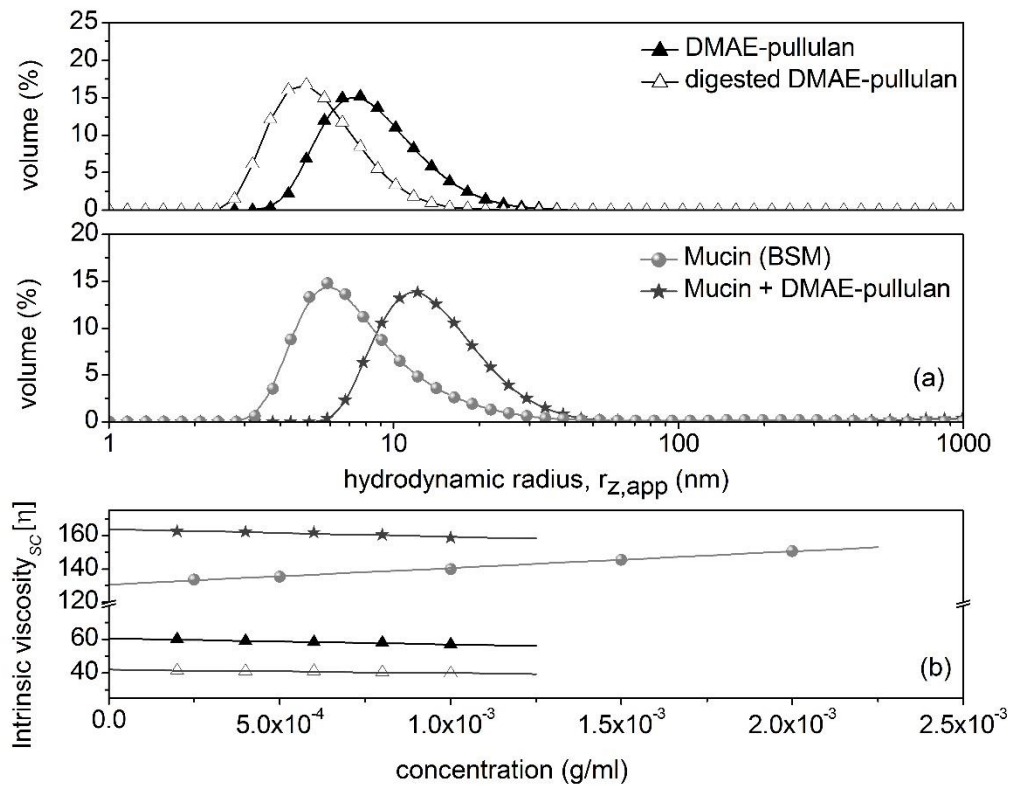


Figure 5.13. DLS results showing changes in the apparent z-average hydrodynamic radii of DMAE-pullulan, BSM, HSA, and the result of their interactions (a), and viscosity results showing the Solomon-Ciuta extrapolation for intrinsic viscosity $[\eta]$ (b). DLS results are given as an average of three measurements. Performed at 20.0°C, in a 1:1 ratio.

Viscosity and DLS results confirmed the ability of HSA to reduce the hydrodynamic particle size $r_{z,app}$ of DMAE-pullulan from ~8 nm to ~5 nm (Figure 5.13a). In the presence of BSM (~6.5 nm) an increase in the size distribution was observed, suggesting mucoadhesive interactions, corresponding to a $r_{z,app}$ of ~12 nm (Figure 5.13.a).

Similarly, we evaluated changes in the intrinsic viscosity (Figure 5.13.b), which corresponded to a $\sim 32\%$ decrease upon the addition of the enzyme. By contrast, the intrinsic viscosity of the DMAE-pullulan/mucin mixture was 23% higher than the viscosity of BSM itself, suggesting a direct complexation (Figure 5.15b). The DLS and viscometry analysis were further reinforced by SV-AUC which allowed us to directly monitor changes in the sedimentation coefficient distribution of DMAE-pullulan upon the addition of HSA and BSM (Figure 5.14.).

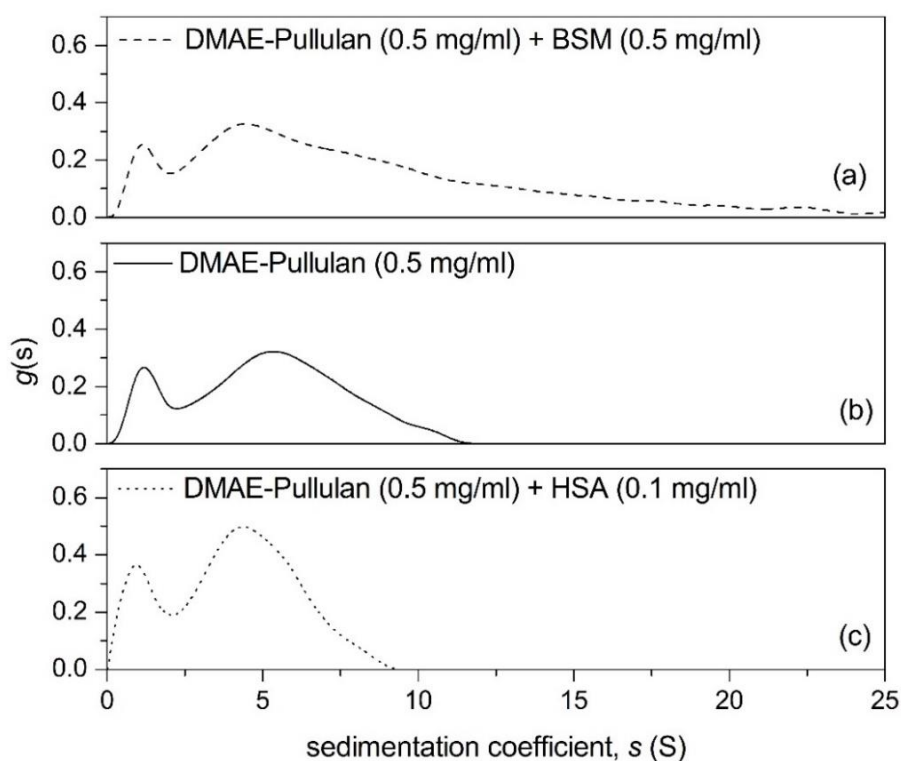


Figure 5.14. Sedimentation velocity, $g(s)$ analysis showing the sedimentation coefficient distributions for DMAE-pullulan at 0.5 mg/ml (b) and the result of the addition of mucin at 0.5 mg/ml (a) and α -amylase at 0.1 mg/ml (b); and the GC-MS volatile analysis from modified and unmodified pullulan and solutions upon the addition of HSA (d). Rotor speed: 45,000 rpm (130,000 g), 20.0 °C.

DMAE-pullulan control revealed a rather broad sedimentation profile, indicative of a polydisperse composition. At a concentration of 0.5 mg/ml, the apparent sedimentation coefficient distribution ranged from 1S to ~12S (Figure 5.14.b). An initial assessment reveals an increase in the sedimentation coefficient distribution increased to ~25S upon the addition of mucin, indicative of binding, although a large proportion of sedimentation species (~70%) has remained unaffected (Figure 5.14.a).

By contrast, the addition of HSA caused a reduction in the weighted average sedimentation coefficient distribution of the modified polymer from ~12S to ~9S (Figure 5.14.c). This translates to a ~25% loss of larger S components, and an increase in the concentration of smaller weight average DMAE-pullulan fractions. To summarise, these values are qualitatively consistent with the results of viscosity and DLS (Figure 5.13.).

5.3.6. General Discussion

Mucoadhesive polymers may be anionic, cationic or non-ionic (Mansuri et al., 2016; Peppas and Huang, 2004; Woertz et al., 2013). However, the natural clearance time of these polymers depends on the application. For most food and orally administered products they are rapidly passed down along the alimentary canal, therefore mucoadhesives are used to slow down the rate of transport of the ingested matrix across the mucosal membranes.

While some food biopolymers have been classed as mucoadhesive (e.g. chitosan) in biomedical applications targeted at the gastrointestinal (GI) region, their ability to increase the bioavailability of flavour compounds

remains modest, considering the marked reduction of mucin concentration. However, such strong interactions are attributed to negative organoleptic properties, including astringency and GI (Cook et al., 2017).

In this work, it was shown that the use of the neutral polymer pullulan may have stronger resonances in flavour applications. Cationic pullulan was synthesised with the aim that it forms complexes with submaxillary mucin while being reduced by salivary α -amylase. Two amino coupling groups were studied: diethylaminoethyl and glycidyltrimethylammonium, but the latter appeared to cause strong mucin and α -amylase aggregation.

The advantage of DMAE compared to previously characterised diethylaminoethyl (DEAE) synthesis, is that the methyl groups as opposed to the ethyl groups, may increase the availability of the positively charged amino groups to the negatively charged carbohydrate residues of mucin. However, current results showed that the ratio of the mucin/polymer complex to that of the mucin ($S_{\text{complex}}/S_{\text{mucin}}$), ranged from 1.1 to 2 (Figure 5.16.a), which is similar to that of DEAE-dextran - still fairly modest compared to some stronger mucoadhesive polymers like chitosan, shown to give sedimentation ratios of up to ~ 50 times larger (Harding, 2003).

In this study it was estimated that up to 30% of DMAE-pullulan interacts with mucin, as given by the area under the sedimentation distribution curve (Figure 5.16.a). However, it is worth suggesting that the interaction mechanisms of DMAE-pullulan may lead to minor changes in the in mouth rheology of the bolus, since the viscosity increase due to adhesive interactions is counterbalanced by the decrease due to enzyme hydrolysis.

Therefore, sensory changes by the food/saliva mixture, i.e. mouthfeel, are suggested to be the minimal. As a result, it is suggested that a food grade cationic pullulan could become a next generation mucoadhesive targeted at the oral cavity. Once a food grade cationic pullulan becomes available, sensory experiments would add to our analysis and provide a clearer picture of its effects on consumer perception.

5.4. Conclusion

The current study has shown that while some anionic polysaccharides are considered to be mucoadhesive, they do not form direct mucin-polymer interactions. While other biopolymers, such as chitosan, have been shown to form larger complexes and enhance the aroma released, applications with chitosan are limited for the oral cavity. In addition, the presence of anionic CMC and cationic chitosan appear to play a role in the interactions with aldehydes, whereby their presence creates an imbalanced aroma concentration. Cationic DMAE-pullulan was synthesised and has shown to enhance the intensity of flavour as a result its specific interactions with the two salivary glycoproteins. While the concept developed here has strong resonances in the release of flavour from liquid foods, it may also be found useful in the controlled delivery of medicines, via the action of pancreatic α -amylase.

6. Chapter 6: Mucin immobilization in calcium alginate: A biomimetic tool for evaluating mucoadhesion and retention of flavour

6.1. Introduction

During product development or reformulation, food and pharmaceutical companies need to assess the release and retention properties of the product onto the target tissues, such as the mouth, skin or gastrointestinal (GI) tract. At the moment, a large number of food products are being tested on animals or animal tissues. It was reported that over 60% of scientific research in the area of mucoadhesion involves the use of laboratory animals, specifically raised for their mucosal surfaces (Cook et al., 2015b). However, the current trend, supported by sustainability campaigns and animal rights organizations, is to discourage industry and academia from performing experiments on animal tissues and aim to use more sustainable options.

Currently, a common alternative is to use byproducts resulting directly from the meat industry. While abattoir discarded animal tissues provide closer representations to human mucosa, there are still a number of issues associated with their use, such as limited shelf life and increased risk of cross contamination (Lehr et al., 1990; Grabovac et al., 2005; Fransen, 2008), making them less than ideal for assessing the retention of bioactive compounds in foods, oral care and other products.

Several new alternatives have been proposed to overcome those limitations (Mortazavi and Smart, 1995; Baloğlu et al., 2003; Mackie et al., 2017b). Some innovations include the development of mammalian epithelial cell lines grown on collagen membranes, which resemble some of the surface morphology of mucus (Sugiyama et al., 1993b; Takahashi et al., 2004b). However, the lengthy and costly nature of such models, combined with the low yield of the final product limit any potential industrial applications (Kavvada et al., 2005b; Keely et al., 2005b).

The most accessible approach is to use commercially available mucin powders, isolated and purified from the bovine or porcine GI tract. Since mucin glycoproteins represent the primary macromolecular constituent of mucus, their use enables the development of a wide array of model systems, from aqueous solutions to partially hydrated films, or grafted onto cellulose membranes or other biomimetic polymer substrate (Harding et al., 1999; Harding, 2006; Venter et al., 2006; Jones et al., 2009; Harding et al. 2016).

Some approaches also moved away from the conventional mucus/mucin-based systems and developed alternative methods purely based on hydrocolloids and/or synthetic polymers. For instance, cellulose, locust bean gum, or carbopol have all been employed as surrogates for bioadhesion assays as they were shown to possess some of the carbohydrate-like rheology of mucus (Anwarul Hasan et al., 2010b; Hall et al., 2011b).

The choice of the model surface is essential for evaluating the mucoadhesive properties of polymers. Cook et al. (2015) analysed an ex-

vivo system based on porcine oral tissue in order to analyse the mucoadhesive strength of three biopolymers: sodium alginate, sodium carboxymethyl-cellulose (CMC) and pectin (DE<30). They previously suggested that pectin was by far the most potent in its ability to enhance the retention of sodium *in-vitro*, but the *ex-vivo* tongue experiments confirmed that CMC was the more potent in increasing salt bioavailability. However, *in-vivo* sensory results recently established that CMC actually reduces sodium perception, despite scoring high for attributes such as adhesion and mouth-coating (Cook et al., 2018b; Gan et al., 2014a). Such disagreements highlight the importance of selecting a suitable model system for evaluating mucoadhesion.

In-vivo studies may provide a clear picture, for example Atmospheric Pressure Chemical Ionization- Mass Spectrometry coupled with the MS-Nose interface can enable the retronasal quantification of volatile compounds present in the oral cavity, but this can be very challenging due to the lack of compound specificity, or the very weak signals detected from real foods (Gan et al., 2014b). Therefore, before consumer phases, *in-vivo* and *ex-vivo* animal testing still remains the primary means of evaluating interactions with the product.

Flavour perception is ultimately determined by the rate of release of aroma and taste compounds from the salivary bolus, towards the aroma and taste receptors, before the food or medicine is ingested. Otherwise flavour, along with other bioactive compounds, is rapidly lost through ingestion and are less available for perception.

The common strategy is to increase the concentration of flavour and taste compounds in food, leading to nutritionally compromised products with high sodium, sugar and excessive levels of flavourings. To combat these issues, new mucoadhesives are being developed. But with a burst in the development of new mucoadhesives, comes the need for new methodologies to assess their properties.

In this study, we developed a rapid and more sustainable model for evaluating the retention of flavour compounds in the presence of different polymer mucoadhesives. Physiological concentrations of mucin were encapsulated in calcium alginate spheres using the well-established ion exchange reaction (Smidsrod and Draget, 1997, Paulsen, 2000).

It is hypothesized that mucin glycoproteins are anchored along the surface of the calcium alginate complex, thus influencing the chemistry of the system. To validate the efficiency of the *in-vitro* model, the surface of an *ex-vivo* bovine tongue was used to assess the ability of the mucoadhesive excipients to retain the flavouring compounds.

Environmental scanning electron microscopy (ESEM), AUC and DLS were used to examine the surface morphology and surface chemistry of the beads. GC-MS was used along with ion conductivity analysis to quantify the release of aroma and salt compounds.

6.2. Materials and Methods

6.2.1. Samples

A stock solution of pig gastric mucin (Sigma-Aldrich, M1778, type III) and sodium alginate (Sigma) were prepared in phosphate-buffered saline (PBS) buffer, pH 7.0, adjusted to an ionic strength $I=0.1\text{M}$ by the addition of NaCl, according to Green, (1993). Deacetylated chitosan (70%) was purchased from Sigma Aldrich (Kitozyme, 740179-5g, Dorset, UK). The carboxymethylcellulose (CMC) and pullulan samples were purchased from Carbosynth, UK. DMAE-pullulan was obtained as described previously (section 5.2.7.).

6.2.2. Mucin beads preparation

A 10 mg/ml pig gastric mucin solution and was prepared in 0.1 M PBS (pH 7.0) and mixed with a 40 mg/ml Na^+ alginate aqueous solution. The final concentrations of mucin and alginate were 5 mg/ml and 20 mg/ml, respectively. A syringe was used to pour even droplets into a 3% calcium chloride solution, and left to harden for 30 minutes under constant stirring.

The control beads (Na^+ alginate) were prepared in the same way, such that the final concentration was 20 mg/ml, but without the presence of mucin. The beads were collected and hydrated in RO water (reverse osmosis) prior to investigation.

6.2.3. Orange drink preparation

Robinson's orange squash was used throughout this investigation, purchased from the local supermarket. Hexanal, octanal and decanal were added in order to assess the interactions with linear aldehydes at concentration of 1 ppm (1.0 mg/l). Then, 2.0 mg/ml stock solutions of CMC, pullulan and DMAE-pullulan were prepared in 0.1 M PBS (pH 7.0) while sodium acetate buffer (pH 5.0) was used to solubilise chitosan. Final solutions were made such that they contain one part orange squash, one part polymer solution, and three parts water. The final polymer concentrations were 0.4 mg/ml, which are below the critical coil overlap concentration c^* , in order to reduce viscosity related effects (Hollowood et al., 2002). The pH of the four drink preparations was in the range of 4-5.

6.2.4. *Ex-vivo* tissue preparation

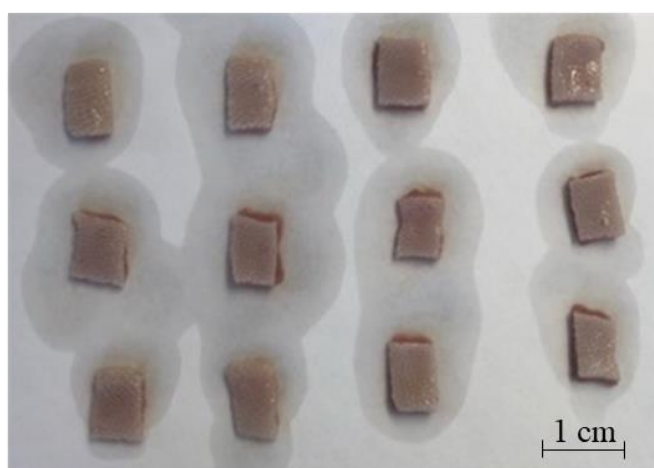


Figure 6.1. The upper layer of the bovine tongue cut into rectangles prior to treatment with different biopolymer solutions.

A freshly cut ox tongue was delivered up to 24 hours post slaughter. Most of the muscle and connective tissues were immediately separated from the upper surface of the tongue, and refrigerated overnight. Freezing was avoided as to reduce undesired damage to the oral mucosa (Hegarty and Naudé, 1973). The dorsal surface of the tongue was gently separated from the remaining muscle tissue using surgical blades and shaped into equal sized rectangles (1x1.5 cm) of around 2 mm in thickness (Figure 6.1.).

The tip and back parts of the tongue were not used to avoid inconsistencies due to their different morphologies, which contain large or an uneven number of very ubiquitous papillae. The sections were immersed in the different orange drink preparations for 5 minutes and then transferred into GC vials for headspace analysis.

6.2.5. Retention analysis and weight experiments

The weight of five control and five mucin beads were recorded before and after immersion in the model drink containing the different polymer solutions. For the GC-analysis, vials containing the mucin beads were placed on a roller mixer for 5 minutes. The beads were drained on a 250 micron sieve to remove excess liquid and were sealed in GC-vials containing 1.0 ml of water to maintain hydration. The experiment was performed in triplicate.

6.2.6. Titratable acidity (TA)

5 ml of the final solution was mixed with 25 ml distilled water. A 0.1N NaOH solution was constantly added in using a 200 µl Gilson's pipette, until the solution reached a pH of ~8. The volume of NaOH solution added was recorded and used to determine the TA of each sample using the following equation:

$$TA = (Vol. NaOH) \times (N NaOH) \times (Eq. factor) / (Wt. sample \times 1000) \times 100$$

6.2.7. Conductivity meter

Changes in the intensity of sodium ions were evaluated using a Mettler Toledo conductivity meter (Ohio, USA). The experimental design was the same as described for the GC analysis. The main difference was that the beads were immersed final solutions contained 1 % (w/v) NaCl. The beads were immersed in 15.0 ml RO water, prior to analysis and allowed to rest for approximately 20 minutes. The conductivity is directly proportional to the amount of Na⁺ ions retained into the bead.

6.2.1. Gas Chromatography-Mass Spectrometry (GC-MS)

The Trace 1300 series Gas Chromatograph coupled with the single-quadrupole mass spectrometer (Thermo Fisher Scientific, Hemel Hempstead, UK) was used (section 2.7.). The column temperature was initially at 40.0 °C for 2 min, then increased by 6.0 °C every minute up until 250.0 °C and held for 5 min. Full scan mode was chosen to measure volatile compounds (mass range from 20 to 300 Da).

6.2.2. Dynamic Light Scattering (DLS)

The experiments were performed using the Zetasizer Nano-ZS detector and low volume disposable sizing cuvettes (Malvern Instruments Ltd, Malvern, UK). The charge was measured at (20.00 ± 0.01) °C using the dip-cell (Malvern Instruments Ltd., Malvern, UK). The bead is held in place between the two electrodes and placed in a standard cuvette (ZEN0112). An applied voltage of 2 mV was used, and the apparent electrophoretic mobility of the bead was measured. It was assumed that the sample does not move during the experiment, therefore no glue was used in the attachment of the beads between the two electrodes. The surface zeta potential cell SOP was employed in automatic mode and repeated 6 times.

6.2.3. Environmental Scanning Electron Microscopy (ESEM)

Mucin beads were kindly analysed by the technical staff at the Nanoscale and Microscale Research Centre (nmRC) using the Thermo-Fisher Scientific (Waltham, USA) FEI Quanta 650 ESEM.

6.2.4. Sedimentation Velocity (SV)

Experiments were performed at 20.0 °C using the Optima XL-I analytical ultracentrifuge with Interference optics as reported in Section 2.1. Samples were analysed at 40, 000 rpm.

6.3. Results and Discussion

6.3.1. Characterization of mucin-alginate beads

It is hypothesized that immobilisation of mucin in alginate beads would result in a mucus mimetic surface having part of the chemical and physical properties of mucins. The beads produced were approximately 4 mm in size. They were subjected to controlled dehydration in the ESEM sample chamber at operating pressures ranging from ~ 4 to ~ 5 Torr.

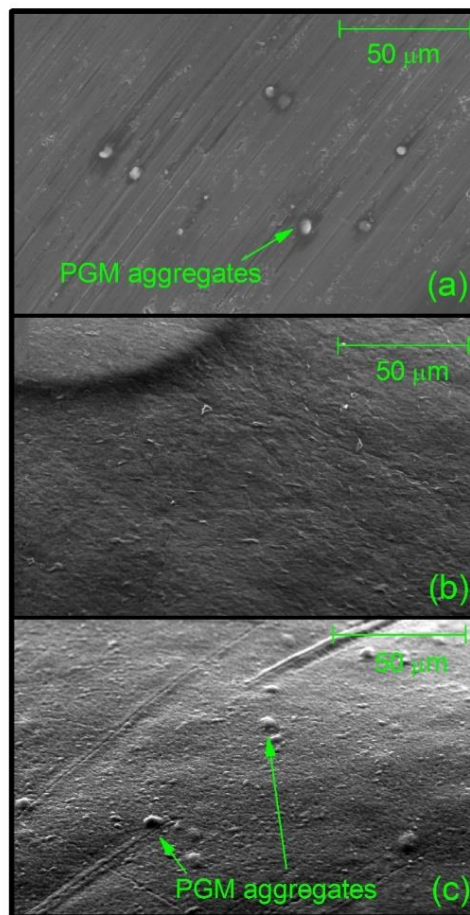


Figure 6.2. Environmental scanning electron micrographs of pig gastric mucin (PGM) suspended in 0.1M PBS, pH 7.0 (a), surface alginate bead (b) and the surface of the alginate-mucin bead (c).

The mucin solution control revealed the formation of larger well-separated globular aggregates ($<1\mu\text{m}$) present on the streaky metal surface of the sample holder (Figure 6.2a). Similar globular features are also visible on the surface of the mucin-alginate bead (Figure 6.2c). By contrast, the surface of the control alginate bead appeared smooth, without the presence of large structures (Figure 6.2b).

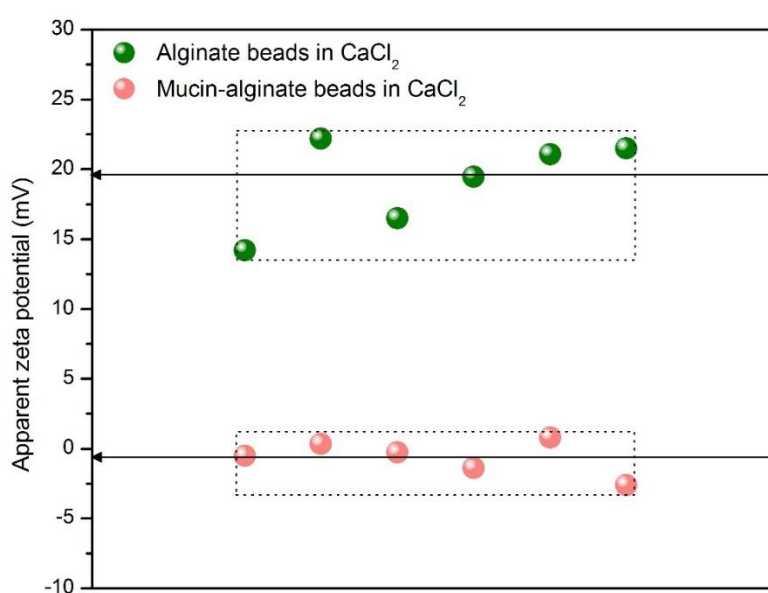


Figure 6.3. Apparent zeta potential of solutions containing calcium alginate control beads and mucin beads (n=6).

The apparent zeta potential was measured by DLS to assess changes in the surface charge of the mucin-alginate bead. Although it was not possible to measure the actual charge, due to the presence of high Ca^{2+} concentrations contributing to overestimates, our values indicate a relative decrease in the zeta potential by ~ 20 mV, after loading with mucin (Figure 6.3.). This is thought to be attributed to the entrapment of mucin within the gelled alginate matrix, thus imparting its anionic properties.

Four different biopolymers were investigated: anionic CMC, neutral non-ionic pullulan, weakly cationic dimethylaminoethyl (DMAE) pullulan and strongly cationic chitosan. All polymers had a weight average molecular weight of approximately 200,000 g/mol. The mucin-alginate beads, along with the control beads (alginate only) were immersed in the different biopolymer formulations.

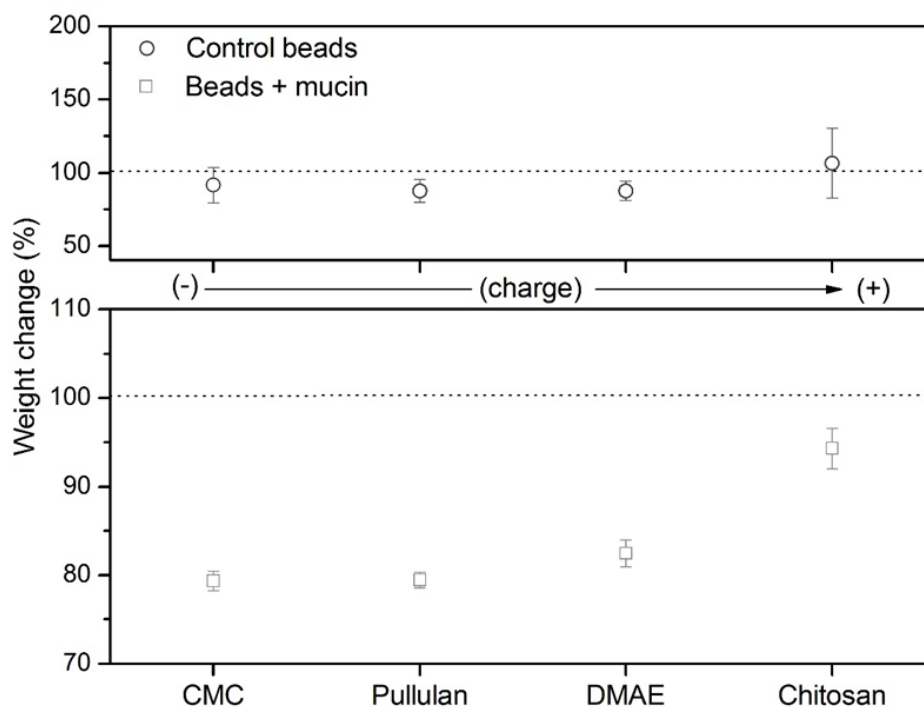


Figure 6.4. Changes in the weight of control and mucin beads after immersion in different biopolymer formulations for 30 min. Weight change is directly proportional to changes in the hydrated radius of the spheres. Values are expressed as mean \pm SD (n = 3).

Changes in the weight of the beads were measured after each treatment and plotted in the order of polymer charge (Figure 6.4.). Within experimental error, there were no differences between the polymer treatments for the control beads, although chitosan led to the largest apparent weight change, which is hypothesized to be due to hydration. By contrast, the different excipients had a pronounced effect on the weight (thus size) of mucin-alginate beads. Firstly, it was observed that all treatments led to a marked decrease the level of hydration of the beads, attributed to ion exchange reactions in the presence of the low ionic strength formulation, such as the migration of calcium ions from the bead. The magnitude of the observed hydration effect was found to be dependent on the net charge of the polymer. For instance, the size of the beads immersed in anionic CMC and neutral pullulan were smallest, as opposed to beads immersed in cationic polymers, which lead to the formation of significantly heavier beads (Figure 6.4. bottom). Based on our hypothesis, this effect is attributed to strong electrostatic interactions between the charged polymer groups and the negatively charged mucins, via their sialic acids or sulfate groups. However, mannuronic or guluronic acid groups of alginate can also interact with chitosan, but the extent of this interaction is reduced by the presence of calcium ions. This has been confirmed by an SV experiment, in the effect of calcium chloride (CaCl_2) on the alginate chitosan interaction was addressed (Figure 6.5.).

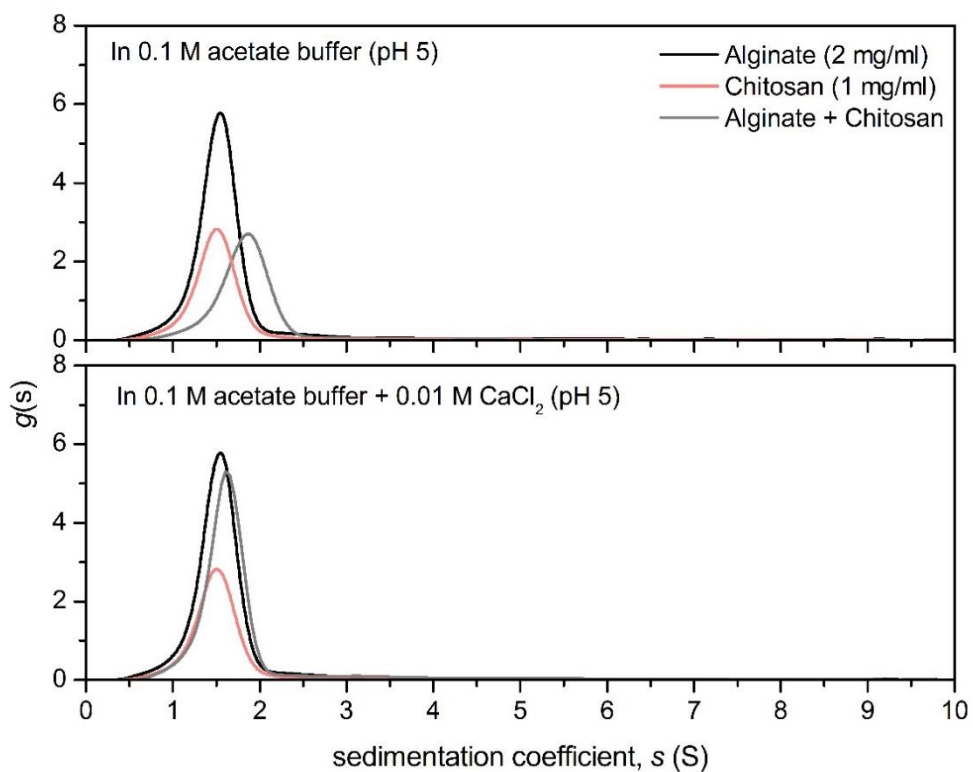


Figure 6.5. Sedimentation velocity, $g(s)$ analysis showing the sedimentation coefficient distributions of alginate (2.0 mg/ml) and the result of its interactions with chitosan (1.0 mg/ml) in the presence and absence of 0.01M CaCl_2 . Rotor speed: 40, 000 rpm (120, 000 g), 20.0 °C.

In the absence of CaCl_2 , the addition of 1 mg/ml chitosan to a 2 mg/ml alginate solution lead to the depletion the alginate concentration and the formation of large supramolecular aggregates of over 200 S (Figure 6.5. top). By contrast, the presence of 0.01 M CaCl_2 appeared to significantly prevent the interaction, although a small proportion of the alginate concentration still decreased (Figure 6.5. bottom).

Very low CaCl_2 concentration were used as to avoid the formation of Ca-alginate gels within the AUC centrepieces. In reality however, the CaCl_2 concentrations used for the formation of the beads would have an even stronger charge shielding effect. Therefore, in the current study, it is implied that interactions with mucin are the main contributors to the differences observed in the hydration of the biomimetic beads.

6.3.2. Retention of aroma and taste compounds

The biopolymers were tested in the presence the real food system: Robinson's orange squash, prepared according to the manufacturer. Hexanal, octanal and decanal were also added to the commercial product, in order to address interactions with linear aldehydes.

There was a distinct effect of each polysaccharide on each aroma compound, for example the strongly cationic chitosan yielded significantly higher concentrations of volatile compounds (Figure 6.6.), when compared to the other biopolymers. A distinct effect was also observed for linear aldehydes, showing a hydrophobicity ($\log P$) dependent effect, where they decrease in intensity with increasing hydrophobicity.

It is also worth mentioning that of the compounds investigated, limonene, nonanal and linalool are the most abundant aroma compounds present in the orange squash product, and correspond to over 80% of all volatiles present.

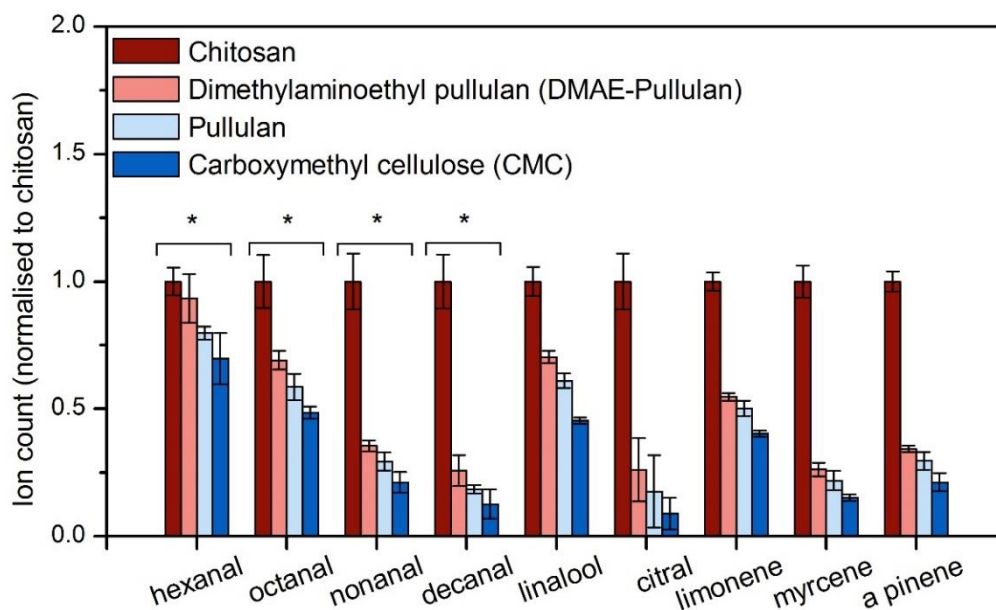


Figure 6.6. GC-MS results showing the relative volatile intensity for the mucin beads after immersion in different biopolymer solutions. Volatile aroma compounds are naturally found in the orange squash formulation while the linear aldehydes were additionally added. The comparison is made by Tukey's post hoc test to calculate the P -values ($P < 0.05^*$). The data are shown as mean \pm SD, ($n=3$).

Significant differences were observed in the retention of the aroma compounds as a function of polymer charge, in the order of chitosan, DMAE-pullulan, pullulan and CMC ($P < 0.05$). With the exception of linalool, limonene and myrcene, minor differences were observed between CMC and pullulan ($P < 0.05$), although the relative intensity was an average of $\sim 10\%$ higher in the presence of pullulan. However, no changes in weight were observed for the two treatments (Figure 6.6.). This may be due to different physiochemical properties between the CMC and pullulan, such

as branching and higher viscosity for CMC, although there were no differences in the viscosity and pH of the dilute orange drinks.

Table 6.1. Titratable acidity (TA) of final orange drinks containing different polymers (error based on $\pm 50 \mu\text{l}$ 0.1N NaOH).

Biopolymer	TA (g/100ml)
CMC	0.34(± 0.01)
Pullulan	0.33(± 0.01)
DMAE-pullulan	0.33(± 0.01)
Chitosan	0.40-0.43 (± 0.01)*

*depending on main acid present i.e. citric (eq. factor 0.064) or acetic (eq. factor 0.060).

Additionally, an experiment was performed to quantify the total acidity (TA) contained within the model food (Table 6.1.). This was performed by exhaustively titrating the liquid drinks until they reach a pH of ~ 8 . Although the pH of the different orange drink formulations was virtually identical ~ 4.5 , small differences in TA were found in the chitosan formulation, attributed to the additional presence of acetic acid used in the solubilisation of chitosan. Therefore, the slightly higher acidity may also contribute to the higher partitioning of aroma compounds (Sadler and Murphy, 2010; Dinu et al. 2019a).

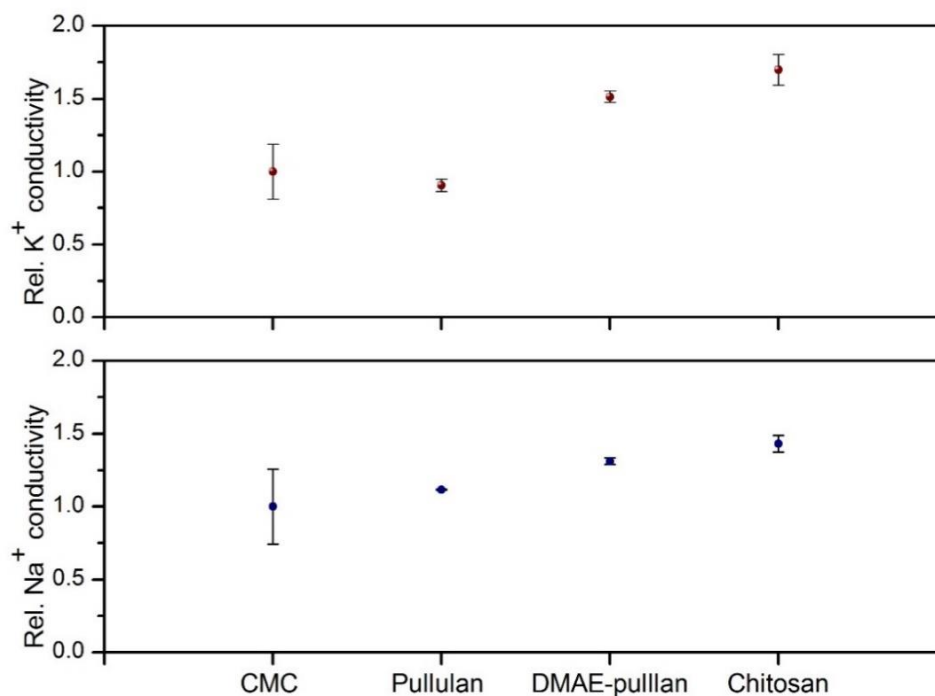


Figure 6.7. Conductivity results showing the relative Na⁺ and K⁺ concentration on the mucin beads after immersion in different biopolymer solutions. Values are determined by subtracting the values of the control beads. Values are expressed as mean ± SD (n = 3).

In an analogous way, the ability of our *in-vitro* surface to retain sodium and potassium was investigated (Figure 6.7.). The results appear to be in complete agreement to the hypothesis, despite the different interaction mechanism of ions with mucin or other ionic polysaccharides present in the system (Janado and Onodera, 1972). This includes charge shielding of carboxylic acids, sialic acid and reduction in polymer viscosity.

Although a similar trend was observed, changes in relative intensity of sodium ions retained in the presence of CMC were not significantly different, possibly due to the small sample size, or via any of the

mechanisms mentioned previously. By contrast to anionic polymers, salt retention in the presence of cationic polymers increased by up to 50%, reinforcing the strong effect of electrostatic interactions in mucoadhesion (Figure 6.7.).

It may be possible sodium retention is related to changes in hydration but also to competition with calcium ions (Figure 6.4.). Another possibility may result from the anionic polymer effect, previously shown to stunt the perception of sodium by reversibly serving as the anion associated with the Na⁺ ions (Ye et al., 1991).

6.3.3. Comparison to the *ex-vivo* tongue surface

The retention of aroma compounds on the *in-vitro* system was next compared to the *ex-vivo* bovine tongue surface (Figure 6.8.). The model used in our study was made from the dorsal layer containing the papillae. Results appeared to be in full agreement with the *in-vitro* findings, with volatile retention being directly correlated to the charge of the polymers.

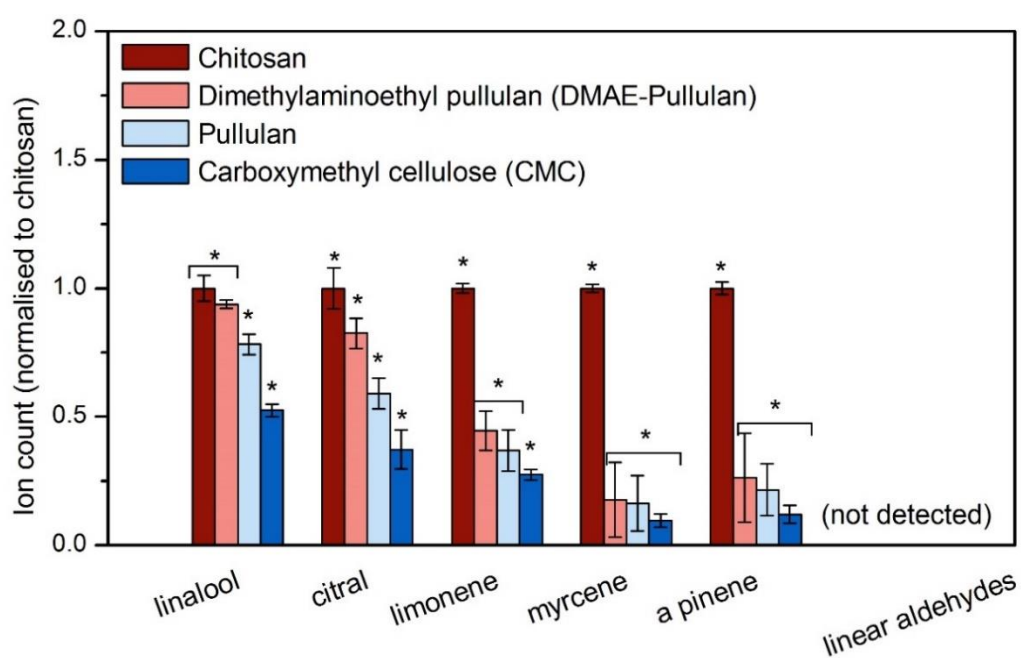


Figure 6.8. GC-MS results showing the relative volatile retention on the mucin beads after immersion in different biopolymer solutions. The comparison is made by Tukey's post hoc test to calculate the *P*-values ($P < 0.05^*$). The data are shown as mean \pm SD, ($n=3$).

Major differences are observed for the extra added linear aldehydes, which were not detected by the GC-MS. Other studies have reported this effect, and is suggested to arise from the formation of irreversible covalent bonds (Schiff bases) between linear aldehydes and amino acids, such as lysine (Godoy-Alcántar et al., 2005; Gremlı, 1974; San George and Hoberman, 1986).

6.3.4. General Discussion

Our previous experiments using pooled human saliva have also confirmed a significant reduction in the headspace concentration of linear aldehydes in green tea, but not to this extent (Dinu et al., 2018b). It is worth highlighting potential issues associated with the validity of the bovine tongue surface and other similar *ex-vivo* tissues (Davidovich-Pinhas and Bianco-Peled, 2014; Cook 2017). It is possible that the excised tissue may not be the most accurate representation of an oral surface after all, due to the higher proportion of exposed meat on the ventral surface of the tongue, uncovered by a mucus layer. This may be an explanation for the loss in the linear aldehyde signal, compounds well known to irreversibly bind to protein groups, which apart from the 'naked' regions present sparsely present in mucus, are absent in the *in-vitro* model.

However, other proteins or enzymes may be encapsulated to provide a more accurate representation of the target tissue. Another advantage is that the gel structures can be tailored to meet specific applications, by varying the concentrations of calcium chloride or sodium alginate. Additionally, the gelled alginate beads can be adjusted in size or moulded into completely different shapes, such as thin sheets, depending on the test needed to assess mucoadhesion.

6.4. Conclusion

Given the anionic properties of mucins, electrostatic interactions with polymers play a key role in mucoadhesion, along with hydrogen bonds and van der Waals forces of attraction. Here, we took advantage of some of these functional properties to validate the ability of the developed *in-vitro* system to retain flavour compounds as a function of the co-ingredient mucoadhesive.

The surfaces are synthesized by using the ion exchange calcium-alginate reaction, which led to the formation of mucin immobilised alginate gel beads. Electron microscopy and Zeta potential results indicated that mucins and mucin aggregates are distributed within the gelled alginate matrix, imparting their characteristic charge to the surface of the beads.

The mucus like surfaces were proven able to retain flavour compounds, naturally present in orange squash formulations in a similar way to the bovine tongue surface, excluding linear aldehydes which are suggested to bind to the dorsal part of the tongue, contaminated from excision. The immobilisation of other relevant proteins may further reduce the gaps in the current system and therefore help to reduce future needs to use animal tissues.

7. Chapter 7: Hydrodynamic interactions of mucin and α -amylase with aroma and taste compounds

7.1. Introduction

The interactions of volatile aroma compounds and various different proteins has been reported previously (Guo et al., 2019; Jouenne and Crouzet, 2000; Landy et al., 1995; Zhou et al., 2014). Aroma/protein interactions are generally classified into three categories (McGorin et al., 1996): (i) binding of flavour compounds, (ii) phase partitioning, i.e. air, water or lipid, or (iii) viscosity effects. Binding can either be reversible or irreversible depending on the strength of the interaction. Ketones and aldehydes are reported to covalently bond with amino groups of proteins (Weerawatanakorn et al., 2015, Meynier et al., 2004). Others have shown that they form weak hydrogen bonds with food or salivary macromolecules containing electronegative clusters of nitrogen, sulphur or oxygen (Reineccius, 2006; Tromelin et al., 2006).

While most mucins are heavily glycosylated, submaxillary mucins are made up of a higher fraction of 'naked' unglycosylated polypeptide, predominantly composed of cysteine, serine, threonine and proline. While cysteine participates in disulphide bonding between mucin subunits, serine and threonine form bridges via their hydroxyl groups with the N-acetylgalactosamine residues of the oligosaccharides chains (Steen et al., 1998). Protein sequencing has confirmed that the serine, threonine,

proline assist in the coiling of the glycoprotein (Harding et al., 1983a, 1983b), which are thought to give rise to potential interaction sites.

Salivary α -amylase (HSA), which is also a glycoprotein, is made up of 496 amino acids, represented by a $(\beta/\alpha)_8$ enzyme barrel structure containing the catalytic core and the Cl^- and Ca^{2+} binding sites. The open catalytic site consists of acidic amino acids such as aspartic acids and glutamine, while the ion binding sites are mainly composed of aspartic acid, arginine, and histidine (MacGregor et al., 2001).

The tertiary and quaternary structure of proteins can expose numerous potential sites for interaction through hydrogen bonding and hydrophobic interactions. It is hypothesised that the exposed amino groups of the amino acids in mucin, α -amylase and other salivary proteins, can participate in aldehyde and ketone binding, which leads to the formation of permanent or non-permanent Schiff bases, or imine adducts. To test this hypothesis, we take advantage of the powerful technique of sedimentation velocity-analytical ultracentrifugation (SV-AUC), along with viscometry and SEC-MALS to illustrate how such protein-aroma interactions might affect some of the solution properties of BSM and HSA.

In addition, taste compound quinine is investigated for its interaction with HSA. It is worth noting that most aroma compounds have a high buoyant force, and a tendency to partition in the gas phase. They are below the detection level for analytical ultracentrifugation in terms of their molar mass (<150 g/mol); nonetheless it may still be possible to assess their effect on the sedimentation properties of the two macromolecules.

7.2. Materials and Methods

7.2.1. Samples

Bovine submaxillary mucin (type I-S, M3895), human salivary α -amylase (type IX-A, A0521) and aroma compounds were purchased from Sigma Aldrich (Dorset, UK). The samples were made in 0.1 M phosphate buffered saline (PBS).

7.2.2. Sedimentation Velocity (SV)

Experiments were performed at 20.0 °C using the Optima XL-I analytical ultracentrifuge (Beckman, Palo Alto, USA) equipped with Rayleigh interference optics. Samples were centrifuged at 30, 000 rpm. A partial specific volume of 0.64 ml/g and 0.74 ml/g were employed for mucin and α -amylase respectively (Fisher et al., 2006).

7.2.3. Raman spectroscopy

Raman spectroscopy was performed using a RamanRXN2 optical system (Kaiser, Boston, USA) as discussed in Section 2.10. A 10 mg/ml stock mucin solution was prepared in 0.1 M PBS and dialysed against a 14000 Da cut off membrane, (Fisher scientific) to remove salts, in order to prevent the formation of salt crystals during drying. The cut-off is based on globular protein assumption which may be significantly less for mucins due to their much larger hydrodynamic volume.

7.2.4. SEC-MALS-Viscostar

The SEC set-up consisted of a Postnova Analysis PN7505 degassing unit (Landsberg am Lech Germany), Shimadzu LC-10AD HPLC Pump (Shimadzu UK, Milton Keynes, UK.), fitted with a Spark-Holland Marathon Basic autosampler (Spark Holland, Emmen, The Netherlands) combined with a TSK Gel guard column (7.5 × 75 mm) and TSK Gel G5000, G6000 columns (7.5 × 300 mm) connected in series (Tosoh Biosciences, Tokyo, Japan), as discussed previously.

The samples were filtered through a 0.45 µm syringe filter (Whatman, Maidstone, England) to remove any insoluble material or dust prior to injection and then injected into the autosampler. A 100 µl aliquot of each solution was injected onto the columns at ambient temperature. The eluent employed was the PBS dialysate at a flow rate of 0.5 ml/min.

7.2.5. E-tongue analysis

Solutions were made to a constant concentration of 20 mM quinine hydrochloride (QHCl) and increasing concentrations of α-amylase. Samples were poured into sample cups for the electronic tongue in triplicate (Taste Sensing System TS-5000Z). Manufactures guidelines were used for analysis and data extraction. The acidic bitterness sensor 'C00' and the ion sensor 'CT0' were used to evaluate the concentrations of QHCl. The analysis was kindly performed by New Food Innovation specialists as according to previous studies (Pein et al., 2014; Tahara and Toko, 2013).

7.2.6. Capillary viscometry

Relative viscosity was measured using the semi-automated (Schott Geräte, Hofheim, Germany) U-tube Ostwald capillary viscometer immersed in a temperature-controlled water bath at 20.00 °C. A constant volume of 2.0 ml was used for sampling. BSM concentrations were remained constant at 0.5 mg/ml while the concentrations of hexanal were varied. The intrinsic viscosity, $[\eta]$ was calculated according to the Solomon-Ciuta equation (eq. 1.4.18) and plotted against the concentration series.

7.3. Results and Discussion

7.3.1. Interactions of BSM with aldehydes and ketones

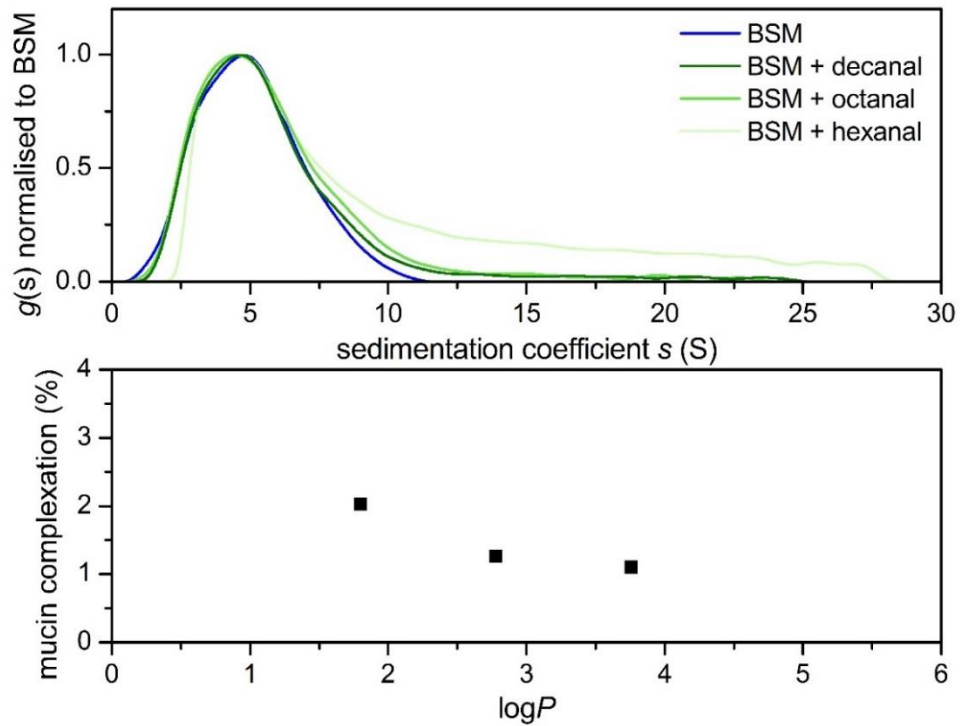


Figure 7.1. Sedimentation velocity, $g(s)$ analysis showing the sedimentation coefficient distributions of BSM (1.0 mg/ml) and the effect of linear aldehydes (5.0 mg/ml) on this distribution; and (lower) plot of hydrophobicity, $\log P$ against % change in mucin complexation. Rotor speed: 30,000 rpm (90,000 g), 20.0 °C.

Figure 7.1. shows the sedimentation coefficient distribution of a 1 mg/ml solution of BSM in the 0.1 M PBS buffer, revealing a broad polydisperse distribution ranging from $\sim 2S$ to $12S$, as shown previously (Dinu et al. 2019a). The addition of different linear aldehydes was shown to increase the peak broadness of the distribution, tailing up to $\sim 28S$ for the more hydrophilic compounds such as hexanal.

The effect was correlated with the partition coefficient $\log P$, which is a measure of compound hydrophobicity (Figure 7.1. lower).

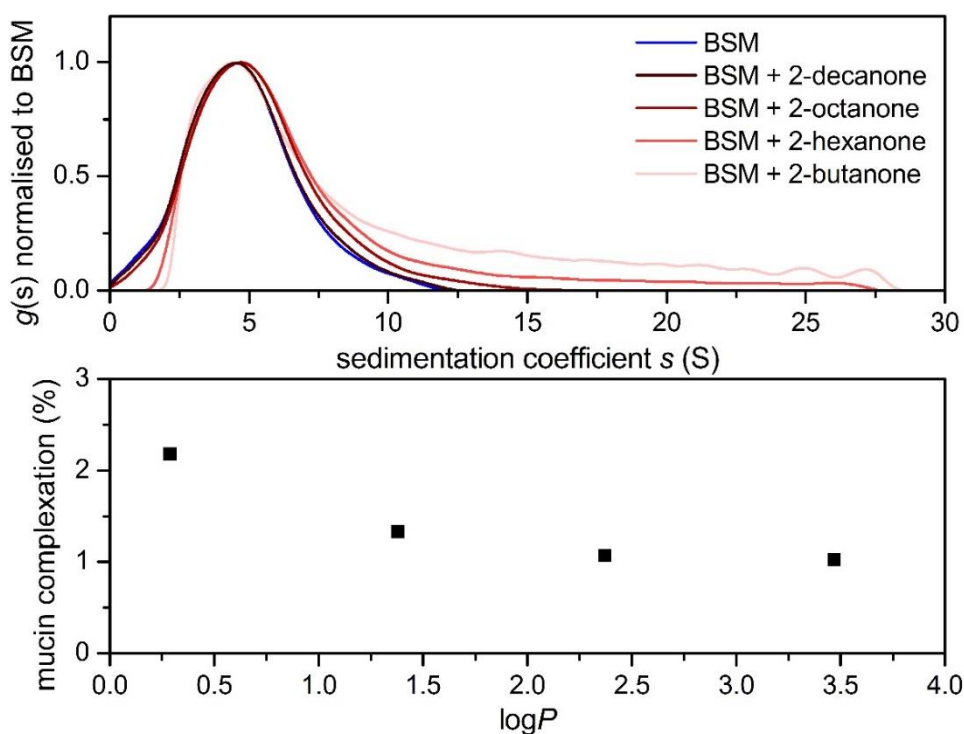


Figure 7.2. Sedimentation velocity, $g(s)$ analysis showing the sedimentation coefficient distributions of BSM (1.0 mg/ml) and the effect of linear ketones (5.0 mg/ml) on this distribution; and (lower) plot of hydrophobicity, $\log P$ against % change in mucin complexation. Rotor speed: 30,000 rpm (90,000 g), 20.0 °C.

A similar effect was observed in the presence of linear ketones, which also revealed a direct relationship with their $\log P$, although the % change in complexation appeared milder. It is suggested that the additional alkyl group reduces the reactivity of their carbonyl groups.

Although the addition of ketones or aldehydes does not result in significant changes in the sedimentation coefficient of the main, the shape of the peak is affected (Figure 7.2.). The weighted average sedimentation coefficient

has shifted from lower to higher S values, as observed in the $\sim 1.5S$ and after the 12S region.

This indicates the formation of mucin aggregates. However, it is also possible that the higher solution density of the more hydrophilic compounds affects the rate of sedimentation of the mucin components to a higher extent than the less hydrophilic compounds. An additional experiment was employed using the SEC-MALS to confirm the results from the AUC, showing the interaction of mucin with hexanal (Figure 7.3.).

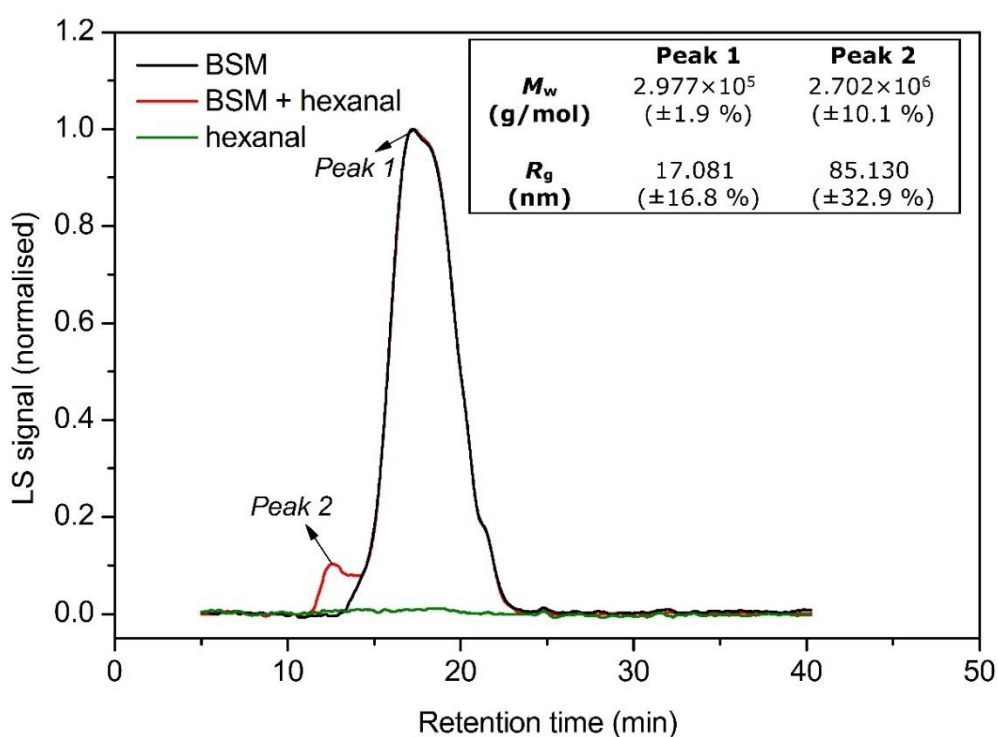


Figure 7.3. SEC-MALS results showing the light scattering (LS) elution profile of BSM, hexanal and the result of their interaction. Insert shows the summary for the hydrodynamic parameters for the main peaks, including weight average molar mass (M_w) and apparent radius of gyration (R_g).

Results reveal a broad multi-component assembly of BSM, ranging from ~16 to 24 min, as in previous reports (Dinu et al., 2019a). The addition of hexanal led to the formation of additional components (Peak 2), which appear to be of higher molecular weight, almost 10 times larger than those of Peak 1. Consequently, the hydrodynamic radius of the new components increased considerably, although the relatively high experimental errors indicate small relative concentrations. However, results from SEC-MALS and SV are indicating an interaction between hexanal and mucin.

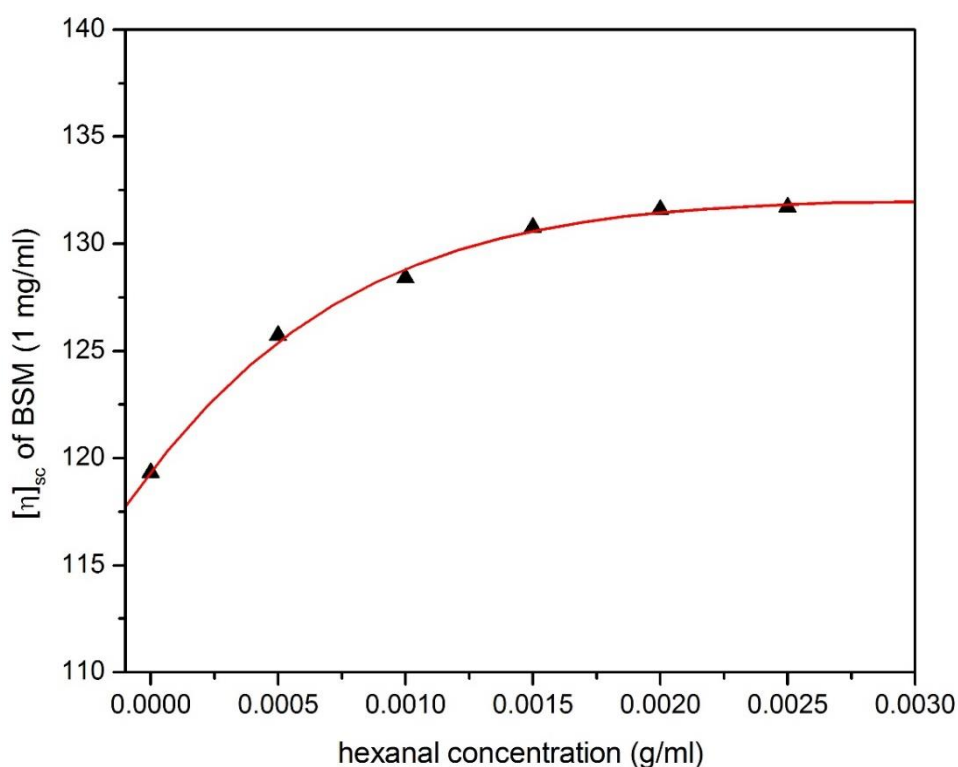


Figure 7.4. Solomon-Ciuta intrinsic viscosity $[\eta]_{sc}$ analysis showing the quantitative effect of hexanal addition to bovine submaxillary mucin (1.0 mg/ml) in 0.1M phosphate buffer saline. The polynomial fit is based on 6 data points derived from separate hexanal/BSM mixtures.

Changes in the intrinsic viscosity of BSM at different concentrations of hexanal are next studied (Figure 7.4.). The intrinsic viscosity $[\eta]$ values of BSM were obtained by using the Solomon-Ciuta relation at a constant mucin concentration of 1.0 mg/ml and plotted against the added concentrations of hexanal (Figure 7.4.).

The addition of hexanal led to an increase in the intrinsic viscosity, gradually plateauing at higher hexanal concentrations, attributed to the low solubility of hexanal in water (~ 2.5 mg/ml at 20.0 °C). This interaction could arise from a direct binding or hexanal induced aggregation leading to an increase in the molecular weight observed by SEC-MALS.

7.3.2. Interactions of BSM with phenolic compounds

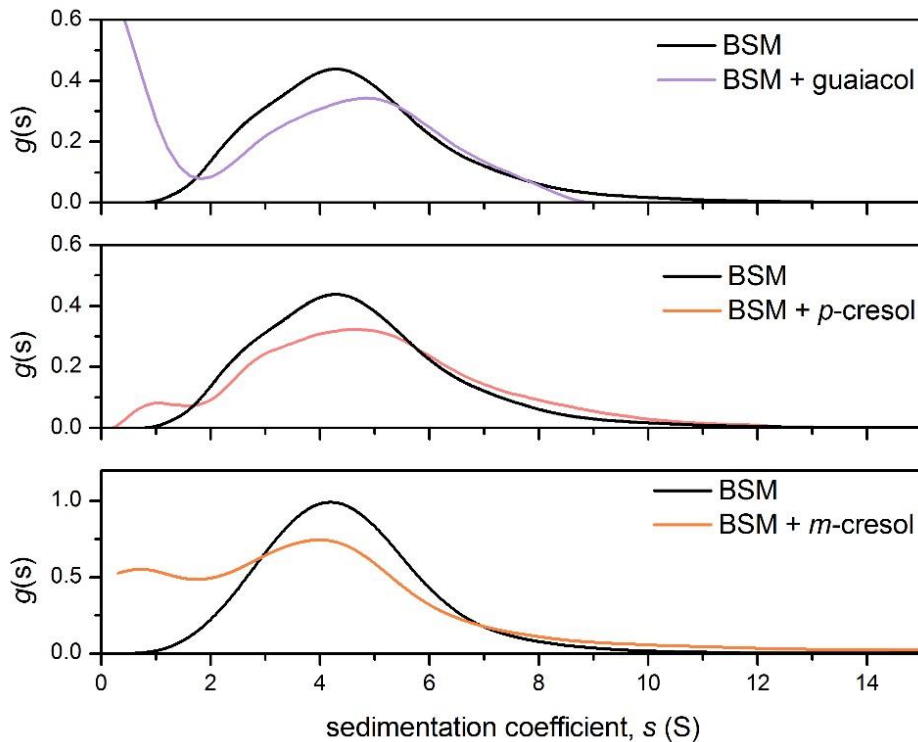


Figure 7.5. Sedimentation velocity, $g(s)$ analysis showing the sedimentation coefficient distributions of BSM (0.5 g/ml) and the result of its interactions with different phenolic compounds (0.5 mg/ml). Rotor speed: 30,000 rpm (90,000 g), 20.0 °C.

In a similar way, it was found that phenolic aroma compounds have the ability to alter the sedimentation coefficient distribution of mucin. Results in Figure 7.5. correspond to changes in the sedimentation coefficient of BSM upon the addition of guaiacol, *p*-cresol and *m*-cresol. Data suggests that the phenols act as chaotropes by inducing changes the molecular distribution of mucins.

It is worth suggesting that guaifenesin, which has the same functional groups as guaiacol, has been considered for reducing the molecular weight

and viscosity of mucus in medication for patients suffering from mucus congestion issues caused by common colds (Rubin, 1999; Seagrave et al., 2011). It was suggested that the hydroxyl group of the phenol ring (phenoxy group), is primarily involved in some type of interaction with mucin glycoproteins (Rubin, 1999; Seagrave et al., 2011).

As a result, the interactions between *p*-cresol and BSM were further investigated by Raman spectroscopy, by examining changes in the vibrational spectrum of BSM before and after the addition of *p*-cresol (Figure 7.6.).

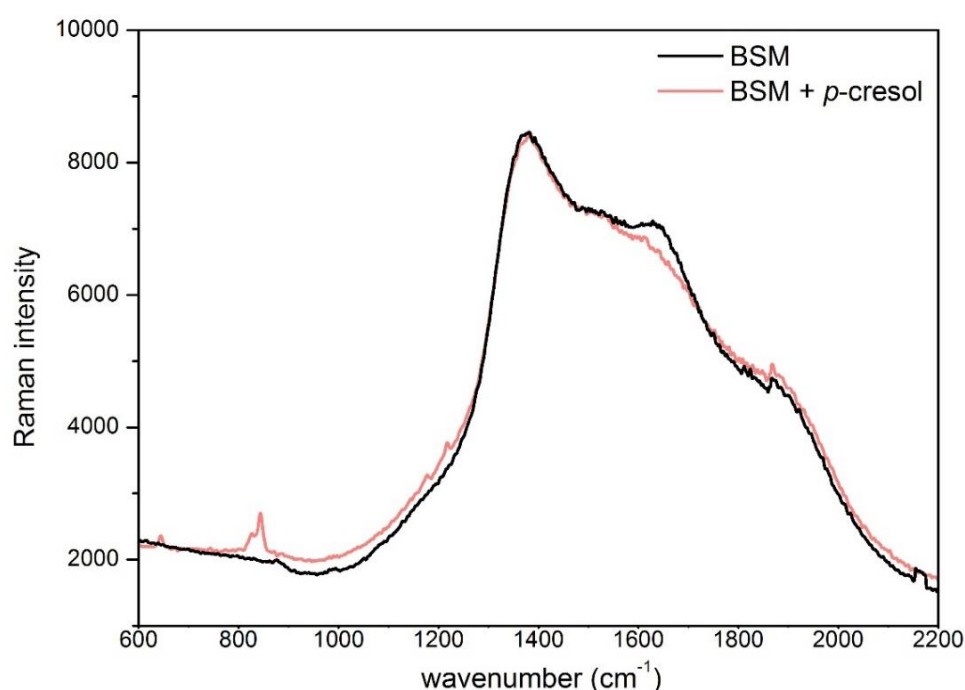


Figure 7.6. Raman spectra of BSM (c= 10 mg/ml) with and without *p*-cresol (1.0 mg/ml). The mixture was dialysed against a 14 kDa membrane prior to analysis to remove excess *p*-cresol. Performed in 0.1 M PBS pH 7.0 at 20.0 °C.

Spectral changes were observed in the 820-850 cm^{-1} region, which represents a Fermi doublet, distinguished by the stronger (840 cm^{-1}) and weaker (810 cm^{-1}) Raman shifts (Arp et al., 2001). The ratio of the doublet is said to provide information on the strength of the hydrogen bonding of the phenoxy group in solution (Arp et al., 2001; Miura and Thomas, 1995). Secondly, a decrease in the intensity of the 1500-1700 cm^{-1} Amide I and II region is observed, indicating changes in the protein region of mucin, thus supporting previous reports.

7.3.3. Interactions between HSA and aroma compounds

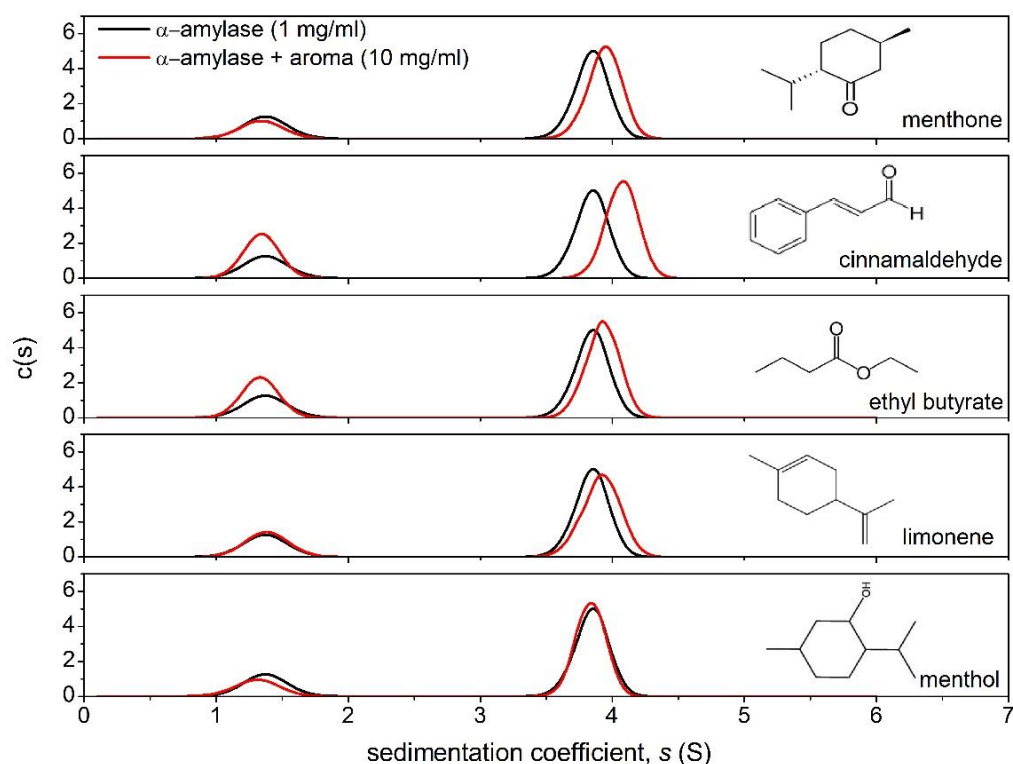


Figure 7.7. Sedimentation velocity, c (s) analysis showing the sedimentation coefficient distributions of HSA (1.0 mg/ml) in 0.1M PBS and the result of its interactions with different aroma compounds. Rotor speed: 40,000 rpm (100,000 g), 20.0 °C.

Interactions between the aroma compounds and α -amylase are surprisingly underexplored, considering the high relative concentrations and function of the enzyme during food processing. A range of aroma compounds/HSA interactions were investigated, including esters, ketones and aldehydes (Figure 7.7.).

In the same way as mucin, it was shown that volatiles containing a carbonyl group had a marked effect, particularly in compounds which have less steric hindrance allowing for nucleophilic attack. For example, the addition of cinnamaldehyde led to the highest increase in the apparent weight average sedimentation coefficient by $\sim 10\%$ from $\sim 3.8S$ to $\sim 4.2S$. This may also be linked to previous findings which showed that cinnamaldehyde can inhibit α -amylase activity (Okutan et al., 2014). By contrast, compounds containing hydroxyl functional groups, such as menthol, led to no apparent changes in the sedimentation coefficient distribution (Figure 7.7.).

Although minor changes, they are fairly reasonable considering the very low molecular weights of aroma compounds and the limited availability binding sites on the α -amylase surface. However, it is difficult to establish whether these interactions are a result of a direct binding or minor changes in conformation due to a decrease in the hydration of the enzyme.

7.3.4. Interactions between quinine and HSA

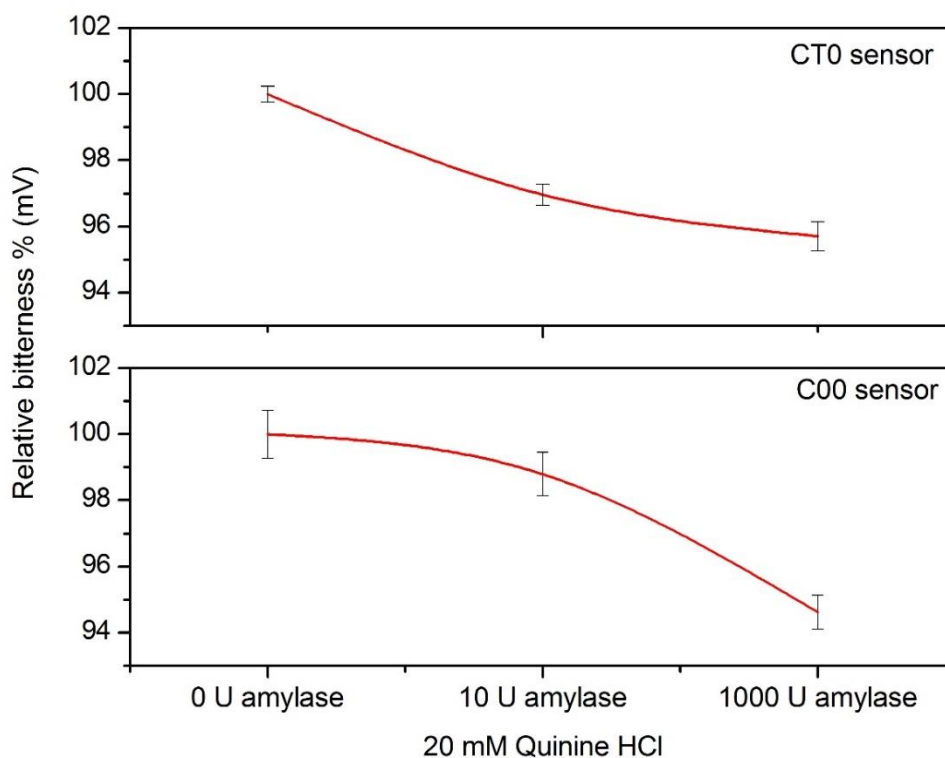


Figure 7.8. Results from the INSENT E-tongue showing the % change in the intensity of bitterness as a result of α -amylase addition. Experiments performed at 20.0 °C. Values are expressed as mean \pm SD (n = 3).

Next, quinine hydrochloride was used as a higher molecular weight taste compound to characterise its interactions with α -amylase. A reduction in the signal for bitterness was observed upon the addition of α -amylase (Figure 7.8.). This is thought indicate either an interaction attributed binding or due to physical obstruction of the probe signal by the increased concentration of enzyme. However, the E-tongue works by detecting changes in electric potential (mV) generated by the molecular functional groups (Latha and Lakshmi, 2012; Woertz et al., 2011). Therefore, these changes are suggested to arise a chemical interaction within the system.

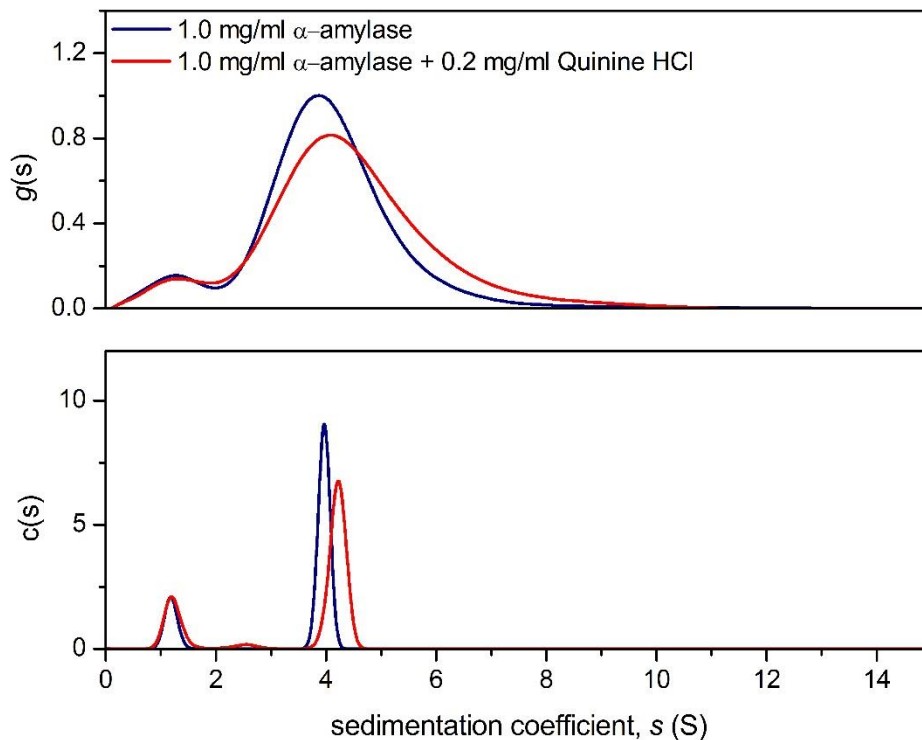


Figure 7.9. Sedimentation velocity, $g(s)$ and $c(s)$ analyses showing the sedimentation coefficient distributions of HSA (1.0 mg/ml) and the result of its interactions with quinine hydrochloride (0.2 mg/ml) in 0.1M PBS. Rotor speed: 30, 000 rpm (90, 000 g), temperature 20.0 °C.

An SV experiment was employed to elucidate the potential mechanism by which the concentration of quinine is reduced (Figure 7.9.). Changes were observed in the sedimentation coefficient distribution of α -amylase upon the addition of quinine hydrochloride, such a decrease in the concentration of the 4S component and an increase in peak broadness and higher S species (Figure 7.9.). This might indicate either a direct binding or aggregation induced by the addition of quinine hydrochloride, which is slightly alkaline having a pK_a of ~ 9 (Schulman et al., 1974).

Other studies have reported an interaction between quinine and bovine serum albumin (BSA). For instance, an increase in the hydrodynamic particle size of BSA has been observed by DLS upon the addition of quinine (Liu et al., 2014). NMR studies also showed that the signal for aromatic protons is higher than that of aliphatic protons, suggesting electrostatic interactions between the benzene ring containing the amino group and acidic amino acids containing carboxyl functions, such as glutamate or aspartate which are actually present in the catalytic core of α -amylase (Liu et al., 2014).

7.3.5. General Discussion

Previous studies have reported that acetaldehyde, the shortest aldehyde, has been linked to the onset of mutagenesis, DNA damage, heart failure or coagulation disorders (Hoffmann et al., 1993; Setshedi et al., 2010). Particularly associated with chronic alcohol consumers, acetaldehyde was shown to increase the risk of developing alcoholic liver disease and hepatocellular carcinoma by promoting adduct formation with the proteins, thus leading to impairment in protein function (Donohue et al., 1983; Stevens et al., 1981). It was found that the interactions between acetaldehyde and proteins can be both permanent and non-permanent (Donohue et al., 1983; Stevens et al., 1981; Tuma et al., 1987).

The amino group of N-terminal amino acids, such as serine and threonine in mucins, are suggested to be the functional groups participating in aldehyde binding. Adducts are mainly characterised as Schiff bases,

sometimes referred to as imines, resulting from the reaction of the aldehyde carbonyl group with primary or secondary amino groups.

Depending on the physiological conditions, such as the pH of the bolus, the carbonyl group of aldehyde or ketone compounds can become prone to nucleophilic attack by amines (Godoy-Alcántar et al., 2005; San-George and Hoberman, 1986). This is sometimes classified as a condensation reaction, although imine reactions are usually characterised in organic solvents, and their formation in water or physiological conditions is not well understood.

One study investigated the binding of more hydrophobic linear aldehydes such as octanal onto the rat olfactory receptors. It was suggested that the odour binding pocket for octanal is predominantly made up of lysine and aspartic acid residues, with the hydrophobic tail of octanal also able to form van de Waals interactions with the hydrophobic pockets (Singer, 2000).

Based on the current study, we have shown that the extent of aldehyde or ketone binding is influenced by compound hydrophobicity and solubility in the aqueous solution. Incidentally, it appears that mucin complexation is stronger as the compounds become more hydrophilic. Interactions between mucin and hexanal were also confirmed by SEC-MALS and intrinsic viscosity, both indicating some aggregate formation. It is worth suggesting that the $\log P$ dependency may also explain why the shortest linear aldehyde, acetaldehyde, has such major effects on the structure-function relationship of proteins.

Interactions between mucins and phenolic compounds such as cresols or guaiacol have not been reported previously. Unlike ketones and aldehydes, the presence of aromatic compounds appeared to also reduce the sedimentation coefficient distribution, indicating destabilisation phenomena, whereby the mucin distribution is separated into smaller fractions.

p-cresol is a by-product of citral degradation, which is a major ingredient in citrus flavoured drinks (Choi et al., 2009). Although, effects are valid at higher concentrations, they are not representative of the actual concentrations found in commercial products (<0.1 mg/l). However, some compounds can be found at excessively high concentration in different products (>2 mg/ml), in which case the effects observed in our study are valid.

Moreover, the main functions of *m*-cresol are known to de-aggregate insulins into their active, monomeric form (Whittingham et al., 1998). Therefore, mechanisms by which they interact with mucin might be of a similar nature. Raman analysis was used to validate the nature of the interactions, indicating changes in the non-glycosylated protein domains, directly related to the disruption of the hydrogen bonds present in the protein regions.

A substituted phenol, guaiacol is a flavouring in whisky or smoky products which appeared to behave in a similar way, with the SV analysis indicating similar changes in the sedimentation coefficient distribution. However, guaiacol was previously already shown to bind proteins and is used as a universal substrate for peroxidase enzymes, shown to interact with glycine

and isoleucine amino acids its phenoxy group (Murphy et al., 2012). A similar mechanism is reported for the mucilatory clearance effects of guaiacol glyceryl ether – or guaifenesin, administered to patients to help thin the mucus (Seagrave et al., 2011).

Similar mechanisms are possible in the current study, although the possibilities of interaction with the carbohydrate regions of mucin should not be excluded. For instance, Tsuji and Osawa, (1986) have studied the attractive interactions between fucose and benzene and found that the stabilisation energies between the benzene ring and the -OH and -CH bonds can be as strong as that of a hydrogen bond.

7.4. Conclusion

So far, this is the first biophysical study revealing changes in the physical properties mucin and α -amylase induced by low molecular weight flavour compounds. Hydrodynamic techniques were used to examine their interactions with submaxillary mucin and α -amylase. It has been shown that aroma molecules containing more reactive carbonyl moieties elicit a higher effect on the hydrodynamic properties of BSM and α -amylase, leading to the formation of aggregates. The effect appears to be correlated with their hydrophobicity ($\log P$), or solubility in aqueous media, with the more soluble compounds having a higher effect.

Secondly, the interactions of mucin with phenolic compounds, complemented by Raman spectroscopy and intrinsic viscosity were further investigated. As indicated by the presence of the Fermi doublet and the decrease in the Amide I and II spectrum, it is suggested that the phenoxy

groups are involved in the interaction with those from the amino acids in the 'naked' polypeptide regions.

Lastly, we have revealed that higher concentration of HSA can inhibit bitterness, possibly through binding phenomena. However, more detailed studies of these interactions need to be investigated. This could lay grounds for new research into the health benefits of flavour compounds.

While the concentrations of flavourings used in the current study are not representative of the very low concentrations found in most food or drinks, they may have significant implications in products such as flavoured electronic cigarettes, where their concentration are up to a million times higher (up to 10 mg/ml), and are directly adsorbed onto the lung mucus surface.

8. Chapter 8: Perspectives, Concluding Remarks and Future Work

8.1. Effect of acidity (pH) and ionic strength (salt)

The aim of this section was to study the effects of dietary acidic pH and salt on the hydrodynamic properties of submaxillary mucin and salivary α -amylase and monitor subsequent changes in the headspace concentrations of aroma compounds.

8.1.1. Bovine submaxillary mucin (BSM) characterisation and pH effects

BSM is a more recent type of mucin employed in research as a surrogate for human salivary mucins. First, BSM was assessed for its molecular integrity at neutral and acidic pH using sedimentation velocity (SV), intrinsic viscosity, dynamic light scattering (DLS) and size exclusion chromatography coupled with multi-angle laser light scattering (SEC-MALS). Preparations were made in 0.1 M phosphate buffer saline, pH 7.0, to simulate the physiological solution conditions of saliva, while the 0.1 M sodium citrate buffer was used to assess the effects of the lower pH, representative of the vast majority of foods (Figures 3.1-3.3).

The weight average molecular weight of BSM was analysed using SEC-MALS and SV (via the more recent Extended Fujita transformation of the $g(s)$ distribution). The MHKS double logarithmic relation showed a good correlation between molar mass and intrinsic viscosity, consistent with random coil molecules. The additional MultiHYDFIT package yielded a persistence length value, L_p of 5.6 nm (± 0.5) and mass per unit length, M_L of ~ 800 g.mol⁻¹/nm, corresponding to a very tightly packed random coil type of molecules in solution (Figure 3.3).

SEC-MALS results were used in the Extended Fujita analysis for the molecular weight and provided an opportunity to assess differences due resulting from acidic solution conditions. Results suggest mild aggregation phenomena and possible changes in conformation to even more tightly packed structures, as the pH decreases closer to the isoelectric point of mucin (pI \sim 2-3). It is suggested that charged carbohydrate residues are neutralised and therefore collapse onto the polypeptide backbone.

However, there are a couple of inconsistencies in the molecular weight and intrinsic viscosity analysis. Firstly, the intrinsic viscosity results obtained from Ostwald U-tube capillary viscometry are lower than the results obtained from the pressure imbalance viscometer 'Viscostar', measured after SEC column separation (Table 3.1). Secondly, there are discrepancies between the weight average molecular weight determined from SEC-MALS and that from sedimentation equilibrium (SE), the latter suggesting significantly lower weight average molar mass. One possible explanation is that the SEC-MALS-Viscostar set-up yields overestimation of molecular mass and intrinsic viscosity, due to the formation of aggregates during separation. The other possibility is that the centrifugation speed employed

for SE was too high, sedimenting part of the larger molecular weight species (larger tail visible on SEC-MALS), and therefore yielding underestimates in weight average molar mass. Although, SE results are only apparent as they were performed at 0.5 mg/ml, which is non-ideal for most mucins. Nevertheless, changes in the hydrodynamic properties at lower pH are evident and are suggested to play a role in the higher intensity of volatile aroma compounds detected.

Sedimentation velocity (SV) was also employed in the analysis of human salivary α -amylase (HSA) as a function of pH (Figure 3.7). Unlike mucin, it was shown that α -amylase is more sensitive to pH, attributed to the reduced or the lack of glycosylation. As a result, this caused significant aggregation and precipitation leading to reduced α -amylase/volatile interactions and therefore a more enhanced headspace concentration of aroma compounds (Figure 3.8.).

8.1.2. Effect of ionic strength

Using the same hydrodynamic approach, changes in the solution structure of BSM and α -amylase were investigated as a function of ionic strength. It was found that an increase in the concentration of sodium chloride reduced the non-ideal behaviour of mucin in solution. This led to changes in the concentration dependent 'Gralen' coefficient and caused a marked reduction in the intrinsic viscosity of mucin (Figure 3.9.). Results suggest that as the salt concentration increases, mucins adopt a more extended

conformation. For α -amylase, which is a globular protein, the gross conformation is unaffected.

The aroma intensity was evaluated from a commercial orange drink in which BSM and α -amylase solutions were included. The addition of sodium chloride resulted in salting out effects, whereby the release of aroma compounds was significantly increased. Some compounds such as myrcene, limonene and α -pinene were not affected by the addition of salt (Figure 3.11.).

It was also found that although the overall aroma concentration was still higher under high salt concentrations (through salting out), the effect of mucin on volatile release was still very pronounced, indicating hydrophobic interactions are predominant. This was not the case for α -amylase. The overall aroma intensity at neutral pH and low salt was significantly lowered by the enzyme (by up to 50%). However, an increase in the concentrations of salt significantly reduced the interactions between the aroma molecules and α -amylase.

8.2. Interactions of food and saliva in their native state

Analytical ultracentrifugation was used in the analysis of the interactions of whole human saliva and green tea. Firstly, stimulated (SS) and unstimulated saliva (US), pooled from five healthy volunteers were analysed by SV. The hypothesis was to fit a sedimentation coefficient

distribution that can be used as a platform for the identification of different components involved in matrix-saliva interactions (Figure 4.1.).

The total protein concentrations of SS and US samples were determined by differential refractometry. It was shown that the SS sample contained a higher overall protein concentration than US. The SV analysis confirmed the presence of a higher concentration of lower S species, attributed to a higher amount of secreted enzymes and low molecular weight proteins upon stimulation. The study continued with the determination of the relative viscosities of SS and US and analysed the effect of α -amylase on the relative viscosity of mucin (BSM). It was shown that an increase in the α -amylase concentration led to a decrease in the relative viscosity of the system (Figure 4.2.).

The interaction between whole saliva and green tea, as a model for a dilute food system was assessed by SV. It was suggested that epigallocatechin-gallate (EGCG), the most abundant polyphenol in tea, especially in green tea, is involved in an interaction with the low S components present in saliva. This was shown to be partly attributed to a direct interaction with α -amylase (Figure 4.6).

During the process, it was revealed that the reaction between green tea and human saliva is responsible for the formation of a characteristic aroma profile, such as a decrease in linear aldehydes (attributed to protein binding) and an increase in the concentration of β -ionone, benzaldehyde and isovaleraldehyde. This formed the basis for the development of a fundamentally new concept of food analysis, by analysing the interactions

of the bolus in its native state, which ultimately affects the rate of release of aroma and taste compounds to the oral/nasal receptors.

8.3. Development and validation of artificial saliva

Based on the sedimentation coefficient distribution fingerprint from SV and the concentration estimations determined for saliva, an artificial saliva analogue was developed and compared to the real saliva for their abilities to modify aroma release. The artificial system consisted of submaxillary mucin and salivary α -amylase as the only macro-constituents. It was concluded that the artificial system can be useful in the analysis of flavour, but only in model flavour systems (aroma suspension), where a cumulative effect of α -amylase and mucin is observed (Figure 4.8.). However, the presence of other salivary proteins in human saliva was shown to play a significant role in the interaction with real food, whereby the artificial system is not valid (Figure 4.9.). Given the cost for other salivary proteins to be included in the composition and their stability in aqueous solutions, it is difficult to develop more robust analogues. Therefore, we recommended that experiments with more complex food systems are to be analysed with *ex-vivo* saliva. In addition, PCA results confirmed that the intensity of more hydrophilic aroma compounds is higher in the presence of mucin, while the intensity of more hydrophobic compounds is higher above the headspace of α -amylase solutions.

8.4. Advances in mucoadhesive applications

Mucoadhesion was proposed to resolve some of the disadvantages of rapid oral transit time and increase the bioavailability of flavour in the oral cavity. Advances in mucoadhesive applications include 1) the development of a cationic pullulan derivative that can be degraded by salivary α -amylase, and 2) the development of a mucus mimetic tool which can be used for the evaluation of mucoadhesion and retention of flavour compounds.

8.4.1. Mucoadhesive biopolymers

The presence of biopolymers and stabilisers physically decrease the release concentration of aroma compounds through their bulky, viscous nature and large molar mass. Therefore, during oral processing, most food hydrocolloids lower the release of the aroma compounds. Some of them have been shown to improve the bioavailability of flavour through synergistic interactions with mucus/mucins. As a result, some anionic polysaccharides such as carboxymethyl-cellulose (CMC) have been classified as mucoadhesive. However, especially in the dilute conditions of the bolus (acidity and ionic strength), there is no evidence to suggest that anionic polysaccharides can bind to mucin glycoproteins.

By contrast, cationic polymers have been well documented for their ability to form stronger electrostatic interactions with mucin in acidic conditions.

Polysaccharides such as chitosan can form large complexes with mucin, as shown in the current investigation. However, the formation of large mucin-polymer complexes is undesirable during oral processing. Besides, the general aroma intensity was not significantly increased, with the exception of linear aldehydes, which appear to increase upon the addition of chitosan.

For starch, a reduction in polymer the chain through hydrolysis has been correlated to an increased perception of flavour. This exceptional property has been applied in the development of a cationic pullulan analogue, which can be broken down by salivary α -amylase (Chapter 5). By developing the cationic polymer, we have, at least in theory, addressed some of the “loss through ingestion” issues, through the adhesion of the polymer to the oral mucin. Dimethylaminoethyl pullulan (DMAE-Pullulan) was synthesised for the first time, and confirmed by FT-IR. Hydrodynamic results suggested that the polymer forms complexes with submaxillary mucin, while still being degraded by the α -amylase. These interactions contributed to an enhanced intensity of flavour compounds.

8.4.2. Development of a biomimetic mucus surface

In Chapter 6, we explored the development of a new mucus-mimetic platform based on mucin immobilisation in calcium alginate beads. It was found that the mucins form micron sized aggregates, uniformly distributed across the calcium-alginate bead, as shown by environmental scanning electron microscopy (ESEM).

Retention of flavour compounds on the mucin-functionalised surface was tested using the orange drink formulation. Different mucoadhesive polymers with varying degree of charge, i.e. anionic, neutral and cationic, including the newly developed DMAE-pullulan, were tested for their ability to interact with mucin and retain flavour compounds onto the mucin-alginate surface. The mucus mimic was validated using the surface of an *ex-vivo* bovine tongue, with the retention results showing a good qualitative agreement. The developed method proved to be an efficient and more convenient tool for providing information on the effectiveness of mucoadhesive polymers without the variability, safety and ethical issues associated with animal tissues.

8.5. Interactions between salivary proteins and flavour compounds

In food, aroma compounds are mostly found at very small concentrations, under 1 ppm or 1 mg/l. However, in certain medicines and consumer products, such as inhalers and E-cigarette liquids, they can be found at excessively high concentrations (over 10 mg/ml).

Experiments were performed to identify any direct interactions between aroma compounds and the salivary glycoproteins (Chapter 7). Generally, it was found that compounds containing a carbonyl function, such as aldehydes and ketones, elicit a marked change in the sedimentation coefficient distributions of mucin and α -amylase. The effect appears to be correlated with their hydrophobicity ($\log P$), and concentration in the

aqueous phase, with more soluble smaller compounds (such as hexanal) having a stronger effect.

Secondly, interactions with phenolic aromatic compounds were also shown to alter the molecular distribution of mucin. Raman spectroscopy suggested that the phenoxy group is involved in the interaction with mucin polypeptide regions, as indicated by the presence of the Fermi doublet at 810-840 cm^{-1} , and a decrease in the Amide I and II spectra at 1500-1700 cm^{-1} .

8.6. Future work

- Currently, experiments were performed using bovine submaxillary mucin (BSM). However, it is unclear whether BSM or other animal salivary mucins are the most appropriate model in oral research. Therefore, isolation and purification of human salivary mucins fractions MG1 (MUC5B) and MG2 (MUC7) would greatly add to these investigations.
- The AUC analysis of the interactions between saliva and food in their native state remains challenging, especially for complex systems. Although the combination of the techniques used in this investigation can provide some useful information about the formation of aroma compounds *in vivo*, it is difficult to study the interactions of different salivary components involved in oral processing. In this work, SV analysis of saliva may be a useful technique provided the food system

is very dilute and has a low degree of heterogeneity (such as green tea), containing at most one or two components.

- Although salivary mucin and α -amylase can make up to 90 % of the total protein concentration in saliva, it was also shown that the presence of other salivary components and as well as other food co-ingredients play a significant role in regulating the concentrations of aroma released. The use of artificial saliva is limited to simple food systems, therefore fresh human saliva or *in-vivo* trials are required, when possible.
- As illustrated in this investigation, the choice of mucoadhesive polymer employed for modulating the release and retention of flavour varies depending on its physical and chemical properties. One of the mechanisms by which aroma intensity can be modified is via the formation of new surfaces at the food-salivary interface, such as new mucin-polymer complexes and degradation fragments, which facilitate the aroma release process. However, most biopolymers currently employed in food are non-digestible, and result in a complex food bolus which physically lowers the bioavailability of aroma and taste compounds.

Should the use of DMAE-pullulan be considered in the future, additional nuclear magnetic resonance (NMR) analyses, toxicological studies and ultimately *in-vivo* studies, such as sensory evaluation, are required to validate current findings.

- With advances in mucoadhesion, efforts to develop mucus mimetic surfaces are also required to test for polymer adhesion. The alternative tool proposed in the current study requires minimal use of resources and was found useful for evaluating the retention of flavour as a function of different polymer mucoadhesives. It is suggested that by encapsulating other relevant oral proteins, alongside mucins, current gaps between *in-vitro* and the *ex-vivo* mucus surfaces may be narrowed.

A possible limitation is that this method can only be employed in homogenous liquid systems, in order to ensure bead hydration and uniform polymer distribution. Furthermore, while ESEM is useful in the visualisation of the bead surface, heat damage from the laser was a problem during sample analysis. Therefore, more suitable techniques include cryo-SEM and high-pressure freezing (HPF) which enable higher resolution and more detailed imaging of hydrated biological samples.

- The effects of aroma compounds on the structural integrity of proteins have so far not been investigated. This could lay grounds for new research into the health aspects of aroma compounds. While the concentrations of flavourings used in our study are not representative of the very low levels found in food or drink (below 1 mg/l), they may have significant consequences in products such as inhalers, cosmetics, and E-cigarettes, where their concentrations are up to a million times higher (i.e. 10 mg/ml) and are directly adsorbed onto the saliva and lung surfaces through inhalation. Would these low molecular weight aroma compounds continue to be analysed by AUC, the use of organic

solvents will aid in their solubility, which would enable their characterisation at such excessive concentration. However, apart from pushing the limits of AUC in terms of their molecular mass, their sedimentation profile depends on the solvent density which, if it is less than their own, they will continue to float and exert counter-ion like effects on the sedimenting species.

- Future recommendations include the use of additional spectroscopic techniques, such as Raman or Circular Dichroism (CD) spectroscopy to gain a better understanding of the secondary and tertiary structures of these biological proteins. Microbiology may also bring a new perspective into the effects of viscosity and protein structure on bacterial motility and implications in disease development.

In addition to laboratory experiments analysing single compounds, machine learning (ML) may also be a useful tool in the identification of possible interaction sites involving the thousands of complex aroma compounds. By its very nature, a continuation of this work would contribute to new advancements in food and health research and lead to new collaborations at the interface of food, chemical and biological sciences.

8.7. Conclusion

In the series of experiments detailed in this thesis, a range of food oral processing interactions between salivary constituents and food co-ingredients were investigated using hydrodynamic techniques, such as analytical ultracentrifugation, viscosity measurements, light scattering and other complementing techniques.

These interactions were studied in order to understand their effect on the intensity of aroma and taste compounds released from their mixture. Findings were able to add to our current understanding of the effects of pH, salt, polyphenols, food polysaccharides, aroma compounds themselves and other co-ingredients present, on the saliva and on its two most abundant salivary glycoproteins: submaxillary mucin and salivary α -amylase.

The research presented here has directly provided the basis for the publication of five peer reviewed scientific publications and will lead into future investigations of saliva and other mucosal surfaces and their role as the first physical barrier between the consumer and the product.

References

Allen, A. (1983). Mucus — a protective secretion of complexity. *Trends in Biochemical Sciences* 8, 169–173.

Allen, F.H., Baalham, C.A., Lommerse, J.P.M., and Raithby, P.R. (1998). Carbonyl–Carbonyl Interactions can be Competitive with Hydrogen Bonds. *Acta Crystallographica B* 54, 320–329.

Allen, J.G., Flanigan, S.S., LeBlanc, M., Vallarino, J., MacNaughton, P., Stewart, J.H., and Christiani, D.C. (2016). Flavoring Chemicals in E-Cigarettes: Diacetyl, 2,3-Pentanedione, and Acetoin in a Sample of 51 Products, Including Fruit-, Candy-, and Cocktail-Flavored E-Cigarettes. *Environmental Health Perspectives* 124, 733–739.

Almutairi, F.M., Cifre, J.-G.H., Adams, G.G., Kök, M.S., Mackie, A.R., de la Torre, J.G., and Harding, S.E. (2016). Application of recent advances in hydrodynamic methods for characterising mucins in solution. *European Biophysics Journal* 45, 45–54.

Anderson, M.T., Harding, S.E., and Davis, S.S. (1989). On the interaction in solution of a candidate mucoadhesive polymer, diethylaminoethyl-dextran, with pig gastric mucus glycoprotein. *Biochemical Society Transactions* 17, 1101–1102.

Anwarul Hasan, MD., Lange, C.F., and King, M.L. (2010a). Effect of artificial mucus properties on the characteristics of airborne bioaerosol droplets generated during simulated coughing. *Journal of Non-Newtonian Fluid Mechanics* 165, 1431–1441.

Arp, Z., Autrey, D., Laane, J., Overman, S.A., and Thomas, G.J. (2001). Tyrosine Raman signatures of the filamentous virus Ff are diagnostic of non-hydrogen-bonded phenoxyls: demonstration by Raman and infrared spectroscopy of p-cresol vapor. *Biochemistry* 40, 2522–2529.

Bachmanov, A.A., Bosak, N.P., Floriano, W.B., Inoue, M., Li, X., Lin, C., Murovets, V.O., Reed, D.R., Zolotarev, V.A., and Beauchamp, G.K. (2011).

Genetics of sweet taste preferences. *Flavour and Fragrance Journal* 26, 286–294.

Baldwin, R.L. (1954). Boundary Spreading in Sedimentation Velocity Experiments. II. The Correction of Sedimentation Coefficient Distributions for the Dependence of Sedimentation Coefficient on Concentration^{1,2}. *J. Journal of the American Chemical Society* 76, 402–407.

Baldwin, R.L. (1996). How Hofmeister ion interactions affect protein stability. *Biophysical Journal* 71, 2056–2063.

Baloğlu, E., Özyazıcı, M., Hızarcıoğlu, S.Y., and Karavana, H.A. (2003). An in vitro investigation for vaginal bioadhesive formulations: bioadhesive properties and swelling states of polymer mixtures. *Il Farmaco* 58, 391–396.

Bank, R.A., Hetteema, E.H., Arwert, F., Amerongen, A.V., and Pronk, J.C. (1991). Electrophoretic characterization of posttranslational modifications of human parotid salivary alpha-amylase. *Electrophoresis* 12, 74–79.

Bansil, R., and Turner, B.S. (2006a). Mucin structure, aggregation, physiological functions and biomedical applications. *Current Opinion in Colloid & Interface Science* 11, 164–170.

Bansil, R., and Turner, B.S. (2006b). Mucin structure, aggregation, physiological functions and biomedical applications. *Current Opinion in Colloid & Interface Science* 11, 164–170.

Bansil, R., and Turner, B.S. (2018). The biology of mucus: Composition, synthesis and organization. *Advanced Drug Delivery Reviews* 124, 3–15.

Baxter, N.J., Lilley, T.H., Haslam, E., and Williamson, M.P. (1997). Multiple interactions between polyphenols and a salivary proline-rich protein repeat result in complexation and precipitation. *Biochemistry* 36, 5566–5577.

Belitz, H.D., Grosch, W. (2009). Aroma Compounds. In *Food Chemistry*, H.-D. Belitz, W. Grosch, and P. Schieberle, eds. (Berlin, Heidelberg: Springer Berlin Heidelberg), pp. 340–402.

Bendoraitiene, J., Kavaliauskaite, R., Klimaviciute, R., and Zemaitaitis, A. (2006). Peculiarities of Starch Cationization with Glycidyltrimethylammonium Chloride. *Starch - Stärke* 58, 623–631.

Bennick, A. (2002). Interaction of Plant Polyphenols with Salivary Proteins. *Critical Reviews in Oral Biology & Medicine* 13, 184–196.

Bernkop-Schnürch, A. (2005). Thiomers: A new generation of mucoadhesive polymers. *Advanced Drug Delivery Reviews* 57, 1569–1582.

Berry, M., and Corfield, A. (2014). Structure and Properties of Mucins. In *Mucoadhesive Materials and Drug Delivery Systems*, (John Wiley & Sons, Ltd), pp. 136–145.

Björk, I., and Lindh, E. (1974). Gross Conformation of Human Secretory Immunoglobulin A and Its Component Parts. *European Journal of Biochemistry* 45, 135–145.

Bohdanecky, M. (1983). New method for estimating the parameters of the wormlike chain model from the intrinsic viscosity of stiff-chain polymers. *Macromolecules* 16, 1483–1492.

Bornhorst, G.M., and Singh, R.P. (2013). Kinetics of in Vitro Bread Bolus Digestion with Varying Oral and Gastric Digestion Parameters. *Food Biophysics* 8, 50–59.

Breslin, P.A.S., and Spector, A.C. (2008). Mammalian taste perception. *Current Biology* 18, R148–R155.

Burchard, W. (1992). Static and dynamic light scattering approaches to structure determination of biopolymers (Royal Society of Chemistry: Cambridge, UK).

Buttery, R.G., and Ling, L.C. (1995). Volatile Flavor Components of Corn Tortillas and Related Products. *Journal of Agricultural and Food Chemistry* 43, 1878–1882.

Carlstedt, I., Sheehan, J.K., Corfield, A.P., and Gallagher, J.T. (1985). Mucous glycoproteins: a gel of a problem. *Essays in Biochemistry* 20, 40–76.

Celli, J.P., Turner, B.S., Afdhal, N.H., Ewoldt, R.H., McKinley, G.H., Bansil, R., and Erramilli, S. (2007). Rheology of Gastric Mucin Exhibits a pH-Dependent Sol–Gel Transition. *Biomacromolecules* 8, 1580–1586.

Chai, W.G., Hounsell, E.F., Cashmore, G.C., Rosankiewicz, J.R., Bauer, C.J., Feeney, J., Feizi, T., and Lawson, A.M. (1992). Neutral oligosaccharides of bovine submaxillary mucin. A combined mass spectrometry and ¹H-NMR study. *European Journal of Biochemistry* 203, 257–268.

Chandrashekar, J., Hoon, M.A., Ryba, N.J.P., and Zuker, C.S. (2006). The receptors and cells for mammalian taste. *Nature* 444, 288.

Channell, G., Dinu, V., Adams, G.G., and Harding, S.E. (2018). A simple cell-alignment protocol for sedimentation velocity analytical ultracentrifugation to complement mechanical and optical alignment procedures. *European Biophysics Journal* 47, 809–813.

Cheaib, Z., and Lussi, A. (2013). Role of amylase, mucin, IgA and albumin on salivary protein buffering capacity: A pilot study. *Journal of Biosciences* 38, 259–265.

Chen, M.-C., Wong, H.-S., Lin, K.-J., Chen, H.-L., Wey, S.-P., Sonaje, K., Lin, Y.-H., Chu, C.-Y., and Sung, H.-W. (2009). The characteristics, biodistribution and bioavailability of a chitosan-based nanoparticulate system for the oral delivery of heparin. *Biomaterials* 30, 6629–6637.

Choi, S.J., Decker, E.A., Henson, L., Popplewell, L.M., and McClements, D.J. (2009). Stability of citral in oil-in-water emulsions prepared with medium-chain triacylglycerols and triacetin. *The Journal of Agricultural and Food Chemistry* 57, 11349–11353.

Cook, D.J., Hollowood, T.A., Linforth, R.S.T., and Taylor, A.J. (2003). Oral Shear Stress Predicts Flavour Perception in Viscous Solutions. *Chemical Senses* 28, 11–23.

Cook, M.T., Smith, S.L., and Khutoryanskiy, V.V. (2015a). Novel glycopolymer hydrogels as mucosa-mimetic materials to reduce animal testing. *Chemical Communications* 51, 14447–14450.

Cook, M.T., Schmidt, S., Lee, E., Samprasit, W., Opanasopit, P., and Khutoryanskiy, V. (2015b). Synthesis of mucoadhesive thiol-bearing microgels from 2-(acetylthio)ethylacrylate and 2-hydroxyethylmethacrylate: novel drug delivery systems for chemotherapeutic agents to the bladder. *Journal of Materials Chemistry B* 3, 6599–6604.

Cook, S.L., Bull, S.P., Methven, L., Parker, J.K., and Khutoryanskiy, V.V. (2017). Mucoadhesion: A food perspective. *Food Hydrocolloids* 72, 281–296.

Cook, S.L., Methven, L., Parker, J.K., and Khutoryanskiy, V.V. (2018a). Polysaccharide food matrices for controlling the release, retention and perception of flavours. *Food Hydrocolloids* 79, 253–261.

Cook, S.L., Methven, L., Parker, J.K., and Khutoryanskiy, V.V. (2018b). Polysaccharide food matrices for controlling the release, retention and perception of flavours. *Food Hydrocolloids* 79, 253–261.

Cooper, R. (2012). Green tea and theanine: health benefits. *Chemical Communications* 63 *Suppl 1*, 90–97.

Correia, J.J., and Stafford, W.F. (2015). Sedimentation Velocity: A Classical Perspective. *Methods in Enzymology* 562, 49–80.

Creeth, J.M., and Denborough, M.A. (1970). The use of equilibrium-density-gradient methods for the preparation and characterization of blood-group-specific glycoproteins. *Biochemical Journal* 117, 879–891.

Creeth, J.M., and Harding, S.E. (1982). Some observations on a new type of point average molecular weight. *The Journal of Biochemical and Biophysical Methods* 7, 25–34.

Dam, J., and Schuck, P. (2003a). Determination of sedimentation coefficient distributions by direct modeling of the sedimentation boundary with Lamm equation solutions. *Methods in Enzymology* 384, 185–21.

Dam, J., and Schuck, P. (2003b). Determination of sedimentation coefficient distributions by direct modeling of the sedimentation boundary with Lamm equation solutions. *Methods in Enzymology* 384, 185–21.

Dam, J., and Schuck, P. (2004a). Calculating sedimentation coefficient distributions by direct modeling of sedimentation velocity concentration profiles. *Methods in Enzymology* 384, 185–212.

Dam, J., and Schuck, P. (2004b). Calculating sedimentation coefficient distributions by direct modeling of sedimentation velocity concentration profiles. *Methods in Enzymology* 384, 185–212.

Damodaran, S., and Kinsella, J.E. (1981). The effects of neutral salts on the stability of macromolecules. A new approach using a protein-ligand binding system. *Journal of Biological Chemistry* 256, 3394–3398.

Davidovich-Pinhas, M., and Bianco-Peled, H. (2014). Methods to Study Mucoadhesive Dosage Forms. In *Mucoadhesive Materials and Drug Delivery Systems*, (John Wiley & Sons, Ltd), pp. 175–196.

Deacon, M.P., McGurk, S., Roberts, C.J., Williams, P.M., Tendler, S.J., Davies, M.C., Davis, S.S., and Harding, S.E. (2000). Atomic force microscopy of gastric mucin and chitosan mucoadhesive systems. *Biochemical Journal* 348 Pt 3, 557–563.

Decourcelle, N., Lubbers, S., Vallet, N., Rondeau, P., and Guichard, E. (2004). Effect of thickeners and sweeteners on the release of blended aroma compounds in fat-free stirred yoghurt during shear conditions. *International Dairy Journal* 14, 783–789.

Denny, P., Hagen, F.K., Hardt, M., Liao, L., Yan, W., Arellanno, M., Bassilian, S., Bedi, G.S., Boontheung, P., Cociorva, D., et al. (2008). The proteomes of human parotid and submandibular/sublingual gland salivas collected as the ductal secretions. *Journal of Proteome Research* 7, 1994–2006.

Dhami, R., Harding, S.E., Jones, T., Hughes, T., Mitchell, J.R., and To, K. (1995). Physico-chemical studies on a commercial food-grade xanthan — I. Characterisation by sedimentation velocity, sedimentation equilibrium and viscometry. *Carbohydrate Polymers* 27, 93–99.

Dinu, V., Liu, C., Ali, J., Ayed, C., Gershkovich, P., Adams, G.G., Harding, S.E., and Fisk, I.D. (2018a). Analytical ultracentrifugation in saliva research: Impact of green tea astringency and its significance on the in-vivo aroma release. *Scientific Reports* 8, 13350.

Dinu, V., Liu, C., Ali, J., Ayed, C., Gershkovich, P., Adams, G.G., Harding, S.E., and Fisk, I.D. (2018b). Analytical ultracentrifugation in saliva research: Impact of green tea astringency and its significance on the in-vivo aroma release. *Scientific Reports* 8, 13350.

Dinu, V., Gillis, R.B., MacCalman, T., Lim, M., Adams, G.G., Harding, S.E., and Fisk, I.D. (2019a). Submaxillary Mucin: its Effect on Aroma Release from Acidic Drinks and New Insight into the Effect of Aroma Compounds on its Macromolecular Integrity. *Food Biophysics* 14, 278-286.

Dinu, V., Yakubov, G., Lim, M., Hurst, K., Adams, G.G., Harding, S.E., and Fisk, I.D. (2019b). Mucin immobilization in calcium alginate: A possible mucus mimetic tool for evaluating mucoadhesion and retention of flavour. *International Journal of Biological Macromolecules* 138, 831-836.

Dion-Fortier, A., Gravel, A., Guérette, C., Chevillot, F., Blais, S., Auger, S., Picard, P., and Segura, P.A. (2019). Signal enhancement in laser diode thermal desorption-triple quadrupole mass spectrometry analysis using microwell surface coatings. *Journal of Mass Spectrometry* 54, 167–177.

Dodd, S., Place, G.A., Hall, R.L., and Harding, S.E. (1998). Hydrodynamic properties of mucins secreted by primary cultures of Guinea-pig tracheal epithelial cells: determination of diffusion coefficients by analytical ultracentrifugation and kinetic analysis of mucus gel hydration and dissolution. *European Biophysics Journal* 28, 38–47.

Dominy, B.N., Perl, D., Schmid, F.X., and Brooks, C.L. (2002). The effects of ionic strength on protein stability: the cold shock protein family. *Journal of Molecular Biology* 319, 541–554.

Donohue, T.M., Tuma, D.J., and Sorrell, M.F. (1983). Acetaldehyde adducts with proteins: binding of [¹⁴C]acetaldehyde to serum albumin. *Archives of Biochemistry and Biophysics* 220, 239–246.

Drobitch, R.K., and Svensson, C.K. (1992). Therapeutic drug monitoring in saliva. An update. *Clinical Pharmacokinetics* 23, 365–379.

Ducker, W.A., Senden, T.J., and Pashley, R.M. (1991). Direct measurement of colloidal forces using an atomic force microscope. *Nature* 353, 239.

Dziemiańczyk, D., Grabowska, S.Z., and Balicki, R. (2005). Evaluation of secretory mucin concentration of patients with squamous cell carcinoma oral cavity. *Roczniki Akademii Medycznej w Białymstoku* 50, 334–338.

Eccles, R. (1994). Menthol and Related Cooling Compounds. *Journal of Pharmacy and Pharmacology* 46, 618–630.

Eisenberg, H. (2003). Modern analytical ultracentrifugation in protein science: look forward, not back. *Protein Science* 12, 2647–2649; discussion 2649–2650.

Escher, F.E., Nuessli, J., and Conde-Petit, B. (2000). Interactions of flavor compounds with starch in food processing. In *ACS Symposium Series*, (Washington, DC; American Chemical Society; 1999), pp. 230–245.

Ferraro, J.R. (2003). *Introductory Raman Spectroscopy* (Elsevier).

Ferry, A.-L., Hort, J., Mitchell, J.R., Lagarrigue, S., and Pamies, B.V. (2004). Effect of Amylase Activity on Starch Paste Viscosity and Its Implications for Flavor Perception. *Journal of Texture Studies* 35, 511–524.

Fiebrig, I., Davis, S.S., Harding, S.E., Hill, S.E., and Mitchell, J.R. (1995a). *Biopolymer Mixtures* (Nottingham University Press, Nottingham).

Firestein, S. (2001). How the olfactory system makes sense of scents. *Nature* 413, 211.

Fisher, S.Z., Govindasamy, L., Tu, C., Agbandje-McKenna, M., Silverman, D.N., Rajaniemi, H.J., and McKenna, R. (2006). Structure of human salivary α -amylase crystallized in a C-centered monoclinic space group. *Acta Crystallographica Section E: Crystallographic Communications* 62, 88–93.

Fransén, N., Björk, E., and Edsman, K. (2008). Changes in the mucoadhesion of powder formulations after drug application investigated with a simplified method. *Journal of Pharmaceutical Sciences* 97, 3855–3864.

Frenkel, E.S., and Ribbeck, K. (2015). Salivary Mucins Protect Surfaces from Colonization by Cariogenic Bacteria. *Applied and Environmental Microbiology* 81, 332–338.

Friel, E.N., and Taylor, A.J. (2001). Effect of salivary components on volatile partitioning from solutions. *Journal of Agricultural and Food Chemistry* 49, 3898–3905.

Flavors & Fragrances Market Size, Share | Industry Report, 2019-2025.

Gan, H.-H., Soukoulis, C., and Fisk, I. (2014a). Atmospheric pressure chemical ionisation mass spectrometry analysis linked with chemometrics for food classification - a case study: geographical provenance and cultivar classification of monovarietal clarified apple juices. *Food Chemistry* 146, 149–156.

Gan, H.H., Yan, B., Linfoth, R.S.T., and Fisk, I.D. (2016a). Development and validation of an APCI-MS/GC-MS approach for the classification and prediction of Cheddar cheese maturity. *Food Chemistry* *190*, 442–447.

García de la Torre, J., and Harding, S.E. (2013). Hydrodynamic modelling of protein conformation in solution: ELLIPS and HYDRO. *Biophysical Reviews* *5*, 195–206.

Gibbins, H.L., and Carpenter, G.H. (2012). Alternative Mechanisms of Astringency – What is the Role of Saliva? - Gibbins - 2013 - *Journal of Texture Studies* - Wiley Online Library.

Gillespie, C., Maalouf, J., Yuan, K., Cogswell, M.E., Gunn, J.P., Levings, J., Moshfegh, A., Ahuja, J.K.C., and Merritt, R. (2015). Sodium content in major brands of US packaged foods, 2009. *The American Journal of Clinical Nutrition* *101*, 344–353.

Gillis, R.B. (2015). Protein polysaccharide complexes: permanent/nonpermanent interactions between polysaccharides and polypeptides. PhD thesis Nottingham.

Gillis, R.B., Adams, G.G., Heinze, T., Nikolajski, M., Harding, S.E., and Rowe, A.J. (2013). MultiSig: a new high-precision approach to the analysis of complex biomolecular systems. *European Biophysical Journal* *42*, 777–786.

Gittings, S., Turnbull, N., Henry, B., Roberts, C.J., and Gershkovich, P. (2015). Characterisation of human saliva as a platform for oral dissolution medium development. *European Journal of Pharmaceutics and Biopharmaceutics* *91*, 16–24.

Godoy-Alcántar, C., Yatsimirsky, A.K., and Lehn, J.-M. (2005). Structure-stability correlations for imine formation in aqueous solution. *Journal of Physical Organic Chemistry* *18*, 979–985.

Gottschalk, A. (1960). Correlation Between Composition, Structure, Shape and Function of a Salivary Mucoprotein. *Nature* *186*, 949.

Goycoolea, F.M., Morris, E.R., Richardson, R.K., and Bell, A.E. (1995). Solution rheology of mesquite gum in comparison with gum arabic. *Carbohydrate Polymers* 27, 37–45.

Grabovac, V., Guggi, D., and Bernkop-Schnürch, A. (2005a). Comparison of the mucoadhesive properties of various polymers. *Advanced Drug Delivery Reviews* 57, 1713–1723.

Grabovac, V., Guggi, D., and Bernkop-Schnürch, A. (2005b). Comparison of the mucoadhesive properties of various polymers. *Advanced Drug Delivery Reviews* 57, 1713–1723.

Gralén, N. (1944). Sedimentation and diffusion. Measurements on cellulose and derivatives. PhD Thesis. PhD Dissertation, Uppsala, Sweden.

Green, A.A. (1933). The Preparation of Acetate and Phosphate Buffer Solutions of Known PH and Ionic Strength. *Journal of the American Chemical Society* 55, 2331–2336.

Gremler, H.A. (1974). Interaction of flavor compounds with soy protein. *Journal of the American Oil Chemists' Society* 51, 95A-97A.

Grosch, W. (2001). Evaluation of the Key Odorants of Foods by Dilution Experiments, Aroma Models and Omission. *Chemical Senses* 26, 533–545.

Gu, J.M., Robinson, J.R., and Leung, S.H. (1988). Binding of acrylic polymers to mucin/epithelial surfaces: structure-property relationships. *Critical Review in Therapeutic Drug Carrier Systems* 5, 21–67.

Gui, J., Fu, X., Zhou, Y., Katsuno, T., Mei, X., Deng, R., Xu, X., Zhang, L., Dong, F., Watanabe, N., et al. (2015). Does Enzymatic Hydrolysis of Glycosidically Bound Volatile Compounds Really Contribute to the Formation of Volatile Compounds During the Oolong Tea Manufacturing Process? *J. Agric. Food Chemistry* 63, 6905–6914.

Guo, J., He, Z., Wu, S., Zeng, M., and Chen, J. (2019). Binding of aroma compounds with soy protein isolate in aqueous model: Effect of preheat treatment of soy protein isolate. *Food Chemistry* 290, 16–23.

Hall, D.J., Khutoryanskaya, O.V., and Khutoryanskiy, V.V. (2011a). Developing synthetic mucosa-mimetic hydrogels to replace animal experimentation in characterisation of mucoadhesive drug delivery systems. *Soft Matter* 7, 9620–9623.

Hall, D.J., Khutoryanskaya, O.V., and Khutoryanskiy, V.V. (2011b). Developing synthetic mucosa-mimetic hydrogels to replace animal experimentation in characterisation of mucoadhesive drug delivery systems. *Soft Matter* 7, 9620–9623.

Haney, M.A. (1985a). The differential viscometer. I. A new approach to the measurement of specific viscosities of polymer solutions. *Journal of Applied Polymer Science* 30, 3023–3036.

Haney, M.A. (1985b). The differential viscometer. II. On-line viscosity detector for size-exclusion chromatography. *Journal of Applied Polymer Science* 30, 3037–3049.

Hans, R., Thomas, S., Garla, B., Dagli, R.J., and Hans, M.K. (2016). Effect of Various Sugary Beverages on Salivary pH, Flow Rate, and Oral Clearance Rate amongst Adults. *Scientifica* 1, 5027283

Harding, S.E. (1989). The macrostructure of mucus glycoproteins in solution. *Advances in Carbohydrate Chemistry* 47, 345–381.

Harding, S.E. (1994). The analytical ultracentrifuge spins again. *TrAC Trends in Analytical Chemistry* 13, 439–446.

Harding, S.E. (1997). The intrinsic viscosity of biological macromolecules. Progress in measurement, interpretation and application to structure in dilute solution. *Progress in Biophysics & Molecular Biology* 68, 207–262.

Harding, S.E. (2003). Mucoadhesive interactions. *Biochemical Society Transactions* 31, 1036–1041.

Harding, S.E. (2006a). Trends in muco-adhesive analysis. *Trends in Food Science & Technology* 5, 255–262.

Harding, S.E., Rowe, A.J., and Creeth, J.M. (1983a). Further evidence for a flexible and highly expanded spheroidal model for mucus glycoproteins in solution. *Biochemical Journal* 209, 893–896.

Harding, S.E., Creeth, J.M., and Rowe, A.J. (1983b). Modelling the conformation of mucus glycoproteins in solution. In *Proc 7th Int Glycoconjugates Conf Olsson-Reklambyra*, 558–559.

Harding, S.E., Horton, J.C., and Cölfen, H. (1997). The ELLIPS suite of macromolecular conformation algorithms. *European Biophysical Journal* 25, 347–359.

Harding, S.E., Davis, S.S.B., Deacon, M.P., and Fiebrig, I. (1999). Biopolymer Mucoadhesives. *Biotechnology and Genetic Engineering Reviews* 16, 41–86.

Harding, S.E., Schuck, P., Abdelhameed, A.S., Adams, G., Kök, M.S., and Morris, G.A. (2011). Extended Fujita approach to the molecular weight distribution of polysaccharides and other polymeric systems. *Methods* 54, 136–144.

Harding, S.E., Adams, G.G., Tombs, M.P., Paulsen, B.S., and Barsett, H. (2016). *An Introduction to Polysaccharide Biotechnology, Second Edition* (Taylor & Francis).

Hassan, E.E., and Gallo, J.M. (1990). A Simple Rheological Method for the in Vitro Assessment of Mucin-Polymer Bioadhesive Bond Strength. *Pharmaceutical Research* 7, 491–495.

Haward, S.J., Odell, J.A., Berry, M., and Hall, T. (2011). Extensional rheology of human saliva. *Rheologica Acta* 50, 869–879.

Hegarty, P.V.J., and Naudé, R.T. (1973). Effect of freezing, thawing and fixatives on the diameter of fibres from pre- and post-rigor skeletal muscles. *Proceedings of the Royal Irish Academy. Section B: Biological, Geological, and Chemical Science* 73, 87–94.

Heinze, T., Haack, V., and Rensing, S. (2004). Starch Derivatives of High Degree of Functionalization. 7. Preparation of Cationic 2-Hydroxypropyltrimethylammonium Chloride Starches. *Starch - Stärke* 56, 288–296.

Henning, H. (1926). Psychologie der chemischen Sinne. In *Receptionsorgane I: Tangorezeptoren · Thermorezeptoren Chemorezeptoren · Phonorezeptoren Statorezeptoren*, W. v. Buddenbrock, M.H. Fischer, M. v. Frey, K. v. Frisch, M. Gildemeister, A. Goldscheider, K. Grahe, H. Held, H. Henning, H. Herter, et al., eds. (Munich: J.F. Bergmann-Verlag), 393–405.

Ho, C.-T., Zheng, X., and Li, S. (2015). Tea aroma formation. *Food Science and Human Wellness* 4, 9–27.

Hoffmann, T., Meyer, R.J., Sorrell, M.F., and Tuma, D.J. (1993). Reaction of acetaldehyde with proteins: formation of stable fluorescent adducts. *Alcoholism: Clinical and Experimental Research* 17, 69–74.

Hollowood, T.A., Linforth, R.S.T., and Taylor, A.J. (2002). The Effect of Viscosity on the Perception of Flavour. *Chemical Senses* 27, 583–591.

Huggins, M.L. (1942). The Viscosity of Dilute Solutions of Long-Chain Molecules. IV. Dependence on Concentration. *Journal of the American Chemical Society* 64, 2716–2718.

Humphrey, S.P., and Williamson, R.T. (2001). A review of saliva: normal composition, flow, and function. *Journal of Prosthetic Dentistry* 85, 162–169.

Hurlimann, J., and Zuber, C. (1968). In vitro protein synthesis by human salivary glands. *Immunology* 14, 819–824.

Institute of Medicine (US) Committee on Strategies to Reduce Sodium Intake (2010). *Strategies to Reduce Sodium Intake in the United States* (Washington (DC): National Academies Press (US)).

Iranshahi, M. (2012). A review of volatile sulfur-containing compounds from terrestrial plants: biosynthesis, distribution and analytical methods. *Journal of Essential Oil Research* 24, 393–434.

Isemura, T., and Kakiuchi, K. (1962). Association and Dissociation of Bacterial α -Amylase Molecule. *Journal of Biochemistry* 51, 385–392.

Jacques, Y., and Buri, P. (1997). An investigation of the physical behaviour of moisture-activated mucoadhesive hydrogels upon contact with biological and non-biological substrates. *Pharmaceutica Acta Helvetiae* 72, 225–232.

Janado, M., and Onodera, K. (1972). Effect of ionic strength in the gel filtration of charged polysaccharides. *Agricultural and Biological Chemistry* 36, 2027–2031.

Joiner, A., Muller, D., Elofsson, U.M., and Arnebrant, T. (2004). Ellipsometry analysis of the in vitro adsorption of tea polyphenols onto salivary pellicles. *European Journal of Oral Sciences* 112, 510–515.

Jones, D.S., Bruschi, M.L., de Freitas, O., Gremião, M.P.D., Lara, E.H.G., and Andrews, G.P. (2009a). Rheological, mechanical and mucoadhesive properties of thermoresponsive, bioadhesive binary mixtures composed of poloxamer 407 and carbopol 974P designed as platforms for implantable drug delivery systems for use in the oral cavity. *International Journal of Pharmaceutics* 372, 49–58.

Jones, D.S., Bruschi, M.L., de Freitas, O., Gremião, M.P.D., Lara, E.H.G., and Andrews, G.P. (2009b). Rheological, mechanical and mucoadhesive properties of thermoresponsive, bioadhesive binary mixtures composed of poloxamer 407 and carbopol 974P designed as platforms for implantable drug delivery systems for use in the oral cavity. *International Journal of Pharmaceutics* 372, 49–58.

Jouenne, E., and Cruzet, J. (2000). Effect of pH on retention of aroma compounds by beta-lactoglobulin. *Journal of Agricultural and Food Chemistry* 48, 1273–1277.

Juan, A.S., Hlawaty, H., Chaubet, F., Letourneur, D., and Feldman, L.J. (2007). Cationized pullulan 3D matrices as new materials for gene transfer. *Journal of Biomedical Materials Research Part A* 82A, 354–362.

Kaneko, S., Kumazawa, K., and Nishimura, O. (2011). Studies on the key aroma compounds in soy milk made from three different soybean cultivars. *Journal of Agricultural and Food Chemistry* 59, 12204–12209.

Kavvada, K.M., Murray, J.G., Moore, V.A., Coombes, A.G.A., and Hanson, P.J. (2005a). A Collagen IV Matrix Is Required for Guinea Pig Gastric Epithelial Cell Monolayers to Provide an Optimal Model of the Stomach Surface for Biopharmaceutical Screening. *Journal of Biomolecular Screening* 10, 495–507.

Keely, S., Rullay, A., Wilson, C., Carmichael, A., Carrington, S., Corfield, A., Haddleton, D.M., and Brayden, D.J. (2005a). In vitro and ex vivo intestinal tissue models to measure mucoadhesion of poly (methacrylate) and N-trimethylated chitosan polymers. *Pharmaceutical Research* 22, 38–49.

Kejriwal, S., Bhandary, R., Thomas, B., and Kumari, S. (2014). Estimation of Levels of Salivary Mucin, Amylase and Total Protein in Gingivitis and Chronic Periodontitis Patients. *Journal of Clinical and Diagnostic* 8, ZC56–ZC60.

Kesen, S. (2013). GC–MS–olfactometric characterization of the key aroma compounds in Turkish olive oils by application of the aroma extract dilution analysis. *Food Research International* 15, 391-401

Khutoryanskiy, V.V. (2011). Advances in Mucoadhesion and Mucoadhesive Polymers. *Macromolecular Bioscience* 11, 748–764.

Kiribuchi, T., and Yamanishi, T. (1963). Studies on the Flavor of Green Tea. *Agricultural and Biological Chemistry* 27, 56–59.

Kostanski, L.K., Keller, D.M., and Hamielec, A.E. (2004). Size-exclusion chromatography-a review of calibration methodologies. *Jornal of Biochemical and Biophysical Methods* 58, 159–186.

Koyama, I., Komine, S., Yakushijin, M., Hokari, S., and Komoda, T. (2000). Glycosylated salivary alpha-amylases are capable of maltotriose hydrolysis and glucose formation. *Comparative Biochemistry and Physiology B* 126, 553–560.

Kraemer, E.O. (1938). Molecular Weights of Celluloses and Cellulose Derivates. *Industrial & Engineering Chemistry Research* 30, 1200–1203.

Krahn, N., Meier, M., Reuten, R., Koch, M., Stetefeld, J., and Patel, T.R. (2019). Solution Structure of *C. elegans* UNC-6: A Nematode Parologue of the Axon Guidance Protein Netrin-1. *Biophysical Journal* 116, 2121–2130.

Kusch, P., Obst, V., Schroeder-Obst, D., Fink, W., Knupp, G., and Steinhaus, J. (2013). Application of pyrolysis–gas chromatography/mass spectrometry for the identification of polymeric materials in failure analysis in the automotive industry. *Engineering Failure Analysis* 35, 114–124.

Lamm, O. (1920). Die Differentialgleichung der Ultrazentrifugierung. *Arkiv för matematik, astronomi och fysik* 2, 1- 4

Landy, P., Druaux, C., and Voilley, A. (1995). Retention of aroma compounds by proteins in aqueous solution. *Food Chemistry* 54, 387–392.

Lang, T., Hansson, G.C., and Samuelsson, T. (2007). Gel-forming mucins appeared early in metazoan evolution. *Proceedings of the National Academy of Sciences of the United States of America* 104, 16209–16214.

Latha, R.S., and Lakshmi, P.K. (2012). Electronic tongue: An analytical gustatory tool. *Journal of Advanced Pharmaceutical Technology & Research* 3, 3–8.

Lee, J.W., Park, J.H., and Robinson, J.R. (2000). Bioadhesive-based dosage forms: the next generation. *Journal of Pharmaceutical Sciences* 89, 850–866.

Lee, J.-Y., Jeong, K.-W., and Kim, Y.-M. (2011). Epigallocatechin 3-gallate Binds to Human Salivary α -Amylase with Complex Hydrogen Bonding Interactions. *Bulletin of the Korean Chemical Society* 32, 2222–2226.

Lee, S., Müller, M., Rezwan, K., and Spencer, N.D. (2005). Porcine Gastric Mucin (PGM) at the Water/Poly(Dimethylsiloxane) (PDMS) Interface: Influence of pH and Ionic Strength on Its Conformation, Adsorption, and Aqueous Lubrication Properties. *Langmuir* 21, 8344–8353.

Legeay, S., Rodier, M., Fillon, L., Faure, S., and Clere, N. (2015). Epigallocatechin Gallate: A Review of Its Beneficial Properties to Prevent Metabolic Syndrome. *Nutrients* 7, 5443–5468.

Lehr, C.-M., Bouwstra, J.A., Tukker, J.J., and Junginger, H.E. (1990a). Intestinal transit of bioadhesive microspheres in an in situ loop in the rat - A comparative study with copolymers and blends based on poly(acrylic acid). *Journal of Controlled Release* 13, 51–62.

Lehr, C.-M., Bouwstra, J.A., Schacht, E.H., and Junginger, H.E. (1992). In vitro evaluation of mucoadhesive properties of chitosan and some other natural polymers. *International Journal of Pharmaceutics* 78, 43–48.

Li, X., Li, W., Wang, H., Bayley, D.L., Cao, J., Reed, D.R., Bachmanov, A.A., Huang, L., Legrand-Defretin, V., Beauchamp, G.K., et al. (2006). Cats Lack a Sweet Taste Receptor. *Journal of Nutrition* 136, 1932S-1934S.

Liao, X., Yuan, D., Tang, J., Yang, H., Liang, B., Cheng, Q., and Li, H. (2016). Probing into the Interaction of Nicotine and Bovine Submaxillary Mucin: NMR, Fluorescence, and FTIR Approaches. *Journal of Spectroscopy*, 9580136.

Linforth, R.S.T., Ingham, K.E., and Taylor, A.J. (1996). Time course profiling of volatile release from foods during the eating process. *Flavour Science: Recent Development* 4, 361–368.

Liu, Y., Chen, M., Wang, S., Lin, J., Cai, L., and Song, L. (2014). New insight into the stereoselective interactions of quinine and quinidine, with bovine serum albumin. *Journal of Molecular Recognition* 27, 239–249.

Llena-Puy, C. (2006). The rôle of saliva in maintaining oral health and as an aid to diagnosis. *Medicina Oral, Patología Oral y Cirugía Bucal* 11, NaN-NaN.

Luther, T., Carrion, C.F., Cobb, N., Le, G., Edwards, C., Schwartz, S., and Streckfus, C. (2010). Methods for analyzing saliva proteins for systemic disease detection. *General dentistry* 58, 110–113.

Lynch, J.W., and Barry, P.H. (1989). Action potentials initiated by single channels opening in a small neuron (rat olfactory receptor). *Biophysical Journal* 55, 755–768.

Lyttleton, J.W. (1964). Bovine salivary mucoprotein: An improved method of Isolation. *New Zealand Journal of Agricultural Research* 7, 228–237.

MacGregor, E.A., Janecek, S., and Svensson, B. (2001). Relationship of sequence and structure to specificity in the alpha-amylase family of enzymes. *Biochimica et Biophysica Acta* 1546, 1–20.

Mach, J.P., Pahud, J.J., and Isliker, H. (1969). IgA with “secretory piece” in bovine colostrum and saliva. *Nature* 223, 952–955.

Mackie, A.R., Goycoolea, F.M., Menchicchi, B., Caramella, C.M., Saporito, F., Lee, S., Stephansen, K., Chronakis, I.S., Hiorth, M., Adamczak, M., et al. (2017a). Innovative Methods and Applications in Mucoadhesion Research. *Macromolecular Bioscience* 17.

Mackie, A.R., Goycoolea, F.M., Menchicchi, B., Caramella, C.M., Saporito, F., Lee, S., Stephansen, K., Chronakis, I.S., Hiorth, M., Adamczak, M., et al. (2017b). Innovative Methods and Applications in Mucoadhesion Research. *Macromolecular Bioscience* 17.

Madsen, J.B., Sotres, J., Pakkanen, K.I., Efler, P., Svensson, B., Abou Hachem, M., Arnebrant, T., and Lee, S. (2016). Structural and Mechanical Properties of Thin Films of Bovine Submaxillary Mucin versus Porcine Gastric Mucin on a Hydrophobic Surface in Aqueous Solutions. *Langmuir* 32, 9687–9696.

Mandel, A.L., Peyrot des Gachons, C., Plank, K.L., Alarcon, S., and Breslin, P.A.S. (2010). Individual differences in AMY1 gene copy number, salivary α -amylase levels, and the perception of oral starch. *PLoS ONE* 5, e13352.

Mansuri, S., Kesharwani, P., Jain, K., Tekade, R.K., and Jain, N.K. (2016). Mucoadhesion: A promising approach in drug delivery system. *Reactive and Functional Polymers* *100*, 151–172.

Mathiowitz, E., and Chickering, D.E. (1999). Definitions, mechanisms and theories of bioadhesion. *Bioadhesive Drug Delivery Systems: Fundamentals, Novel Approaches and Development*, Marcel Decker, New York *1*.

McGorin, R.J., 1951-, and Leland, J.V. (1996). *Flavor-food interactions* (American Chemical Society).

Mehrotra, R., Thornton, D.J., and Sheehan, J.K. (1998). Isolation and physical characterization of the MUC7 (MG2) mucin from saliva: evidence for self-association. *Biochemical Journal* *334*, 415–422.

Menini, A., Picco, C., and Firestein, S. (1995). Quantal-like current fluctuations induced by odorants in olfactory receptor cells. *Nature* *373*, 435.

Meynier, A., Rampon, V., Dalgalarrodo, M., and Genot, C. (2004). Hexanal and t-2-hexenal form covalent bonds with whey proteins and sodium caseinate in aqueous solution. *International Dairy Journal* *14*, 681–690.

Miura, T., and Thomas, G.J. (1995). Raman Spectroscopy of Proteins and Their Assemblies. In *Proteins: Structure, Function, and Engineering*, B.B. Biswas, and S. Roy, eds. (Boston, MA: Springer US), pp. 55–99.

Morris, G.A., Adams, G.G., and Harding, S.E. (2014). On hydrodynamic methods for the analysis of the sizes and shapes of polysaccharides in dilute solution: A short review. *Food Hydrocolloids* *42*, 318–334.

Mortazavi, S.A. (1995). An in vitro assessment of mucus/mucoadhesive interactions. *International Journal of Pharmaceutics* *124*, 173–182.

Mortazavi, S.A., and Smart, J.D. (1995). An investigation of some factors influencing the in vitro assessment of mucoadhesion. *International Journal of Pharmaceutics* 116, 223–230.

Murphy, E.J., Metcalfe, C.L., Nnamchi, C., Moody, P.C.E., and Raven, E.L. (2012). Crystal structure of guaiacol and phenol bound to a heme peroxidase. *Federation of European Biochemical Societies* 279, 1632–1639.

Nafee, N.A., Ismail, F.A., Boraie, N.A., and Mortada, L.M. (2004). Mucoadhesive Delivery Systems. I. Evaluation of Mucoadhesive Polymers for Buccal Tablet Formulation. *Drug Development and Industrial Pharmacy* 30, 985–993.

Narukawa, M., Kimata, H., Noga, C., and Watanabe, T. (2010). Taste characterisation of green tea catechins. *International Journal of Food Science & Technology* 45, 1579–1585.

Okutan, L., Kongstad, K.T., Jäger, A.K., and Staerk, D. (2014). High-resolution α -amylase assay combined with high-performance liquid chromatography-solid-phase extraction-nuclear magnetic resonance spectroscopy for expedited identification of α -amylase inhibitors: proof of concept and α -amylase inhibitor in cinnamon. *Journal of Agricultural and Food Chemistry* 62, 11465–11471.

van den Oord, A.H.A., and van Wassenaar, P.D. (1997). Umami peptides: assessment of their alleged taste properties. *Z Lebensm Unters Forsch* 205, 125–130.

Ortega, A., and García de la Torre, J. (2007). Equivalent radii and ratios of radii from solution properties as indicators of macromolecular conformation, shape, and flexibility. *Biomacromolecules* 8, 2464–2475.

Pagès-Hélary, S., Andriot, I., Guichard, E., and Canon, F. (2014). Retention effect of human saliva on aroma release and respective contribution of salivary mucin and α -amylase. *Food Research International* 64, 424–431.

Pamies, R., Hernández Cifre, J.G., del Carmen López Martínez, M., and García de la Torre, J. (2008). Determination of intrinsic viscosities of macromolecules and nanoparticles. Comparison of single-point and dilution procedures. *Colloid and Polymer Science* 286, 1223–1231.

Parker, J.K., Elmore, S., and Methven, L. (2014). *Flavour Development, Analysis and Perception in Food and Beverages* (Elsevier).

Parnis, J.M., and Oldham, K.B. (2013). Beyond the Beer–Lambert law: The dependence of absorbance on time in photochemistry. *Journal of Photochemistry and Photobiology A: Chemistry* 267, 6–10.

Patel, M.M., Smart, J.D., Nevell, T.G., Ewen, R.J., Eaton, P.J., and Tsibouklis, J. (2003). Mucin/poly(acrylic acid) interactions: a spectroscopic investigation of mucoadhesion. *Biomacromolecules* 4, 1184–1190.

Payza, N., Robert, M., and Herp, A. (1970). THE MOLECULAR WEIGHT OF BOVINE and PORCINE SUBMAXILLARY MUCINS. *International Journal of Protein Research* 2, 109–115.

Pedro, A.S., Cabral-Albuquerque, E., Ferreira, D., and Sarmento, B. (2009). Chitosan: An option for development of essential oil delivery systems for oral cavity care? *Carbohydrate Polymers* 76, 501–508.

Pein, M., Gondongwe, X.D., Habara, M., and Winzenburg, G. (2014). Interlaboratory testing of Insent e-tongues. *International Journal of Pharmaceutics* 469, 228–237.

Peppas, N.A., and Buri, P.A. (1985). Surface, interfacial and molecular aspects of polymer bioadhesion on soft tissues. *Journal of Controlled Release* 2, 257–275.

Peppas, N.A., and Huang, Y. (2004). Nanoscale technology of mucoadhesive interactions. *Advanced Drug Delivery Reviews* 56, 1675–1687.

Perez, E., and Proust, J.E. (1987). Forces between mica surfaces covered with adsorbed mucin across aqueous solution. *Journal of Colloid and Interface Science* 118, 182–191.

Perez-Vilar, J., and Hill, R.L. (1999). The structure and assembly of secreted mucins. *Journal of Biological Chemistry* 274, 31751–31754.

Perlmann, G.E., and Kaufman, D. (1945). The Effect of Ionic Strength and Protein Concentration in the Electrophoretic Analysis of Human Plasma^{1,2}. *Journal of the American Chemical Society* 67, 638–641.

Piggott, J.R. (2000). Dynamism in flavour science and sensory methodology. *Food Research International* 33, 191–197.

Proctor, G.B., and Carpenter, G.H. (2014). Salivary secretion: mechanism and neural regulation. *Monogr Oral Sci* 24, 14–29.

Qian, M., and Reineccius, G. (2003). Static Headspace and Aroma Extract Dilution Analysis of Parmigiano Reggiano Cheese. *Journal of Food Science* 68, 794–798.

Ralston, G.B. (2004). INTRODUCTION TO ANALYTICAL ULTRACENTRIFUGATION. Beckman Coulter.

Ramos-Pineda, A.M., Carpenter, G.H., García-Estévez, I., and Escribano-Bailón, M.T. (2019). Influence of Chemical Species on Polyphenol–Protein Interactions Related to Wine Astringency. *Journal of Agricultural and Food Chemistry* 67, 12833–12843

Rao, K.V.R., and Buri, P. (1989). A novel in situ method to test polymers and coated microparticles for bioadhesion. *International Journal of Pharmaceutics* 52, 265–270.

Redman, R.S. (2012). Morphologic diversity of the minor salivary glands of the rat: fertile ground for studies in gene function and proteomics. *Biotechnic & Histochemistry* 87, 273–287.

Reineccius, G. (2006). Flavor release from foods. *Flavour Chemistry and Technology* 139–159.

Richards, E.G., and Schachman, H.K. (1959). Ultracentrifuge Studies with Rayleigh Interference Optics.I. General Application. *Journal of Physical Chemistry* 63, 1578–1591.

Richards, E.Glen., Teller, D.C., and Schachman, H.K. (1968). Ultracentrifuge studies with Rayleigh interference optics. II. Low-speed sedimentation equilibrium of homogeneous systems. *Biochemistry* 7, 1054–1076.

Rodriguez, M.S., Albertengo, L.A., Vitale, I., and Agullo, E. (2003). Relationship Between Astringency and Chitosan-Saliva Solutions Turbidity at Different pH. *Journal of Food Science* 68, 665–667.

Roussel, P., Lamblin, G., Lhermitte, M., Houdret, N., Lafitte, J.-J., Perini, J.-M., Klein, A., and Scharfman, A. (1988). The complexity of mucins. *Biochimie* 70, 1471–1482.

Rubin, B.K. (1999). An In Vitro Comparison of the Mucoactive Properties of Guaifenesin, Iodinated Glycerol, Surfactant, and Albuterol. *Chest* 116, 195–200.

Ruth, S.M.V., Roozen, J.P., and Cozijnsen, J.L. (1995). Changes in flavour release from rehydrated: Diced bell peppers (*Capsicum annuum*) by artificial saliva components in three mouth model systems. *Journal of the Science of Food and Agriculture* 67, 189–196.

van Ruth, S.M., Grossmann, I., Geary, M., and Delahunty, C.M. (2001). Interactions between artificial saliva and 20 aroma compounds in water and oil model systems. *Journal of Agricultural and Food Chemistry* 49, 2409–2413.

Rwei, S.-P., Chen, Y.-M., Lin, W.-Y., and Chiang, W.-Y. (2014). Synthesis and rheological characterization of water-soluble glycidyltrimethylammonium-chitosan. *Marine Drugs* 12, 5547–5562.

Sadler, G.D., and Murphy, P.A. (2010). pH and Titratable Acidity. In *Food Analysis*, S.S. Nielsen, ed. (Boston, MA: Springer US), 219–238.

Salih, E., Siqueira, W.L., Helmerhorst, E.J., and Oppenheim, F.G. (2010). Large-scale phosphoproteome of human whole saliva using disulfide–thiol interchange covalent chromatography and mass spectrometry. *Analytical Biochemistry* 407, 19–33.

San George, R.C., and Hoberman, H.D. (1986). Reaction of acetaldehyde with hemoglobin. *Journal of Biological Chemistry* 261, 6811–6821.

Sandberg, T., Blom, H., and Caldwell, K.D. (2009). Potential use of mucins as biomaterial coatings. I. Fractionation, characterization, and model adsorption of bovine, porcine, and human mucins. *Journal of Biomedical Materials Research Part A* 91, 762–772.

Sanderson, G.W., and Grahamm, H.N. (1973). Formation of black tea aroma. *Journal of Agricultural and Food Chemistry* 21, 576–585.

Sas, R., and Dawes, C. (1997). The intra-oral distribution of unstimulated and chewing-gum-stimulated parotid saliva. *Archives of Oral Biology* 42, 469–474.

Schachman, H.K. (1989). Analytical ultracentrifugation reborn. *Nature* 341, 259.

Schneyer, L.H., and Levin, L.K. (1955). Rate of secretion by exogenously stimulated salivary gland pairs of man. *Journal of Applied Physiology* 7, 609–613.

Schömig, V.J., Käsdorf, B.T., Scholz, C., Bidmon, K., Lieleg, O., and Berensmeier, S. (2016). An optimized purification process for porcine gastric mucin with preservation of its native functional properties. *RSC Advances* 6, 44932–44943.

Schuck, P. (2000). Size-distribution analysis of macromolecules by sedimentation velocity ultracentrifugation and lamm equation modeling. *Biophysical Journal* 78, 1606–1619.

Schuck, P. (2013). Analytical ultracentrifugation as a tool for studying protein interactions. *Biophysical Reviews* 5, 159–171.

Schuck, P., and Rossmanith, P. (2000). Determination of the sedimentation coefficient distribution by least-squares boundary modeling. *Biopolymers* 54, 328–341.

Schuck, P., Gillis, R.B., Besong, T.M.D., Almutairi, F., Adams, G.G., Rowe, A.J., and Harding, S.E. (2014a). SEDFIT-MSTAR: molecular weight and molecular weight distribution analysis of polymers by sedimentation equilibrium in the ultracentrifuge. *Analyst* 139, 79–92.

Schuck, P., Gillis, R.B., Besong, T.M.D., Almutairi, F., Adams, G.G., Rowe, A.J., and Harding, S.E. (2014b). SEDFIT-MSTAR: molecular weight and molecular weight distribution analysis of polymers by sedimentation equilibrium in the ultracentrifuge. *Analyst* 139, 79–92.

Schulman, S.G., Threatte, R.M., Capomacchia, A.C., and Paul, W.L. (1974). Fluorescence of 6-methoxyquinoline, quinine, and quinidine in aqueous media. *Journal of Pharmaceutical Sciences* 63, 876–880.

Scott, D.J., Harding, S.E., and Rowe, A.J. (2005). UltraScan - A Comprehensive Data Analysis Software Package for Analytical Ultracentrifugation Experiments. In *Analytical Ultracentrifugation*, 210–230.

Seagrave, J., Albrecht, H., Park, Y.S., Rubin, B., Solomon, G., and Kim, K.C. (2011). Effect of guaifenesin on mucin production, rheology, and mucociliary transport in differentiated human airway epithelial cells. *Experimental Lung Research* 37, 606–614.

Sémon, E., Arvisenet, G., Guichard, E., and Le Quéré, J.-L. (2018). Modified proton transfer reaction mass spectrometry (PTR-MS) operating conditions for in vitro and in vivo analysis of wine aroma. *Journal of Mass Spectrometry* 53, 65–77.

Setshedi, M., Wands, J.R., and de la Monte, S.M. (2010). Acetaldehyde adducts in alcoholic liver disease. *Oxidative Medicine and Cellular Longevity* 3, 178–185.

Sheehan, J.K., Oates, K., and Carlstedt, I. (1986). Electron microscopy of cervical, gastric and bronchial mucus glycoproteins. *Biochemical Journal* 239, 147–153.

Sheffner, A.L. (1963). The reduction in vitro in viscosity of mucoprotein solutions by a new mucolytic agent, N-acetyl-L-cysteine. *Annals of the New York Academy of Sciences* 106, 298–310.

Shen, J., Wang, Y., Ping, Q., Xiao, Y., and Huang, X. (2009). Mucoadhesive effect of thiolated PEG stearate and its modified NLC for ocular drug delivery. *Journal of Control Release* 137, 217–223.

Silva, A.C., Amaral, M.H., González-Mira, E., Santos, D., and Ferreira, D. (2012). Solid lipid nanoparticles (SLN)--based hydrogels as potential carriers for oral transmucosal delivery of risperidone: preparation and characterization studies. *Colloids and Surfaces B: Biointerfaces* 93, 241–248.

Singer, M.S. (2000). Analysis of the molecular basis for octanal interactions in the expressed rat 17 olfactory receptor. *Chemical Senses* 25, 155–165.

Singh, A., and Singh, N. (2015). Effect of salt concentration on the stability of heterogeneous DNA. *Physica A: Statistical Mechanics and Its Applications* 419, 328–334.

Smart, J.D. (2005). The basics and underlying mechanisms of mucoadhesion. *Advanced Drug Delivery Reviews* 57, 1556–1568.

Smidsrod, O., and Draget, I. (1997). Alginate gelation technologies. In *Food Colloids: Proteins, Lipids and Polysaccharides*, E. Dickinson, and B. Bergenstahl, eds. (Cambridge, UK: Royal Society of Chemistry), 279–293.

Smith, B. (2012). Perspective: Complexities of flavour. *Nature* 486, S6.

Smith, B.F., Peetermans, J.A., Tanaka, T., and LaMont, J.T. (1989). Subunit interactions and physical properties of bovine gallbladder mucin. *Gastroenterology* 97, 179–187.

Snary, D., and Allen, A.S. (1971). Studies on gastric mucoproteins. The isolation and characterization of the mucoprotein of the water-soluble mucus from pig cardiac gastric mucosa. *Biochemical Journal* 132, 845-853

Snary, D., Allen, A., and Pain, R.H. (1974). Conformational changes in gastric mucoproteins induced by caesium chloride and guanidinium chloride. *Biochemical Journal* 141, 641-646.

Sogias, I.A., Williams, A.C., and Khutoryanskiy, V.V. (2008). Why is chitosan mucoadhesive? *Biomacromolecules* 9, 1837-1842.

Solms, J. (1986). Interactions of non-volatile and volatile substances in foods. *Interactions of Food Components* 6, 189-210.

Solomon, O.F., and Ciuta, I.Z. (2019). Détermination de la viscosité intrinsèque de solutions de polymères par une simple détermination de la viscosité - Solomon - 1962 - *Journal of Applied Polymer Science* - Wiley Online Library.

Steen, P.V. den, Rudd, P.M., Dwek, R.A., and Opdenakker, G. (1998). Concepts and Principles of O-Linked Glycosylation. *Critical Reviews in Biochemistry and Molecular Biology* 33, 151-208.

Stelzer, G.I., and Klug, E.D. (1980). Carboxymethylcellulose. In Davidson R. L. *Handbook of Water-Soluble Gums and Resins*, (New York: McGraw-Hill), 414-428.

Stetefeld, J., McKenna, S.A., and Patel, T.R. (2016). Dynamic light scattering: a practical guide and applications in biomedical sciences. *Biophysical Reviews* 8, 409-427.

Stevens, V.J., Fantl, W.J., Newman, C.B., Sims, R.V., Cerami, A., and Peterson, C.M. (1981). Acetaldehyde adducts with hemoglobin. *Journal of Clinical Investigation* 67, 361-369.

Stuart, B. (2015). Infrared Spectroscopy. In *Kirk-Othmer Encyclopedia of Chemical Technology*, (American Cancer Society), 1-18.

Sugiyama, N., Tabuchi, Y., Horiuchi, T., Obinata, M., and Furusawa, M. (1993a). Establishment of Gastric Surface Mucous Cell Lines from Transgenic Mice Harboring Temperature-Sensitive Simian Virus 40 Large T-Antigen Gene. *Experimental Cell Research* 209, 382–387.

Sugiyama, N., Tabuchi, Y., Horiuchi, T., Obinata, M., and Furusawa, M. (1993b). Establishment of Gastric Surface Mucous Cell Lines from Transgenic Mice Harboring Temperature-Sensitive Simian Virus 40 Large T-Antigen Gene. *Experimental Cell Research* 209, 382–387.

Svedberg, T., and Nichols, J.B. (1926). THE MOLECULAR WEIGHT OF EGG ALBUMIN I. IN ELECTROLYTE-FREE CONDITION. *Journal of the American Chemical Society* 48, 3081–3092.

Tahara, Y., and Toko, K. (2013). Electronic Tongues—A Review. *IEEE Sensors Journal* 13, 3001–3011.

Takahashi, T., Matsumoto, T., Nakamura, M., Matsui, H., Kiyohara, H., Sasakawa, C., and Yamada, H. (2004a). A novel in vitro infection model of helicobacter pylori using mucin-producing murine gastric surface mucous cells. *Helicobacter* 9, 302–312.

Takahashi, T., Matsumoto, T., Nakamura, M., Matsui, H., Kiyohara, H., Sasakawa, C., and Yamada, H. (2004b). A novel in vitro infection model of helicobacter pylori using mucin-producing murine gastric surface mucous cells. *Helicobacter* 9, 302–312.

Takehara, S., Yanagishita, M., Podyma-Inoue, K.A., and Kawaguchi, Y. (2013). Degradation of MUC7 and MUC5B in Human Saliva. *PLOS ONE* 8, e69059.

Takeuchi, H., Thongborisute, J., Matsui, Y., Sugihara, H., Yamamoto, H., and Kawashima, Y. (2005). Novel mucoadhesion tests for polymers and polymer-coated particles to design optimal mucoadhesive drug delivery systems. *Advanced Drug Delivery Reviews* 57, 1583–1594.

Takeuchi, T., Matsushima, T., and Sugimura, T. (1975). Separation of human alpha-amylase isozymes by electro-focusing and their immunological properties. *Clinica Chimica Acta* 60, 207–213.

Taylor, A.J. (1999). Flavour Matrix Interactions. In *Current Topics in Flavours and Fragrances: Towards a New Millennium of Discovery*, K.A.D. Swift, ed. (Dordrecht: Springer Netherlands), 123–138.

Taylor, A.J. (2002). Release and Transport of Flavors In Vivo: Physicochemical, Physiological, and Perceptual Considerations. *Comprehensive Reviews in Food Science and Food Safety* 1, 45–57.

T. Cook, M., A. Schmidt, S., Lee, E., Samprasit, W., Opanasopit, P., and V. Khutoryanskiy, V. (2015). Synthesis of mucoadhesive thiol-bearing microgels from 2-(acetylthio)ethylacrylate and 2-hydroxyethylmethacrylate: novel drug delivery systems for chemotherapeutic agents to the bladder. *Journal of Materials Chemistry B* 3, 6599–6604.

Theisen, A., Johann, C., Deacon, M.P., and Harding, S.E. (2000). *Refractive increment data-book for polymer and biomolecular scientists* (Nottingham: Nottingham University Press).

Tierney, P.A., Karpinski, C.D., Brown, J.E., Luo, W., and Pankow, J.F. (2016). Flavour chemicals in electronic cigarette fluids. *Tobacco Control* 25, 10–15.

Tissières, A., and Watson, J.D. (1958). Ribonucleoprotein Particles from *Escherichia Coli*. *Nature* 182, 778.

Topkas, E., Keith, P., Dimeski, G., Cooper-White, J., and Punyadeera, C. (2012). Evaluation of saliva collection devices for the analysis of proteins. *Clinica Chimica Acta* 413, 1066–1070.

Tromelin, A., Andriot, I., and Guichard, E. (2006). Protein-flavour interactions. In *Flavour in Food*, (Woodhead Publishing Limited), p. 320 p.

Tsuiki, S., Hashimoto, Y., and Pigman, W. (1961). Bovine submaxillary mucin. *Nature* *189*, 399.

Tsuji, T., and Osawa, T. (1986). Carbohydrate structures of bovine submaxillary mucin. *Carbohydrate Research* *151*, 391–402.

Tuma, D.J., Newman, M.R., Donohue, T.M., and Sorrell, M.F. (1987). Covalent binding of acetaldehyde to proteins: participation of lysine residues. *Alcoholism: Clinical and Experimental Research* *11*, 579–584.

Ulla, H., Antti, K., Oskar, L., and Mari, S. (2016). Genetic basis of flavor sensitivity and food preferences. In *Flavor*, P. Etiévant, E. Guichard, C. Salles, and A. Voilley, eds. (Woodhead Publishing), 203–227.

Vaisey, M., Brunon, R., and Cooper, J. (1969). Some Sensory Effects of Hydrocolloid Sols on Sweetness. *Journal of Food Science* *34*, 397–400.

Van Holde, K.E., Johnson, W.C., and Ho, P.S. (2006). *Principles of physical biochemistry* (Upper Saddle River, N.J: Pearson/Prentice Hall).

Van Ruth, S.M., and Roozen, J.P. (2000). Influence of mastication and saliva on aroma release in a model mouth system. *Food Chemistry* *71*, 339 - 345.

Vas, G., and Vékey, K. (2004). Solid-phase microextraction: a powerful sample preparation tool prior to mass spectrometric analysis. *Journal of Mass Spectrometry* *39*, 233–254.

Venter, J.P., Kotzé, A.F., Auzély-Velty, R., and Rinaudo, M. (2006a). Synthesis and evaluation of the mucoadhesivity of a CD-chitosan derivative. *International Journal of Pharmaceutics* *313*, 36–42.

Venter, J.P., Kotzé, A.F., Auzély-Velty, R., and Rinaudo, M. (2006b). Synthesis and evaluation of the mucoadhesivity of a CD-chitosan derivative. *International Journal of Pharmaceutics* *313*, 36–42.

Wales, M., and Holde, K.E.V. (1954). The concentration dependence of the sedimentation constants of flexible macromolecules. *Journal of Polymer Science* *14*, 81–86.

Walker, S., and Prescott, J. (2000). The Influence of Solution Viscosity and Different Viscosifying Agents on Apple Juice Flavor. *Journal of Sensory Studies* 15, 285–307.

Weerawatanakorn, M., Wu, J.-C., Pan, M.-H., and Ho, C.-T. (2015). Reactivity and stability of selected flavor compounds. *Journal of Food and Drug Analysis* 23, 176–190.

West, T.P., and Strohfus, B. (1996). A pullulan-degrading enzyme activity of *Aureobasidium pullulans*. *Journal of Basic Microbiology* 36, 377–380.

Whittingham, J.L., Edwards, D.J., Antson, A.A., Clarkson, J.M., and Dodson, G.G. (1998). Interactions of phenol and m-cresol in the insulin hexamer, and their effect on the association properties of B28 pro --> Asp insulin analogues. *Biochemistry* 37, 11516–11523.

WHO (2011). Global status report on noncommunicable diseases 2010. (Geneva: WHO Library Cataloguing-in-Publication Data).

Woertz, C., Preis, M., Breitzkreutz, J., and Kleinebudde, P. (2013). Assessment of test methods evaluating mucoadhesive polymers and dosage forms: an overview. *European Journal of Pharmaceutics and Biopharmaceutics* 85, 843–853.

Woertz, K., Tissen, C., Kleinebudde, P., and Breitzkreutz, J. (2011). Taste sensing systems (electronic tongues) for pharmaceutical applications. *International Journal of Pharmaceutics* 417, 256–271.

Wyatt, P.J. (1993). Light scattering and the absolute characterization of macromolecules. *Analytica Chimica Acta* 272, 1–40.

Yakubov, G.E., Gibbins, H., Proctor, G.B., and Carpenter, G.H. (2014). Oral Mucosa: Physiological and Physicochemical Aspects. In *Mucoadhesive Materials and Drug Delivery Systems*, (John Wiley & Sons, Ltd), 1–38.

Yamakawa, H., and Fujii, M. (1973). Translational Friction Coefficient of Wormlike Chains. *Macromolecules* 6, 407–415.

Ye, Q., Heck, G.L., and DeSimone, J.A. (1991). The anion paradox in sodium taste reception: resolution by voltage-clamp studies. *Science* 254, 724–726.

Yilmazer-Musa, M., Griffith, A.M., Michels, A.J., Schneider, E., and Frei, B. (2012). Inhibition of α -Amylase and α -Glucosidase Activity by Tea and Grape Seed Extracts and their Constituent Catechins. *Journal of Agricultural and Food Chemistry* 60, 8924–8929.

Yu, T., Macnaughtan, B., Boyer, M., Linforth, R., Dinsdale, K., and Fisk, I.D. (2012). Aroma delivery from spray dried coffee containing pressurised internalised gas. *Food Research International* 49, 702–709.

Zakowski, J.J., and Bruns, D.E. (1985). Biochemistry of human alpha amylase isoenzymes. *Critical Reviews in Clinical Laboratory Sciences* 21, 283–322.

Zhou, F., Zhao, M., Su, G., and Sun, W. (2014). Binding of aroma compounds with myofibrillar proteins modified by a hydroxyl-radical-induced oxidative system. *Journal of Agricultural and Food Chemistry* 62, 9544–9552.